UCLA
UCLA Electronic Theses and Dissertations

Title
One-Dimensional Modeling of Secondary Settling Tanks

Permalink

Author
Li, Ben

Publication Date
2016

Peer reviewed|Thesis/dissertation

UNIVERSITY OF CALIFORNIA

Los Angeles

One-Dimensional Modeling of Secondary Settling Tanks

A dissertation submitted in partial satisfaction of the

requirements for the degree Doctor of Philosophy

in Civil Engineering

by

Ben Li

2016

ABSTRACT OF THE DISSERTATION

One-Dimensional Modeling of Secondary Settling Tanks

by

Ben Li

Doctor of Philosophy in Civil Engineering

University of California, Los Angeles, 2016

Professor Michael K. Stenstrom, Chair

Sedimentation is one of the most important processes that determine the performance of the activated sludge process, and secondary settling tanks (SSTs) have been investigated with the mathematical models for design and operation optimization. However, the practical application of SST models still remains a challenge due to several difficulties, such as the lack of efficient (high accuracy and low computation cost) solution techniques and reliable model calibration strategies. To facilitate the practical application of SST models, this dissertation focuses on the one-dimensional (1-D) modeling of SSTs, including the numerical analysis to introduce and select efficient solution techniques, sensitivity and practical identifiability analysis to reliably calibrate the 1-D SST models, and evaluation of the implications of SST modeling on the design and control of waste water treatment plants.

To improve the understanding of 1-D modeling of SSTs, this dissertation provides a comprehensive literature review of the batch settling methodology and the flux theory, which

played a significant role in the early stage of SST investigation. The literature review also contains an explicit introduction of the established 1-D SST models, including the relevant physical laws, various settling behaviors, the constitutive functions, available solution techniques and calibration strategies.

As the only available method for analytical solution development of ideal continuous settling model, the method of characteristics has been successfully implemented to investigate the dynamics of SST for various solids loading conditions. This dissertation also introduced the Yee-Roe-Davis method, which able to capture solution discontinuities based on gradient, thus providing numerical solutions with second-order accuracy. By using the method of characteristics as a reference, the convergence analysis of Methods Simplified-Godunov, Godunov and Yee-Roe-Davis shows that all are reliable, since they are able to provide arbitrarily close approximations to the reference solutions as discretization is refined. For a given discretization level, the Yee-Roe-Davis method is most efficient in reducing error, and provides the most accurate approximations. However, this advantage of high accuracy of the Yee-Roe-Davis method is at the cost of larger computation time and coding complexity.

To facilitate model calibration, the important parameters for 1-D SST model calibration were identified under non-ideal flow and settling conditions using global sensitivity analysis (GSA). This dissertation also demonstrated that reliable reduction of 1-D SST models can be achieved based on GSA results; for example under the bulking condition, the hindered-compression-dispersion model can be reduced to the hindered-dispersion model without impacting model accuracy. The model uncertainty analysis efficiently evaluates model reduction reliability.

In terms of developing batch settling methodology for reliable model calibration, this dissertation found that the hindered settling parameters are more influential in situations where only batch

settling data are available, while the sensitivity to compression parameters can be greatly increased if concentration profile observations are included. The practical identifiability analysis further showed that parameter estimates obtained from data sets that only include batch settling data or the concentration profiles cannot generally predict concentration profiles and batch settling curve observations, respectively. Because of the application of local sensitivity functions, the parameter identifiability analysis can be sensitive to the initial parameter value selection. Estimates obtained by identifiable parameter subsets estimation are conditional on the values of fixed parameters.

From the view of optimizing the process design and control, this dissertation demonstrated that the bioreactor and SST should be designed as a whole, and a safety constraint can be introduced in the design process to greatly improve the system's efficiency and reliability. A comprehensive selection of the designed alternatives should consider three aspects: economic plausibility, contaminant removal efficiency, and system robustness. Least-cost points can usually be attained, but their locations will vary depending on the weighting of the relative cost factor.

The dissertation of Ben Li is approved.

Eric M.V. Hoek

Keith D. Stolzenbach

Christopher R. Anderson

Michael K. Stenstrom, Committee Chair

University of California, Los Angeles

2016

Dedication to my parents Xiubao Li and Zhenhui Wang

Table of Contents

List of Figures

List of Tables

ACKNOWLEDGEMENTS

VITA

Education

2007 – 2011 B.S. in Environmental Engineering, Zhejiang University of Technology

2011 – 2012 M.S. in Civil Engineering, University of California, Los Angeles

Publications

Ben Li and M.K. Stenstrom, "One-Dimensional Modeling of Secondary Clarifier Tanks and Design Impacts of Sizing", *Wat. Research*, **50**, 160-170, 2014

Ben Li and M.K. Stenstrom, "Dynamic One-Dimensional Modeling of Secondary Settling Tanks and System Robustness Evaluation", *Wat. Sci. & Tech,* **69**(11), 2339-2349, 2014.

Ben Li and M.K. Stenstrom, "Research Advances and Challenges in One-Dimensional Modeling of Secondary Settling Tanks - A Critical Review", *Wat. Research*, **65**, 40-63, 2014.

Ben Li and M.K. Stenstrom, "Construction of Analytical Solutions and Numerical Methods Comparison of the Ideal Continuous Settling Model", *Computers & Chemical Engineering*, **80**, 211-222, 2015.

Ben Li and M.K. Stenstrom, "Practical Identifiability and Uncertainty Analysis of the One-Dimensional Hindered-Compression Continuous Settling Model", *Wat. Research*, 90, 235-246, 2016.

Ben Li and M.K. Stenstrom, "A Sensitivity and Model Reduction Analysis of One-Dimensional Secondary Settling Tank Models Under Wet-weather Flow and Sludge Bulking Conditions", *Chemical Engineering Journal*, 288, 813-823, 2016.

Ben Li, Yingxia Li, Yuping Qiu, Yang Yu, M.K. Stenstrom, " Significance of Reactive Secondary Settling Tank Models On the Simulation of WWTP Performance Under Ideal and Non-Ideal Flow and Settling Conditions", submitted to *Wat. Research* and under review.

Ben Li and M.K. Stenstrom, "Dynamic One-Dimensional Modeling of Secondary Settling Tanks and System Robustness Evaluation", 5th IWA ASPIRE Conference, Daejeon Korea, 2013. (Oral presentation)

Ben Li and M.K. Stenstrom, " Research Advances and Challenges in One-Dimensional Mathematical Modeling of Secondary Settling Tanks—A Critical Review", 86th WEFtec Conference, Chicago, IL, 2013. (Oral presentation)

Ben Li and M.K. Stenstrom, "Comparison of Global Sensitivity Methods for the Activated Sludge Model No.3: A Case Study of the West County Wastewater Reclamation Plant," 6th IWA ASPIRE Conference, Beijing, China, 2015. (Oral presentation)

Ben Li and M.K. Stenstrom, " A Comprehensive comparison of one-dimensional continuous settling models based on sensitivity and uncertainty analysis", 88th WEFtec Conference, Chicago, IL, 2015. (Oral presentation)

1. Introduction

1.1. Background

Biological secondary treatment processes are widely used in wastewater treatment plants to remove organic matter and reduce nutrients such as nitrogen and phosphorus. In most cases, efficient operation requires the biomass to be removed from the wastewater by sedimentation, filtration or other solids-liquid separation processes.

Several types of treatment processes can achieve solids-liquid separation, but secondary settling tanks (SSTs) are most commonly used. SSTs, also known as clarifiers, sedimentation basins or solids-liquid separators, use gravity to separate the biomass from the fluid, and have two similar but distinct functions: clarification and thickening. Clarification is the removal of finely dispersed solids from the liquid to produce a low turbidity effluent; thickening is the process of increasing the sludge concentration in order for it to be recycled or disposed in less volume. In SSTs, the clarification process occurs in the upper zone while thickening occurs near the bottom. The result is an effluent from the top, low in suspended solids, and a second stream of settled, concentrated biomass from the bottom, suitable for recycling or disposal.

As one of the most important units in wastewater treatment process, the SST is often a "bottle neck," limiting the capacity of the wastewater treatment process (Ekama et al. 1997a, Ekama and Marais 2002a). The SST sizing must be combined with the bioreactor sizing to provide the minimum necessary conditions, such as the solids retention (SRT) or food-to-mass (F/M ratio) to meet design conditions, as well as maintaining a safety factor to handle shocks and upsets. If the SST does not produce a highly clarified effluent, or cannot thicken biomass to the required

recycle concentration, excessive effluent solids will result, causing effluent permit violations and resultant loss biomass from the reactor. Therefore, two commonly used parameters: overflow rate and solids flux, have been developed for SST design and evaluation.

Since wastewater characteristics vary, such as temperature, flow rate and contaminant concentrations, traditional design procedures for SSTs tend to be empirical and conservative by introducing averaged parameters with safety factors (Coe and Clevenger 1916). Therefore SST performance can suffer unanticipated fluctuations, which may cause process control problems and increase the risks of failure. Stringent standards for effluent quality and the need for optimization of WWTP performance have made such variations in effluent quality undesirable, and have encouraged the use of dynamic controls for wastewater treatment process.

A mathematical modeling approach, where the bioreactor models are coupled with SST models, is encouraged in WWTP studies for overall process design and control optimization. Scientific knowledge on characterizing the biomass growth and contaminant removal is well-developed, whereas the various settling behaviors within the SST are still poorly understood, thus causing the difficulty in effluent quality prediction, biomass inventory estimation (Plósz et al. 2011). Great efforts have been made to rigorously predict SST performance. According to different practical application purposes, the modeling approaches can be divided into three main categories:

1. One-dimensional (1-D) dynamic model: 1-D models are based mostly on flux theory and Kynch's assumption that the solids gravity settling velocity is only determined by the local sludge concentration. The hydraulic flow is simplified as downward/upward flow to simulate the recycling/effluent flow and satisfy the 1-D assumption.

2. Two-dimensional (2-D) hydraulic model: compared with 1-D models, 2-D models are developed using computational fluid dynamics (CFD) techniques. Therefore, instead of simplifying or omitting the hydraulic flow impacts, 2-D models can incorporate hydrodynamics such as density currents, turbulence, and artifacts of unfavorable SST geometry. Flocculation behavior can also be modeled, if coupled with a sub-flocculation model (Zhou and Mccorquodale 1992a, b). A frequent application of 2-D models is to improve SST geometry design and optimize performance.

3. Three-dimensional (3-D) hydraulic model: the motivation of developing 3-D approaches is to understand non-symmetric features: for example the heat exchange caused by the varying temperatures and wind effects. Very detailed computation grids are now feasible in order to capture geometric features as small as several inches (Gong et al. 2011, Xanthos et al. 2011, Ramalingam et al. 2012). However, the high resolution grids also incur large computation cost which may limit the 3-D models' practicability.

In current engineering practice, 1-D SST models are mostly used due to their relative simplicity and low computation cost. As the most prevalent one, the 1-D 10-layer SST model, also known as the Takács model (Takács et al. 1991), has been implemented in most commercial simulators as a reference model. Although the Takács model has achieved a degree of success in predicting the SST performance, such as the effluent concentration, the underflow concentration and the sludge blanket level, its shortcomings are not negligible, which can be summarized as two aspects:

1. Insufficient description of various settling behavior. With the ad-hoc assumption that hindered settling mostly determines the SST performance, the Takács model only

includes the first-order convection term (hindered settling term) to describe the solids transport within the SST, while other significant settling processes, such as the compression settling, are not considered.

2. Inaccuracy of numerical solutions. The PDE solver using the flux constraint embedded in the Takács model can only provide reliable numerical solutions under ideal conditions (dry-weather and good settling), and may lead to unphysical solution oscillation under non-ideal conditions, such as wet-weather and sludge bulking (Bürger et al. 2012). Meanwhile, the numerical dispersion introduced by the low discretization level (10-layer) also prevents a detail investigation of the settling dynamics, as reported by Jeppsson and Diehl (1996).

In the last two decades, to overcome the limitations of the Takács model, several advanced SST models have been developed as reliable alternatives, which can be classified into three groups based on their advantages:

1. First-order model with reliable numerical techniques: for these models, the model formula remains the same as the Takács model by only considering the hindered settling behavior, while more reliable numerical techniques, such as the Godunov numerical flux are used to construct both numerically and physically acceptable solutions (Jeppsson and Diehl 1996).

2. Second-order hindered-compression model: the improved understanding of activated sludge rheology has facilitated the development of phenomenological theory of sedimentation-consolidation, and then the phenomenological theory is expressed in the compression model, which allows a more rigorous description of the compression settling

behavior (Bürger 2000, Bürger et al. 2000a). Compared with the hindered-only model, the hindered-compression model is expected to provide more realistic prediction of the sludge blanket level and the underflow concentration.

3. Second-order hydraulic dispersion model: for these models, an explicit hydraulic dispersion term is added to the model formula to account for the potential impact of hydraulics on the biomass settling behavior (Plósz et al. 2007, Ramin et al. 2014a). The hydraulic dispersion model possesses the advantage of simulating the hydraulics of SSTs in a wider range of dynamic flow conditions (Ramin et al. 2014c). From the numerical point of view, adding the flow-dependent dispersion term also avoids the shock problem occurring in the hindered-only model.

Despite the advantages of these advanced models, their practical application is limited, which can be potentially attributed to the lack of guidance to facilitate the model calibration and the difficulty of selecting SST models for specific simulation purposes (sludge blanket level prediction, sludge retention time calculation etc). Therefore, given that the currently available SST models cannot always provide satisfactory predictions and their implementation strategies are not well developed, further research is strongly needed to improve the performance of 1-D SST models, as well as facilitate their application in engineering practice.

1.2. Objectives

In order to improve the model reliability as well as facilitate its practical application, the main objectives of this dissertation are (i) to provide a comprehensive literature review, which includes the significant research topics related to the 1-D SST modeling, such as the batch settling test methodology, model formula development, reliable solution calculation and efficient

model calibration; (ii) to focus on the numerical analysis of 1-D SST models with the aim of introducing and selecting efficient numerical techniques for model solving; (iii) to investigate the application of 1-D SST models on the design and control of wastewater treatment plants (WWTPs), such as improving the understanding of interactions between bioreactor and SST, and demonstrate that the design and control decision-making of WWTP operations is sensitive to the selection of 1-D SST models; (IV) to develop efficient calibration strategy of 1-D SST models by identifying parameter subsets suitable for calibration under various flow and settling conditions, and evaluate the parameter identifiability based on different experimental layouts; (V) to investigate the 1-D SST model reduction based on sensitivity analysis results, and evaluate the reliability of model reduction based on uncertainty analysis.

1.3. Outline

Chapter 2 of this dissertation provides a comprehensive literature review of the 1-D modeling of SSTs. This chapter starts with a review of the development of settling theory, focusing on batch settling methodology and the flux theory, since they played an important role in the early stage of SST investigation. The second part of this chapter is an explicit review of the established 1-D SST models, including the relevant physical law, various settling behaviors (hindered, transient, and compression settling), the constitutive functions. The third part is a discussion of reliable numerical techniques needed for solving the models' governing equations. The last part focuses on the calibration of 1-D SST models, which is specifically important in terms of the increasing complexity of SST model itself.

Chapters 3, 4 and 5 of this dissertation mainly focuses on the numerical analysis of SST models and implications of SST models on the design and control of WWTPs. For the ideal SST model

(hindered-only model), its analytical solutions under different operating conditions are constructed in Chapter 4 based on method of characteristics. The analytical solutions are also compared with experiment data to show the validity of the SST model in predicting the sediment height and solids concentration distribution as a function of time and loading conditions. In Chapters 3 and 5, the reliable numerical technique based on the Yee-Roe-Davis method is introduced to calculate both physically and numerically acceptable solutions, and the efficiency of different alternative numerical techniques are evaluated based on their comparison with the analytical solution in Chapter 4. Chapter 3 and 5 also investigate the feasibility of applying the SST models in the design and control of WWTPs, such as optimizing the sizes of bioreactor and SST, and evaluate the influence of SST simulation on control and decision-making.

Chapters 6 and 7 provide the methodology of reliable model calibration in different experimental layouts, and the guidance of model reduction for specific simulation purposes. In Chapter 6, the parameter subsets suitable for model calibration are identified based on sensitivity analysis, and influence of imposed flow and settling conditions on the sensitivity of model outputs on parameters are assessed as well. Chapter 6 further demonstrates that reliable model reduction can be achieved based on sensitivity analysis, and provides the guidance of SST model selection based on specific simulation purposes. The primary concern of Chapter 7 is the reliable calibration of SST models in various experimental layouts. The practical identifiability analysis of SST models is provided in Chapter 7 to determine identifiable parameter subsets based on different experimental layouts. Chapter 7 also investigates the influence of initial parameter value selection on parameter identifiability analysis, and the bias of parameter estimates caused by fixing unidentifiable parameters.

2. Literature review

Sedimentation is one of the most important processes that determine the performance of the activated sludge process (ASP), and SSTs have been frequently investigated with the mathematical models for design and operation optimization. Nevertheless their performance is often far from satisfactory. The first part of this chapter is a review of the development of settling theory, focusing on batch settling methodology and the development of flux theory, since they played an important role in the early stage of SST investigation. The second part is an explicit review of the established 1-D SST models, including the relevant physical law, various settling behaviors (hindered, transient, and compression settling), the constitutive functions, and their advantages and disadvantages. The third part is a discussion of numerical techniques required for reliable model output calculation, and the last part mainly focuses on the calibration of 1-D SST models.

2.1. Batch settling methodology and flux theory development

Because of the similarities between batch settling and continuous settling processes, many early researchers investigating activated sludge thickening and clarification predicted continuous settling behavior from batch settling tests. Coe and Clevenger (1916) provided one of the earliest examples relating batch settling phenomenon to the design and operation of the SST, and in their classical paper, the settling behavior in a batch thickening column was qualitatively indentified in four distinctive zones: 1) the clear supernatant zone at the top with low turbidity; 2) the uniform settling zone with constant concentration equal to initial concentration; 3) the transition zone between the constant concentration and compression zones, and 4) the compression zone formed by the compression from overlaying sludge and the mechanical support of the lower

bottom. Among each zone in the batch settling test, the constant settling zone was found to govern the SST area requirement; however Coe and Clevenger (1916) believed that the SST depth, in their case of using pulp and paper sludge, should be large enough to provide sufficient storage time, thus making the sludge retention long enough within the SST to squeeze the water out of sludge sediment to obtain more condensed recycling flow. As an extension of this conclusion, the requirement of SST area was characterized as the finding the minimum solids handling capacity for any intervening values from the initial concentration to the bottom (Coe and Clevenger 1916).

As the only established quantitative approach, Coe and Clevenger's empirical procedure was widely accepted and used in the first half of the 20th century, having a profound impact on SST design and operation. Nevertheless, the remaining difficulties of theoretically examining the settling process still prevented the in-depth understanding of the batch settling process, as well as the continuous process.

In order to simplify the problem without having to understand the detailed force acting on particles, Kynch (1952) presented the constitutive relation, now known as Kynch's assumption, that the hindered settling velocity is uniquely determined by the local solids concentration. On the basis of Kynch's assumption, the batch settling process was modeled by the mass continuity equation of the solid phase as eq.(2.1) with proper constitutive functions, initial and boundary conditions, and the mass flux was introduced for solids conveyance calculation:

$$\frac{\partial \phi}{\partial t} + \frac{\partial (\phi v_s)}{\partial z} = 0 \tag{2.1}$$

where ϕ is the solid concentration, v_s is the gravity settling velocity, t is time, z is the spatial axis

in vertical direction.

In solving eq.(2.1), solution discontinuities are expected to occur as a function of time and height, and these discontinuities can be physically interpreted as the sediment interfaces or blanket heights observed in experiments and full-scale operations. Therefore, eq.(2.1) is satisfactory in capturing concentration discontinuities without knowing their physical mechanisms, although it fails to distinguish various settling behaviors (Kynch 1952, Concha and Bürger 2003). As Kynch said in his celebrated paper " a considerable amount can be learned by the single main velocity assumption, though further experiments are necessary to verify its validity" (Kynch 1952). His theory greatly improved the understanding of the settling problem, and usually has been applied as the first step in batch and continuous settling data analysis.

Since the starting point of Kynch's work is a mathematic development and analysis of eq.(2.1), he did not provide suggestions for practical application of his theory. The first attempt of introducing Kynch's theory to SST design was proposed by Talmage and Fitch (1955). In their design procedure, the slope of a tangent to the interface subsidence curve of a batch settling test was thought to be equal to the settling velocity of the layer with the initial concentration, shown as Fig 2.1, which is consistent with Kynch's theory. Therefore, the settling velocity information can be obtained through the initial and final equilibrium states, and the settling flux curve can be synthesized from a single batch settling test.

Shortly thereafter, Talmage and Fitch made the assumption that the thickening capacity is governed by the concentration which exists at the solid-liquid interface as the solids enter the compression zone. If solids enter the compression zone more rapidly that they can pass through it to the underflow, accumulation occurs. Hence, the accuracy of their design procedure is highly

dependent on precisely determining the time of compression (t_c). Several empirical methods are available: Roberts' (1949) procedure based on Coe and Clevenger's hypothesis that the loss of water in the compression zone is a function of time and Eckenfelder and Melbinger's (1957) tangents crossing method .
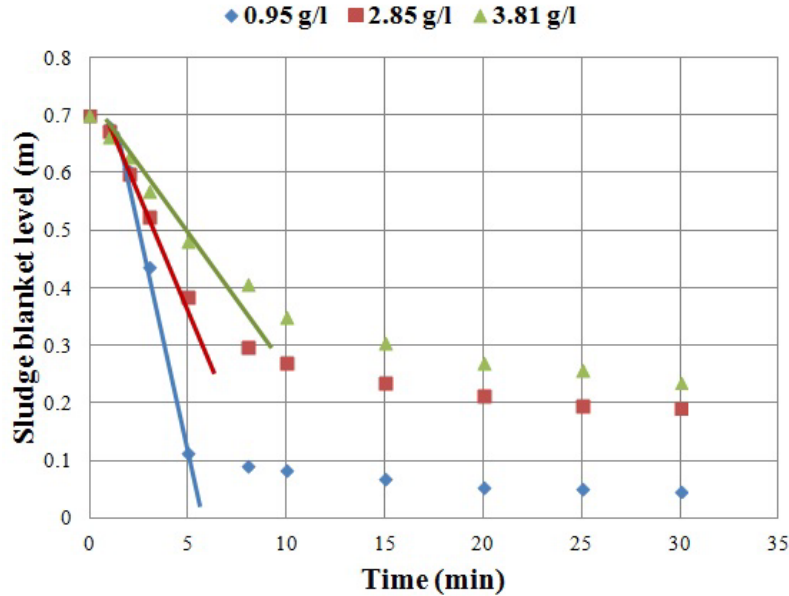
Fig. 2.1 - Sludge blanket height *vs.* time (Grieves and Stenstrom (1976)).

In additional to the difficulty of determining the compression time, the Talmage-Fitch procedure subsequently has been shown to yield conservative SST size design by many investigators (Hassett 1958, Fitch 1962, Alderton 1963). One explanation for this result is that the settling velocity is not only determined by concentration in compression zone but also impacted by various other factors, such as the compressive force, which invalidates Kynch's original assumption. However, acknowledging its shortcomings, the Talmage-Fitch procedure was still advocated by a number of researchers, because it requires only one batch settling test , as

opposed to multiple batch settling experiments required by the Coe and Clevenger method (Moncrieff 1964, Scott 1968a, b).

The reason the Talmage and Fitch method leads to a conservative design rests on two important assumptions: the first is that the settling velocities observed in laboratory batch settling test can truly represent those found in full scale SSTs, and the second is the validity of the Kynch assumption itself.

To understand the potential artifacts of small scale equipments, factors such as the cylinder size, the initial sludge height were investigated. When the diameter of the batch settling cylinder becomes fairly small with respect to the particle size, for example in 1 L graduate cylinder (diameter=3 cm), the "wall effect" will be greatly magnified by "arching" or "bridging" of the sludge with the wall, which could retard the normal settling process (Kammermeyer 1941, Vesilind 1968b). Dick (1965) showed that the "wall effect" was more profound with the concentrated sludge than with dilute one. Generally, the small diameter column can produce higher settling velocity in the dilute range, but lower velocities in the concentrated range (Vesilind 1968b). Small size cylinders are more convenient to use since they require less test sludge, and obtaining uniform initial sludge concentration throughout the cylinder is easier. Non-uniform sludge concentrations may invalid the 1-D assumption may also change floc characteristics (Tracy 1973). For these reasons small size cylinders are still desirable, and slow speed mixers have been recommended to avoid wall effects (Work and Kohler 1940, Behn 1957), as well as model the rake effect found in full-scale SSTs (Eckenfelder and Melbinger 1957, Vesilind 1968b).

Differences in observed settling velocities have been attributed to the initial depth of the sludge. Several researchers (Work and Kohler 1940, Kammermeyer 1941) showed that the initial settling depth exerts a profound influence in concentrated sludge experiments while having much less influence in dilute sludge experiments. Later, more detailed investigations from Dick and Ewing (1967) showed that the height effect was closely related to the type of sludge; for example activated sludge was much more influenced by initial depth than a suspension of sand. Shannon and Alderton (1966) used glass beads with a Gaussian size distribution to demonstrate the independence of settling velocity with the initial height, and Kynch's theory was applicable for interface height prediction (Shannon et al. 1963). This discrepancy was caused by the fact that the activated sludge deviates greatly from the ideal particle assumption (Tracy 1973). The validity of Kynch's theory in compression zone was proven by Tory and Shannon (1965), and they stated that the settling velocity in compression zone can still largely be approximated as a function only of concentration.

The settling velocity function is significant for SST design using solid flux theory (Cho et al. 1993), and a variety of theoretical or empirical functions have been proposed (Steinour 1944, Vand 1948, Richardson and Zaki 1954, Yoshioka et al. 1957b, Scott 1966, Vesilind 1968b, Vaerenbergh 1980, Takács et al. 1991, Cho et al. 1993, Cacossa and Vaccari 1994, Bürger 2000, Kinnear 2002, Zhang et al. 2006). Various factors, for example the particle size, shape, sludge viscosity, density and porosity have been used to characterize the settling velocity, while in practical engineering application, empirical functions are preferred due to their simplicity and practicality. For applications relating to municipal wastewater treatment, the most popular are the exponential functions (Vesilind 1968b, Takács et al. 1991), which have been shown to better fit the experimental data than other functions (Smollen and Ekama 1984). Most empirical

approaches primarily determine the hindered settling velocity as a function of the sludge concentration, although a few functions, consider the velocity in the compression zone, which deviates with Kynch's assumption, and will be discussed later.

The main difference in the continuous settling process as compared to batch settling, is the bulk solids transport caused by hydraulic flows, and in ideal 1-D conditions, these hydraulic flows are simplified as the upward and downward bulk flow, which convey the sludge towards the SST effluent weir and bottom, respectively. On the basis of considering the hydraulic bulk transportation, Yoshioka *et al.* (1957b) and Hassett (1958) independently developed two widely used graphical methods for the limiting flux and SST operation condition analysis. The former one plots gravity flux only, while the later shows both gravity and total flux (total flux =gravity flux +bulk flux). The SST area requirement is governed by the local minimum flux point, which is therefore termed as the limiting flux, and the recycling solids concentration is estimated from mass conservation around the SST bottom. Scott (1968a, b) noted that since both methods were based on batch flux data, they might overestimate the limiting flux and recycling concentration, because batch settling tests do not included a deep compression zone required for compression.

Different batch settling materials or sludges, including the carbonate sludge, lime softening sludge and activated sludge have been used to verify limiting flux theory, and good agreement between observed thickening performance and prediction based on batch flux analytical methods were obtained in all cases (Yoshioka et al. 1957b, Hassett 1958, Javaheri 1971). Thereafter, Keinath *et al.*(1977) and Keinath (1985) extended these methods to the state point concept, where the state point is the intersection of the recycle flow and overflow lines on the settling flux plot. State point analysis is now commonly used to evaluate SST performance over a range of

different operating conditions (underloading condition, critical loading condition and overloading condition), as well as predicating the vertical concentration profiles.

Despite its prevalence, the solids flux theory still has two remaining problems: 1) it is an experiment observation result more than a theoretical proved conclusion; 2) it can deal with steady states, but fails in dynamically investigating the settling behavior within SSTs. During the 1990s, the development of 1-D SST model and mathematic techniques of nonlinear hyperbolic PDEs provide the opportunity of further understanding the solids flux theory. Chancelier *et al.* (1997) found that the flux theory can be confirmed and extended in a natural way within the context of the nonlinear hyperbolic PDEs, and the flux theory conclusions are closely related to the stationary solutions of the 1-D model governing equations. By describing the solids flux theory within nonlinear PDEs theory, many defined conceptions as the limiting flux, feed layer, sludge blanket height and loading condition can be interpreted by a first-order hyperbolic PDE model, hence making the SST dynamic behaviors predictable (Diehl 1995, 1996, Bürger and Narvaez 2007, Bürger and Karlsen 2008, Diehl 2008). Obviously, compared with the stationary solutions of the flux theory, the 1-D SST model owns the specific advantage in dynamic or transient conditions predictions, for example the shock hydraulic loading caused by rainfall, or the sludge bulking problem caused by filament growth. This explains why the research interests was changed to develop reliable 1-D SST model for more comprehensively quantitative investigation of SST design and operation, which will be discussed in the following section.

2.2. Mathematical modeling of SSTs

SSTs have been investigated with mathematical models for design and operation optimization purposes. Although several 2-D and 3-D SSTs models have been developed, 1-D models are mostly used because of their simplicity and lower computational demands. Before discussing 1-D SST models and their development, it is informative to define the expected capabilities of an acceptable model (Tracy 1973). Firstly, the 1-D model should be able to predict both effluent and underflow concentrations during transient operating conditions, which corresponds to clarification and thickening processes. The second main function is to approximate the concentration profile and sludge blanket level during unsteady-state operating condition in order to avoid system failure. Moreover, the model should be able to integrate with available bioreactor models to provide an overall secondary treatment simulation for system design and operation optimization purposes.

Given the complexity of real system conditions (e.g., viscosity, dispersion, turbulence, rake effect, various settling behaviors) and the need to simply the model, several ad hoc assumptions are usually introduced to limit application to an ideal suspension (a continuum) and 1-D modeling conditions, as follows:

1. the SST is circular and central-feed with constant section area;

2. the reaction rates are zero in the SST, and the particle properties (not concentrations) are uniform and constant in the SST;

3. the hydraulic flows are vertically, and horizontally uniform (no density currents or wind effects) and the solids concentration are uniform across any horizontal cross-section of SSTs;

4. the mechanical sludge scraper does not impact the settling process and wall effects are negligible.

Based on these assumptions, Shannon *et al.* (1963) presented the concept of an ideal 1-D SST, and an number of later researchers have advanced these concepts (Bryant 1972b, Stenstrom 1976a, Bustos et al. 1990b, Bürger et al. 2011). Fig 2.2 shows the schematic overview of an ideal SST . In general, SSTs can be divided into three major zones according to their distinct functions: clarification zone, thickening zone and feed zone. In the clarification zone, influent flow is clarified to produce low turbidity effluent, while the thickening zone provides concentrated solids for recycling and disposal. The feed zone is the place where the input sludge is introduced and well mixed for initial settling. For 1-D modeling, the hydraulic flow divides and is upward flow (Q_e) towards the effluent weir and the downward flow (Q_u) towards the SST bottom. As can be seen, compared with the static sedimentation process in batch tests, the feeding and discharge flows in SSTs are continuous.
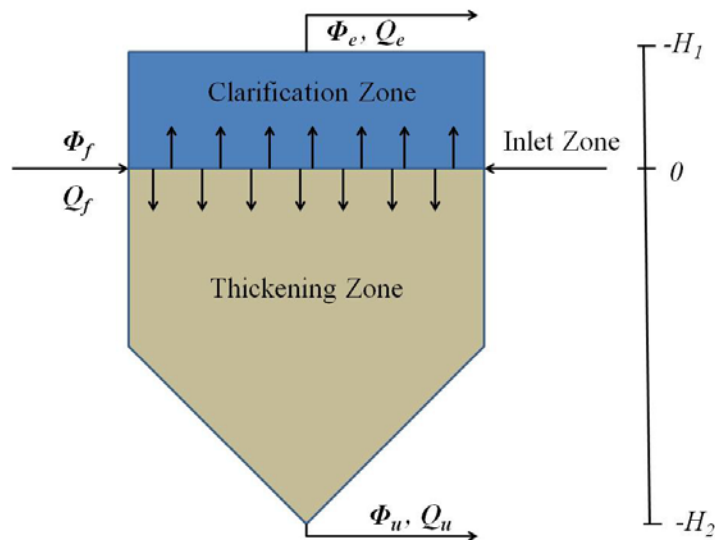
Fig. 2.2 - Schematic overview of an ideal one-dimensional SST.

Instead of the sole gravity settling in batch settling tests, the hydraulic bulk transport caused by the upward and downward hydraulic flows can also greatly impact the sludge settling behavior in the continuous settling process. Therefore, the combination of the sedimentation knowledge learned from batch settling tests and the concept of an ideal SST forms the fundamental theory framework of the 1-D SST modeling. The problem then becomes how to mathematically describe the continuous settling behavior based on this framework.

2.3. The mass conservation model

Generally, the starting point of mathematical modeling work is the physical law (Bürger et al. 2011). The mostly used one in 1-D SST modeling is the mass conservation law of the solid phase, which requires that the substance change per unit time in a finite region equals to the net flux into the region pluses the net mass production in the region, and usually the net mass production is negligible because of the zero reaction assumption. Using the ideal1-D assumptions, the solids concentration is a function of space (z) and time (t).

The mass conservation law model is also known as the layer model, which was originally presented by Bryant (1972b) and Stenstrom (1976a) for thickening process modeling, and broadened by Vitasovic (1986a) by adding the layer above the inlet level for effluent flow quality prediction. The SST is divided into a fixed number of layers with uniform concentration in each layer, and the mass conservation law is imposed around each layer to generate the following nonlinear hyperbolic PDE formations (Takács et al. 1991, Diehl and Jeppsson 1998, Diehl 2000) by modeling the feed flux as point source:

$$\frac{\partial \phi}{\partial t} + \frac{\partial F(\phi)}{\partial z} = v_f \phi_f \delta(z)$$

$$F(\phi) = \begin{cases} -v_e \phi & \textit{effluent zone} \quad (z < -H_1) \\ v_s \phi - v_e \phi & \textit{clarification zone} \quad (-H_1 < z < 0) \\ v_s \phi - v_e \phi + v_u \phi & \textit{inlet zone} \quad (z = 0) \\ v_s \phi + v_u \phi & \textit{thickening zone} \quad (0 < z < H_2) \\ v_u \phi & \textit{underflow zone} \quad (z > H_2) \end{cases} \qquad (2.2)$$

where H_1 is the height of the clarification zone, the feed point is located as $z=0$, H_2 is the depth of the thickening zone, see Fig 2.2; $\delta(z)$ is the Dirac impulse; v_e is the effluent flow velocity, v_u is the downward flow velocity, v_f is the feed flow velocity, ϕ_f is the feed concentration. Compared with the batch settling governing equation (eq.(2.1)), the continuous settling PDE framework includes two bulk terms ($v_e \phi$ and $v_u \phi$) to capture the hydraulic transport process. After adding suitable initial and boundary conditions, solving eq. (2.2) is a problem with one equation and two unknowns. As in the batch settling modeling approach, the constitutive relation (Kynch's hindered settling velocity assumption) is again used to provide a unique solution. The validity of Kynch's concentration discontinuity theory in predicting sludge blanket level propagation in SST has also been demonstrated by solving eq.(2.2) with reliable analytical or numerical techniques (Bustos et al. 1990a, Diehl 1996, 2000, Bürger et al. 2003). Because of its success in hindered settling modeling, others (Fitch 1983, Font 1988) have added compression effect terms based on Kynch's theory. However, this kind of modification encountered several problems that are not easy to solve within Kynch's theory (Concha and Bürger 2003), which will be discussed in the compression effect modeling section.

2.3.1. Settling velocity determination

The determination of the appropriate settling velocity function is essential in the 1-D SST modeling process (Cho et al. 1993). Though the settling velocity is physically a function of the particle and fluid properties, including the particle shape, size distribution, fluid and floc density, fluid viscosity and the hydrodynamic resistance, most available settling velocity models are still empirical with the model parameters determined by experimental curve fitting techniques, such as the single batch settling curve fitting method (Cacossa and Vaccari 1994, Vanrolleghem et al. 1996).

The two mostly used settling functions are the power law function (eq.(2.3)) and exponential law function (eq.(2.4)):

$$v_s = k\phi^{-n} \tag{2.3}$$

$$v_s = k\exp(-n\phi) \tag{2.4}$$

The power function was first suggested by Yoshioka *et al.* (1957b). However, the accuracy of the power law model deteriorates in dilute sludge region (below $2 kgm^{-3}$ (Pitman 1980) or below $3 kgm^{-3}$ (Riddell et al. 1983)) and becomes infinite at zero concentration. This problem can be solved by two alternative approaches: artificially imposing a maximum velocity value or using another velocity function for the dilute concentration zone (De Clercq et al. 2008).

The exponential model is also known as the Vesilind model (Vesilind 1968b) that distinct from the power one in both the dilute and condensed zone prediction. It provides a reasonable maximum when the concentration approaches zero, and lower velocity in the high sludge

concentration range compared with the power law model predictions. Smollen and Ekama (1984) also showed that the exponential model gave a better fit with the experimental data than the power model. Although the exponential model has special advantages over the power model, it is still fully empirical and the parameter values depend upon the fitting experimental data.

From a practical standpoint, Takács *et al.* (1991) questioned the validity of the exponential model in the dilute zone believing that the dilute zone settling velocity be impacted by the flocculation process and non-settleable solids fraction. They modified the exponential model to eq.(2.5), now known as the Takács model, to account for these factors:

$$v_s = \max\left(0, \min\left(v_{0,max}, v_0\left(\exp^{-n_1(\phi-\phi_{min})} - \exp^{-n_2(\phi-\phi_{min})}\right)\right)\right) \tag{2.5}$$

The term $(v_0 exp^{(-n_1(\phi-\phi_{min}))})$ reflects the settling velocity of the large, well flocculated particles, while the term $(v_0 exp^{(-n_2(\phi-\phi_{min}))})$ is the velocity correction factor of the smaller slowly settling particles. ϕ_{min} indicates the non-settable solids fraction. The Takács and Vesilind models only differ in the dilute sludge region, which impacts the predicted effluent TSS concentration.

There have also been efforts to derive the settling velocity from fundamental analyses of mass and force acting in the two phase flow (Cho et al. 1993, Cacossa and Vaccari 1994, Kinnear 2002). Starting from the Carman-Kozeny equation which is accepted universally for porous media modeling, Cho *et al.* (1993) deduced the settling velocity function by adding the sludge viscosity term. Eq. (2.6) uses the viscosity as an exponential function, eq.(2.7) is valid when the sludge volume fraction is negligible of the total volumetric concentration (low sludge concentration) and eq.(2.8) is the situation where the viscosity term is constant.

$$v_s = k\left(1-n_1\phi\right)^4 \exp\left(-n_2\phi\right)/\phi \tag{2.6}$$

$$v_s = k\exp(-n\phi)/\phi \tag{2.7}$$

$$v_s = k\left(1-n\phi\right)^4/\phi \tag{2.8}$$

Comparison of data and models showed that this model can perform well without causing the infinite problem in dilute range, and also can be easily used within the limit flux theory (Cho et al. 1993).

To complement the velocity model for compression zone calculation, Cacossa and Vaccari (1994) originally developed the model in terms of the total suspended solids concentration, the dynamic pressure gradient and the gradient corresponding to the compressive yield stress as shown in eq. (2.9).

$$v_s = v_0\left(1-\left(\partial\phi/\partial z\right)/K\right) \tag{2.9}$$

where K is defined as the compressibility function, which describes the sludge compressive properties. As opposed to the Kynch assumption based models, the settling velocity in this model is defined as a function of the solids concentration, as well as gradient in solids concentration. The batch setting verification results showed that it may over predict the solid-liquid interface level in the compression region, and a more elaborate expression of the compressibility function (K) is required for more accurate prediction (Cacossa and Vaccari 1994). Kinnear (2002) followed this suggestion, and provided an improved velocity model by using more fundamental properties prameters, such as the solids volumetric concentration (ε), intrinsic permeability (k),

floc and liquid density (ρ_f and ρ_l), specific surface area of the primary particle (S_0), sludge viscosity (μ), gel concentration (ε_g) and effective compression stress (P_0). The model was developed from the mass and momentum continuity equations of two phase flow. The hydrodynamic interaction coefficient was related to the intrinsic permeability, which was calculated by the Carman-Kozeny equation. The effective solids stress was determined by Buscall and White's (1987) empirical function, thus making the final settling velocity formulation expressed as:

$$v_s = \frac{(\rho_f - \rho_l)g(1-\varepsilon)^3}{5S_0^2 \varepsilon \mu} \qquad for \ \varepsilon < \varepsilon_g \qquad\qquad (2.10)$$

$$v_s = \frac{\left[\varepsilon(\rho_l - \rho_f)g + P_0\left(\dfrac{\varepsilon}{\varepsilon_g}\right)^m \dfrac{\partial(1-\varepsilon)}{\partial z}\right](1-\varepsilon)^3}{5S_0^2 \varepsilon^2 \mu} \qquad for \ \varepsilon > \varepsilon_g \qquad\qquad (2.11)$$

In contrast to the empirical models, eq. (2.10) and (2.11) incorporate the basic physical factors that may determine the sludge settleability, and their derivation does not rely on Kynch's assumption. Again, the settling velocity is function of both the solids concentration and concentration gradient as in the Cacossa-Vaccari model.

Most velocity functions discussed so far, and especially the power and exponential models, are only appropriate for hindered/compression region modeling, and extending these functions into the flocculation region can produce unrealistic results (Kinnear 2002). Incorporating a more complex flocculation model, as in the Takács model, by introducing a term to reflect the settling velocity of large, well-flocculated particles, or simply setting a constant settling velocity that can be measured during pilot testing, which is the same strategy as used in the power model to limit the overprediciton of the settling velocity in the dilute region.

Table 2.1 - Overview and comments of gravity settling velocity functions.

Model Type	Model Formula	Source	Comments
Polynomial models	$v_s = k(1 + n_1\phi + n_2\phi^2 + n_3\phi^3 + n_4\phi^4)$	Shannon *et al.* (1963)	➢ empirical model; ➢ not often used in practical engineering application; ➢ provides unreliable approximation in low concentration range ➢ requires more parameters than other models;
	$v_s = k\phi(1-\phi)$	Scott (1966)	
	$v_s = \sqrt{n_1 \Big/ \left(n_2 + n_3\phi + n_4\phi^2 + n_5\phi^3\right)}$	Stenstrom (1976)	
Power models	$v_s = k\left(1-n\phi\right)^{4.65}$	Richardson and Zaki (1954)	➢ empirical model; ➢ often used in practical engineering application; ➢ overestimate settling velocity when concentration is small; ➢ singular when concentration approaches to 0;
	$v_s = k\phi^{-n}$	Yoshioka *et. al* (1957)	
	$v_s = k\left(1-n_1\phi\right)^{n_2} \Big/ \phi$	Scott (1966), Cho *et al.* (1993)	
	$v_s = k\left(1-n_1\phi\right)^{n_2}$; $v_s = k_1\left(1-n_1\phi\right)^{n_2} + k_2$	Vaerenbergh (1980)	
Exponential models	$v_s = k\left(1-n_1\phi\right)^2 \exp\left(-n_2\phi\right)$	Steinour (1944)	➢ empirical model; ➢ often used in practical engineering application; ➢ provide reasonable velocity estimation in all concentration domains; ➢ includes other effects, such as flocculation settling, non-settleable particle fraction;
	$v_s = k\left(1-n_1\phi\right)^2 \exp\left(-n_2\phi/(1-n_3\phi)\right)$	Vand (1948)	
	$v_s = k\exp(-n\phi)$	Vesilind (1968)	
	$v_s = \max\left(0, \min\left(v_{0,max}, v_0\left(\exp^{-n_1(\phi-\phi_{min})} - \exp^{-n_2(\phi-\phi_{min})}\right)\right)\right)$	Takács *et al.* (1991)	
	$v_s = k\exp\left(-n\phi\right)/\phi$; $v_s = k\left(1-n_1\phi\right)^{n_2}\exp\left(-n_3\phi\right)/\phi$	Cho *et al.* (1993)	
Compression effect including models	$v_s = v_m(1-(\partial\phi/\partial z)/K)$ $\begin{cases} v_m = (2-\phi/\phi_g)(n_1/(\phi_g - n_2)) & \text{if } \phi < \phi_g \\ v_m = (n_1/(\phi_g - n_2)) & \text{if } \phi \geq \phi_g \end{cases}$	Cacossa and Vaccari (1994)	➢ semi-empirical model derived from mass and momentum conservation law; ➢ often used in compression settling behavior studies; ➢ most parameters have physical meaning, and can be estimated by experiment measurements instead of curve fit;
	$v_s = v_{hs}(\varepsilon)$ if $\varepsilon < \varepsilon_g$; $v_s = v_{hs}(\varepsilon)\left(1 - \dfrac{\rho_s\sigma'_e(\varepsilon)}{\varepsilon_g\Delta\rho}\dfrac{\partial\varepsilon}{\partial z}\right)$ if $\varepsilon \geq \varepsilon_g$	Bürger *et al.* (2000)	
	$v_s = \dfrac{(\rho_l - \rho_s)g(1-\varepsilon)^3}{5S_0^2\varepsilon\mu}$ if $\varepsilon < \varepsilon_g$; $v_s = \dfrac{\left(\varepsilon(\rho_l - \rho_s)g + \sigma'_e(\varepsilon)\partial(1-\varepsilon)/\partial z\right)}{5S_0^2\varepsilon\mu}(1-\varepsilon)^3$ if $\varepsilon \geq \varepsilon_g$	Kinnear (2002)	

Table 2.1 summarizes the structure of various settling velocity functions, and their proper modeling domains. To estimate the performance of these velocity functions, we provided a typical function calibration example, based on the full-scale data collected by Grieves and Stenstrom (1976a) and Levenberg-Marquardt algorithm (More 1978b). Fig 2.3 shows the data fitting result. It is noticeable that almost all velocity models can fit the data in medium concentration range very well, but they deviate significantly in both dilute and high concentration conditions, which also has been demonstrated in previous studies.
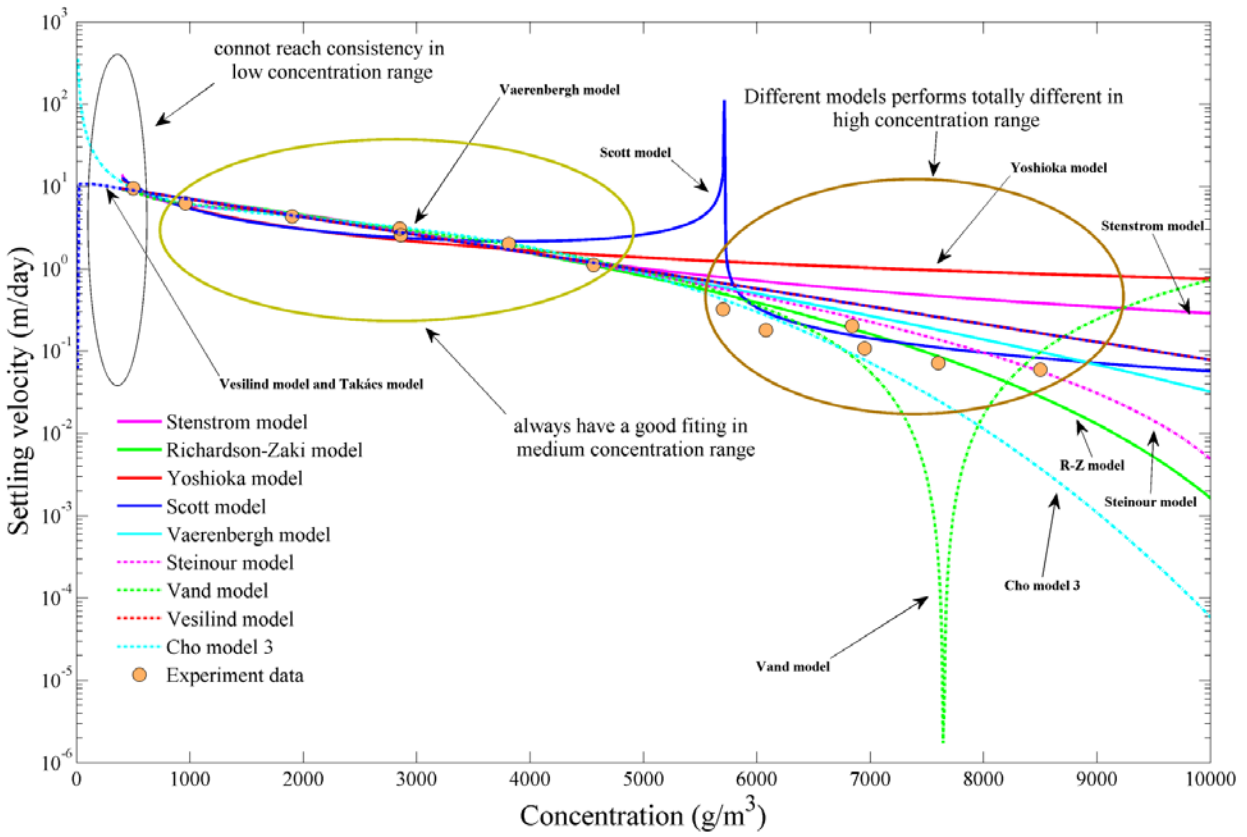
Fig.2.3 - The fit of various settling velocity functions to the experiment data.

2.3.2. The Stenstrom flux constraint analysis

The well-known flux constraint was originally suggested by Stenstrom (1976a) to limit the mass flux for solids overloading simulation. Based on the assumption that the settling mass flux into the lower layer can never exceed the flux the layer is capable to transmit, the flux constraint can be expressed as eq.(2.12).

$$F_{i+1/2}^{S} = \min\left(v_{s,i}\phi_i, v_{s,i+1}\phi_{i+1}\right) \tag{2.12}$$

where S is the Stenstrom numerical flux, i denotes the layer i. Although this flux limiting constraint is empirical, it is "consistent", which means the numerical flux should be a function related to adjacent layers instead of the local single layer (Bürger et al. 2011). By implementing this numerical flux constraint, Stenstrom's model was capable of capturing the sludge blanket change under various operating conditions, thus making the SST failure predictable. Bürger *et al.* (2011) showed that this constraint is indeed a specific numerical flux for unique solution calculation rather than a physically existing one, and noted it as the Stenstrom flux. However, this flux constraint is not nostrum, and will cause unphysical solution oscillations under several conditions such as in the negative concentration gradient case. A site specific threshold concentration was recommended to be set below which the constraint is inactive (Vitasovic 1986a, Takács et al. 1991). The best well-known work following the Stenstrom flux constraint is the Takács' 10-layer model (Takács et al. 1991), which has been mostly used in WWTP modeling.

Watts *et al*. (1996) tested the Takács model in various discretization levels (10, 20,50 layers) without changing the model parameters, and found that only 10-layer provided good agreement

with Pflanz's data (Pflanz 1969). Increasing the number of layer will considerably deteriorate the model performance, which is contradictory to the fundamental principle that the finer discretization should provide more accurate predictions. Further investigation of the Stenstrom flux constraint implied that the function of the flux constraint equals to a layer thickness dependent dispersion term, and its function disappears as the layer thickness approaches to zero, which explains the Takács model deterioration with the increasing discretization level (Watts et al. 1996). To correct this problem, Watts *et al.* (1996) added a dispersion term, hence improving its fit to the Pflanz in finer discretization condition.

Despite analyzing the Stenstrom flux constraint physically, the studies from the standpoint of numerical techniques demonstrated that the inclusion of the Stenstrom flux constraint is correct in the way of preventing the creation of shock wave and any inverse gradients in the concentration profile (Jeppsson and Diehl 1996, De Clercq 2006, Bürger et al. 2011, Bürger et al. 2012, Bürger et al. 2013). However, the model integrated with the Stenstrom flux constraint, such as the Takács model, can only fit the experiment data well in 10-layer condition, which is insufficient to resolve the detailed behavior of SSTs, and at least 30-layer is recommended for reliable predictions (Jeppsson and Diehl 1996). To uniquely determine the reliable solution, both the 'consistent' principle and entropy condition which analogous to the second law of thermodynamic should be fulfilled (Bürger et al. 2011). The Stenstrom flux constraint satisfies the 'consistent' principle, but not always takes the entropy condition into account, which in return results unphysical solutions (oscillation) (Bürger et al. 2011, Bürger et al. 2012, Bürger et al. 2013). Bürger *et al.* (2013) suggested the approach of upgrading the Stenstrom flux constraint to the reliable Godunov flux, since they have similar mathematical expressions. As a conclusion, although the application of the Stenstrom flux constraint in 1-D SST modeling has achieved

some degree of success, more fundamental numerical techniques are still encouraged to being introduced for entire reliable solution solving (for detailed information, see the numerical technique section).

2.3.3. The convection-dispersion model development

The success of the Kynch's theory in settling behavior analysis provided a firm foundation for the development of 1-D SST modeling studies. The mathematical discontinuities predicted by the Kynch theory, however, cannot exist in a practical system (Fitch 1993), which has been confirmed by various experiment cases with continuous concentration profiles (Pflanz 1969, Anderson 1981, Bergstrom et al. 1992, Kinnear 2002). A parabolic second-order PDE can provide a continuous or smooth concentration profile, and inclusion of a eddy turbulent diffusion term in the first-order hyperbolic PDE (eq.(2.2)) converts the governing PDE to a parabolic one (Anderson 1981, Vitasovic 1986a). This approach was implemented by Hamilton *et al.* (1992) and modified by Lee *et al.* (1999) with constant dispersion coefficients as eq. (2.13) shows, and this model is capable of providing non-uniform, monotonically increasing concentration profiles with depth as expected.

$$\frac{\partial \phi}{\partial t} + \frac{\partial F(\phi)}{\partial z} - D\frac{\partial^2 \phi}{\partial z^2} = v_f \phi_f \delta(z) \tag{2.13}$$

where *D* is the dispersion coefficient as a constant for the overall SST domain. Grijspeerdt *et al.* (1995) compared several established 1-D SST models and found Hamilton's and Takács's models are more reliable for fitting data because of their dispersion characteristics, even though the Takács model does not include a physical dispersion term. This can be explained by Watts' conclusion that in low discretization level, the function of the Stenstrom flux constraint equals to

28

a layer thickness dependent dispersion term (Watts et al. 1996). Takács (2008) further demonstrated that in "rough" discretization condition, such as 10-layer, imposing the Stenstrom flux constraint introduces significant numerical dispassion that effective in smooth concentration profile developing. Nevertheless, the drawback of this smooth profile finding approach is the lack of control over the dispersion effect to best model calibration of various operating conditions (Plósz et al. 2011). A finer discretization, when the layer thickness approaches to zero, can seriously deteriorate the Takács model performance, since the dispersion function vanishes; discretization of 10-layers for the Takács generally approximates the dispersion expected in an SST.

To correct this problem, a modification of the concentration dependent dispersion coefficient is necessary, and one approach is to incorporate a dispersion coefficient that is a function of the hydrodynamic dispersion phenomenon caused by the turbulent currents. Even though the dispersion term is analogous with the Fick's constitutive relation for particle diffusion, it represents the hydrodynamic dispersion phenomenon caused by the turbulence rather than the thermal diffusion process (Anderson 1981, Bürger et al. 2011). Watts *et al.* (1996) determined the dispersion coefficient as a function of the feed flow velocity which creates mixing in the inlet region, where most energy dissipation and turbulence occur. The dispersion term was also expected to approximate the processes that affect the sludge settling other than the bulk convection and gravity settling (De Clercq et al. 2003). De Clercq *et al.* (2003) proposed that since the flow conditions may differ in the clarification zone and the thickening zone, the dispersion term should not be only governed by the feed hydraulic flow, but both the upward and downward bulk flow:

$$D_1 = D_{11}e^{\alpha\frac{Q_e(t)}{Q_f(t)}} \quad \textit{Clarification Zone}$$

$$(2.14)$$

$$D_2 = D_{22}e^{\beta\frac{Q_u(t)}{Q_f(t)}} \quad \textit{Thickening Zone}$$

where D_{11}, D_{22}, α and β are dispersion parameters that need to be calibrated.

Plósz *et al.* (2007) investigated the factors that degrade 1-D SST model performance by incorporating the dispersion in terms for both the effluent solids concentration and the sludge blanket height, and found that though the dispersion model can account for the SST hydrodynamic flow effect on the thickening process, the clarification efficiency is limited by flow boundary conditions. The model was optimized to enhance clarification prediction by introducing a hydraulic dispersion term as a function of the upward flow velocity-dependent term. In most recent studies, the mixing currents were assumed to occur in certain locations, such as the SST inlet region, and the dispersion coefficient forms were highly dependent on location. For example, the dispersion term in the SST inlet region is a function of the hydraulic feed flow velocity (Bürger et al. 2011, Bürger et al. 2012, Bürger et al. 2013), and influenced by factors in other regions of the SST. The recent global parameter sensitivity analysis of the whole WWTP modeling shows that selecting of 1-D SST model, convection dominant (first-order) or convection-dispersion (second-order) models, not only impacts the SST behavior prediction, but also greatly influences the parameter selection and the calibration procedure of the WWTP models (Ramin et al. 2014b).

Table 2.2 summarizes of currently available hydraulic dispersion functions. Despite the convection and dispersion effect modeling, the mass conservation law SST model can also involve some other impact factors, for example the current density can be accounted for by

adjusting the inlet height according to the feed sludge concentration (Dupont and Dahl 1995), but the maximum of the inlet height should be restricted to 53% of the SST depth (Plósz et al. 2007). For short-circuit simulation, a short-circuit factor Ω was introduced, which is a dilution factor that can be found by a simple mass balance over the SST, when the flow and concentration of influent and return sludge flow are measured, as well as the concentration at the bottom of the SST (Dupont and Dahl 1995).

2.4. The mass and momentum conservation law model

As can be seen from the above discussion, the cornerstone of the mass continuity model is Kynch's assumption that the settling velocity of a particle depends only on the local solids concentration. Its validly, however, can only be proved in the zone settling region (Dixon 1977a), even Kynch himself admitted in his celebrated paper that "until the details of the forces on the particles can be specified, it is impossible to state when our hypothesis is valid, even for a dispersion of identical particles." (Kynch 1952). This uncertainty gives rise to some important controversies, such as the determination of SST capacity, and compression settling behavior modeling.

By taking into account of force action during thickening process, Dixon (1977a, b, 1978) showed that there is no flux limitation associated with the hindered zone because of the absence of necessary retarding forces, which contradicts the previous conclusion that the hindered settling zone determines the SST thickening capacity as the increase of the compression zone height can compact the sludge by squeezing water out of the sludge structure which then can accelerate the sludge conveyance in this zone (Coe and Clevenger 1916, Kynch 1952, Fitch 1962). For most real settling materials, in particular, these well flocculated slurries such as activated sludge, they

31

form compressible sediment layers which are characterized by curved iso-concentration lines rather than the straight characteristics predicted by the Kynch model (Bürger 2000, De Clercq et al. 2008). Therefore, the mass continuity model based on the Kynch assumption is not sufficient for various type sedimentation problems, and the investigation of the momentum conservation law model with a detailed force balance is necessary to provide a more complete understanding of continuous settling behavior, especially in the compression zone where the Kynch's assumption may not apply.

Generally, given the complexity of the two-phase flow problem, two points of view have been developed for problem analysis and governing equation deviation (Zuber 1964):

1). Internal flow approach: the flow of the fluidized system is considered as a flow through a porous medium with limited permeability, and solid-liquid relative movement could be modeled by Darcy's law through porous media (Shirato et al. 1970, Kos 1977, Cho et al. 1993, Fitch 1993, Diplas and Papanicolaou 1997, Holdich and Butt 1997, Zheng and Bagley 1998, Karl and Wells 1999).

2). External flow approach: the hydraulic flow is considered as the external flow around a particle located in the suspension. The well-known Stokes settling velocity is modified for hindered settling velocity calculation, and the compression process is characterized by semi-empirical equations stemmed from the rheology studies (Zuber 1964, Buscall and White 1987, Auzerais et al. 1988, Auzerais et al. 1990, Buscall 1990, Bürger 2000, Bürger et al. 2000a, Kinnear 2002, Usher and Scales 2005, De Clercq 2006, Usher et al. 2006, Grassia et al. 2011).

Table 2.2 - Overview and comments of different hydraulic dispersion functions.

Hydraulic Dispersion Function*			
Model Type	**Model Formula**	**Source**	**Comments**
Fickian dispersion term	$D_{(z,t)} = $ constant (13 m^2/day)	Hamilton *et al.* (1992)	➢ cannot properly characterize the dispersion effect caused by the hydraulic turbulence but not the molecular diffusion; ➢ greatly decrease the complexity of numerically difficulty in solving the governing PDE;
	$D_{(clarification\ zone,t)} = $ constant$_1$; $D_{(thickening\ zone,t)} = $ constant$_2$	Lee *et al.* (1999)	
Function of hydraulic bulk flow rate	$\begin{cases} D_{i,i+1} = D_{max} (1 + \beta (\sqrt{C_i C_{i+1}} - C_{crit}) \exp^{-\beta(\sqrt{C_i C_{i+1}} - C_{crit})}), & if \sqrt{C_i C_{i+1}} > C_{crit} \\ D_{i,i+1} = D_{max} & if \sqrt{C_i C_{i+1}} \leq C_{crit} \end{cases}$	Watts *et al.* (1996)	➢ empirical model; ➢ properly indicate the hydraulic dispersion effect caused by the hydraulic bulk flow; ➢ parameters determination depends on concentration profile fit; ➢ often imposed around the SST inlet zone to simulate energy dispassion;
	$D_{(clarification\ zone,t)} = D_{11} \exp^{\alpha Q_e / Q_f}$; $D_{(clarification\ zone,t)} = D_{22} \exp^{\beta Q_u / Q_f}$;	De Clercq *et al.* (2003)	
	$D_C = D_{C,0} \quad if\ v_{ov} < v_{ov,C}$; $D_C = D_{C,0} + \gamma (v_{ov} - v_{ov,C}) \quad if\ v_{ov} \geq v_{ov,C}$	Plósz *et al.* (2007)	

* Numerical dispersion or dissipation introduced by the numerical methods is discussed separately.

2.4.1. Force action analysis and model development

The fundamental basis of a momentum based model is the identification of the specific forces acting on the particles, but it is also the most difficult step. Benefiting from the last half century's developments in fluid dynamics and rheology analysis techniques, the detailed sedimentation information, such as the fundamental force analysis, particle interaction in different density ranges now is detectable, and provide new 1-D SST modeling approaches.

As discussed above, the batch settling process can be described as four various concentration zones within the a settling suspension: the clear supernatant zone, the hindered settling zone, the transient zone, as well as the compression zone (Coe and Clevenger 1916). The totally different settling behaviors within these zones necessitate the imposition of force action analysis separately rather than investigating them as a whole. The force acting analysis for the supernatant zone, compared with the other three, is much more straightforward. The gravity, the buoyancy, and the drag forces are the three dominant forces, and their calculation follows the classical approaches. A stochastic Brownian force also exists, but it is negligible due to the large Peclet number.

Before introducing the hindered settling analysis, it is useful to review the definition of hindered settling: when hindered settling occurs, the contacting particles tend to settle as a zone or "blanket", maintaining the same relative position with respect to each other (Metcalf&Eddy 2002). The two distinctive characterizations of hindered settling are the absence of direct particle-particle interaction and uniform concentration profile, such as the uniform initial concentration zone in batch settling. Since there is no direct particle-particle interaction and the settling particles remain relatively stationary to the neighboring ones, only the equilibrium

34

between drag and gravity forces limits settling velocity (Dixon 1977a). The increased concentration in the hindered settling region creates a hydrodynamic interaction between particles, and settling velocity no longer conforms to Stokes settling behavior as it did in the supernatant clear zone (Buscall and White 1987, Buscall 1990, Landman and White 1992, de Kretser et al. 2003). This hydrodynamic interaction mainly impacts the hydrodynamic drag coefficient, which can be multiplied by a hindered settling factor, $R(\phi)$, to quantify the inter-phase drag effect (for detailed information, see the drag coefficient determination section).

Few studies refer to the transient zone, since it is not always observable in batch or continuous settling tests (Coe and Clevenger 1916, Dixon 1977a). The existence of this region is usually viewed as a smooth transition between the zone and compression settling regions, and the settling behavior in this region is usually physically unstable: the settling plots frequently provide inconsistent results (Shirato et al. 1970). In most conditions, the transient zone is characterized by a gradually increasing concentration gradient, and is described by Fitch's concentration gradient study (Fitch 1993). As Fitch stated, a positive concentration gradient leads to a reduced settling velocity due to the dominant solids pressure gradient. Though Kynch's theory succeeds in predicting a concentration gradient, the settling velocity within a region of large concentration gradient is determined not as the hindered settling velocity, but a transition velocity, caused by retarding phenomenon associated with the concentration gradient. When the solids pressure gradient is positive, the suspension is mathematically "in compression", and four kinds of solids compression force can be physically identified: elastic, static, osmotic and dynamic (Fitch 1993):

Elastic compression force is caused by the random motion and collisions of particles (thermal diffusion), which can be modeling by adding a diffusion term ($D\delta\phi/\delta z$). However, even though existence of this force can be proven, its magnitude compared with the gravitational force and hydrodynamic drag force is much smaller, thereby making it insignificant in retarding the settling process.

Static compression force is also known as the compressive yield stress and arises when a continuous network is formed within strong inter-particle interactions (de Kretser et al. 2003). This stress can be transmitted directly throughout the network, and the settling process, if this stress occurs, will be irreversibly retarded (Buscall 1990). However, the static compression force only occurs above the gel point (the point where interparticle force results in a self supported network), while the transient zone concentration is expected at concentrations no greater than the gel point. Hence, the retarding phenomenon within the transient zone cannot be completely defined by static compression force theory.

Osmotic compression force occurs when the concentration spatially varies, such as a monotonically varying concentration, and the suspension is in a non-equilibrium state (Auzerais et al. 1988). The origin of this force can be illustrated as the force both particles and fluid molecules experience in proportion to the gradients of their respective chemical potentials (Batchelor 1976). The colloidal solids within the well-flocculated suspension, however, only constitute a relatively small fraction of the total weight, hence their contributed osmotic press could be indeed insufficient to retard the settling behavior (Fitch 1993).

Dynamic compression force is characterized as the force that causes the particle deceleration as it approaches the discontinuity or settles within a region having a concentration gradient, such as

the transient zone (Dixon 1977a, b, 1978, 1981). It originates from the excess local pressure required to squeeze fluid out interstitial floc areas to make them more concentrated (Fitch 1993). The mathematical formulation of this force still has not been well defined, and the difficulty of including it in the governing equation prevents the further investigation of its impact to the settling process. The formation of the transient settling zone is the result of one or more retarding forces, and further studies are still needed to indentify the mechanism of their contribution to the retardation process.

The study of compression effects is significant for applications as diverse as filtration and centrifugation of suspensions in the mineral industries, or sludge dewatering in wastewater treatment process to reduce the final disposed sludge volume (de Kretser et al. 2003). Dixon (1977a) stressed the importance of compression effect as having a critical role in sludge settling retardation which he associated with determining SST solids handling capacity. The existence of compression zones has been confirmed by many studies, and the terminology "compression settling " can be interpreted from different perspectives. For instance, Fitch (1993) stated that the suspension is in a mathematical compression condition when the pressure gradient term is positive. In more recent studies, from the view of " compressive rheology", the compression settling zone is defined as the zone with particle concentration over the gel point, and also characterized by the strong compressive yield stress transmitted in this zone (Buscall et al. 1987, Buscall and White 1987, Buscall 1990, de Kretser et al. 2003, Usher and Scales 2005, Usher et al. 2006).

The study of compression effects date back to the 1920s when Terzaghi (1925) originally developed the consolidation theory in the field of solid mechanics. This theory was then applied

by Behn (1957) for the settling of compressive slurries because of its mathematical analogy independent of magnitude of the stress gradients. The compression behavior of flocculated particles (Kaolinite) were firstly addressed by Michaels and Bolger (1962b), and the compression settling was assumed to be governed by gravitational force (gravity and buoyancy), hydrodynamic drag force and the stresses transmitted throughout the condensed network. Shirato *et al.* (1970) stated that the compression-permeability (C-P) cell method (Ruth 1946, Grace 1953, Tiller and Shirato 1964) widely used for internal flow analysis, can lead to substantial errors from wall effects in batch settling tests, and used zinc oxide and ferric oxide floc data to determine sediment compressibility and permeability. The numerical solutions of higher concentration conditions were solved, and showed a favorable agreement with experimental results (Shirato et al. 1970). For shock (concentration discontinuity) investigation purposes, Auzerais *et al.* (1988, 1990) started their work with a comprehensive analysis of all forces active in both liquid and solid phases, including the gravitational force, inertial force, viscous, and interparticle stresses.

Most of the investigators discussed above emphasized the critical role that compressive pressure plays in compression settling. The origin of this stress and how to quantify it to determine the sediment compressibility still remain unclear. In the view of compression rheology, for sedimentation at high concentrations, direct particle interaction allows energy to be stored elastically within the particle network. The accumulation of these solids close to the cylinder bottom causes a concentration gradient, and adding the compression stress arising from the accumulated, unbuoyed weight of the particles to the force balance, accounts for this phenomenon (Buscall and White 1987, Buscall 1990). For colloidally-stable suspension or a well-flocculated suspension below the gel point, this stress is only the osmotic pressure, while

for concentrations greater than the gel point, the stress is elastic, which is characterized as the physically measurable network strength: the compressive yield stress (Buscall et al. 1987, Buscall and White 1987, Buscall 1990, de Kretser et al. 2003).

Meanwhile, several parallel theories starting from geotechnical approaches (Terzaghi and Peck 1948, Bürger et al. 1999, Bürger et al. 2000a, Garrido et al. 2000, Bürger et al. 2001) and filtration research (Tiller and Shirato 1964, Tiller and Yeh 1987, Lee et al. 2000) also made important contributions to the understanding of compression settling behavior using the effective solids stress (σ) and the solids pressure (p_s) to quantify the sediment compressibility. However, compared with the compression rheology approach of defining the compressive yield stress as an intrinsic 'material property', both the effective solids stress and pressure, in most cases, are defined as volumetric concentration dependent functions, thereby making them numerically equivalent to the compressive yield stress. Except for the significant conceptual difference, these compressibility quantifying approaches have the a similar rheological basis, and the relationship between volumetric concentration and the compressive stress (the effective solids stress, the solids stress and compressive yield stress) need to be defined for parameter estimation (de Kretser et al. 2003).

As a conclusion, with a comprehensive force action analysis of various settling zones, the five forces (gravity, buoyancy, liquid pressure, hydrodynamic drag force, and compressive yield stress) acting on a floc-phase control volume in 1-D condition can be explicitly shown in Fig 2.4 with proper force directions. The gravity and buoyancy forces can be expressed as a net gravitational force and the hydrodynamic drag force originates from particle-liquid relative motivation. The osmotic pressure arises from the spatial concentration variation while the

compressive yield stress only exists above the gel point where a self-supported network is formed. Therefore, a typical batch settling process can be modeled using the following four governing equations: liquid and solid continuity equations [eq.(2.15) and eq.(2.16)], liquid and solid momentum continuity equation [eq.(2.17) and eq.(2.18)]:

Liquid continuity equation

$$\frac{\partial(1-\varepsilon)}{\partial t}+\frac{\partial\left((1-\varepsilon)v_l\right)}{\partial z}=0 \tag{2.15}$$

Solid continuity equation

$$\frac{\partial(\varepsilon)}{\partial t}+\frac{\partial\left(\varepsilon v_s\right)}{\partial z}=0 \tag{2.16}$$

Liquid momentum equation

$$(1-\varepsilon)\rho_l\frac{\partial v_l}{\partial z}+(1-\varepsilon)\rho_l v_l\frac{\partial v_l}{\partial z}=-\left(1-\varepsilon\right)\rho_l g-(1-\varepsilon)\gamma\left(v_l-v_s\right)-\left(1-\varepsilon\right)\frac{\partial p}{\partial z} \tag{2.17}$$

Solid momentum equation

$$
\begin{aligned}
\varepsilon\rho_s\frac{\partial v_s}{\partial z}+\varepsilon\rho_s v_s\frac{\partial v_s}{\partial z}&=-\varepsilon\rho_s g+(1-\varepsilon)\gamma\left(v_l-v_s\right)-\varepsilon\frac{\partial p}{\partial z} && \varepsilon<\varepsilon_g \\
\varepsilon\rho_s\frac{\partial v_s}{\partial z}+\varepsilon\rho_s v_s\frac{\partial v_s}{\partial z}&=-\varepsilon\rho_s g+(1-\varepsilon)\gamma\left(v_l-v_s\right)-\varepsilon\frac{\partial p}{\partial z}-\frac{\partial p_y}{\partial z} && \varepsilon>\varepsilon_g
\end{aligned} \tag{2.18}
$$

where ε is the solids volumetric friction; ρ_l and ρ_s are the liquid and solid density; v_l and v_s are the liquid and solid velocity; g is the gravity acceleration; γ is the hydrodynamic drag coefficient; p is the fluid static pressure; p_y is the compressive yield stress;
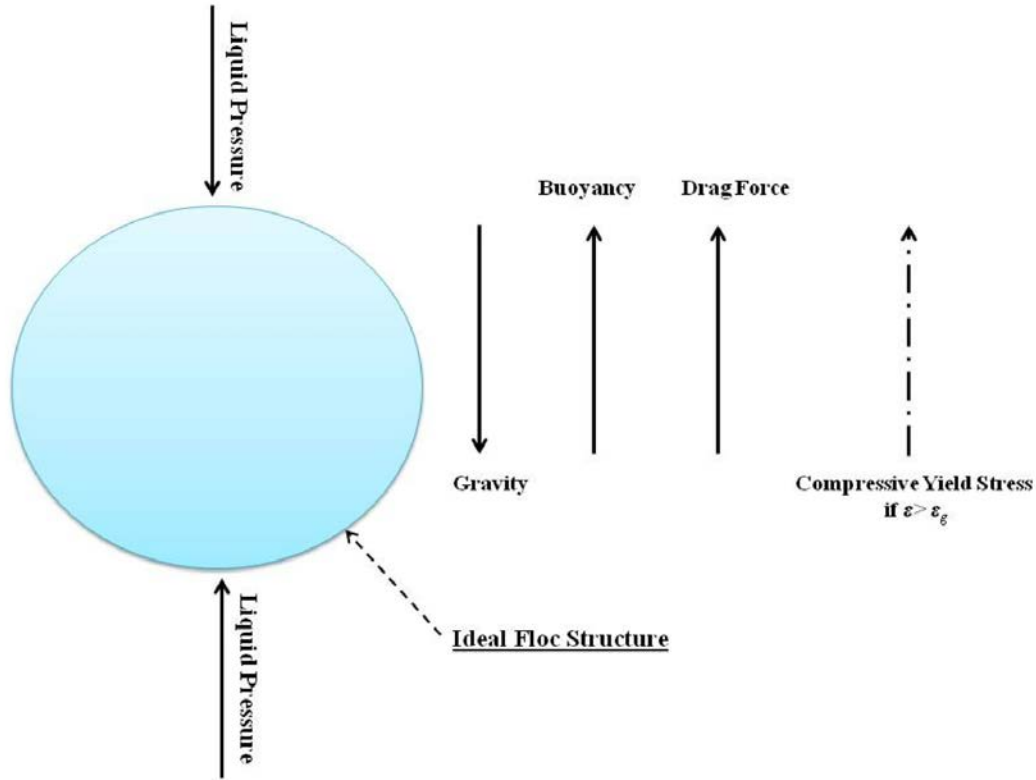
Fig.2.4 - Force acting analysis of ideal floc structure.

The inertial term is always thought to be negligible, since it is many orders of magnitude less than the other terms (Auzerais et al. 1988, Karl and Wells 1999, Bürger 2000, Kinnear 2002). Hence, the four governing equations can be simplified as the following equation:

$$\frac{\partial \varepsilon}{\partial t} + \frac{\partial}{\partial z}\left(\varepsilon\left(\left(\varepsilon(\varepsilon-1)(\rho_s - \rho_l)g + (\varepsilon-1)\frac{\partial p_y}{\partial z}\right)\Big/\gamma \right)\right) = 0 \qquad (2.19)$$

where $p_y = 0$ if $\varepsilon < \varepsilon_g$, and $p_y > 0$ if $\varepsilon > \varepsilon_g$. According to Dixon *et al.* (1976), the inertial term cannot always be ignored in sedimentation analysis due to its great significance in the interface between suspension and sedimentation where rapid velocity occurs. Fitch (1993) further stated that in the concentration gradient-occurring region, for example a transition settling region, various forces,

including the inertial force, together with the dynamic pressure, osmotic pressure, and static pressure will be present, and if their resultant is negative, the inertial model is applicable due to the velocity augmentation of the inertial force. Therefore, compared with the simplification model (eq.(2.19)), the original model (eq. (2.15), (2.16), (2.17), (2.18)) is more capable of describing an interface discontinuity, which is especially important for the sludge blanket level estimation in 1-D SST model. Obviously, additional proper constitutive functions are needed for the hydrodynamic drag coefficient and the compressive yield stress determination to make the model solvable.

2.4.2. Hydrodynamic drag coefficient estimation

Accurate calculation of the hydrodynamic drag force is especially important to describe hindered settling, since it is the only retarding force that can balance the positive gravitational force (Dixon 1977a). At sufficiently low Reynolds number, the hydrodynamic drag force is proportional to the liquid-solid relative velocity, and can be expressed as eq. (2.20):

$$F_d = \gamma \left(v_l - v_s \right) \tag{2.20}$$

Notice that v_l and v_s are the solutions of eq. (2.17) and eq.(2.18). Therefore, calculating the hydrodynamic drag force is equivalent to determining the hydrodynamic drag coefficient. Although various methods and constitutive functions have been developed for the drag coefficient estimation, most of them can be classified in three categories: the hindered settling factor approach (Richardson and Zaki 1954, Michaels and Bolger 1962b, a, Batchelo.Gk 1972, Batchelor 1976, Dixon et al. 1976, Buscall and White 1987, Auzerais et al. 1990, Buscall 1990, Landman and White 1992, Chen et al. 1996, de Kretser et al. 2003, Usher and Scales 2005,

Usher et al. 2006), the Darcy's Law approach (Steinour 1944, Javaheri and Dick 1969, Davies et al. 1976, Cho et al. 1993, Islam and Karamisheva 1998, Zheng and Bagley 1998, Karl and Wells 1999, Kinnear 2002) and the Kynch batch flux density approach (Bürger 2000, Bürger et al. 2000a, Bürger et al. 2005, De Clercq et al. 2008, Bürger et al. 2011).

At a finite dilution with unbounded fluid, the hydrodynamic drag coefficient is the Stokes drag coefficient (λ_{st}); for instance, 6π for spheres, and the particle motion is balanced by the hydrodynamic drag and gravitational force. With the increase of solids concentration in hindered settling region, the indirect interaction (hydrodynamic interaction) between particles leads to a deviation of the Stokes settling behavior (de Kretser et al. 2003). In the hindered settling factor approach, a volumetric friction-dependent hindered settling factor, $r(\varepsilon)$, is introduced to account for this deviation, and the hydrodynamic drag as follows:

$$F_d = \frac{\lambda_{st}\varepsilon r(\varepsilon)}{V_p(1-\varepsilon)}(v_s - v_l)$$
(2.21)

where η_s is the liquid viscosity, V_p is the particle volume. In the infinite dilution condition, $r(\varepsilon)$ approaches to zero to reflect the fact that the single particle sedimentation is unaffected by the neighboring particles. The maximum close packed concentration limits ε to less than 1, preventing $r(\varepsilon)$ from becoming infinite (de Kretser et al. 2003). Batchelor (1972) defined $r(\varepsilon)$ as a linear function of ε, while Buscall *et al.* (1982) showed that $r(\varepsilon)$ increases exponentially as the volumetric friction increases, and established the empirical relation based on experimental data curve fitting:

$$r(\varepsilon) = (1-\varepsilon)^{-4.5}$$
(2.22)

Given the fact that the most real systems are poly-disperse, and $r(\varepsilon)$ is invariably linked to the quantity λ_{st}/V_p , it is more convenient to measure $\lambda_{st}\, r(\varepsilon)\, /V_p$ as a whole, which is defined as the hindered settling function $R(\varepsilon)$ (de Kretser et al. 2001, Usher et al. 2001, de Kretser et al. 2003). The general formula of $R(\varepsilon)$ is shown as follows:

$$R(\varepsilon) = w(1-\varepsilon)^m \tag{2.23}$$

$$R(\varepsilon) = r_a \left(\varepsilon - r_g \right)^{r_n} + r_b \tag{2.24}$$

where w, m, r_a, r_b, r_n and r_b are empirical fitting parameters. Although $R(\varepsilon)$ is termed as the hindered settling function, it spans the entire concentration region, including the compression settling zone, to quantify the hydrodynamic drag associated with various settling behaviors. The experimental methods of characterizing $R(\varepsilon)$ specifically depend on the solids concentration: in the low to intermediate concentration range, a batch sedimentation test is the only available approach, while centrifugation and filtration techniques can be used over gel point to account for the compression effect (de Kretser et al. 2003).

If the internal flow approach is applied, the flow is regarded as a flow through a porous medium with limited permeability, and the upward water experiences more and more resistance with an increase of the solids concentration. The friction force experienced by a particle equals to that experienced by water, which can be determined by the Darcy's law:

$$F_d = K(\varepsilon)(v_s - v_l) \tag{2.25}$$

where $K(\varepsilon)$ is reciprocal of the hydraulic conductivity as a numerical equivalent of the hydrodynamic drag coefficient. It is a function of volumetric friction, and independent of the

flow velocity (Zheng and Bagley 1998). Zheng and Bagley (1998, 1999) defined an empirical function for $K(\varepsilon)$ based on the Vesilind equation as follows:

$$K(\varepsilon) = \frac{g(\rho_s - \rho_f)\varepsilon \exp(n_1\varepsilon)}{\rho_s k_1} \tag{2.26}$$

where n_1 and k_1 are Vesilind equation parameters, which can be determined by experiment data curve fitting approach. Another approach is to associate $K(\varepsilon)$ with certain physically meaningful variables for more theoretical formula derivation (Karl and Wells 1999, Kinnear 2002):

$$K(\varepsilon) = \frac{\mu\varepsilon}{k} \tag{2.27}$$

where μ and k are the liquid viscosity and intrinsic permeability, respectively. The intrinsic permeability, k, can be determined by either an empirical approach (eq. (2.28)) (Dixon et al. 1976, Karl and Wells 1999) or a theoretical formula (eq.(2.29)) known as the Carman-Kozenny equation (Lee et al. 1996, Kinnear 2002):

$$k(\varepsilon) = \alpha \exp(\beta\varepsilon) \tag{2.28}$$

$$k(\varepsilon) = \frac{\varepsilon^3}{5S_0^2(1-\varepsilon)^2} \tag{2.29}$$

where α and β are model parameters, S_0 is the specific surface area of the primary particle. Landman *et al.* (1988) demonstrated that the hindered settling factor approach and the Darcy's law approach only differ in the representation of the drag coefficient, but have a similar, even identical rheological basis.

The Kynch batch flux density (f_{bk}) refers to the flux density (εv_s) used in the mass continuity calculation based on Kynch's theory. The relationship between the Kynch batch flux density and the resistance coefficient ($\alpha(\varepsilon)$) is defined by Bürger *et al.* (2000a) as eq.(2.30):

$$f_{bk} = \frac{(\rho_s - \rho_l) g \varepsilon^2 (1-\varepsilon)^2}{\alpha(\varepsilon)} \qquad (2.30)$$

de Kretser *et al.* (2003) showed that the Kynch batch flux density and the hindered settling factor approaches are identical, differing only in nomenclature; f_{bk} can be related to the hindered settling function, $R(\varepsilon)$, by follows:

$$f_{bk} = \frac{(\rho_s - \rho_l) g \varepsilon (1-\varepsilon)^2}{R(\varepsilon)} \qquad (2.31)$$

Therefore, similar experiment techniques including transient batch sedimentation test, centrifugal and filtration techniques can also be used for f_{bk} and $R(\varepsilon)$ determination. In conclusion, because of the similar rheological basis, the hindered settling factor approach, the Darcy's law approach and the Kynch batch flux density approach have are equally useful in determining the hydrodynamic drag coefficient, and the choice of approach strongly depends on experiment techniques and the available data sets.

2.4.3. Compressive yield stress calculation

When the suspension concentration exceeds the gel point where the self-supported network is formed to resist gravity and compression , the compressive yield stress arises from the unbouyed weight of the overlying particles, and is transmitted throughout the sediment to prevent the irreversible net framework collapse. Since the compressive yield stress only occurs over the gel

point, proper methods are required to determine the gel point value before the compressive yield stress calculation.

As intrinsic properties, both the gel point and compressive yield stress depend implicitly upon the particle size, shape, the strength of aggregation, and the number, strength, arrangement of inter-particle bonds (Buscall 1990, de Kretser et al. 2003). However, direct determination of the gel point still remains a problem because of its difficulty of measurement. For example, when the solids concentration at the top of the sludge blanket is at the gel point, the compressive yield forces present would raise the average bed solids above the gel point (Tien 2002, de Kretser et al. 2003). Instead of considering the gel point as intrinsic property, Channell and Zukoski (1997) used the following constitutive function to define the gel point as a model parameter by the compressive yield stress curve fitting:

$$p_y = k \left(\left(\frac{\varepsilon}{\varepsilon_g} \right)^n - 1 \right) \tag{2.32}$$

where k and n are parameters. This fitting approach should be applied with caution due to broad fit over a range of the gel point values (de Kretser et al. 2003). Since the gel point value could be a time-dependent value (Diplas and Papanicolaou 1997, Kinnear 2002, De Clercq 2006, De Clercq et al. 2008), De Clercq *et al.* (2008) determined the gel point as the concentration where the concentration gradient becomes less than 200g/l/m, a site specific value, within the sludge blanket rather than a certain gel point value. Other more theoretical methods based on the sediment equilibrium force balance are also available (Tiller and Khatib 1984, Green 1997), the estimated gel point, however, is still lower and more detailed study utilizing both shear and compressive techniques is required (de Kretser et al. 2003).

In most previous studies, the compressive yield stress is always expressed empirically as a function of solids concentration or solids volumetric concentration by using polynomial, power or exponential laws (Buscall and White 1987, Auzerais et al. 1988, Auzerais et al. 1990, Buscall 1990, Font 1991, Bergstrom 1992, Holdich and Butt 1997, Karl and Wells 1999, Bürger 2000, Gustavsson and Oppelstrup 2000, Kinnear 2002). However, Zheng and Bagley (1998, 1999) suggested that the compressive yield stress is a function of both the solids concentration and the concentration change rate as eq. (2.33) shows, which is in accordance with Dixon's hypothesis (Dixon 1978).

$$p_y = k \frac{d\varepsilon}{dt} \frac{1}{\varepsilon} \tag{2.33}$$

where k is the model parameter. Hence, their compressive yield stress model greatly differs from the traditional concentration dependent models in the constant concentration region, such as the zone settling region. Because of the absence of a concentration gradient, Zheng and Bagley's model predicts zero compressive yield stress in constant concentration zones without making any additional assumption, as other models require. De Clercq *et al.* (2008) stated that the most frequently used power or exponential model cannot accurately describe the calculated compressive yield stress, especially for batch settling tests at high initial concentration. This deviation is attributed to the increasing gradient that exists at higher concentration, which do not conform to experiment observations. A logarithmic function with two parameters, α and β, is presented to overcome this shortcoming:

$$p_y = \alpha \ln\left(\frac{\varepsilon - \varepsilon_g + \beta}{\beta}\right) \tag{2.34}$$

Table 2.3 summarizes the mostly used compressive yield stress functions. Polynomial, exponential and power models are almost equivalent in compressive yield stress calculation, while the logarithmic model is developed to capture the logarithmic behavior of the stress that cannot be modeled by the other three.

Table 2.3 - Overview and comments of different compressive yield stress function.

Compressive Yield Stress (effective stress)			
Model Type	Model Formula	Source	Comments
Polynomial model	$\phi = a + b\sigma_e + c\sigma_e^2 + d\sigma_e^3$	Font (1991)	➢ empirical model; ➢ these models only differ in model formula, but almost identical in compressive yield stress approximation; ➢ some introduce the gel concentration or the maximum package concentration as model parameters; ➢ provide a increasing stress gradient for higher concentration range;
Exponential model	$\sigma_e = a \exp^{(b\phi)}$	Karl and Wells (1999)	
Power model	$\sigma_e = a\left(\left(\phi/\phi_g\right) - 1\right)^b$; $\sigma_e = a\left(\left(\phi/\phi_g\right)^b - 1\right)$	Landman et al. (1988)	
	$\sigma_e = a\phi^b/\left(\phi_{max} - \phi\right)$	Bergstrom (1992)	
	$\sigma_e = \left(\phi/a\right)^b$	Holdich and Butt (1997)	
Logarithmic model	$\sigma_e = \alpha \ln\left(\left(\phi - \phi_g + \beta\right)/\beta\right)$	De Clercq et al. (2008)	➢ empirical model; ➢ developed to capture the logarithmic behavior of σ_e which cannot modeled by the exponential or power models;

2.5. Numerical technique discussion

For typical batch sedimentation modeling without considering the dispersion and compression effects, the model governing equation can be expressed as eq. (2.1) as a combination of Kynch's assumption and the mass conservation law, that can be written as follows:

$$\frac{\partial \phi}{\partial t} + \frac{\partial \left(f_{bk}\left(\phi \right) \right)}{\partial z} = 0 \tag{2.35}$$

The numerical challenge of solving this equation is the non-linear hyperbolic property. The dispersion and compression effects can be added, without increasing the complexity of solution, but have limited value unless the hyperbolic problem is first solved (Bürger et al. 2011). Therefore, eq.(2.35) is generally used as the primary objective function in most numerical analysis studies (Kynch 1952, Petty 1975, Bustos 1988, Bustos et al. 1990a, Bustos et al. 1990b, Bustos and Concha 1992, Diehl 1996, 2000, Bürger et al. 2003, Bürger et al. 2010, Bürger et al. 2012). As a first-order nonlinear hyperbolic PDE, the solution to eq.(2.35) is constant along the characteristic lines which are given by:

$$\frac{dz}{dt} = f_{bk}'\left(\phi \right) \tag{2.36}$$

Obviously, the characteristics are straight lines, which means a constant concentration ϕ_0 propagates with the speed f_{bk}' (ϕ_0) in a z-t coordinate plane. Two characteristics with different concentrations may intersect during the propagation and then a shock (solution discontinuity) occurs (Diehl 2000). Kynch (1952) developed the first characteristics (iso-concentration line) analysis approach for batch sedimentation, and succeeded in capturing the shock (the interface of sediment and supernatant). Because of its great success in the sludge blanket level prediction,

this characteristics analysis approach was further developed to build the framework of the well-known flux theory for SST design and operation investigations (Keinath et al. 1977, Keinath 1985, Chancelier et al. 1997, Diehl 2008). Petty (1975) extended Kynch's procedure to the continuous sedimentation, and provided an explicit shock analysis for the transient state, while Bustos et al. (1990a) constructed the global weak solutions based on the method of characteristics for various initial data and operating conditions. Diehl (2000) applied characteristic analysis to SST analysis with a further consideration of the impact of the converging cross-sectional area and various boundary conditions at top, bottom and inlet. As a conclusion, the method of characteristics or the characteristics analysis is currently the only available approach to obtain exact solutions of the nonlinear hyperbolic governing PDEs, however, it requires considerably more effort of its implementation in engineering practice, and further investigations are needed.

Because of the existence of solution discontinuities, eq.(2.35) does not have closed-form solutions, and reliable numerical techniques are encouraged to produce approximate solutions that converges to the exact one as the grid mesh is refined (Bürger et al. 2011). To obtain both numerically and physically acceptable solutions, eq.(2.35) cannot be straightforwardly discretized, and numerical schemes specially designed to solve the scalar conservation law equation are needed to satisfy three fundamental principles: the Courant-Friedrichs-Lewy condition (CFL condition) to ensure stability, the "consistent" numerical flux, a function of the concentration in neighboring layers, and the entropy condition to reject unphysical discontinuities. Great effort has been made to obtain a suitable numerical technique, and the earliest, but the most used one in environmental engineering field is the Stenstrom numerical flux, as shown in eq.(2.12), which originated as a method for predicting solids overloading.

Nevertheless, it may invalidate the entropy condition, and produces unphysical solutions which is demonstrated by Bürger *et al.* (2011) and Li and Stenstrom. Bürger *et al.* (2012) further showed that the Stenstrom flux is only sufficient for standard batch sedimentation and normal operation SST modeling, where the concentration is increasing as a function of the depth. The well-known Godunov numerical flux (F^G) was first introduced for SST simulation by Jeppsson and Diehl (1996), and also used by Plósz *et al.* (2007). The Godunov numerical flux in clarification zone can be shown as eq.(2.37):

$$F^G_{i+\frac{1}{2}} = \begin{cases} \min_{\phi_i \leq \phi \leq \phi_{i+1}} \left(v_s \phi - \dfrac{Q_e}{A} \phi \right) & \text{if } \phi_i \leq \phi_{i+1} \\[4mm] \max_{\phi_{i+1} \leq \phi \leq \phi_i} \left(v_s \phi - \dfrac{Q_e}{A} \phi \right) & \text{if } \phi_i > \phi_{i+1} \end{cases}$$

(2.37)

It is noticeable that the F^G differs from F^S in the flux calculation by including the bulk transport, and the concentration inverse situation where the concentration is decreasing as a function of the depth. Based on the Godunov numerical flux, Bürger *et al.* (2010) derived Method G, which is first-order correct. Another alternative method called Method EO, based on the Engquist-Osher numerical flux (Engquist and Osher 1981) was developed by Bürger *et al*. (2005) and further refined by De Clercq *et al.* (2008).

Though both Method G and Method EO are reliable for SST modeling, and yield similar or identical solutions in many cases, their selection as a PDE solver is subjected to several competing principles: the complexity of implementation, the solution accuracy, and the computation cost which is indicated by the CPU time. The comparison study (Bürger et al. 2012) showed that the Method EO is too complicated for a straightforward application as the PDE solver in practical engineering cases, and for a given discretization level, the Method G is

capable of producing acceptable and faster solutions than Method EO. However, Method EO reduces numerical error more efficiently than the Method G, which may favor Method EO for calculating of high accuracy numerical solutions.

For the convection-dispersion model (eq.(2.13)), including the dispersion term transforms the original nonlinear hyperbolic PDE to a parabolic PDE, which is significantly easier to solve numerically. David *et al.* (2009a, 2009b) proposed the Method of Lines (MOL) strategy for this problem, based on the use of finite difference methods and time integrators. Generally, MOL proceeds in two steps (David et al. 2009a):

1. approximating the spatial derivatives by using finite-difference or spectral methods;
2. the resulting system of semi-discrete (discrete in space but continuous in time) equations are integrated in time;

The efficiency and flexibility of MOL's implementation in practical analysis and control have been demonstrated by various numerical simulation tests of the convection-dispersion model.

When the compression effect term is imposed, the phenomenological analysis of the various settling materials yields a degenerate parabolic PDE model (eq.(2.19)), which means the governing PDE is nonlinear hyperbolic if $\phi < \phi_g$, but nonlinear parabolic if $\phi > \phi_g$. Because of its mixed nonlinear hyperbolic-parabolic nature, the solution of the convection-compression model can also be discontinuous, hence making it difficultly to be discretized straightforwardly as in the convection-dispersion model case (Bürger et al. 2000b, Berres et al. 2003, Bürger et al. 2006). The developed Method G, Method EO and Method YRD can be used for the nonlinear convection term discretization, while for the nonlinear compression term discretization, if the

primitive con not be expressed in closed form, it can be approximated by numerical integration (Bürger et al. 2013).

If the inertial effect is further considered, the complete model format is a mixed hyperbolic-parabolic equation system (eq.(2.15, 2.16, 2.17, 2.18)). In Karl and Wells' approach (Karl and Wells 1999), eq.(2.16) was first solved to determine ϕ at the new time level $(n+1)$, and then, eq.(2.18) was solved for v_s at the new time level $(n+1)$ based on the solution of eq.(2.16). An explicit upwind scheme was introduced to discrete eq.(2.16) shown as follows:

$$\frac{\phi_i^{n+1} - \phi_i^n}{\Delta t} = \frac{\left(\phi v_s\right)_{i+1/2}^n - \left(\phi v_s\right)_{i-1/2}^n}{\Delta z} \tag{2.38}$$

where n is the time index. Because this technique is unconditionally unstable for convection-dominate systems, Karl and Wells (1999) also added an artificial numerical diffusion term to smooth the shock during the calculation. The momentum equation (eq.(2.18)) can be solved either implicitly or explicitly, as well as being discretized with either a central difference or upwind scheme. The numerical simulation tests showed that the fully explicit formula of the momentum equation needed a very small time step (Δt), which greatly increases computation cost, while the implicit method allows for larger time steps (Karl and Wells 1999). The selection of the upwind or central difference methods does not seriously impact the final simulation solutions.

Table 2.4 summarizes most alternative techniques that can be used for accurate analytical or numerical solutions solving. Until now, none of these strategies can completely satisfy the requirement of high solution accuracy and low computation cost, and more studies are needed in

the future to develop solution calculation technique, which is not only efficient in accurate solution calculation, but also easy for implementation in practical application.

Table 2.4 - Overview and comments of different numerical techniques used in solving the model governing PDEs.

Numerical Technique				
Model Type	Formula Type	Numerical Method	Source	Comments
Convection model	Nonlinear hyperbolic PDE	Method of characteristics	Petty (1975)	➤ Method of characteristics is the only available approach for analytical solution calculation, but it is difficult for implementation; ➤ Stenstrom flux constraint is easy for implementation, but can be problematic in several situations, such as the negative concentration gradient condition; ➤ Method G and EO converge to the physically relevant solutions, but only own first-order accuracy in both discontinuity and smooth regions; ➤ Method YRD converges to the physically relevant solutions, and owns second-order accuracy in both discontinuity and smooth regions;
		Stenstrom flux constraint	Stenstrom (1976)	
		Godunov scheme (Method G)	Jeppsson and Diehl (1996)	
		Engquist-Osher scheme (Method EO)	Bürger et al. (2005)	
		Yee-Roe-Davis scheme (Method YRD)	Li and Stenstrom (2014)	
Convection-Dispersion model	Linear parabolic PDE	Central-differencing scheme	Hamilton et al. (1992)	➤ compared with the nonlinear hyperbolic PDE, adding the hydraulic dispersion term greatly reduces the complexity of the numerical solution calculation; ➤ Both central-differencing scheme and Method of lines are easy for implementation;
		Method of lines	David et al. (2009a)	
	Nonlinear parabolic PDE	Upwind scheme	Watts et al. (1996)	
Convection-compression model	Degenerate hyperbolic-parabolic PDE	Numerical techniques used for convection model solving is applicable for the convection term discretization; the conservative scheme is used for the compression term discretization;	Bürger et al. (2000) Berres et al. (2003) Bürger et al. (2006)	➤ the model formula type is nonlinear hyperbolic if $\phi < \phi_g$, nonlinear parabolic if $\phi > \phi_g$; ➤ the numerical techniques used for convection model are suitable for the convection term discretization, while the nonlinear compression term requires special conservative schemes; ➤ for the compression term discretization, if the primitive cannot be expressed in closed form, it can be approximated by numerical integration;
		Operator splitting methods	Bürger et al. (2000)	
Convection-dispersion-compression model	Mixed hyperbolic-parabolic PDE	Numerical techniques used for convection model solving is applicable for the convection term discretization; the conservative scheme is used for the compression term discretization; central differencing scheme is used for the hydrodynamic dispersion term discretization;	Bürger et al. (2011) Bürger et al. (2012) Bürger et al. (2013)	➤ the model formula type is nonlinear hyperbolic if $\phi < \phi_g$, nonlinear parabolic if $\phi > \phi_g$; ➤ solving this type of model requires the combination of the various numerical techniques used in the models discussed above;

2.6. Calibration of 1-D SST models

Given the variety of simulation conditions, such as the sludge settleability and compressibility, 1-D settling models are not considered to be universal for all SST systems, and model parameter adjustment based on experiment data, usually referred as model calibration, is usually required for specific SST simulations. The calibration methodology of the hindered-only settling models are well developed, and can be classified into two categories: 1) the conventional approach using hindered settling velocities obtained from multiple batch settling tests; 2) the direct parameter estimation approach by fitting a single batch settling curve (Vanderhasselt and Vanrolleghem 2000). It is noticeable that the hindered-compression settling models cannot be calibrated straightforwardly following these two approaches because of the inclusion of the additional compression parameters. Several proposed calibration methods require the use of advanced techniques, such as radiotracing, to measure the dynamic concentration distribution during batch settling experiments (Kinnear 2002, De Clercq et al. 2005, De Clercq et al. 2008), which is beyond the accessibility of most practical application cases (Ramin et al. 2014d). Therefore, to promote the application of the hindered-compression settling model, great efforts are needed to facilitate its calibration. For example Ramin et al. (2014a, 2014c, 2014d) identified the potential parameter subsets suitable for the calibration of WWTP models under various simulation conditions, and further reported that calibrating the hindered-compression model based on the additional measurement of the batch bottom concentration, beside the batch settling curves, has achieved some degree of success.

The limited observational data of practical batch experiments naturally gives rise to the problem of the poorly identifiable parameters, which means it is difficult to identify a unique set of all

parameters used in the hindered-compression models due to possible parameter correlation (Brun et al. 2002, Brockmann et al. 2008). To avoid this problem, it is important to understand the practical identifiability of the model and select a suitable subset of parameters which can be reliably identified by the available experiment measurements (Weijers and Vanrolleghem 1997, Brun et al. 2001, Ruano et al. 2007).

In the wastewater treatment process modeling field, two alternative approaches have been most used to analysis the parameter identifiability problem. The first method is on the basis of scalar functions calculated from the Fisher Information Matrix (FIM), and the D and mod-E criteria can be used to select the best identifiable parameter subset (Weijers and Vanrolleghem 1997). The second method developed by Brun et al. (2001) uses a diagnostic regression and focuses on the analysis of parameter interdependency by calculating the collinearity index. Both methods are proven to be efficient in selecting the best identifiable parameter subset from limited experiment measurements (Weijers and Vanrolleghem 1997, Brun et al. 2001, Ruano et al. 2007, Brockmann et al. 2008). Recently, the Generalized Likelihood Uncertainty Estimation (GLUE) method has also been demonstrated as a reliable alternative for the identifiability analysis of the hindered-compression settling model by Torfs et al. (2013).

Nevertheless, despite the efficiency of the two most used approaches in addressing parameter identifiability problem, they still have drawbacks which may greatly impact the analysis results, at least in the hindered-compression settling model study. Both approaches are based on the calculation of local sensitivity functions for a set of reasonable parameters values within the parameter space, and in most activated sludge model (ASM) identifiability studies, the initial parameter set is determined as default values reported in literature. For example the practical

identifiability analysis of ASM2d by Brun et al. (2002) used the default values presented by Henze et al. (1999) as the starting point values. Given the fact that very limited parameter values have been reported in hindered-compression settling model studies, especially those related to the compression rheology, the initial parameter set values cannot be determined by the default value strategy, which implies that the choice of the initial parameter values may significantly impact the parameter identifiability. Beyond that, fixing some parameters, such as the non-influential parameters determined by the local sensitivity analysis, at prior values according to lecture and practical experience can introduce bias to the parameter estimates, which have been reported in pervious investigations (Weijers and Vanrolleghem 1997, Brun et al. 2001, Omlin et al. 2001, Brun et al. 2002).

From a practical point of view, the uncertainty analysis of wastewater treatment plant models is particularly important for design and operation decision making, and one of main uncertainty sources is the model input uncertainty, such as characterizing the model parameter values over a reliable range to reflect the limited knowledge of their exact values (Sin et al. 2009). To facilitate the practical application of the hindered-compression settling models by providing a guidance for experiment design, it is important to know which parameters can be obtained under what experimental conditions, and how large the model prediction uncertainties can be. This knowledge can be very beneficial in understanding the uncertainties of SST performance, such as the sludge blanket height (SBH), the recycle solids concentration under wet-weather and sludge settleability deterioration conditions.

3. Dynamic 1-D modeling of SSTs and system robustness evaluation

3.1. Introduction

Activated sludge is the most prevalent secondary treatment process and commonly uses secondary settling tanks (SSTs) to achieve efficient solid-liquid separation. The major functions of SSTs can be described as two similar but distinct actions: clarification and thickening. Clarification is the removal of suspended particles from effluent, and occurs in the clarification zone (above the inlet), and thickening is the process of increasing the underflow sludge concentration in the thickening zone (below the inlet). Free settling is always observed in clarification process, while hindered and compression settling dominate the thickening process to produce a more concentrated underflow. Therefore, the settling behavior in the clarification and thickening zones is totally different.

Traditional design and control procedures for SSTs tend to be more empirical and conservative regardless of changes in wastewater characteristics such as flow rate and contaminant concentration. For SST design and operation optimization purposes, mathematical models have been used in engineering practice; for example the one-dimensional (1-D) models are used to evaluate the sludge blanket level (Li and Stenstrom 2014a), the two-dimensional (2-D) and three-dimensional (3-D) models are used for the SST geometry design, such as the inlet structure (Zhou and Mccorquodale 1992b, Mazzolani et al. 1998).

Although different SST models are available, one-dimensional (1-D) SST models are most often used for their relative simplicity and low computation cost. Based on solids flux theory (Kynch, 1952), 1-D SST models describe sludge transport within the SST by the scalar conservation

partial differential equation (PDE) with a discontinuous flux, and are able to predict both the effluent and recycling solids concentration as well as the sludge blanket level. However, presently available 1-D sedimentation models are highly dependent upon empirical functions to express clarification, thickening and compaction processes and these functions can be an error source that profoundly affects simulation results. A second challenge is lack of reliable numerical methods to provide a high accuracy solution at low computational cost. Further research is still needed to improve the performance of 1-D models.

Nomenclature		t	time [h]
A	cross-sectional area of SST [m^2]	z	height above SST bottom [m]
C	sludge concentration [g/m^3]	*Greek letters*	
C_{min}	non-settleable solids concentration [g/m^3]	Δt	the time step [h]
F	(convection) flux function [g/(m^{2}h)]	Δz	the time step [h]
h	SST inlet depth [m]	Φ	the flux limiter
H	SST depth [m]	θ	the averaging factor
N	number of layers	δ	the YRD method parameter
Q	flow rate [m^3/h]	*Subscripts*	
r	Veslind settling parameter [m^3/kg]	B	bottom
r_h	Takács settling parameter [m^3/kg]	e	effluent
r_p	Takács settling parameter [m^3/kg]	f	feed
R	The ratio of solution difference	i	index of model layer
v	velocity [m/h]	u	underflow
v_0	Veslind settling parameter [m/h]	T	top
$v_{0,\ max}$	Takács settling parameter [m/h]	*Superscripts*	
v_s	hindered settling velocity [m/h]	n	index of time

The goal of this chapter is to briefly review the development of 1-D SST models and currently available numerical techniques used as the model governing PDE solver, then to provide a new, reliable numerical technique (based on the Yee-Roe-Davis method) for accurate numerical solution calculation. The second goal is providing an analysis of SST behavior at different operating conditions (underloading and overloading) based on numerical simulation results. The final goal is to show how the choice of numerical methods impact the model outputs, which has implications on the design and operation strategies.

3.2. Methodology

3.2.1. Model structure development

In order to simplify the problem and satisfy a 1-D modeling condition, several assumptions are necessary to be introduced as following: 1) the SST is circular and central-feed with constant area; 2) reaction rates are zero, and the sludge properties are uniform and constant in the SST; 3) no density currents exist (the hydraulic flow is vertical, and horizontally uniform); 4) loading rate is uniform and there are no wall effects; 5) the mechanical sludge scraper does not affect the sludge settling behavior.

In most previous SST modeling studies, the SST is divided into three functional zones, namely the clarification zone (above the inlet), thickening zone (below the inlet) and inlet zone to characterize the various settling behaviors: clarification, thickening and the mixture of input solids. Because of assumption 3), the hydraulic flow in the clarification zone is an upward effluent flow (Q_e), which conveys the solids toward the SST effluent weir, while the downward underflow (Q_u) in thickening zone transports solids to the SST bottom to produce a concentrated

recycle flow. Hence, the 1-D SST model should include both the bulk hydraulic transport and gravity settling.

In addition to the gravity settling and hydraulic transport, other factors can also impact the continuous settling process, for example the density current in the inlet region (Plósz et al. 2007), the hydraulic dispersion around the inlet (Hamilton et al. 1992, Watts et al. 1996, De Clercq et al. 2003, Plósz et al. 2007, Bürger et al. 2011, Bürger et al. 2012), sludge compression caused by its own weight at the SST bottom (Buscall and White 1987, Landman et al. 1988, Landman and White 1992, Cacossa and Vaccari 1994, Kinnear 2002, de Kretser et al. 2003, Usher and Scales 2005, Gladman et al. 2006, Usher et al. 2006, De Clercq et al. 2008, Gladman et al. 2010a, Bürger et al. 2011). Any attempt to model hydraulic dispersion and compression must introduce a diffusion term (a second-order derivative term) to the model formula that smoothes concentration profiles (Bürger et al. 2011, Bürger et al. 2012, Bürger et al. 2013). However, solution may still have discontinuous in the region where local concentration less than the critical concentration (gel point), which means no compression effect occurs. The governing PDE remains nonlinear hyperbolic in these regions, and cannot be easily discretized due to solution discontinuities. For either the convention dominant model, such as the well-known 10-layer model (Takács *et al.* 1991) only including the convection process, or the convention-diffusion model which also simulates hydrodynamic dispersion and compression, it is necessary to introduce reliable numerical techniques for accurate numerical solution calculation and discontinuity capture, which is primary goal of this study. Since solving either the convection dominant model or the convection-dispersion model requires capturing the solution discontinuities and avoiding oscillation at the discontinuity, these two alternative models possess

similar characteristics in their numerical solutions. We chose the convection dominant model as our model, because of its greater utility in current engineering practice.

The convection dominant model can be written as the following nonlinear hyperbolic PDEs based on the mass conservation law:

$$\frac{\partial C}{\partial t} + \frac{\partial \left(v_s C - v_e C\right)}{\partial z} = 0 \qquad \textit{above the inlet zone} \qquad (3.1)$$

$$\frac{\partial C}{\partial t} + \frac{\partial \left(v_s C + v_u C - v_e C\right)}{\partial z} = v_f C_f \qquad \textit{the inlet zone} \qquad (3.2)$$

$$\frac{\partial C}{\partial t} + \frac{\partial \left(v_s C + v_u C\right)}{\partial z} = 0 \qquad \textit{below the inlet zone} \qquad (3.3)$$

As can be seen, the SST model is one equation with two unknowns (C and v_s). Therefore, an additional constitutive relation is required, and the Kynch's assumption (Kynch 1952) is most often used, which states that the hindered settling velocity is solely determined by the local solids concentration. The two commonly used constitutive formulas are the Vesilind (Vesilind 1968a) function, eq.(3.4), and the double-exponential function (Takács *et al.* 1991), eq.(3.5) :

$$v_s = v_0 \exp^{-rC} \qquad (3.4)$$

$$v_s = \max(0, \min(v_{0,\max}, v_0 \left(\exp^{-r_h\left(C-C_{\min}\right)} - \exp^{-r_p\left(C-C_{\min}\right)}\right))) \qquad (3.5)$$

Though both formulas are suitable for hindered settlings, the Vesilind function may overestimate the settling velocity at low solids concentration (Li and Ganczarczyk 1987). The improvement of the two-exponential function relates to the non-settleable fraction in the feed sludge and the

discrete settling behavior at low solids concentration region. Therefore, the double-exponential function is applied in this study for gravity settling velocity calculation, thus making the solids concentration (*C*) the only unknown in the model.

The mass conservation law should also hold on the upper and bottom boundaries, which requires the flux of particle leaving the SST to equal the flux entering the effluent and recycling pipes (Diehl 2000, Bürger et al. 2012). The mass conservation law of boundaries can be expressed as follows:

$$v_s C_T - \frac{Q_e}{A} C_T = -\frac{Q_e}{A} C_e \qquad \text{the top boundary} \tag{3.6}$$

$$v_s C_B + \frac{Q_u}{A} C_B = \frac{Q_u}{A} C_u \qquad \text{the bottom boundary} \tag{3.7}$$

The sludge settling velocity parameters are site specific and depend upon the condition of the biomass (i.e., filaments, etc). In this chapter, Grieves and Stenstrom's (1976b) data are used. The measurement error has been checked to be Gaussian and uncorrelated, and Levenberg–Marquardt algorithm (More 1978a) is used for model parameter identification. The results are shown as normal sludge in Table 3.1.

Table 3.1 - Parameter sets of gravity settling velocity (normal and deterioration).

Parameter set of settleability		
	Normal sludge	Deterioration
$v_{0,max}$ [m/h]	9.63	9.63
v_0 [m/h]	20	20
r_p [m^3/kg]	0.01	0.01
r_h [m^3/kg]	0.00063	0.003
C_{min} [g/m^3]	10	12

3.2.2. Numerical technique introduction

Equation (3.1)-(3.3) are hyperbolic and cannot be straightforwardly discretized because of the shock problem (discontinuous solutions), which requires determination of unique solutions along the shock, and rejection of unstable discontinuities. To obtain both numerically and physically acceptable solutions, reliable numerical techniques specially designed for scalar conservation PDE are needed to satisfy the three fundamental principles: Courant-Friedrichs-Lewy (CFL) condition, consistent numerical flux and the entropy condition to ensure the calculation stability and accuracy (Bürger *et al.* 2011).

Kynch (1952) first introduced the characteristics (iso-concentration line) analysis in a vessel with constant cross section area to capture the path of concentration gradients (shocks) in batch settling tests. Petty (1975) extended Kynch's procedure to continuous sedimentation, and provided an explicit shock analysis for the transient state, while Bustos *et al.* (1990a) constructed the global weak solutions based on method of characteristics for various initial data and operating conditions. Diehl (2000) complemented the characteristics analysis by resolving the problem with special boundary conditions at top, bottom and inlet, as well as considering the conical effect near the SST bottom. Successful examples of the characteristics analysis are the estimate of the batch-settling flux function from experimental data (Diehl 2007), and the mathematical analysis of the well-known solids-flux theory (Diehl 2008). On the basis of the method of characteristics, Burger *et al.* (2004) also developed a front tracking method, which is efficient for shock capture. As a conclusion, the method of characteristics or the characteristics analysis is currently the only available approach to obtain exact solutions of the nonlinear hyperbolic governing PDEs, however, it requires considerably more effort of its implementation

in engineering practice, and further investigations are needed.

Compared with analytical approaches, numerical techniques have advantages in dynamic process simulations. One of the earliest numerical flux descriptions used in 1-D SST modeling is the Stenstrom-Vitasovic- Takács (SVT) flux (Stenstrom 1976a, Vitasovic 1986a, Takács et al. 1991) shown as follows:

$$F_{i+1/2}^{SVT} = \min\left(v_{s,i}C_i, v_{s,i+1}C_i\right) \tag{3.8}$$

Several studies used the SVT flux, and the most well-known one is the 10-layer model (Takács *et al.* 1991) with the SVT flux as the key ingredient. Bürger *et al.* (2011, 2012, 2013) showed that the SVT flux can invalidate the entropy condition, and generates unphysical solutions in low concentration region. The Godunov numerical flux, shown as eq.(3.9), is the another widely used numerical technique in 1-D SST modeling, which is derived from the unique exact solutions (Jeppsson and Diehl 1996), and also used by Plósz *et al.* (2007).

$$F_{i+1/2}^{G} = \begin{cases} \min\limits_{C_i \leq C \leq C_{i+1}} \left(v_s C - \dfrac{Q_e}{A}C\right) & \text{if } C_i \leq C_{i+1} \\[4mm] \max\limits_{C_{i+1} \leq C \leq C_i} \left(v_s C - \dfrac{Q_e}{A}C\right) & \text{if } C_i > C_{i+1} \end{cases} \tag{3.9}$$

An explicit numerical method (Method EO) with the Enquist-Osher numerical flux (Engquist and Osher 1981) was presented by Bürger *et al.* (2005), and De Clercq *et al.* (2008) employed it for batch settling simulation. Another numerical technique presented by Bürger *et al.*(2010) is Method G, based on the Godunov numerical flux. Though both Method G and Method EO are reliable for SST modeling, which means they are able to provide approximate solutions that converge to the unique physically relevant solutions, and in many cases, they yield similar, even

identical solutions, the selection as a PDE solver is subjected to three competing principles: the complexity of implementation, the solution accuracy, and the computation cost. The comparison study (Bürger *et al.* 2012) showed that the Method EO is too complicated for a application as the PDE solver in practical engineering problems, and for a given discretization level, Method G is capable of producing solutions faster than the Method EO. However, the Method EO reduces numerical error more efficiently than the Method G, which means the larger CPU time needed by Method EO results in higher quality numerical solutions.

3.2.3. Numerical discretization and integration

Because of the possible solution discontinuities (shocks) during the calculation, the nonlinear hyperbolic governing PDE cannot be straightforwardly discretized, and specific numerical techniques designed for scalar conservation PDE solving are often applied to avoid the shock, for example the flux averaging technique. Rather than choosing one method such as a first-order upwind method, the flux averaging starts with two or more established methods, then chooses one method or averages them. The averaging flux can be shown as follows:

$$\hat{F}_{i+1/2}^{n} = \theta_{i+1/2}^{n}\hat{F}_{i+1/2}^{(1)} + \left(1 - \theta_{i+1/2}^{n}\right)\hat{F}_{i+1/2}^{(2)} \tag{3.10}$$

where $\hat{F}_{i+1/2}^{n}$ is the averaging numerical flux, $\hat{F}_{i+1/2}^{(1)}$ is the conservative numerical flux of numerical method 1, $\hat{F}_{i+1/2}^{(2)}$ is the conservative numerical flux of numerical method 2, and $\theta_{i+1/2}^{n}$ is the averaging factor, sometimes called the shock switch. An equivalent way of writing eq.(3.10) is eq.(3.11) shown as follow:

$$\hat{F}_{i+1/2}^{n} = \hat{F}_{i+1/2}^{(1)} + \phi_{i+1/2}^{n}(\hat{F}_{i+1/2}^{(2)} - \hat{F}_{i+1/2}^{(1)}) \tag{3.11}$$

where $\phi_{i+1/2}^n$ equals to $\left(1-\theta_{i+1/2}^n\right)$, and is called the flux limiter. This flux averaging method is called the flux-limiter method. After determining the two first-generation methods, the next step is choosing suitable flux limiter, which strongly depends on distinguishing shocks from the smooth regions. Generally, shocks are indicated by the ratios of solution differences, which can be expressed as eq.(3.12):

$$R_i^+ = \frac{C_i^n - C_{i-1}^n}{C_{i+1}^n - C_i^n}, \quad R_i^- = \frac{C_{i+1}^n - C_i^n}{C_i^n - C_{i-1}^n} \tag{3.12}$$

where R is the ratio of solution difference, and has the following properties:

- $R_i^\pm \geq 0$ if the concentration is monotone increasing or decreasing:

- $R_i^\pm \leq 0$ if the solution has a maximum or a minimum;

- $\left|R_i^+\right|$ is large and $\left|R_i^-\right|$ is small if the solution differences decrease dramatically from left to right;

- $\left|R_i^+\right|$ is small and $\left|R_i^-\right|$ is large if the solution differences decrease dramatically from right to left;

A large decrease or increase of the ratio of solution differences always indicates shocks. The flux-limit technique directly leads to the popular total variation diminishing (TVD) methods, which enforces the nonlinear stability by using the freedom of flux averaging. The Yee-Roe-Davis (YRD) numerical technique introduced in this study is a typical flux-limited method, which has the TVD property. The two first-generation methods used in YRD numerical technique are the forward-time central-space (FTCS) method (eq.(3.13)) and Roe's first-order upwind method (eq.(3.14)).

$$\hat{F}_{i+1/2}^{FTCS} = \frac{F\left(C_{i+1}^n\right) + F\left(C_i^n\right)}{2} \tag{3.13}$$

$$\hat{F}_{i+1/2}^{ROE} = F\left(C_{i+1}^n\right) - \left|a_{i+1/2}^n\right|\left(C_{i+1}^n - C_i^n\right) \tag{3.14}$$

where

$$F(C_i^n) = \begin{cases} C_i^n v_i^n - \dfrac{Q_e}{A} C_i^n & \text{the clarification zone} \\[2mm] C_i^n v_i^n + \dfrac{Q_u}{A} C_i^n & \text{the thickening zone} \end{cases} \tag{3.15}$$

In the original ROE's first-order upwind method, $a_{i+1/2}^n$ is given by eq.(3.16):

$$a_{i+1/2}^n = \begin{cases} \dfrac{F\left(C_{i+1}^n\right) - F\left(C_{i+1}^n\right)}{C_{i+1}^n - C_i^n} & \text{for } C_i \neq C_{i+1} \\[3mm] F'\left(C_i^n\right) & \text{for } C_i = C_{i+1} \end{cases} \tag{3.16}$$

In the YRD method, $\left|a_{i+1/2}^n\right|$ is replaced by $\psi\left(a_{i+1/2}^n\right)$, as eq.(3.17) shows:

$$\psi\left(a_{i+1/2}^n\right) = \begin{cases} \dfrac{a_{i+1/2}^n + \delta^2}{2\delta} & \text{for } \left|a_{i+1/2}^n\right| < \delta \\[3mm] \left|a_{i+1/2}^n\right| & \text{for } \left|a_{i+1/2}^n\right| > \delta \end{cases} \tag{3.17}$$

Here, δ is an arbitrary small value, which is determined as 10^{-20} in this study. The final step is determining the flux limiter $\phi_{i+1/2}^n$, and Yee et al. (1990) suggested three possible flux limiters:

$$\phi\left(R_i^+, R_{i+1}^-\right) = \text{minmod}(1, R_i^+, R_{i+1}^-) \tag{3.18}$$

$$\phi\left(R_i^+, R_{i+1}^-\right) = \text{minmod}(2, 2R_i^+, 2R_{i+1}^-, \frac{1}{2}\left(R_i^+ + R_{i+1}^-\right)) \tag{3.19}$$

$$\phi\left(R_i^+, R_{i+1}^-\right) = \text{minmod}(1, R_i^+) + \text{minmod}(1, R_{i+1}^-) - 1 \tag{3.20}$$

where minmod is the minimum modulus. The minmod function returns the argument closest to zero if all of its arguments have the same sign, and it returns zero if any two of its arguments have different signs. In this study, we choose the first one, eq.(3.18) as the flux limiter, and the explicit Yee-Roe-Davis method is

$$C_i^{n+1} = C_i^n - \frac{\Delta t}{\Delta z}\left(\hat{F}_{i+1/2}^n - \hat{F}_{i-1/2}^n\right) \tag{3.21}$$

where

$$\hat{F}_{i+1/2}^n = \frac{1}{2}\left(F_i^n + F_{i+1}^n\right) + \frac{1}{2}\psi\left(a_{i+1/2}^n\right)\left(\phi_{i+1/2}^n - 1\right)\left(C_{i+1}^n - C_i^n\right) \tag{3.22}$$

The YRD method determines what to do in terms of the solution gradient rather than considering the solution's stability and accuracy in the same fashion throughout the entire domain. Therefore, the YRD method can work well in both regions simultaneously with small tradeoffs, and possesses second-order accuracy. Since the SVT numerical flux is mostly often used in current engineering practices, we use it as a reference method to show the improvement of applying the YRD method.

3.2.4. SST behavior investigation under underloading and overloading conditions

Wastewater flow rate and contaminant concentration vary, which means control strategies for

SST must make appropriate adjustments. Hence, it is significant to understand SST's behavior in different operating conditions. SSTs are usually operated at underloading conditions, which requires the operating flux to be less than the limiting flux. Overloading can occur from hydraulic shock loading or sludge bulking.

In this study, we use both SVT flux model and YRD flux model to investigate the SST's response to different operating conditions (parameter set shown in Table 3.2). According to discretization sensitivity study that numerical solution converges when the number of layer exceeds 50 (Li and Stenstrom 2014a), the discretization level is determined as 50-layers.

Table 3.2 - Parameter set to generate different operating conditions.

Parameter set of different operating conditions			
	Underloading Condition	Overloading Condition 1	Overloading Condition 2
A [m^2]	100	100	100
H [m]	4	4	4
h [m]	2	2	2
Q_e [m^3/h]	200	200	200
Q_u [m^3/h]	60	60	60
C_f [g/m^3]	2500	4000	9000

3.2.5. System robustness study

SSTs may experience failure due to two primary causes: hydraulic shock loading and deterioration of sludge settleability. Time-to-failure is defined as the time interval between the beginning of an upset and failure, and can be used as an important indicator for system robustness evaluation (Diehl 2005, 2006). The longer time-to-failure indicates a more robust process. System robustness is closely related to SST size, since SST size can greatly impact

several important operating factors, such as operating flux and limiting flux. To quantitatively investigate the relationship between system robustness and SST size, we simulated solids overloading for both hydraulic shock loading and sludge settleability deterioration, for SST surface area from 100m^2 to 400m^2. All variations are imposed as step functions with the initial condition of zero concentration throughout the SST:

● Hydraulic shock loading: At t=0 h, Q_e=200 m^3/h to reach steady state. At t=2 h, Q_e is increased from 200 m^3/h to 800 m^3/h. C_f is fixed as 2000 g/m^3.

● Sludge settleability deterioration: Q_e and C_f are fixed as 200m^3/h and 2000 g/m^3. At t=0 h, the settling parameters are set to normal as shown in Table 3.1. At t=2h, the settling velocity parameters change to deterioration (Table 3.1) in order to model a change to poor settleability condition (e.g., bulking).

3.3. Results and discussion

3.3.1. Numerical solution accuracy

To evaluate solution accuracy, we created a hypothetical but typical overloading condition (A=100m^2, C_f=4000 mg/l), with normal settling parameters as shown in Table 3.1. As can be seen from the predicted concentration profiles (Fig.3.1), both models are able to predict the sludge blanket level movement; however the model solved by the SVT method provides smooth profiles rather than sharp discontinuities shown in the YRD one. The predications also diverge with differences in the sludge blanket level, solids concentration in each layer and the underflow concentration. The sludge blanket level predicted by the SVT method is higher, while the concentration profile solved by the YRD method has an increased solids concentration in each

layer, including the bottom one (the underflow concentration). Using the YRD method also provides a more accurate prediction of the discontinuities at the edge of the blanket. It is also significant to notice the overestimation of the sludge blanket level may encourage designing larger SSTs.
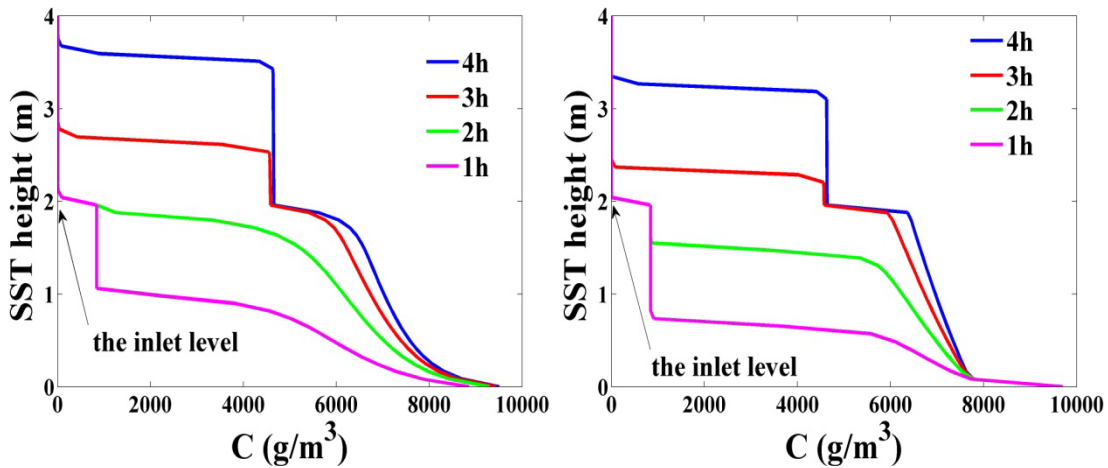
Fig.3.1 -Typical overloading concentration profiles.

(left: the SVT method; right: the YRD flux method)

In order to further demonstrate the reliability of the YRD method, we ran both the YRD method and the SVT method with the same scenario as in Fig.7 of Bürger *et al* (2012), and the simulation results are shown as Fig.3.2. The concentration profiles constructed by the YRD method and the Method G are similar, which demonstrates that the YRD method is reliable to produce entropy-satisfying solutions, and can be an equivalent alternative as the G and EO methods. However, the SVT method provides solutions different from the YRD, G and EO methods, and it is also sensitive to the discretization level.
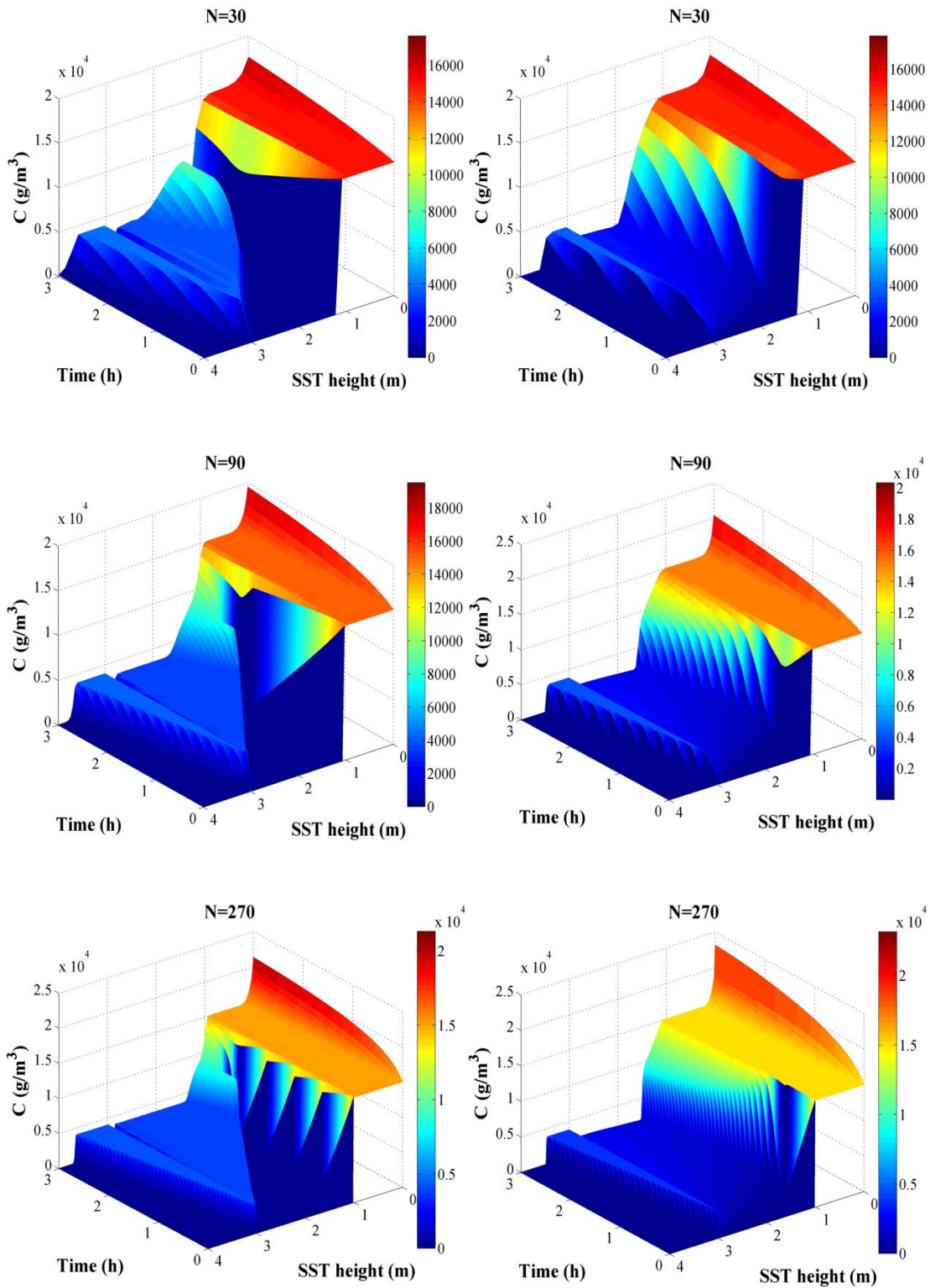
Fig. 3.2 - Concentration profiles of the SVT method and the YRD method.

(left: the SVT method; right: the YRD method)

3.3.2. SST behaviors in various operating conditions

As can be seen in Fig.3.3, SSTs can convey most feed sludge towards to the bottom and produce low turbidity effluent in underloading case, which matches the previous experiments observations (Tracy 1973). Sludge is thickened in the thickening zone for further recycle and disposal. Since the SVT numerical flux limits the gravity settling flux, the downward bulk flux is the only source for sludge transfer during the initial thickening time, which can cause a numerical delay. Therefore, an obvious sludge accumulation occurs in the SVT method results compared with the normal smooth concentration prediction of the model solved by the YRD method.

When C_f is 4000 g/m^3 (overloading 1), the operating flux is larger than the limiting flux, and overloading occurs. Both models show that the sludge blanket will rise, though the predicted sludge blanket growth rate is different (2.7m for the SVT method versus 2.2m for the YRD method). This result supports the earlier statement that the model solved by the SVT method overestimates the sludge blanket height. Another key variable is the underflow concentration (C_u). Fig.3.3 shows that C_u is independent of sludge blanket height, and is approximately 10000 g/m^3, matching the flux diagram prediction (Hassett 1958).

The SST behavior can be totally different after C_f increases to 9000 g/m^3 (overloading 2), though the operating condition is still defined as solids overloading. In this case, instead of settling to the thickening zone, most sludge will be directly conveyed to the SST effluent weir by the effluent flow. Rather than a gradual sludge blanket growth from SST bottom, we can observe both sludge blanket rise in thickening and clarification, and the latter one is even more rapid than the former one as shown in Fig.3.3. Finally, the sludge blanket will exceed the effluent weir, and cause an

effluent validation, known as clarification failure. The solutions solved by these two methods are totally different in this case. The predicated concentration difference in clarification zone is 2000 g/m^3 (8500 g/m^3 *Vs.* 6500 g/m^3). The recycling concentration solved by the SVT method is 8000 g/m^3, while if the YRD method is used as the PDE solver, it remains the same as overloading 1 (10000 g/m^3). For the sludge blanket level, the SVT method provides a higher value in the clarification zone, but lower value in the thickening zone compared to the solutions solved by the YRD method.

3.3.3. System robustness

SSTs with larger surface area are usually considered to be more robust compared with smaller ones in terms of offering more sludge storage capacity and smaller operating flux. However, this cannot always be correct, since the associated limiting flux can also decrease with the increase of size. Hence, in order to quantitatively investigate this problem, time-to-failure is selected as a system robustness indicator. Generally, a lengthy time to reach failure implies a more stable process. Fig.3.4 illustrates time-to-failure after a 20-h hydraulic shock loading simulation (Fig.3.4 left) and deterioration of sludge settleability (Fig.3.4 right).

It is notable that the estimated time-to-failure based on the solutions solved by the SVT method is much smaller than what the YRD method provides. This corresponds well to the conclusion presented earlier in the numerical accuracy section that the model solved by the SVT method overestimates the sludge blanket height due to numerical inaccuracies. As a consequence, the time-to-failure solved by the YRD method is used for system robustness analysis.
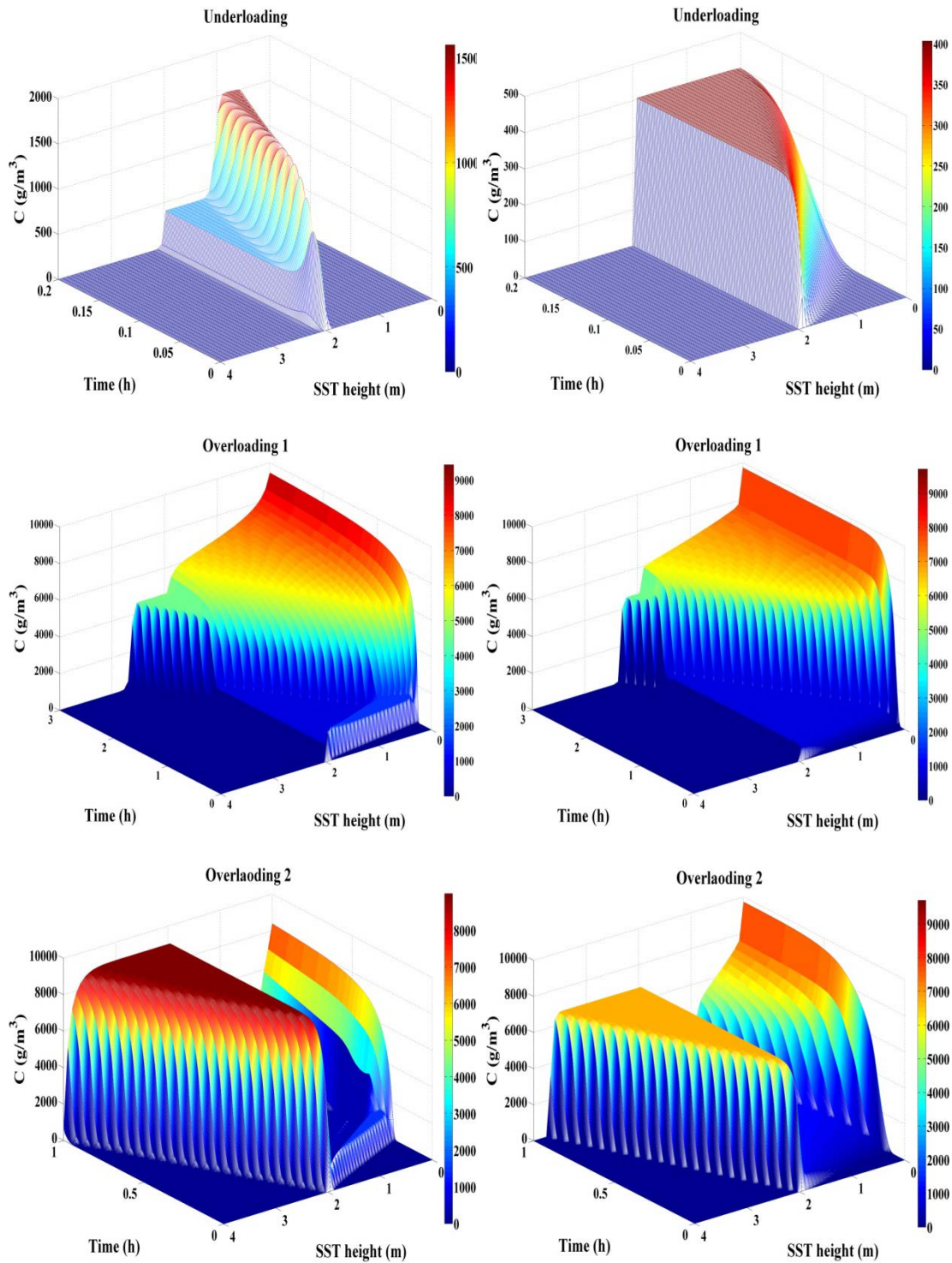
Fig. 3.3 - Concentration profiles of different solids loading conditions.

(left: the SVT method; right: the YRD method)

According to Fig. 3.4 (left), the hydraulic shock loading failure time of smaller SST alternatives (A=100 to 135 m^2) is less than 0.1 h. It increases to 1.5-4 h, a great improvement, when SSTs are enlarged to medium size (A=140 to 250 m^2). No failure will occur if the SST is larger than 250 m^2. For the case of a small SST, most biomass is directly conveyed to the clarification zone by the overflow instead of settling to the thickening zone, causing a clarification failure in less than 0.1h. This helps explain why small SSTs have extremely short time-to-failure. A gradual sludge blanket rise is observed in medium SSTs, and causes a thickening failure when it reaches the feed point. An area of 140 m^2 is the demarcation point between clarification failure and thickening failure. Compared with a clarification failure, the thickening failure is a relatively slow process as the sludge blanket must rise from the bottom to top, which usually occurs over several hours. If the SST can afford large enough limiting flux, the system can always maintain an underloading condition. For this reason, neither clarification nor thickening failure occurs when the SST area is greater than 260 m^2.

Compared to hydraulic shock loading, where the failure is caused by a sudden increase of operating flux, failure due to poor biomass settleability (sludge bulking), is attributed to a decrease in the limiting flux. Fig.3.4 (right) shows a similar failure time change tendency observed in hydraulic shock loading: a rapid to gradual process. In this case, failure can be avoided only by increasing the limiting flux, such as changing the recycle rate or contacting pattern (Stenstrom and Andrews 1979a).
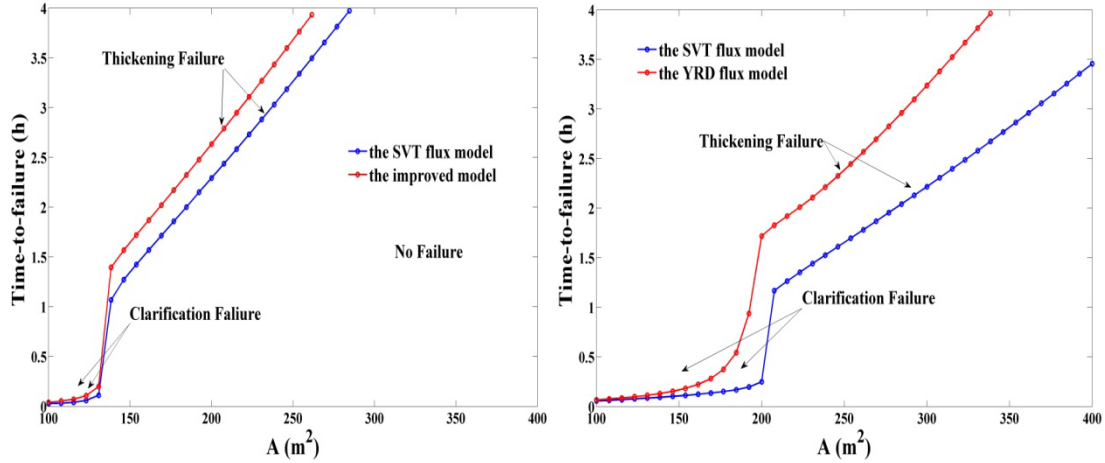
Fig.3.4 - Failure time in the hydraulic shock loading (left) and the settleability deterioration (right).

3.4. Conclusion

The conclusions of this chapter can be summarized as follows:

- Instead of applying the empirical SVT method as the nonlinear hyperbolic governing PDE solver, the YRD method determines the calculation behavior in terms of the solution gradient, and provides both numerically and physically acceptable solutions that satisfy the CFL condition and entropy condition. Therefore, the YRD method is a reliable numerical technique for solving the nonlinear hyperbolic PDE of the SST model, and can be an acceptable alternative to the G and EO methods.

- Both clarification and thickening failure can occur during overloading with the magnitude of the overloading determining the type of failure. Clarification failure occurs with greater overloading. The model solved by the SVT method is likely to produce unrealistic solids accumulation during under loading but both models perform well in thickening failure predication (overloading 1). For clarification failure (overloading 2), the model solved by the YRD method provides more accurate recycle solids concentration and sludge blanket

81

level predication.

- The choice of numerical methods can greatly impact the model solutions, for instance the time-to-failure evaluation. Compared with the exact time-to-failure solved by the YRD method, the SVT method can underestimate the time-to-failure, and lead to conservative design and operation strategies. Therefore, reliable numerical techniques, such as the YRD method, are strongly recommended for 1-D SST model solving.

4. Construction of analytical solutions and numerical methods comparison of the ideal continuous settling model

4.1. Introduction

Continuous sedimentation, a gravity driven solid-liquid separation process, has various applications in industrial areas including the wastewater treatment, water reuse, mineral waste manage and processing. However, in current engineering application, the design and operation of the continuous settling tanks still remain as a difficult task, and generally, empirical and conservative strategies are applied, which may cause both capital and land waste, as well as the unanticipated performance flocculation of the settling tank itself (Northcott et al. 2005, Li and Stenstrom 2014a, Li and Stenstrom 2014d). For the purposes of understanding the continuous settling behavior and optimizing settling tank performance, mathematical models are encouraged to being used, and in most commercial simulators, the ideal one-dimensional (1-D) continuous settling model (without compression effect) is equipped due to its relative well understanding and less computation burden, especially if long term simulation is needed (Bürger et al. 2011).

Given the complexity of real system conditions (e.g., viscosity, dispersion, turbulence, rake effect, various settling behaviors), the concept of the ideal thickener was introduced by Shannon *et al.*(1963) to simplify the modeling task. In an ideal 1-D condition, the secondary settling tank (SST) possesses a constant cross-section with uniform solids concentration in each horizontal layer, and the complex hydrodynamics are simplified as the upward effluent flow to the top and downward underflow to the bottom, as shown in Fig.4.1. The distribution of solids are determined by both gravity settling and the bulk hydraulic transport, and the mass conservation

law holding in each layer can be expressed as the partial differential equation, eq.(4.1) (Diehl 1997, Diehl and Jeppsson 1998):

$$\frac{\partial \phi}{\partial t} + \frac{\partial F(\phi)}{\partial x} = s\delta(x)$$

$$F(\phi) = \begin{cases} -v_e\phi_e = g_e & x < -H \\ f_{bk}(\phi) - v_e\phi = g(\phi) & -H < x < 0 \\ f_{bk}(\phi) + v_u\phi = f(\phi) & 0 < x < D \\ v_u\phi_u = f_u & x > D \end{cases} \tag{4.1}$$

where F is the flux function, $\delta(z)$ is the Dirac impulse , $\phi(x,t)$ denotes the solid concentration, x is the depth from the feed inlet, t is the time, $s=v_f\phi_f$, denotes the feed solids flux (ϕ_f is the feed solid concentration and v_f is the feed flow velocity), f_{bk} is the Kynch batch flux function and the solid mass fluxes leaving at the effluent weir and bottom are $g_e=v_e\phi_e$ (v_e is the effluent flow velocity and ϕ_e is the effluent solids concentration) and $f_u=v_u\phi_u$ (v_u is the underflow velocity and ϕ_u is the underflow solids concentration) respectively.

It is noticeable that eq.(4.1) only can be solvable with proper constitutive relations. The fundamental constitutive relation for hindered settling modeling is the Kynch's assumption that the hindered settling velocity is solely determined by the local solids concentration. Based on the Kynch's assumption, three alternative methods have been established to develop the required constitutive function: the hindered settling factor approach (Buscall and White 1987, Landman et al. 1988, Usher and Scales 2005, Gladman et al. 2010b), the Darcy's Law approach (Karl and Wells 1999, Kinnear 2002) and Kynch flux density approach (Bürger et al. 2000a, Bürger et al. 2005). However, the Kynch's assumption is not a nostrum, since it can only provide a complete settling behavior description of Kynchian suspensions with no compressive behavior at any

concentration. Otherwise, its validity can only be proved in hindered settling region, where the concentration is sufficiently low that no weight-bearing network formed (Dixon 1977a).
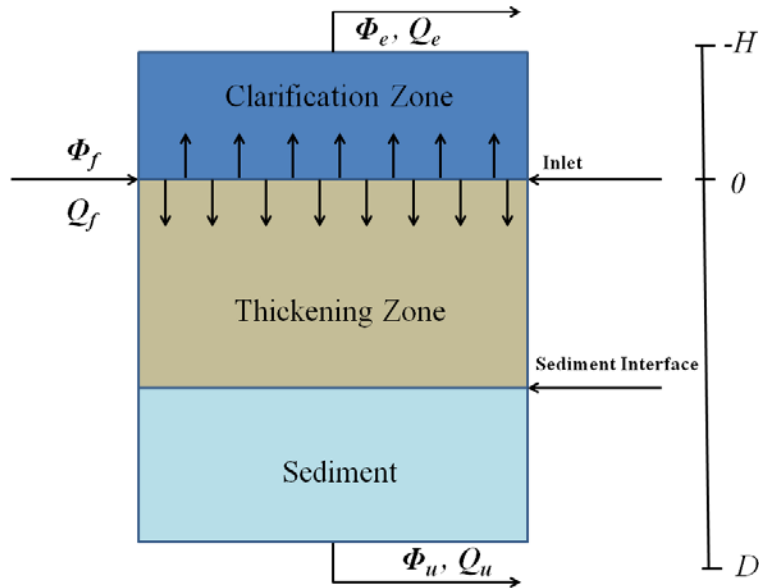
Fig.4.1 - Schematic overview of ideal continuous settling tank with constant cross-section area.

When in high concentration range, where strong particle-particle interaction exists, compression settling occurs because of the compressive stress transmitted through the formed net structure (de Kretser et al. 2003), and modeling the compression settling process is significant for applications as diverse as thickening, dewatering, filtration and centrifugation. Two parallel theories have been developed to interpret the compression settling: geotechnical approach (Bürger 2000, Bürger et al. 2001), which quantifies the sediment compressibility by using effective solids stress or the solids pressure; compression rheology approach (Buscall et al. 1987, Buscall and White 1987), where the compressibility is characterized as the physically measurable network strength: compressive yield stress. The effective solid stress and solid pressure are usually defined as solid volumetric concentration dependent functions rather than the intrinsic material property as the compressive yield stress is. Except for the significant conceptual difference, these two

approaches actually have a similar rheological basis, thus making them parallel (de Kretser et al. 2003).

The development of settling theory including the hindered and compression rheology is the first step for model formula complementation, and solving these PDEs, which means accurately solution calculation, is equivalently important for reliable model predications. When hindered settling dominates, the model governing equation can be written as eq.(4.1), nonlinear hyperbolic PDEs, known as the convection-dominant model. The compression effect can be modeled by adding a nonlinear diffusion term to eq.(4.1), and then the model formula becomes strongly degenerate parabolic PDEs, known as the convection-compression model (Bürger et al. 2012). Though differing in rheology basis, both convection-dominant and convection-compression models possess the similar mathematical characteristics, and solving the compression including model will not greatly increase the solution technique complexity (Bürger et al. 2012). Therefore, from a mathematical point of view, it is informative to fully understand the mathematical implication of eq.(4.1) before investigating more complex models (Diehl 2000).

Based on the mass continuity law and Kynch's assumption, the advantage of eq.(1) is that it is capable to capture the movement of large concentration discontinuities without knowing their physical mechanisms (Kynch 1952). However, solution discontinuities, which can be physically interpreted as the concentration gradients, are expected to occur as a function of time and height in solving eq.(4.1), and greatly increases the complexity of required solution techniques. Solving eq.(4.1) can be either numerical or analytical: numerical techniques including Method G (Jeppsson and Diehl 1996), Method EO (Bürger et al. 2005), Method YRD (Li and Stenstrom 2014a, c) *et al*. have achieved some degree of success in shock capturing and solution calculation,

but cannot always satisfy practical application standards, such as high accuracy but low computation burden; the only available approach for analytical solution construction is the method of characteristics (MOC), which avoids complicate discretization procedure but provide high accuracy solutions. Therefore, it is worthwhile further investigating the implementation strategy of MOC in 1-D continuous settling modeling.

The application of MOC to gravity settling problem can trace its history to 1950s, when Kynch (1952) analyzed the solids concentration distribution within the batch settling cylinder by using constant concentration lines, or iso-concentration lines, which is mathematically equivalent to characteristics. Thereafter, this approach was widely applied in practical SST design and operation (Fitch 1979, 1983, 1993). In recent studies, Diehl (2007) showed that the inverse problem of estimating of the batch settling flux function from experimental data can also be well addressed by using MOC. The first MOC study in continuous settling modeling was provided by Petty (1975) to show that the limiting flux, commonly observed in lab and full scale tests, is an intrinsic nonlinear phenomenon of the governing nonlinear hyperbolic PDEs, which is lately supported by Chancelier *et al.* (1997) and Diehl (2008), and the propagation of solution discontinuities from bottom boundary is caused by interaction of rarefaction waves. Nevertheless, Petty's work is a MOC based continuous settling behavior analysis more than an analytical solution developing study. Hence, further investigations were motivated to complement the MOC theory in continuous settling study, including the global weak solution construction (Bustos 1988, Bustos et al. 1990b, Diehl 1997), boundary condition determination (Bustos and Concha 1992, Diehl 1996, 2000), and control theory development (Buscall et al. 1982, Bustos et al. 1990b, Diehl 2005, 2006).

The first goal of this chapter is to construct solutions of the ideal SST model that includes hindered settling and hydraulic bulk transport with dynamic loading conditions on the basis of the previously developed MOC implementation strategy. The MOC solutions are compared with experimental continuous settling data to demonstrate the accuracy of MOC solutions in predicting dynamic continuous settling behaviors. Given that numerical solution techniques are often used for continuous settling models, the second part of this chapter focuses on the convergence analysis of three representative numerical methods: Method SG, Method G and Method YRD by using the MOC solutions as reference solutions. Accuracy and computation cost of these three methods are also investigated to compare their efficiency for practical engineering applications. The techniques demonstrated here for solving hyperbolic PDEs are applicable in other chemical engineering problems; for example, modeling of two-phase flow in heterogeneous media (Vanduijn et al. 1995) and the investigation of multicomponent separation (adsorption, ion exchange, chromatography) when the liquid phase is plug flow (Loureiro and Rodrigues 1991).

4.2. MOC theory review in ideal continuous settling model solving

To improve the understanding of the MOC theory in ideal continuous settling process and its implementation stretegy, we proived a brief reivew of the MOC theory and its implementation stretegy which is developed in previous publicitions (Diehl 1996, 1997, 2000). For the overall SST domain, as shown in Fig.4.1, the height of the clarification zone is H, and the depth of thickening zone is D. The downward direction is defined as the positive direction of the x-axis, and settling velocity and flux are positive in downward direction. The direction of feed flow (Q_f), effluent flow (Q_e), and underflow (Q_f) are also shown in Fig.4.1. The Kynch's assumption

(Kynch 1952), is assumed to hold, therefore the settling velocity (v_s) as well as the Kynch batch flux function $f_{bk}=v_s\phi$ is only determined by local solids concentration ϕ. The mass conservation law model equation, eq.(4.1), inside the SST domain, can be written as eq.(4.2) (Diehl 2000):

$$
\begin{aligned}
\frac{\partial \phi}{\partial t} - v_e \frac{\partial \phi}{\partial x} &= 0 & x < -H \\
\frac{\partial \phi}{\partial t} + (f_{bk}^{'}(\phi) - v_e)\frac{\partial \phi}{\partial x} &= 0 & 0 > x > -H \\
\frac{\partial \phi}{\partial t} + (f_{bk}^{'}(\phi) + v_u)\frac{\partial \phi}{\partial x} &= 0 & D > x > 0 \\
\frac{\partial \phi}{\partial t} + v_u \frac{\partial \phi}{\partial x} &= 0 & x > D
\end{aligned}
\tag{4.2}
$$

where $f_{bk}^{'}(\phi) = d(f_{bk}(\phi))/d\phi$. As a nonlinear hyperbolic PDE, eq.(4.2) possesses the property that, the initial concentration value, $\phi(x,0)$, propagates with the speed $f_{bk}^{'}(\phi(0,x))$, along a straight line x_l with slope $x_l^{'} = f_{bk}^{'}(\phi(0,x))$. These straight lines with constant solutions are called *characteristics*. If the initial concentrations are not uniform, characteristics with different slopes can intersect in the positive direction of t and generate solution discontinuities, which means for a discontinuity $X=X(t)$, the solutions are ϕ^{x+} and ϕ^{x-} on the left and right side respectively, instead of being continuous.

Since the differential formula requires differentiable solutions, it cannot model the possible nondifferentiable discontinuities, thus making eq.(4.2) not sufficient to completely describe the settling processes in both smooth and discontinuous regions. To provide a unique solution, the differential formula, eq.(4.2), is supplemented by a jump condition (Rankine-Hugoniot relations), which is derived from the integral form, and expressed as a discontinuity $X=X(t)$, propagating at a speed of S:

$$S = z^{'}(t) = \frac{f_{bk}\left(\phi^{x+}\right) - f_{bk}\left(\phi^{x-}\right)}{\phi^{x+} - \phi^{x-}} \tag{4.3}$$

And eq.(4.3) implies that

$$S = f_{bk}^{'}\left(\xi\right) \tag{4.4}$$

where ξ is between ϕ^{x+} and ϕ^{x-}. However, given the fact that the flux function, f_{bk}, is always nonconvex, the jump condition for nonconvex scalar conservation law is not sufficient to select the unique ϕ^{x+} and ϕ^{x-} along discontinuities. A stronger condition called Oleinik entropy condition (Oleinik 1964), is always introduced as an algebraic inequality to reject unstable discontinuities, shown as eq.(4.5):

$$\frac{f_{bk}\left(\xi\right) - f_{bk}\left(\phi^{x-}\right)}{\xi - \phi^{x-}} \geq S = \frac{f_{bk}\left(\phi^{x+}\right) - f_{bk}\left(\phi^{x-}\right)}{\phi^{x+} - \phi^{x-}} \geq \frac{f_{bk}\left(\xi\right) - f_{bk}\left(\phi^{x+}\right)}{\xi - \phi^{x+}} \tag{4.5}$$

for all ξ between ϕ^{x+} and ϕ^{x-}. The Oleinik entropy condition is derived from the second law of thermodynamics, and states that the flux function, f_{bk} here, lies entirely above the chord connecting ϕ^{x+} and ϕ^{x-} for $\phi^{x+} > \phi^{x-}$, or the flux function f_{bk} lies entirely below the chord connecting ϕ^{x+} and ϕ^{x-} for $\phi^{x+} < \phi^{x-}$, thus no intersection is allowed between the flux function curve and the chord.

Because of the discontinuities of flux functions at three boundaries (*x=-H, x=0, x=D*), the solutions of the governing PDE, eq.(4.2), are also discontinuous, which can be defined as following:

$$\phi^{-H+} = \lim_{\varepsilon \searrow 0}\phi(-H+\varepsilon,t), \ \phi^{-H-} = \lim_{\varepsilon \searrow 0}\phi(-H-\varepsilon,t) \qquad \textit{top outlet boundary}$$

$$\phi^{0+} = \lim_{\varepsilon \searrow 0}\phi(0+\varepsilon,t), \ \phi^{0-} = \lim_{\varepsilon \searrow 0}\phi(0-\varepsilon,t) \qquad\qquad \textit{inlet boundary} \qquad\qquad (4.6)$$

$$\phi^{D+} = \lim_{\varepsilon \searrow 0}\phi(D+\varepsilon,t), \ \phi^{D-} = \lim_{\varepsilon \searrow 0}\phi(D-\varepsilon,t) \qquad \textit{bottom outlet boundary}$$

The mass conservation law should also hold on the three boundaries, yielding the following jump conditions:

$$-v_e\phi^{-H-} = v_s\phi^{-H+} - v_e\phi^{-H+} \ \Rightarrow \ g_e\left(\phi^{-H-}\right) = g\left(\phi^{-H+}\right) \quad \textit{top outlet boundary}$$

$$v_s\phi^{0+} + v_u\phi^{0+} = v_s\phi^{0-} - v_e\phi^{0-} + s \Rightarrow f\left(\phi^{0+}\right) = g\left(\phi^{0-}\right) + s \quad \textit{inlet boundary} \qquad (4.7)$$

$$v_u\phi^{D+} = v_s\phi^{D-} + v_u\phi^{D-} \ \Rightarrow \ f\left(\phi^{D-}\right) = f_u\left(\phi^{D+}\right) \quad \textit{bottom outlet boundary}$$

Accurately determining the six boundaries solutions are especially significant, since they are not only the solutions of the governing PDEs, but also the required model outcomes, such as the effluent solids concentration (ϕ^{-H-}) and the recycle solids concentration (ϕ^{D+}). However, the jump conditions (eq.(4.3) and eq.(4.7)) are not sufficient to determine the unique discontinuous solutions at three boundaries for a given initial condition. In order to select the physically acceptable boundary solutions, MOC theory at boundaries are supplemented by the *condition Γ* (Diehl 1995, 1996), which is a generalization of Oleinik entropy condition (eq,(4.5)) and motivated physically by a conservative numerical method: Godunov method (Godunov 1959).

- top outlet boundary: to construct the physically correct ϕ^{-H-} and ϕ^{-H+}, two auxiliary functions are developed, including the non-increasing function $\breve{g}_e$ and the non-decreasing function $\hat{g}$, as shown in eq.(4.8):

$$\breve{g}_e = g_e = -v_e \phi$$

$$\hat{g} = \begin{cases} \min_{\alpha \in [\phi,\phi_0]} g(\phi), & 0 \le \phi \le \phi_0 \\ \max_{\alpha \in [\phi_0,\phi]} g(\phi), & \phi_0 \le \phi \le \phi_{max} \end{cases} \tag{4.8}$$

where ϕ_{max} is the maximum packing concentration, an intrinsic property of the settling material.

Condition Γ states that the effluent boundary flux γ is the value of the intersection of $\breve{g}_e$ and $\hat{g}$, and the boundary solutions ϕ^{-H-} and ϕ^{-H+} satisfy:

$$g_e\left(\phi^{-H-}\right) = \gamma = g\left(\phi^{-H+}\right) \tag{4.9}$$

inlet boundary: the most complex behavior of the SST occurs at the inlet, and in a fashion similar to the top outlet boundary, two auxiliary functions are introduced: the non-increasing function $\breve{g}$ and the non-decreasing function $\hat{f}$, shown as eq.(4.10).

$$\breve{g} = \begin{cases} \max_{\alpha \in [\phi,\phi_0]} g(\phi) + s(t), & 0 \le \phi \le \phi_0 \\ \min_{\alpha \in [\phi_0,\phi]} g(\phi) + s(t), & \phi_0 \le \phi \le \phi_{max} \end{cases}$$

$$\hat{f} = \begin{cases} \min_{\alpha \in [\phi,\phi_0]} f(\phi), & 0 \le \phi \le \phi_0 \\ \max_{\alpha \in [\phi_0,\phi]} f(\phi), & \phi_0 \le \phi \le \phi_{max} \end{cases} \tag{4.10}$$

Condition Γ states that the flux value γ at *the* feed boundary is the value of the intersection of the $\breve{g}\left(\phi^{0-}\right)$ and $\hat{f}\left(\phi^{0+}\right)$, and ϕ^{0-} and ϕ^{0+} satisfy:

$$f\left(\phi^{0+}\right) = \gamma = g\left(\phi^{0-}\right) + s(t) \tag{4.11}$$

• bottom outlet boundary: the bottom outlet boundary solutions are constructed by defining another two auxiliary functions: a non-increasing function $\breve{f}$ and a non-decreasing function $\hat{f}_u$:

$$\breve{f} = \begin{cases} \max_{\alpha \in [\phi, \phi_0]} f(\phi), & 0 \le \phi \le \phi_0 \\ \min_{\alpha \in [\phi_0, \phi]} f(\phi), & \phi_0 \le \phi \le \phi_{\max} \end{cases}$$ (4.12)

$$\hat{f}_u = f_u = v_u \phi$$

Condition Γ states that the flux value γ at *the* feed boundary is the value of the intersection of the $\breve{f}\left(\phi^{D-}\right)$ and $\hat{f}_u\left(\phi^{D+}\right)$, and ϕ^{D-} and ϕ^{D+} satisfy:

$$\breve{f}\left(\phi^{D-}\right) = \gamma = \hat{f}_u\left(\phi^{D+}\right)$$ (4.13)

As can be seen, the MOC theory in continuous settling includes two main parts: determining the unique correct solutions inside the SST domain by considering the jump condition and Oleinik entropy condition, and determining the unique boundary solutions by applying *condition Γ*. The most important but difficult task when using MOC is to correctly determine possible discontinuities, and the corresponding discontinuity solutions. To avoid presenting the complicated mathematics, we assume that readers are familiar with the techniques and concepts discussed above, and more information about the jump condition, Oleinik entropy condition, and *condition Γ*, can refer to (Oleinik 1964, Diehl 1995, 1996, 2000).

4.3. Continuous sedimentation experiments and model parameter estimation

It is well known that the solids handling capacity of a SST is limited, and the maximum solids flux that can be transported to the tank bottom outlet without causing changes, such as the sediment height propagation, is defined as the limiting flux (Diehl 2005). Hence, the SST's operating conditions can be divided into three categories: 1) underloading condition if the feed flux is less than the limiting flux; 2) critical loading if the feed flux equals to the limiting flux; 3)

overloading if the feed flux is larger than the limiting flux. The SST is normally underloaded, while overloading can be caused by hydraulic shock loading (wet weather) or settleability deterioration, and often leads to process failure.

Tracy (1973) conducted a lab-scale investigation of the impact of various feeding conditions on continuous settling behavior, especially the responses of the recycle concentration and sediment height. Ferric hydroxide was used as the settling material, and its settleability was characterized by the Kynch batch settling function (f_{bk}) based on the Vesilind equation (Vesilind 1968b), shown as eq.(14):

$$f_{bk} = v_s \phi$$
$$v_s = v_0 \exp(-n\phi) \quad (Vesilind\ equation)$$

(4.14)

In this study, the Vesilind parameter estimation (V_0 and n) is performed by fitting the Vesilind equation on the measured settling velocity data, and the objective function used to quantify the quality of the fit is the sum of squared errors. Table 3.1 shows the tank configuration and Kynch batch settling function parameters. Three transients are imposed: underloading-to-underloading, underloading-to-overloading, overloading-to-underloading by two influent forcings, and the operating condition for each transient is given in Table 3.2. In next section, we will show the implementation strategy of MOC to construct solutions of these three transients.

4.4. MOC solutions construction of three transients

Each of the following three cases is designed to show how the ideal continuous settling model can be solved with MOC to show the dynamic performance. The selected cases show important and commonly observed conditions for full scale SSTs.

- Underloading-underloading transient: in this case, the change of feed flux causes a change of the recycle concentration. Hence, the MOC solution is expected to accurately predict the recycle solids concentration.

- Underloading-overloading transient: in this case, the change of feed flux causes the propagation of sediment from SST bottom, and the increase of the recycle concentration. Hence, the MOC solution is expected to accurately predict the sediment interface level and the recycle concentration to prevent process failure.

- Overloading-underloading transient: in this case, the sediment interface rises to the top due to the overloading condition and then decreases due to a reduction in feed flux. The decrease of feed flux also causes a decrease in the recycle concentration. The MOC solution is expected to accurately predict the sediment interface change including both the increase and decrease, and the recycle concentration change.

Table 4.1 - SST configuration and Vesilind equation parameters.

SST configuration		Vesilind equation parameters	
Cross-section area [m^2]	0.0153	V_0 [m/h]	3.163
SST height [m]	2.44	n [m^3/kg]	0. 936
Inlet height (m)	1.83		

Table 4.2 - Operation conditions for the underloading-underloading, underloading-overloading, and overloading-underloading transients from Tracy (1973).

Underloading-to-underloading			Underloading-to-overloading			Overloading-to-underloading		
Operating Parameter	Underloading (0-5 h)	Underloading (5-12 h)	Operating Parameter	Underloading (0-5 h)	Overloading (5-16h)	Operating Parameter	Overloading (0-10 h)	Underloading (10-30h)
Influent flow rate (l/h)	13.02	9.72	Influent flow rate (l/h)	9.72	13.02	Influent flow rate (l/h)	15.84	15.84
Underflow rate (l/h)	3.456	3.456	Underflow rate (l/h)	2.538	2.538	Underflow rate (l/h)	3.96	3.96
Influent solids concentration (g/l)	1.435	1.335	Influent solids concentration (g/l)	1.28	1.435	Influent solids concentration (g/l)	1.4	1

4.4.1. Underloading-to-underloading

For the first transient experiment, the column is initially filled with liquid, which means the initial value of the governing formula is 0. At $t=0$, the tank is fed at a constant concentration ($\phi_f=1.435$ kg/m^3, $s_1=1.22$ kg/(m^{2}h)). The graphs of auxiliary functions $\hat{f}\left(\phi;\phi^{0+}\right)$ and $\breve{g}\left(\phi;\phi^{0-}\right)+s$ where $\phi^{0+}=\phi^{0-}=0$ are shown in Fig.4.2 (top left). Their intersection occurs at the concentration ϕ_1^{0+} and the flux value s_1. Therefore, as the *condition Γ* states, the unique boundary condition concentrations at inlet ($x=0$) are $\phi_1^{0+}=0.58$ kg/m^3 and $\phi_1^{0-}=0$ kg/m^3, and holds until the feed concentration changes to $\phi_f=1.335$ kg/m^3, $s_2=0.848$ kg/(m^{2}h) at $t=5$ h. As shown in Fig.4.2 (bottom left), Z_1 is the region where characteristics with slope $f^{'}(0)$ propagate, thus making solutions at this region equal to 0. Similarly, the solution at Z_3 is $\phi_1^{0+}=0.58$ kg/m^3 determined by the characteristics with slope $f^{'}(\phi_1^{0+})$.

Between Z_1 and Z_3, there is an expansion wave (Z_2) consisting all concentrations between the solution of Z_1 ($\phi^{0+}=0$ kg/m3) and the solution of Z_3 ($\phi_1^{0+}=0.58$ kg/m^3). The solution $\phi(x,t)$ within Z_2 can be uniquely solved by eq.(4.15) (the monotonic decreasing of $f^{'}$ at the left side of the inflection point ensures the invertibility of $f^{'}$):

$$\phi(x,t)=\left(f^{'}\right)^{-1}(x/t) \tag{4.15}$$

The recycling concentration (ϕ^{D+}) remains 0, until the expansion wave reaches the bottom ($z=D$) at t_1. Then ϕ^{D+} generally increases from 0 to ϕ_1^{D+} (5.406 kg/m^3) the values predicted by the

condition Γ as the intersection of $\breve{f}\left(\phi;\phi_1^{D-}\right)$ and $\hat{f}_u$ as shown in Fig.4.2 (top left). Any recycle concentration between t_1 and t_2 can be determined by eq.(4.16) based on the mass conservation law:

$$v_u \phi^{D+}\left(D,t\right) = f\left(\left(f'\right)^{-1}\left(D/t\right)\right) \tag{4.16}$$

At $t=5h$, the operation condition becomes to $\phi_f=1.335$ kg/m^3, $s_2=0.848$ kg/(m^{2}h), and correspondingly, the inlet boundary concentrations change to $\phi_2^{0+}=0.33$ kg/m^3 and $\phi_2^{0-}=0$ kg/m^3 predicted by the *condition* Γ as the intersection of $\hat{f}\left(\phi;\phi^{0+}\right)$ and $\breve{g}\left(\phi;\phi^{0-}\right) + s$ ($\phi^{0+}=\phi_1^{0+}$, $\phi^{0-}=0$), Fig.4.2 (top right) shows. The change of inlet boundary concentration generates the new characteristics with slope $f'\left(\phi_2^{0+}\right)$, thus making Z_4 an uniform solution region ($\phi\left(x,t\right)=\phi_2^{0+}$) as Z_1 and Z_3. Since $f'\left(\phi_2^{0+}\right) > f'(\phi_1^{0+})$, a solution discontinuity ($X_1(t)$) originates at point (5,0), and propagates towards bottom. The slope of X_1 follows the jump condition as eq.(4.17):

$$X_1' = \frac{f\left(\phi_2^{0+}\right) - f\left(\phi_1^{0+}\right)}{\phi_2^{0+} - \phi_1^{0+}} \tag{4.17}$$

At $t=t_3$, X_1 reaches the bottom ($x=D$) as shown in Fig.4.2 (bottom left), and causes a sudden decrease of recycling concentration from ϕ_1^{D+} (*5406* g/m^3) to ϕ_2^{D+} (*3755* g/m^3). Fig.4.2 (bottom right) shows that the recycling concentrations change predicted by MOC solutions (the generally increase from 0 to ϕ_1^{D+} (5.406 kg/m^3) at time interval (t_1 - t_2), and the decrease from ϕ_1^{D+} (5.406 g/m^3) to ϕ_2^{D+} (3.755 g/m^3) at t_3) matches the experiment data very well.
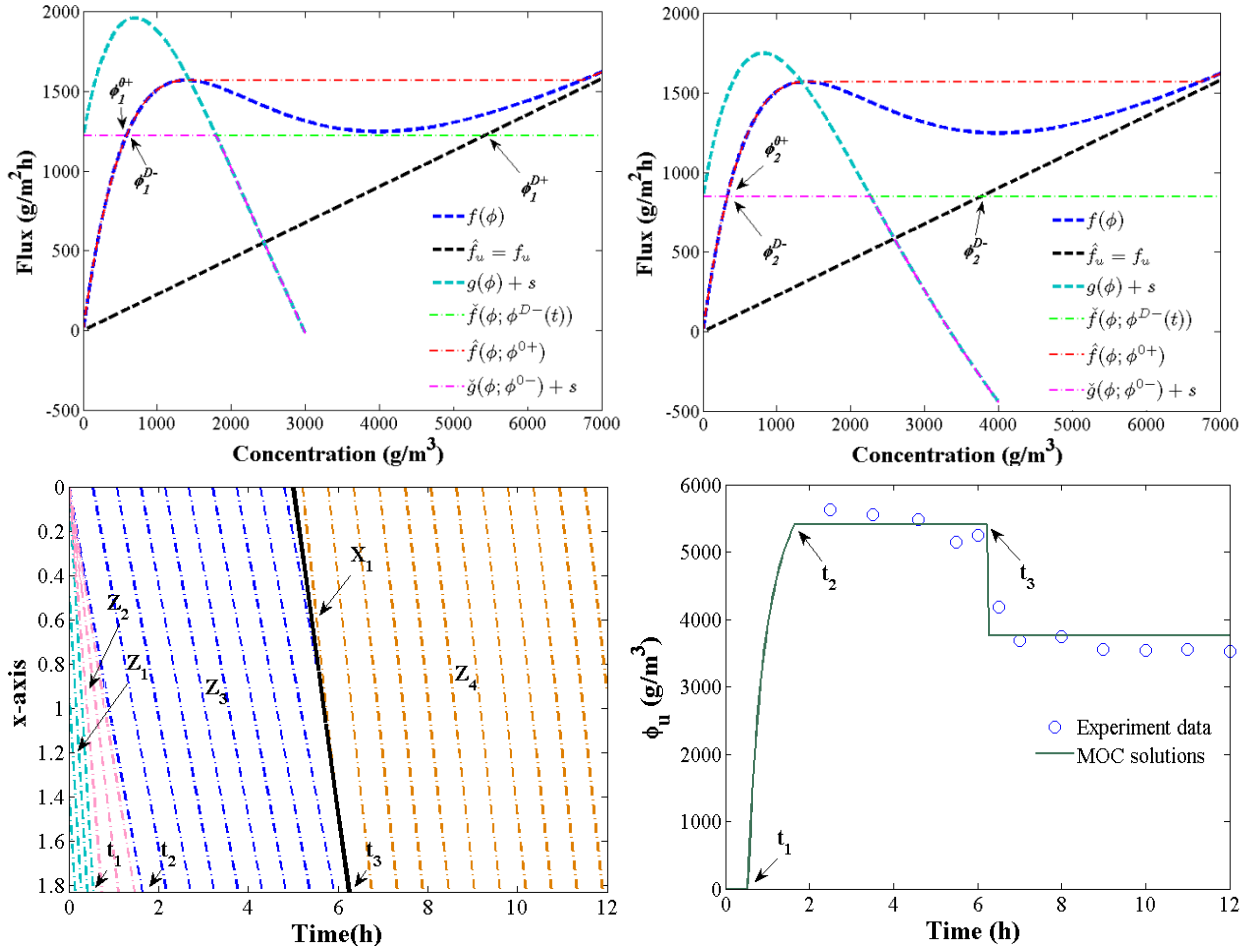
Fig.4.2 - Top: flux and auxiliary functions of the first underloading operation (left); flux and auxiliary functions of the second underloading operation (right). Bottom: MOC solutions of the underloading-underloading transients (left); the MOC prediction of the recycle concentration compared with the experiment observation (right).

4.4.2. Underloading-to-overloading

The SST is filled with liquid as before in the underloading-to-underloading case, thus making the initial value as 0. The underloading condition is imposed by continuously feeding the tank with the constant ferric hydroxide flow (ϕ_f=1.28 kg/m^3, s_1=0.81 kg/(m^{2}h)). Fig.4.3 (top left) shows the graphs of flux and auxiliary functions used to construct boundary concentrations. The unique inlet boundary concentrations are ϕ_1^{0+} =0.32 kg/m^3 and ϕ_1^{0-} =0 kg/m^3, determined by the

intersection of $\hat{f}\left(\phi;\phi^{0+}\right)$ and $\breve{g}\left(\phi;\phi^{0-}\right)+s$ ($\phi^{0+}=\phi^{0-}=0$). Solutions are shown in Fig.4.3 (bottom) in terms of characteristics and discontinuities. Z_1(characteristic slope= $f'\left(\phi_1^{0-}\right)$) and Z_3 (characteristic slope= $f'\left(\phi_1^{0+}\right)$) are constant solution regions with solutions as 0 kg/m^3 and 0.32 kg/m^3 respectively. The expansion wave (Z_2) between Z_1 and Z_3 includes all the concentrations between $\phi^{0+}=0$ kg/m^3 and $\phi_1^{0+}=0.32$ kg/m^3, and solutions within Z_2 can also be uniquely determined by eq.(4.15). The recycle concentration (ϕ^{D+}) generally increases from 0 to ϕ_1^{D+}(4.9 kg/m^3) after the expansion wave reaches the bottom, and can be calculated by eq.(4.16) as well. Therefore, the steady-state boundary concentrations are: the inlet boundary $\phi_1^{0+}=0.32$ kg/m^3 and $\phi_1^{0-}=0$ kg/m^3; the bottom boundary $\phi_1^{D+}=4.9$ kg/m^3 and $\phi_1^{D-}=0.32$ kg/m^3.
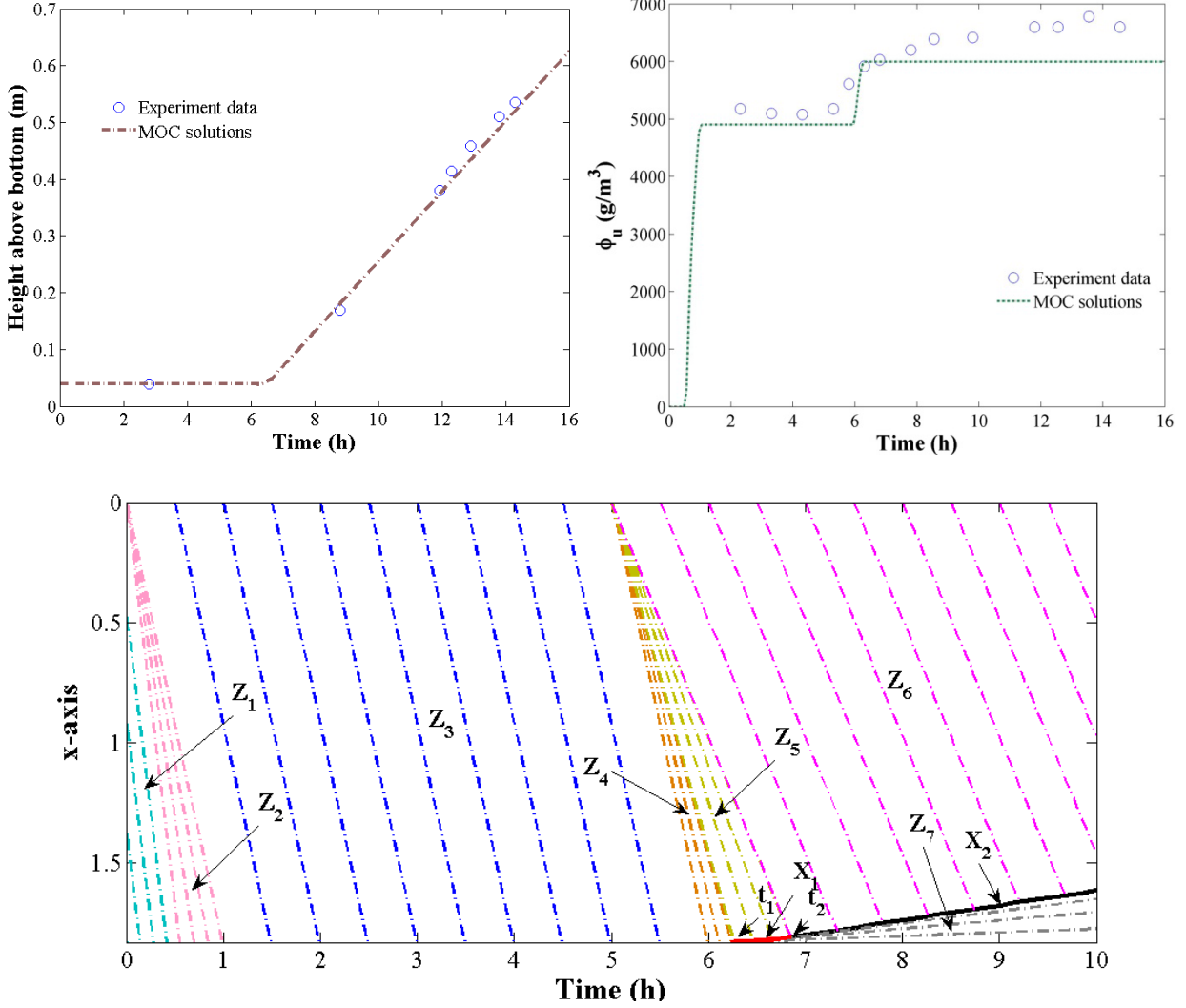
Fig.4.3 - Top: flux and auxiliary functions of the first underloading operation (left); flux and auxiliary functions of the second overloading operation (right). Middle: MOC prediction of sediment interface compared with the experiment observation (left); the MOC prediction of the recycle concentration compared with the experiment observation (right). Bottom: MOC solutions of the underloading-overloading transients.

At t=5 h, the tank is overloaded by increasing ϕ_f to 1.435 kg/m^3 (s_2=1.22 kg/(m^{2}h)). The intersection of $\hat{f}\left(\phi;\phi_1^{0+}\right)$ and $\breve{g}\left(\phi;\phi_1^{0-}\right)+s$ indicates that the inlet boundary concentrations changes to ϕ_2^{0+} = 0.62 kg/m^3 and ϕ_2^{0-} =0 kg/m^3, see Fig.4.3 (top right). Since $f'\left(\phi_1^{0+}\right)>f'\left(\phi_2^{0+}\right)$, both Z_4 and Z_5 in Fig.4.3 (bottom) are expansion wave regions, at which solutions can be determined by eq.(4.15), but they differ in the recycling concentration (ϕ^{D+}) change. Similar as

Z_2, Z_4 causes the recycle concentration increase from ϕ_1^{D+} to ϕ_2^{D+} (6.0 kg/m³). However, at $t=t_1$ (6.32 h), when Z_5 reaches the bottom, instead of continuously increasing the recycle concentration, a contact discontinuity $(X_1(t))$, emanates from point (D,t_1), and propagates towards the inlet ($x=0$). Therefore, after t_1, the recycle concentration remains as ϕ_2^{D+} (6.0 kg/m³). The solution below X_1 increases from ϕ_I to ϕ_2^{D-} , and the solution above X_1 increases from ϕ_L (the smaller solution of $f(\phi)=f(\phi_2^{D-})$) to ϕ_2^{0+} as Fig.4.3 (top right) shows. Complete analytical solution construction requires the determination of the formula of $X_1(t)$, the most significant but also most challenging task. Denote ϕ^{X_1-} ($\phi_L \leq \phi^{X_1-} \leq \phi_2^{0+}$) and ϕ^{X_1+} ($\phi_I \leq \phi^{X_1-} \leq \phi_2^{D-}$)as the left and right solution limits at discontinuity X_1, which satisfy eq.(4.18):

$$f'\left(\phi^{X_1+}\right) = \frac{f\left(\phi^{X_1+}\right) - f\left(\phi^{X_1-}\right)}{\phi^{X_1+} - \phi^{X_1-}} \tag{4.18}$$

Starting from (6.23,1.83), X_1 (t) can be defined by eq.(4.19):

$$\frac{X_1(t) - 0}{t - 5} = f'\left(\phi^{X_1-}\right)$$
$$\frac{dX_1(t)}{dt} = f'\left(\phi^{X_1+}\right) \tag{4.19}$$

Since $f'\left(\phi^{X_1+}\right)$ can be approximated as a linear function of $f'\left(\phi^{X_1-}\right)$ with $R^2=0.998$, as Fig.4.4 (left) shows, the formula of $X_1(t)$ can be determined by the following procedure:

$$\frac{dX_1(t)}{dt} = 0.1235 * \frac{X_1(t) - 0}{t - 5} - 0.1823 \Rightarrow \begin{cases} X_1(t) = \lambda * (t-5)^{0.1235} - 0.208 * (t-5) \\ (1.83, 6.23) \end{cases} \Rightarrow$$
$$\Rightarrow X_1(t) = 2.0332 * (t-5)^{0.1235} - 0.208 * (t-5)$$

At (1.808,6.853), the intersection of X_1 and characteristics emanating at (0,5) with slope $f'(\phi_2^{0+})$, X_1 is replaced by the discontinuity X_2, which emanates tangentially from X_3. The formula of X_2 can be easily determined as $X_2(t) = X_1'(t_2)*(t-t_2)+1.808$, $t_2 = 6.853$. Z_6 is a constant solution zone with $\phi(t,x) = \phi_2^{0+}$. The solution in Z_7 is determined by characteristics emanate tangentially from X_1, and for any point (x_{z_7}, t_{z_7}) in Z_7, the corresponding tangent point ($X_1(t^*)$, t^*) can be determined by eq.(4.20):

$$X_1'(t^*) = \frac{x_{z_7} - X_1(t^*)}{t_{z_7} - t^*}$$
(4.20)

To accurately solve eq.(4.20), numerical techniques, for example Newton's method (Traub 1964), are needed to solve nonlinear equations. And then, the solution at (x_{z_7}, t_{z_7}) is solved based upon eq.(4.21):

$$f'\left(\phi\left(x_{z_7},\ t_{z_7}\right)\right) = X_1'(t^*)$$
(4.21)

103
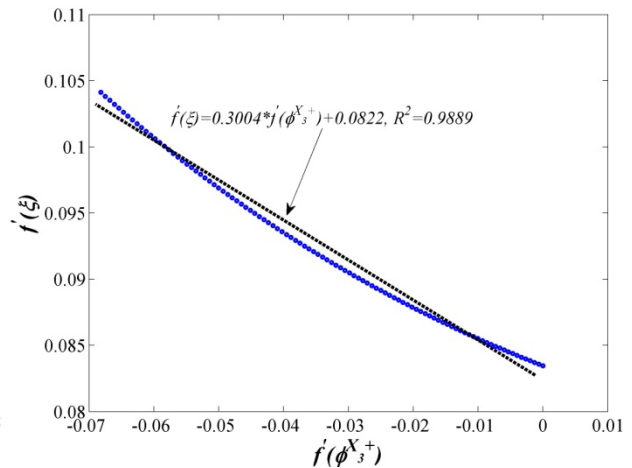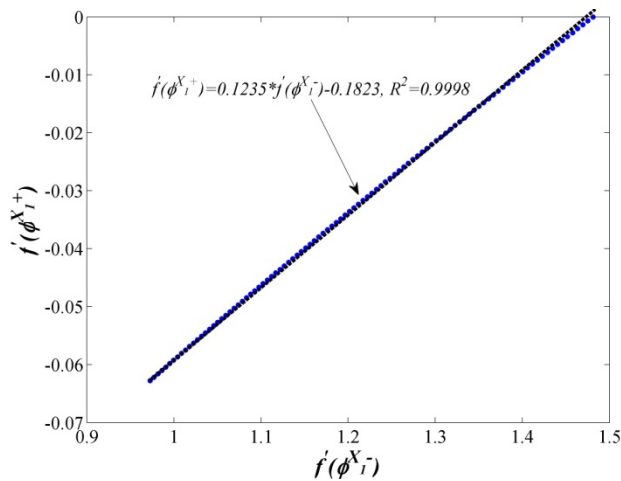
Fig.4.4 - Approximating $f'\left(\phi^{X_1+}\right)$ as a linear function of $f'\left(\phi^{X_1-}\right)$ in underloading-overloading transient (left); approximating $f'(\varepsilon)$ as a linear function of $f'\left(\phi^{x_3+}\right)$ in overloading-underloading transient (right).

Fig.4.3 (middle left) demonstrates the accuracy of MOC solution in sediment interface (solution discontinuities) prediction by comparing with experiment data. MOC solutions can also capture the change of recycling concentration as shown in Fig.4.3 (middle right). However, the recycling concentration (6.0 kg/m^3) predicted by MOC solution in overloading condition is smaller than the experiment observation (6.6 kg/m^3). This incongruity can be attributed to the fact that the coning effect (onset of coning at the bottom of tank increases the recycling concentration but not greatly impact continuous settling behavior) and compression effect (compression effect caused by the sediment with high solids concentration produces a more concentrated recycling flow) are magnified in overloading condition, which is not considered in the ideal continuous settling model.

4.4.3. Overloading-to-underloading

Since settling characteristics of solids in the overloading-underloading transient cannot be adequately described by the collected batch settling data (Tracy 1973, George and Keinath 1978) , the measured sediment interface level and recycle concentration data can be no longer used to test the MOC solution accuracy. In this case, the Vesilind parameters remain the same, and the tank operating parameters are given by Table 4.2.

To simplify the overloading problem analysis, the initial concentration is assumed to be the constant ϕ_0 (0.94 kg/m^3) which determined by eq. (4.22) in the thickening zone, and the constant ϕ_0 (0 kg/m^3) in the clarification zone, which means the overloading will cause a sludge blanket

rise in the thickening zone as time progresses, but no clarification failure in the clarification zone.

$$f\left(\phi_0\right)=\phi_f \frac{\left(Q_e+Q_u\right)}{A}=s_1 \qquad (4.22)$$

Similarly, the inlet boundary concentrations are determined by the intersection of $\hat{f}\left(\phi;\phi^{0+}\right)$ and

$\breve{g}\left(\phi;\phi^{0-}\right)+s$ as ϕ_1^{0+} =0.94 kg/m^3 and ϕ_1^{0-} =0 kg/m^3, as Fig.4.5 (top left) shows. It is noticeable

that since $\phi_0=\phi_1^{0+}$ ($f'\left(\phi_0\right)=f'\left(\phi_1^{0+}\right)$), Z_1 is a constant solution zone with the solution as ϕ_1^{0+}

(0.94 kg/m^3), and the contact discontinuity X_1 emanates from bottom at t=0 h, and propagates

towards the inlet as a straight line. Denote the left and right solution limits of X_1 as ϕ^{X_1-} and ϕ^{X_1+}.

ϕ^{X_1-} equals to ϕ_1^{0+}, and ϕ^{X_1+} can be determined by eq.(4.23) (Ballou 1970, Diehl 2000):

$$f'(\phi^{X_1+})=\frac{f\left(\phi_1^{0+}\right)-f\left(\phi^{X_1+}\right)}{\phi_1^{0+}-\phi^{X_1+}} \qquad (4.23)$$

Therefore, the formula of X_1 is $X_1=f'(\phi^{X_1+})*t+1.83$. Below X_1, the concentration increases from

ϕ^{X_1+} to ϕ_1^{D-}, and the recycling concentration remains as ϕ_1^{D+} (4.98 kg/m^3) until t_2, as shown in
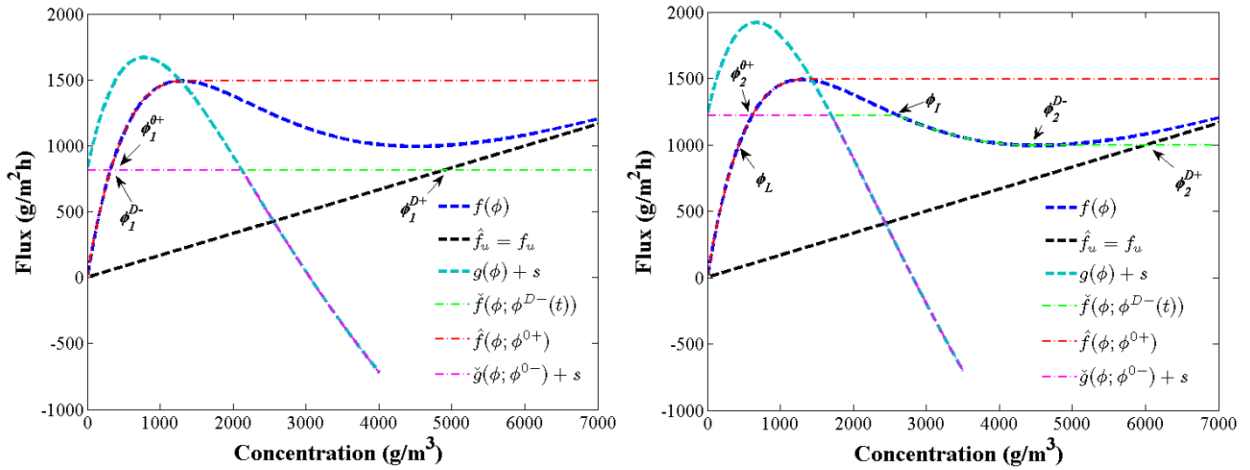
Fig.4.5 (bottom).
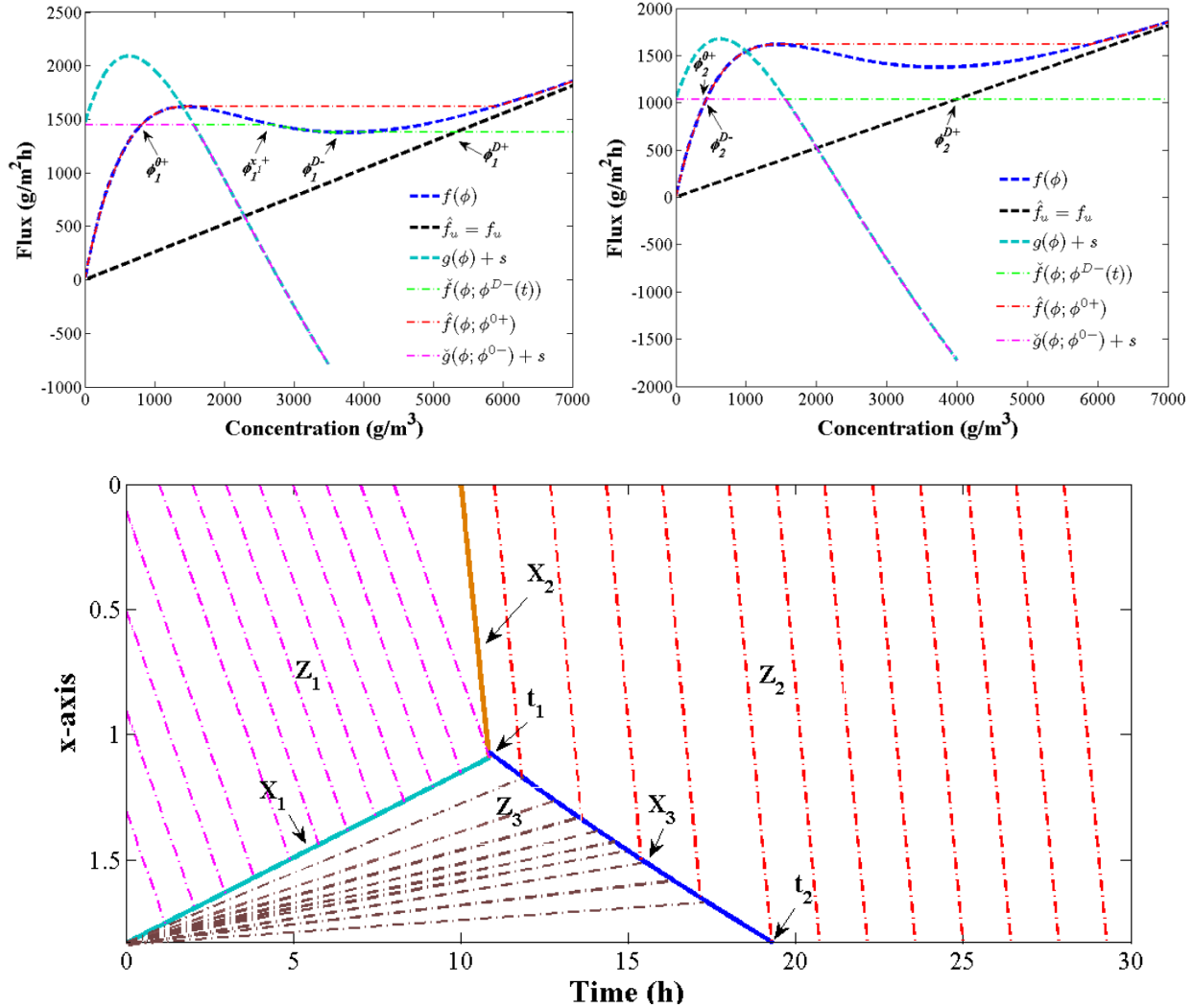
Fig.4.5 - Top: flux and auxiliary functions of the first overloading operation (left); flux and auxiliary functions of the second underloading operation (right). Bottom: MOC solutions of the overloading-underloading transients.

At t=10 h, the operating condition is changed to underloading, and correspondingly, the inlet boundary concentrations change to ϕ_2^{0+} (0.45 kg/m^3) and ϕ_2^{0-} (0 kg/m^3), as Fig.4.5 (top right) shows. Since $f'\left(\phi_2^{0+}\right) > f'(\phi_1^{0+})$, a solution discontinuity ($X_2(t)$) originates at point (0,10), and propagates towards bottom. The formula of X_2 is $X_2(t) = X_2' *(t\text{-}10)$, where

$$X_2' = \frac{f\left(\phi_2^{0+}\right) - f\left(\phi_1^{0+}\right)}{\phi_2^{0+} - \phi_1^{0+}}$$ (4.24)

Z_2 is a constant concentration zone with the solution of ϕ_2^{0+}. At $t=t_1$ (*10.83* h), the interaction of X_1 and X_2 at (1.1, 10.83) generates the third discontinuity $X_3(t)$. Denote the left and right solution limits of X_3 as ϕ^{X_3-} and ϕ^{X_3+}. ϕ^{X_3-} equals to ϕ_2^{0+}, while ϕ^{X_3+} is in the range of ϕ_I and ϕ_1^{D-}. $X_3(t)$ is governed by eq.(4.25):

$$\frac{dX_3(t)}{dt} = \frac{f\left(\phi^{X_3-}\right) - f\left(\phi^{X_3+}\right)}{\phi^{X_3-} - \phi^{X_3+}} = f'(\varepsilon)$$

$$\frac{X_3(t) - 1.83}{t - 0} = f'\left(\phi^{X_3+}\right)$$ (25)

where ε is between ϕ^{X_3-} and ϕ^{X_3+}. Fig.4.4 (right) shows that $f'(\varepsilon)$ can be approximated as a linear function of $f'\left(\phi^{X_3+}\right)$ with R^2=*0.9889*. Hence, the formula of X_3 can be determined by the following procedure:

$$\frac{dX_3(t)}{dt} = -0.3004 * \frac{X_3(t) - 1.83}{t - 0} + 0.0822 \Rightarrow \begin{cases} X_3(t) = \dfrac{1.83 * t + 0.0632 * t^2}{t} + \dfrac{\lambda}{t^{0.3004}} \Rightarrow \\ (1.1, 10.83) \end{cases}$$

$$\Rightarrow X_3(t) = \frac{-2.8113 * t + 1.83 * t^{1.3004} + 0.0632 * t^{2.3004}}{t^{1.3004}}$$

The solution in Z_3 can be determined by solving eq.(4.26) :

$$f'\left(\phi\left(t_{z_3}, x_{z_3}\right)\right) = \frac{x_{z_3} - 1.83}{t_{z_3} - 0}$$ (4.26)

4.5. Convergence analysis and efficiency comparison of numerical methods

Although MOC has been successfully implemented to develop analytical solutions, as shown previously, its application as an alternative solution technique in commercial simulators remains as a challenge for two reasons: 1). the model formula cannot always be expected to have analytical solutions, especially when it is extended to capture more physical phenomena, such as the hydrodynamic dispersion and the compression effects; 2). MOC's theoretical complexity requires considerably more effort to implement in engineering practice. Therefore, numerical solution techniques are often needed to provide accurate results.

Applied mathematical investigations have led to several alternative numerical methods, represented here by Method G based on the Godunov numerical flux (Jeppsson and Diehl 1996, Diehl and Jeppsson 1998), Method EO based on the Engquist-Osher numerical flux (Bürger et al. 2005), and Method YRD, a total variation diminishing (TVD) method based on flux-limit technique (Li and Stenstrom 2014a). All these numerical methods are expected to be reliable, which means they produce approximate solutions that converge to the exact solutions as the discretization is refined (Bürger et al. 2012). However, due to the difficulty of proving convergence, only the convergence of Method EO has been proven by Bürger *et al.* (2005). An approach to evaluating the accuracy of the other methods is to use solutions generated by solving the model formula with Method EO at extreme high discretization level, such as 2430-layer (Bürger et al. 2012) and use this as the reference for other solutions. The successful implementation of MOC, in this study, provides another alternative approach of using analytical solutions as reference solutions.

Since the convergence of Method EO has already been proven, we did not include it in the convergence test, but added another alternative method: Method SG (simplified Godunov), which was originally proposed by Bürger *et al.* (2012, 2013). As the name implies, Method SG is derived from Method G, and eq. (4.27) compares methods G and SG, for the thickening zone.

$$F_{i+1/2}^G = \begin{cases} \min_{C_i \leq C \leq C_{i+1}} \left(v_s \phi + v_u \phi \right) & \text{if } \phi_i \leq \phi_{i+1} \\ \max_{C_{i+1} \leq C \leq C_i} \left(v_s \phi + v_u \phi \right) & \text{if } \phi_i > \phi_{i+1} \end{cases}$$

$$F_{i+1/2}^{SG} = \begin{cases} \min_{C_i \leq C \leq C_{i+1}} \left(v_s \phi \right) + v_u \phi & \text{if } \phi_i \leq \phi_{i+1} \\ \max_{C_{i+1} \leq C \leq C_i} \left(v_s \phi \right) + v_u \phi & \text{if } \phi_i > \phi_{i+1} \end{cases}$$

(4.27)

where i is layer index; F^G is the Godunov numerical flux; F^{SG} is the simplified Godunov numerical flux. As can be seen, both of Method G and Method SG are based on Godunov numerical flux, but differ in the numerical flux application: Method G applies the Godunov flux to the total flux, while Method SG applies the Godunov flux only to the nonlinear settling flux ($v_s\phi$); the linear bulk flux ($v_u\phi$) is unchanged. This adjustment leads to a simplification in determining the local extrema: Method G, Method EO, Method YRD require keeping track of two local extremum of the total flux function, which may vary with the change of underflow rate, while Method SG only requires the determination of only one local extrema that does not vary with underflow rate, thus making Method SG easier to implement with the algorithm given by Bürger *et al* (2013).

To evaluate convergence, various model outputs have been obtained using a reliable solution technique, which are then used as a reference solution. For example, Bürger *et al.* (2012) used the concentration profile from Method EO to validate Method G. In this study, the sludge blanket level is selected for comparison for two reasons: 1). sludge blanket level is one of the most

significant model outputs for system robustness evaluation; 2). the shock path (sludge blanket level) function developed by MOC can be directly applied to test the shock capturing accuracy, generally the most challenging task in a numerical solution. The spatial and time steps are same for all three methods, and the discretization level starts at 40-layer as Jeppsson and Diehl (1996) recommended. Solutions of the underloading-overloading scenario (scenario 1) and overloading-underloading scenario (scenario 2) as shown in Table 4.2 are solved with Methods SG, G and YRD to demonstrate and compare their convergences.

The sludge blanket levels for both loading conditions at discretization levels of 40, 100 and 200-layer by Methods SG, G and YRD are shown in Fig.4.6, and compared with the MOC solution. As can be seen, all these three methods are able to track the change of the sludge blanket level regardless of the discretization level. For each method, the approximate solution for 40-layer deviates most from the reference, but as the discretization increases (increasing number of layers), the approximate solutions converge to the reference solutions, as demonstrated. The convergence rate with increasing discretization is rapid at first, but greatly decreases as the number of layers approaches 500, which is most evident in the Method SG simulation results.

Even though Fig.4.6 qualitatively shows that all three methods are able to converge to reference solutions, at least in these two scenarios, it does not mean they are equally efficient in practical engineering applications. An efficient numerical method is defined as high in approximation accuracy and low in computation cost. To further quantify the efficiency of these three alternatives, computation cost is characterized by the required CPU time, and accuracy is evaluated using the error measurement defined in eq.(4.28)

$$e_h = \frac{\sum_{j=1}^{m} (\left| h_j^N(t) - h_j^R(t) \right| / h_j^R(t))}{m} \qquad (4.28)$$

where e_h is the averaged relative error in sludge blanket level; j is the time index; m is the overall time step used; h denotes the sludge blanket level; N is the discretization level, and R denotes the reference solution. The amount of required memory can also be important in defining efficiency, but it is not important in this case since the needed memory can be provided by a typical desk top computer.
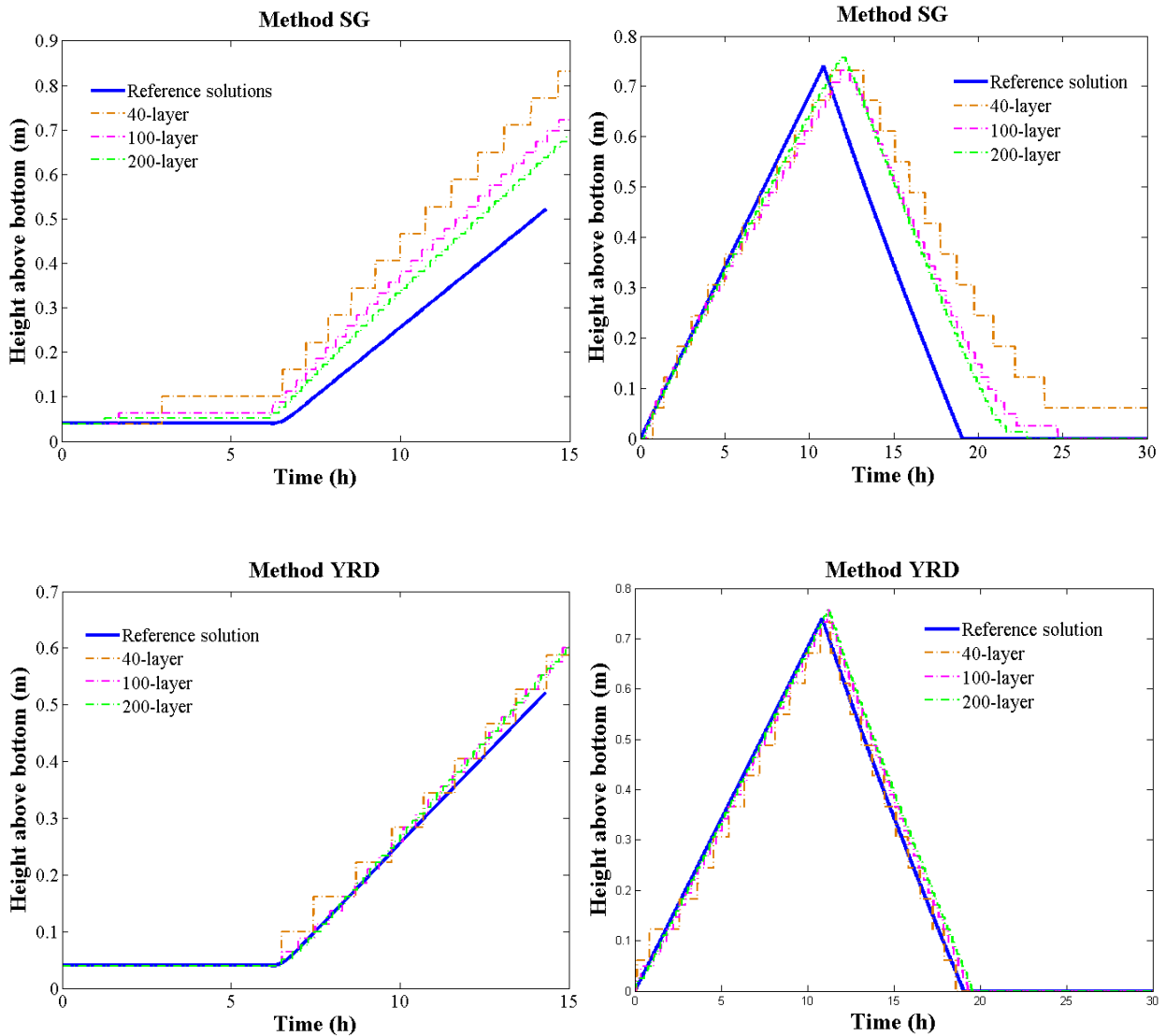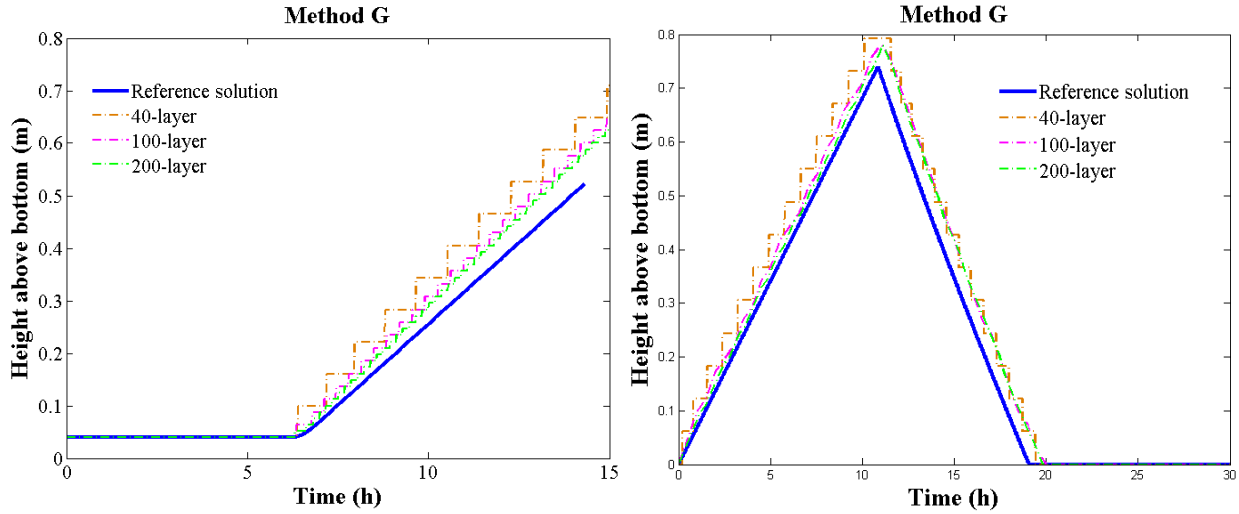
Fig.4.6 - Comparison of solution convergences for Methods SG, YRD and G (top to bottom, respectively) for the two cases of under loading-to-overloading and overloading-to-under loading (left to right, respectively) at *N*=40,100,200.

Fig.4.7 (left) shows the e_h change with increasing discretization, and quantitatively confirms the conclusion made previously that for these three methods, increasing discretization can effectively improve the quality of numerical solutions, but yields diminishing returns when using a large number of layers. Method YRD shows the most relative improvement with increased number of layers, but its absolute accuracy is much greater that Method G and SG for any fixed *N*. For example, Method YRD using 40-layer has approximately the same accuracy as Method G using 200-layer and much more accurate than Method SG using 200-layer. This difference in accuracy can be attributed to the fact that Method YRD possesses second-order accuracy in both smooth and discontinuous regions, while Method G is first-order accurate. At the same discretization level, Method SG can be no more accurate than Method G because the simplification in numerical flux that facilitates implementation results in increased numerical errors (Bürger et al. 2012, Li and Stenstrom 2014a).
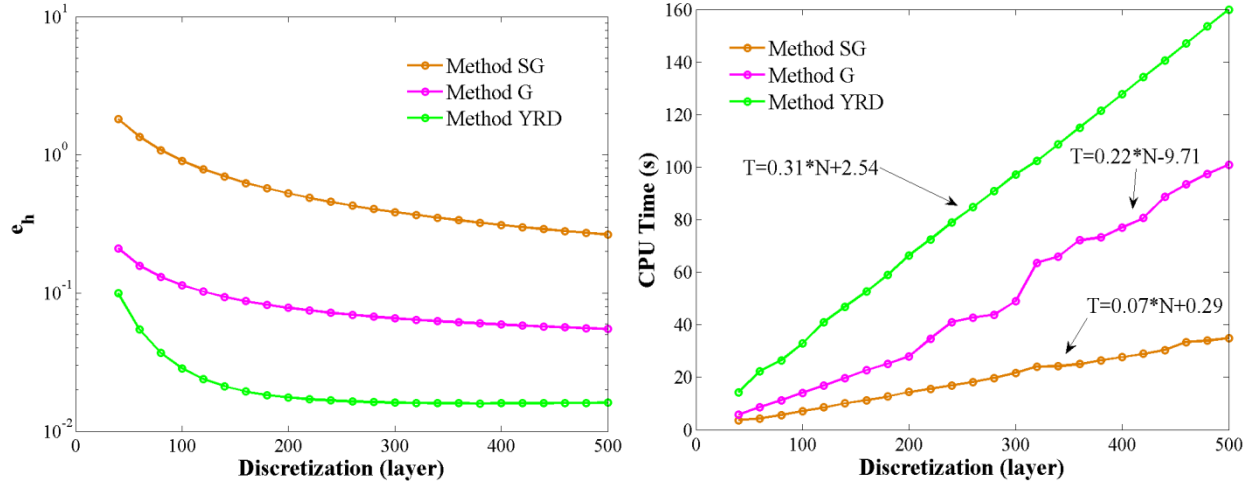
Fig.4.7 - Errors of the underloading-overloading transient simulation at various layer numbers (left); CPU times of the underloading-overloading transient simulation at various layer numbers (right).

Nevertheless, Method YRD's error reduction is at the cost of more computation, which is quantitatively indicated by the increase of CPU time shown in Fig.4.7 (right); less CPU time means fewer computations and faster simulations. Method SG produces approximations faster than the other two methods for any given N. If CPU time is further approximated as a linear function of the discretization, the rate of computation increase for Method YRD, Method G and Method SG is 0.31 s/layer, 0.22 s/layer, 0.07 s/layer, respectively, which implies that Method YRD requires much more computations than the other two. For example the computation cost of Method YRD at 100-layer equals to it of Method G at 197-layer and Method SG at 475-layer. It seems that we might be able to continuously refine the discretization of Method G and Method SG to make them as accurate as Method YRD in numerical calculation but with the same or even less computation cost. Nevertheless, this strategy is questionable for two reasons: 1) continuously refining discretization requires smaller time steps to guarantee calculation stability, which may invalidate the observed linear relations and make the real computation cost much

more than the predicated one; 2) as shown in Fig.4.6 (left), the rate of error decrease with increasing discretization decreases. Methods SG and G will require greater levels of discretization to obtain a specified accuracy. The choice of method will depend upon the required accuracy and the availability of computing resources.
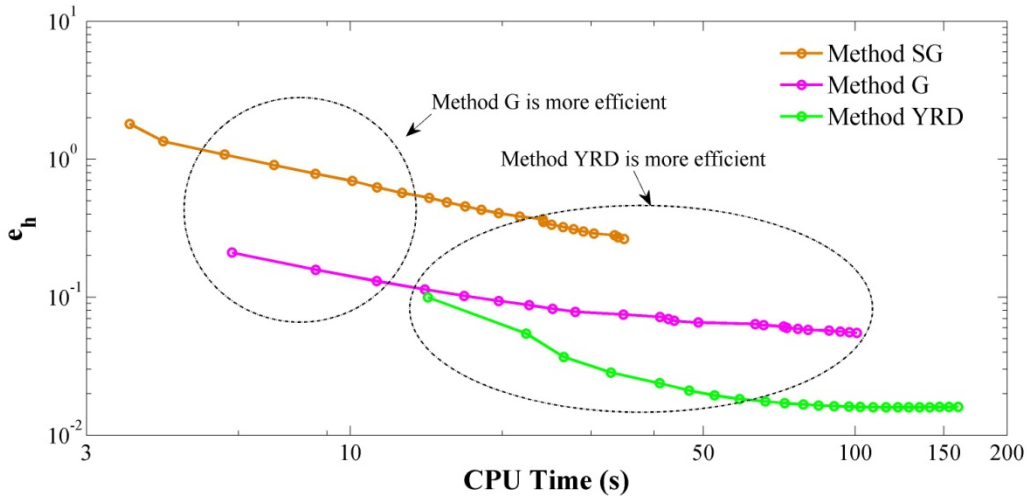
Fig.4.8 - Efficiency lines (error *vs.*CPU time) of Methods SG, G and YRD for different layer numbers.

Fig.4.8 shows the efficiency line of each method based Fig.4.6. If the computation cost is the priority (CPU time < *20*s), Method G and Method SG can be the only two alternatives, and Method G is more efficient than Method SG as its efficiency line lies below that of Method SG. However, if the accuracy is the priority ($e_h<10^{-1}$), Method YRD is the most efficient one regardless of its high implementation complexity. The implementation complexity (complexity of the computer code) of the three methods cannot be included in Fig.4.8, since it is difficult to quantify. Based on our knowledge, more accurate calculation of the numerical flux usually complicates implementation; the simplification of the Godunov numerical flux calculation makes the implementation of Method SG much easier than it of Method G, while the flux limited technique

114

used in Method YRD to ensure a second-order accuracy can greatly increase the implementation complexity.

4.6. Conclusion

Accurately solving the ideal continuous settling model is challenging because of solution discontinuities. As the only available method for analytical solution development of ideal continuous settling model, the method of characteristics has been successfully implemented to investigate the dynamics of SST for three typical solids loading transients: underloading-underloading, underloading-overloading and overloading-underloading. The comparison of experiment continuous settling data and MOC solutions demonstrates that the ideal continuous settling model solved by MOC can accurately predict the recycle concentration and sediment interface change at various operation conditions. However, because of the complexity of implementing MOC, further studies are required to develop more efficient implementation strategies.

To avoid the complexity of MOC, alternative solution techniques are available but have not been extensively verified as to convergence and efficiency. By using the MOC solution as reference, the convergence analysis of Methods SG, G, and YRD shows that all are reliable, since they are able to provide arbitrary close approximations to the reference solutions as discretization is refined. An efficiency comparison based upon three completing principles: easy implementation, high accuracy and low computation cost is provided. For a given discretization level, Method YRD is most efficient in reducing error, and provides the most accurate approximations. However, this advantage of high accuracy of Method YRD is at the cost of larger computation time and coding complexity when compared with Methods SG and G. The simplified numerical

flux calculation technique used in Method SG increases error, but greatly reduces the coding complexity and computation cost. Method G performs well in both accuracy and computation cost comparisons. Therefore, the selection of the most desirable numerical solution technique depends on the ease of implementation, accuracy and computation cost.

5. Dynamic 1-D modeling of SSTs and design impacts of sizing decisions

5.1. Introduction

Biological secondary treatment processes are widely used in wastewater treatment plants to remove organic matter and reduce nutrients such as nitrogen and phosphorus. In all cases, efficient operation requires the sludge to be removed from the wastewater by sedimentation, filtration or other solids-liquid separation processes.

For sedimentation to be successful, the biomass must be composed of large particles or flocs, which have sufficient settling velocity to be removed in a settling tank of manageable size. To achieve this goal, it is necessary to grow the biomass to select floc-forming organisms as well as understanding solids-liquid separation processes (Parker, et al. 2004).

Several types of treatment processes can achieve the solids-liquid separation, but secondary settling tanks (SSTs) are most commonly used. SSTs, also known as sedimentation basins or solids-liquid separators, use gravity to separate the biomass from the fluid, and have two similar but distinct functions: clarification and thickening. Clarification is the removal of finely dispersed solids from the liquid to produce a low turbidity effluent; Thickening is the process of increasing the sludge concentration in order for it to be recycled or disposed in less volume. In SSTs, the clarification process occurs in the upper zone while thickening occurs near the bottom. The result is an effluent from the top, low in suspended solids, and a second stream of settled, concentrated solids from the bottom, suitable for recycling or disposal.

As one of the most important units in wastewater treatment process, the SST is often a "bottle neck," limiting the capacity of the wastewater treatment process (Ekama et al. 1997b, Ekama and

Marais 2002b). The SST sizing must be combined with the bioreactor sizing to guarantee the minimum necessary performance to meet the design basis, as well as maintaining required efficiency for contaminant removal. If the SST does not remove solids from the effluent, or fails to produce a recycle stream, process failure occurs with effluent permit violations and loss of biomass from the reactor. Therefore, two commonly used parameters: overflow rate and solids flux, have been developed for SST design and evaluation.

Nevertheless, given the fact that the wastewater characteristics vary, such as flow rate and contaminant concentrations, traditional design procedures for SSTs tend to be more empirical and conservative by introducing averaged parameters with safety factors (Coe and Clevenger 1916). Therefore SST performance can suffer unanticipated fluctuations, which may cause process control problems and increase the risks of failure. Stringent standards for effluent quality and the need for optimization of WWTP performance have made such variations in effluent quality undesirable, and have encouraged the use of dynamic controls for wastewater treatment process. For the purpose of developing such an automatic control system to provide consistent effluent water quality, great effort has been made to create accurate mathematic descriptions of wastewater treatment process (mathematical models), and the one-dimension (1-D) SST model for predicting the time dependent responses to transient process inputs of SSTs is a good example.

1-D SST models, based on solids-flux theory (Kynch 1952), describe sludge transport by a scalar conservation partial differential equation (PDE). Although many 1-D SST models are available and some of them, especially Takács model (Takács et al. 1991), have been widely utilized in engineering practice, the predication of the sludge settling characteristics and concentration

profiles in and out of a SST is still far from satisfactory.

The presently available 1-D models are highly dependent upon empirical equations to express clarification, thickening and compaction process and these equations or functions can be an error source that can profoundly affect simulation results. A second challenge is the difficulty of making full-scale measurements in working SSTs that has caused a lack of data sets for model calibration and verification. As a consequence, further research is still needed to improve the performance of the 1-D model.

The first goal of this chapter is to review the previous, major developments in SST design and analysis to show how they have been used to develop 1-D models. The second goal is to review the 1-D models especially with regard to the numerical methods used to solve the resulting PDE, and to provide an improved method for solving the PDE. The final goal is to show how the 1-D model can be used in the design process to better understand the interaction between bioreactor and SST, particularly with regard to dynamic inputs, such as the time-to-failure after a shock load or appearance of filamentous bulking organisms.

5.2. Background

5.2.1. Flux theory and state point analysis

As theoretical foundations of solids-liquid separation, flux theory and state point analysis are widely used in SST studies, such as SST design, capacity analysis, and optimizing daily operations. For the purposes of quantifying biosolids settling characteristics, the starting point of both flux theory and state point analysis is usually the batch settling test. Table 5.1 lists the major contributors to solids flux theory and shows that Coe and Clevenger (1916) performed one of the

119

earliest batch settling studies. Their major contribution was a comprehensive method to understand and utilize batch settling test results, and confirm SSTs' limited capacity in clarification/thickening, now known as limiting flux theory.

Because of the difficulty in analyzing the details of forces on particles during sedimentation, a complete theoretical analysis of solids settling cannot be completed. Though Coe and Clevenger's method was widely accepted, it was still considered an empirical rather than a "first-principles" analysis. One of the most well-known theoretical analyses was given by Kynch (1952), also shown in Table 5.1. Kynch approached the problem by introducing a simple but critical assumption that hindered settling velocity is only determined by the local solids concentration, thus making the solids concentration the dominant factor in sedimentation processes. The solids transport then can be calculated using mass flux ($\Phi = v_s C$, a function only related to *C*), which is the rudiment of flux theory. Therefore, the batch settling process can be mathematically expressed as a continuous function based on scalar mass conservation law:

$$\frac{\partial C}{\partial t} + \frac{\partial (v_s C)}{\partial z} = 0 \tag{5.1}$$

Talmage and Fitch (1955, 1962) interpreted Kynch's result by suggesting the slope of the tangent to the interface subsidence curve of a batch settling test was equal to the settling velocity of the layer with the same solid concentration. Their experimental results matched Kynch's theory.

However, one remaining question in flux theory was whether the free settling velocity obtained in laboratory scale batch settling conditions can accurately represent the observed velocity in the full-scale continuous SSTs, since batch settling can be affected by various factors, such as the size of cylinders, wall effects, the non-uniform shape and size particles. Dick *et al* (1967, 1970)

compared batch settling processes with similar initial concentrations in different sized cylinders, and recommended using a slow speed mixer to offset the wall effect and reduce lag time. Tory and Shannon (1965) investigated the non-uniform shape and size problem by using Gaussian distribution spheres, and found that zone settling was independent of particle shape and size.

Yoshioka *et al* (1957a) and Hassett (1958) independently developed two widely accepted graphical methods of analyzing batch flux data on the basis of flux theory. The former plots the gravity flux only, while the later shows on both gravity and total fluxes. However, both of them use batch test results for continuous settling predication, such as underflow solids concentration and limiting flux, thus making the SST performance predictable.

One of the most well known concepts in flux theory is a limiting flux that is normally used to estimate SST solids handling capacity. Thickening and clarification failure may occur when the solids loading flux exceeds the limiting flux, which can be caused by either hydraulic shock loading or deterioration of settling characteristics. Keinath (1985) extended flux theory, creating what has become known as state point analysis, by integrating clarification requirements into the flux diagram. State point analysis considers feed flow rate, underflow rate and feed solids concentration, and is now routinely used for operation analysis of activated sludge systems and solids inventory control strategies. Table 5.1 summarizes the major advances of these pioneering studies and summarizes the contribution of each researcher.

Table 5.1- Major contributions to SST behavior analysis and comments.

Author	Major contribution	Comments
Coe and Clevenger (1916)	Conducted one of the earliest batch settling tests and developed a comprehensive method to understand and utilize batch settling results.	Their work connected batch settling tests and continuous settling study, and had a profound impact on the SST studies for the first half of the 20th century.
Kynch (1952)	Assumed that gravity settling velocity is only determined by the local solids concentration, and mathematically expressed the mass conveyance as a partial differential equation (PDE).	The velocity assumption made the settling process mathematically describable, thus greatly improving the understanding of solid-liquid separation.
Talmage and Fitch (1955)	Suggested the slope of the tangent to the interface subsidence curve of a batch settling test was equal to the settling velocity of the layer with the same solid concentration, and developed a procedure to obtain the settling velocity information.	It was one of the earliest ramifications of Kynch theory, and the batch settling velocity can be easily determined. The accuracy of this procedure was highly depended on the determination of the compression point.
Yoshioka *et al* (1957) Hassett *et al* (1958)	Independently developed two widely accepted graphical methods of analyzing batch flux data (the gravity flux and bulk flux), and the flux analysis was related to a concentration profile in SST.	Both are convenient methods to estimate several significant parameters, such as underflow solids concentration and limiting flux, therefore making the SST performance predictable.
Shannon and Tory (1965) Dick *et al* (1967)	Recommended using a slow speed mixer to offset the wall effects and to reduce lag time, and showed that the batch settling results were independent to the initial settling height, the particles' shape and size.	Since the free settling velocity obtained in batch settling tests can represent the observed velocity in full-scale continuous SST, the batch settling results can be used as reference of continuous SST deign and control.
Keinath (1985)	Extended the flux theory to the state point analysis, a comprehensive analysis of the relationships among various operating parameters (MLSS, overflow rate, underflow rate *et al*)	The state point analysis provided a fundamental description of solids handling characteristics of the SST, and could be used to develop effective SST control strategy and optimize its performance.

Nomenclature

A	cross-sectional area of SST [m^2]
C	sludge concentration [g/m^3]
C_{min}	non-settleable solids concentration [g/m^3]
C_T	total ASP cost [dollar]
G	flux [g/(m^{2}h)]
G_s	gravity settling flux [g/(m^{2}h)]
h	SST inlet depth [m]
H	SST depth [m]
H_s	Sludge blanket level [m]
n	Veslind settling parameter [m^3/kg]
Q	flow rate [m^3/h]
r_h	Takács settling parameter [m^3/kg]
r_p	Takács settling parameter [m^3/kg]
R_c	relative cost coefficient
S	biodegradable substrate concentration [g/m^3]
v	settling velocity [m/h]
v_0	Veslind settling parameter [m/h]

V	bioreactor volume [m^3]
$v_{0,\,max}$	Takács settling parameter [m/h]
v_s	hindered settling velocity [m/h]
t	time [h]
z	height above SST bottom [m]

Greek letters

Φ	flux [g/(m^{2}h)]
Φ_l	limiting flux [g/(m^{2}h)]
μ/Y	F/M ratio ((kg BOD$_5$/kg MLSS) d^{-1})

Subscripts

e	effluent
f	feed
i	index of model layer
in	incoming
u	underflow
w	waste

Superscripts

n	index of time

5.2.2. Modeling of continuous settling process

The previous discussion traced the development of flux theory for SSTs and all the analyses were steady state analysis. To extend these results to more realistic conditions, a dynamic procedure is needed. Considerable efforts have been made to develop dynamic models to better understand and predict SST performance. Bryant (1972a) improved Kynch's batch continuity equation by adding extra terms to simulate the bulk mass thickening near the SST bottom and established the following fundamental model structure:

$$\frac{\partial C}{\partial t} + \left(v_u + \frac{\partial (v_s C)}{\partial C} \right) \frac{\partial C}{\partial z} = 0 \tag{5.2}$$

However, Bryant realized that the eq. (5.2) cannot predict a limiting flux and solids overloading condition without proper PDE solver.

Tracy (1973) developed an inventory model by dividing the SST into clarification, dilution, thickening, and compression zones. Tracy adjusted the volume of each zone to conserve mass and adhere to the limiting flux by using solids concentrations calculated from Hasselt's flux graphing method. The utility of his model is the ability to simulate overloading by adjusting the thickening zone volume to represent sludge blanket level rise as a function of solids overloading, and even predicting time-to-failure with continued overloading. The limitation of this model is its inability to dynamically change concentrations in each zone as a function of hydraulic changes. It is interesting to note that Tracy never actually solved eq. (5.1) or (5.2).

Stenstrom (1976b) modified Bryant's model eq.(5.2) in order to make it conform to the limitations of solids flux theory by using an empirical constraint eq. (5.3) on gravity settling flux.

$$G_{s,i+1/2} = \min\left(v_{s,i}C_i, v_{s,i+1}C_i\right) \tag{5.3}$$

He divided the SST into layers or finite differences, and limited the solids flux out of each layer into the lower layer. Fluxes were calculated from the batch settling velocity relationship, and an upper layer was limited to the flux that the lower layer could pass. The constraint, while based on a physical concept, does have a theoretical basis, since it satisfies a mathematical principle called 'consistent', which means the numerical flux should be a function related to adjacent layers instead of the local single layer (Bürger et al. 2011). Vitasovic (1986b) found this constraint may cause oscillations at low concentrations, and recommended to setting a threshold concentration below which the constraint is not active. He chose 3,000 g/m^3 and noted the value is site specific. The best well-known work using Stenstrom and Vitasovic's work is the Takács model (Takács et al. 1991), which has become the most widely used 1-D SST model.

Although the studies discussed above have partially solved the one-dimension SST modeling problem, the increasingly strict standard for WWTPs stability and reliability calls for efforts to provide more accurate and practicable continuous models; and approaches to improve model quality can be identified into two categories: improvements to the numerical solution technique, and more accurate description and implementation of the sedimentation mechanism.

The settling model, a typical nonlinear hyperbolic PDE, is not easy to solve because of possible solution discontinuities, which are difficult to detect. Authors (Jeppsson and Diehl 1996, David et al. 2009a, Bürger et al. 2011) have discussed better methods for providing more reliable solutions of eq. (5.2).

In addition to the gravity and hydraulic flux, other effects can also influence continuous settling

process: for example dispersion, compression, density currents and short-circuiting. Several approaches now are available to estimate possible impacts. Dispersion is usually modeled by a second-order dispersion term (Watts et al. 1996, Plósz et al. 2007, Bürger et al. 2011), and compression is caused by solid-solid and solid-water interaction in a high concentration zone, and modeled by the second-order compression term (De Clercq et al. 2008). Usually, 1-D models have difficulty in accounting for hydraulic flow impacts, but the density current and short-circuiting are predictable with inlet height and feed flow rate adjustment (Dupont and Dahl 1995).

5.3. Model improvement

5.3.1. Model structure development

The SST is idealized as one dimension with constant cross-sectional area, no net organism growth, no density currents and no short-circuiting. Therefore the SST feed solids concentration can be assumed to equal the bioreactor solids concentration.

Other effects, such as dispersion and compression affect SST performance, but modeling them can greatly increase the model's complexity. Therefore, to maintain the model complexity at a reasonable level for practical application, in this study, the model mathematic expression is determined, giving

$$\frac{\partial C}{\partial t} + \frac{\partial \left(v_s C - v_e C \right)}{\partial z} = 0 \qquad \textit{above the inlet layer} \qquad (5.3)$$

$$\frac{\partial C}{\partial t} + \frac{\partial \left(v_s C + v_u C - v_e C \right)}{\partial z} = v_f C_f \qquad \textit{the inlet layer} \qquad (5.4)$$

$$\frac{\partial C}{\partial t} + \frac{\partial \left(v_s C + v_u C \right)}{\partial z} = 0 \qquad \textit{below the inlet layer} \qquad (5.5)$$

A relationship between the C and v_s is required. Based on Kynch's settling velocity assumption (Kynch 1952), two commonly used functions are Vesilind's equation (Vesilind 1968a) and the double-exponential equation (Takács et al. 1991):

$$v_s = v_0\, \mathrm{e}^{-nC} \tag{5.7}$$

$$v_s = \max\left(0, \min\left(v_{0,\max}, v_0\left(e^{-r_h(C - C_{\min})} - e^{-r_p(C - C_{\min})}\right)\right)\right) \tag{5.8}$$

Both of equations are suitable in hindered settling zone, while Vesilind's equation may overestimate the settling velocity at low solids concentration (Li and Ganczarczyk 1987, David et al. 2009a). Therefore, the double-exponential formulation is used in this study.

The sludge settling velocity parameters are site specific and depend upon the condition of the biomass (i.e., filaments or no filaments, etc). For this chapter, the data collected by Stenstrom (1976b) and Tracy (1972) were used. The measurement error has been checked to be Gaussin and uncorrelated. Therefore, the estimation used the Levenberg–Marquardt algorithm (More 1978a). The results are shown as normal sludge in Table 5.2.

For most situations where an SST is overloaded, the limit occurs because of the rise of the sludge blanket in the hindered settling zone, which is less than the gel point concentration. Compression settling only occurs near the SST bottom region, which can impact the sludge blanket level rise and sludge recycling. However, the rise in the compression zone usually does not limit operation. In cases where more thickening is involved, such as with gravity thickeners, modeling this compression zone will be more important. Notice that the major improvement of this model is the use of reliable numerical techniques, and the solids settling description still follows the double-exponential formulation, which is not designed for compression settling modeling.

Several researchers (Buscall and White 1987, Cacossa and Vaccari 1994, Bürger 2000, Kinnear 2002, De Clercq et al. 2008, Gladman et al. 2010b) have studied the compression zone, and provided approaches and guidance for modeling two-phase flow and compression settling.

5.3.2. Numerical discretization and integration

The first-order nonlinear hyperbolic PDE mathematic structure can produce numerical discontinuities during the calculation. However, computing these discontinuities generates severe challenges, since numerical oscillations may occur near the discontinuous point.

Though great efforts have been done to improve model solution accuracy, problems still remain. For example, when using the flux constraint (Stenstrom, 1976) the result is sensitive to the number of discretization layers used in the model, and can cause numerical oscillation at low concentrations; Both Godunov's first-order method and Engquist and Osher's upwind method routinely treat every part of numerical solutions same, regardless of how these solutions behave, thus causing a sharp tradeoff between accuracy and stability.

In this study, the SST model is improved by introducing a second-order accurate total variation diminishing (TVD) numerical technique- the Yee-Roe-Davis scheme (Yee et al. 1990), which is specifically designed for the scalar conservation law solving. To capture the solution discontinuity and avoid oscillation across the shock, the solution difference calculation and flux limiter technique are used. For smooth region, the solution difference can be very small, while it can be relative large through the shock. And instead of the straightforward discretization, the flux limiter is used to satisfy the nonlinear stability condition. Eq. (5.9) is used as the flux limiter in this study.

$$\phi\left(r_i^+, r_{i+1}^-\right) = \text{minmod}(1, r_i^+, r_{i+1}^-) \tag{5.9}$$

where

$$r_i^+ = \frac{C_i^n - C_{i-1}^n}{C_{i+1}^n - C_i^n}, \ r_i^- = \frac{C_{i+1}^n - C_i^n}{C_i^n - C_{i-1}^n} \tag{5.10}$$

The explicit Yee-Roe-Davis flux limited scheme is

$$C_i^{n+1} = C_i^n - \frac{\Delta t}{\Delta z}\left(\overline{G}_{i+1/2}^n - \overline{G}_{i-1/2}^n\right) \tag{5.11}$$

where

$$\overline{G}_{i+1/2}^n = \frac{1}{2}\left(G_i^n + G_{i+1}^n\right) + \frac{1}{2}\psi\left(a_{i+1/2}^n\right)\left(\phi_{i+1/2}^n - 1\right)\left(C_{i+1}^n - C_i^n\right) \tag{5.12}$$

$$\psi\left(a\right) = \left\{\frac{a^2 + \delta^2}{2\delta}, |a| < \delta; |a|, |a| > \delta\right\}, \ a = \frac{dG}{dC} \tag{5.13}$$

In this study, δ is determined as 10^{-20}. As a solution sensitive technique, the Yee-Roe-Davis technique is able to determine what to do in terms of the solution gradient rather than considering the solution's stability and accuracy in the same way throughout the entire solution domain. Therefore, the improved model can work well at both discontinuity and smooth regions simultaneously with small tradeoffs.

Given the fact that solids concentration depends on two variables (z, t), discretization is required for both time axis and spatial axis: the SST is divided into several layers with equal height, volume and a uniform concentration within the layer. Specifying the number of layers must be

done carefully, because it greatly impacts the calculated concentration profile (Jeppsson and Diehl 1996). Sensitivity to the number of layers is a numerical artifact; the solution should be independent of the number of layers. Hence, a favorable 1-D model is required to be consistent with respect to number of layers. Fig.5.1 shows discretization sensitivity of the improved model and Takács model in a solids overloaded simulation.
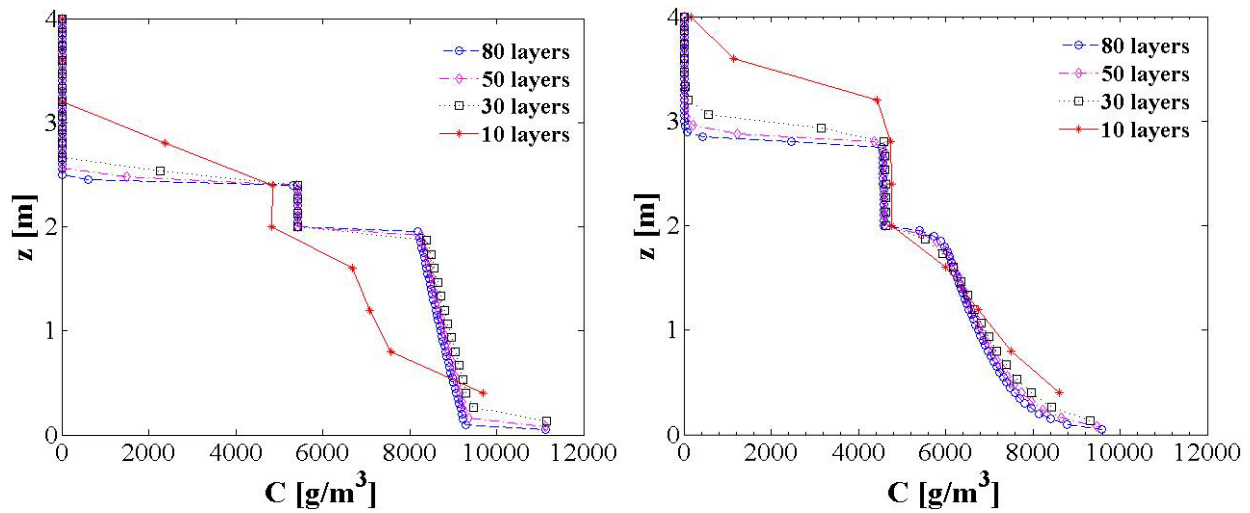
Fig.5.1 - Typical overloading concentration profiles of different discretization levels.

(left: the improved model; right: Takács model)

5.3.3. Numerical solution accuracy

For the SST modeling, what interests us most is the SSTs' response to solids overloading, since effluent violations are likely to occur with solids overloading. To evaluate sensitivity, we created a hypothetical but typical overloading condition (A=100m^2, C_f=4000 mg/l), with normal settling parameters as shown in Table 5.2. As can be seen from the predicted concentration profiles (Fig.5.1), both models are able to detect the sludge blanket propagation regardless of the number of layers, but the results diverge with differences in the sludge blanket level, solids concentration in each layer and the recycling solids concentration. The Takács model predicts a higher sludge

blanket height (~3m), while the improved model has a larger solids concentration in each layer, including the bottom layer. Using the Yee-Roe-Davis technique as PDE solver, the improved model more accurately predicts the discontinuities at the edges of the blankets. It is also important to notice the overestimation of the sludge blanket height (~3 m versus ~2.5 m) that may lead to designing for a larger SST area, to accommodate the excessive blanket height.

Table 5.2 - Parameter sets of ASP design and gravity settling velocity (normal and deterioration).

Parameter set of ASP design		Parameter set of settleability		
Q_f	260		Normal sludge	Deterioration
Q_e	200	$v_{0,max}$	20	20
Q_u	60	v_0	9.63	9.63
S_{in}	300	r_p	0.01	0.01
F/M	0.3	r_h	0.00063	0.003
H	4	C_{min}	10	12
h	2			

5.3.4. Layer number sensitivity test

Fig.5.1 is the solids concentration profile for four different layer-number conditions. Except for the case of 10 layers, no obvious differences within each model's results can be observed. Clearly, 10-layer is not enough for either model. The 10-layer model, especially for the Takács model, predicts too much sludge storage within the SST. When the model layer number exceeds 30, the

predicted concentration profiles within each model, will be similar.

5.3.5. Model verification of SST responses to solids flux overloading

In current engineering practice, the underflow solids concentration and the sludge blanket level predications are the two key 1-D SST model outputs, since they are closely related to ASP system robustness and contaminant removal efficiency. To further investigate the model performance, the data collected by Tracy (1973) in continuous ferric hydroxide suspension settling is introduced for both the Takács model and the improved model verification. The response of the height of the sludge blanket level and the predicted and actual underflow solids concentration are shown in Fig.5.2. For the sludge blanket level predication, the improved model simulation (6.82 cm/h) closely approximates the actual sludge blanket rising rate (6.71cm/h), while the Takács model predication is 7.25 cm/h, which agrees well with the conclusion above that the Takács model overestimates the sludge blanket level. The underflow solids concentration predicted by the Takács model ($5850g/m^3$) is also much smaller than the measured concentration, as expected. The improved model provides a steady state value $6480g/m^{3,}$ which is virtually the same as the measured value $6650g/m^3$, and the underflow concentration change tendency predicated by the improved model is more rapid than data. These incongruities can be explained by the impact of compression settling. Because of the compression settling impact, the thickening process will be retarded during the initial solids overloading period, which can accelerate the sludge blanket rise and decelerate the underflow concentration increasing rate. However, with the sludge blanket increase, the weight of the overlying sludge in the compression zone promotes thickening, which can decelerate the sludge blanket rise but can accelerate the increase in underflow concentration.
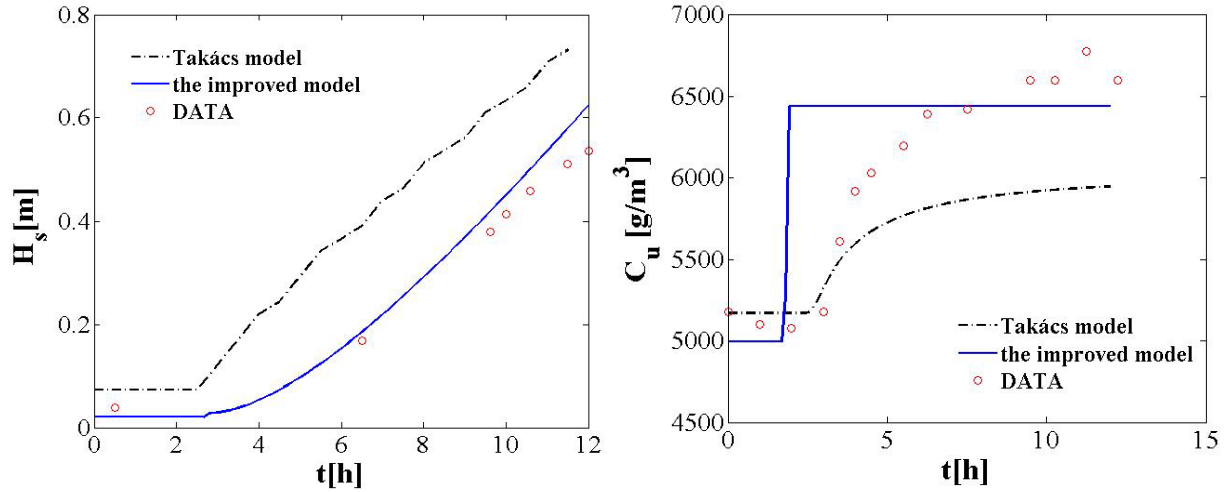
Fig. 5.2 - SST response to step increase in influent solids flux (Data from Tracy, 1973).

5.4. Practical model application

5.4.1. Activated sludge process design

Mathematic models including ordinary differential equations (ODEs) for bioreactor and PDEs for SST are frequently used for activated sludge process (ASP) design and evaluation (Diehl and Faras 2012). Here, we present a traditional ASP design to demonstrate practical value of the improved SST model. Assume that dissolved oxygen in bioreactor is sufficiently high; the bioreactor is completely mixed; Q_w and S at steady state are much smaller than Q_e and S_0, respectively. Design parameters and sludge settling parameters (normal sludge) are given in Table 5.2.

The substrate mass balance around the bioreactor yields the following ODE:

$$V\frac{dS}{dt} = Q_e S_{in} - (Q_e - Q_w)S - Q_w S_w - \frac{\mu}{Y}C_f V \tag{5.14}$$

Sedimentation process in SST is modeled by a series of PDEs, eq. (5.4~5.6). At steady state, S_{in}, Q_e, V, F/M ratio are constant, and Q_w and S are much smaller than Q_e and S_0. Thus, the steady

133

state C_f can be expressed as:

$$C_f = \frac{Q_e S_{in}}{V(\mu/Y)}$$ (5.15)

In solids flux theory, the SST solids input is defined as the operating flux, and the maximum SST solids handling capacity must equal to or be less than the limiting flux. To maintain ASP stability and reliability, process loading at critical or under loading conditions is preferable, which means operating flux must be less than or equal to the limiting flux. Otherwise, thickening or clarification failure may occur. In this study, we set this requirement as a safety constraint safeguarding ASP efficiency and stability, and express it as the following inequality:

$$\frac{(Q_e + Q_u)}{A} \cdot \frac{Q_e S_{in}}{V(\mu/Y)} \leq \Phi_l$$ (5.16)

If steady state Q_u is also set as a constant 30% of Q_e, Φ_l can be obtained from the graphic total flux method (Hassett 1958) for various areas indicated in Fig.5.3. A restricted range (100-400 m^2) was evaluated which is within the proper overflow rate (0.5-2 m/h). As a result, the bioreactor volume and SST area are the two only variables in this inequality, and their effect on process performance can be plotted.

5.4.2. Selection of different-sized ASP

Various combinations of V and A can satisfy the safety constraint, so three extra criterions are established to evaluate the quality of the design:

1. Economic plausibility;

2. Contaminants removal efficiency at steady state;

3. Robustness to solids overloading;

Most ASP cost optimizations treat the designed treatment capacity as the dominant components, while few recognized the capital cost is closely related to reactors' size (Keinath et al. 1977). In this study, the cost estimation strategy follows the latter one, and unit cost of bioreactor and SST are respectively expressed as dollar/m^3 and dollar/m^2 in terms of their volume and area. Providing an explicit cost analysis is beyond the scope of this research, but a hypothetical yet realistic example is achieved by fixing the bioreactor unit cost as 1 dollar/m^3, and then introducing a relative-cost coefficient for SST cost calculation as eq. (5.17):

$$C_T = 1 \cdot V + R_c \cdot A \tag{5.17}$$

The relative cost coefficient will vary and be site specific, and three typical values (1, 1.5, 3) are selected here (David 1968).

At steady state, the biomass distribution between the bioreactor and SST will reach equilibrium. Total biomass in the reactor is an important factor in contaminants removal evaluation, and retaining most biomass in bioreactor is preferable for maximizing overall treatment efficiency. The steady state C_f is solved by the following ODE:

$$\frac{dC_f}{dt} = \frac{C_u Q_u - C_f Q_f}{V} \tag{5.18}$$

Here, we only discuss the contaminant removal efficiency in the underloading condition, because it is most prevalent. A typical underloading condition is modeled by fixing Q_e=100 m^3/h, half of the designed capacity with a simulation time interval as 3 h.

Though the safety constraint considerably improves system stability and reliability, SST may still experience failure problems attributed to two chief causes: hydraulic shock loading and deterioration of sludge settleability. The time-to-failure or failure time is defined as the time interval between the beginning of an upset and failure, and can be used as an important indicator for process robustness evaluation. Obviously, a longer time-to-failure indicates a more robust process. All variations are imposed as step functions in solids overloading endurance test:

- Hydraulic shock loading: At t=0 h, Q_e=200 m^3/h to reach steady state. At t=2 h, Q_e is increased from 200 m^3/h to 800 m^3/h, four times of the designed flow rate.

- Slurry settleability deterioration: Q_e is fixed as 200m^3/h. At t=0 h, the settling parameters are set to normal as shown in Table 5.2. At t=2h, the settling velocity parameters change to deterioration (Table 5.2) in order to simulate a change to poor settleability condition (e.g., bulking).

5.5. Process size results and discussion

5.5.1. ASP unit sizes

Fig.5.3 shows the limiting flux decreasing with increasing SST area. This occurs because a larger area provides smaller hydraulic bulk flux towards SST bottom. A smaller limiting flux does not simply mean less reliability, because enlarging the SST's area meanwhile decreases the operating flux to less than or equal to the limiting flux.
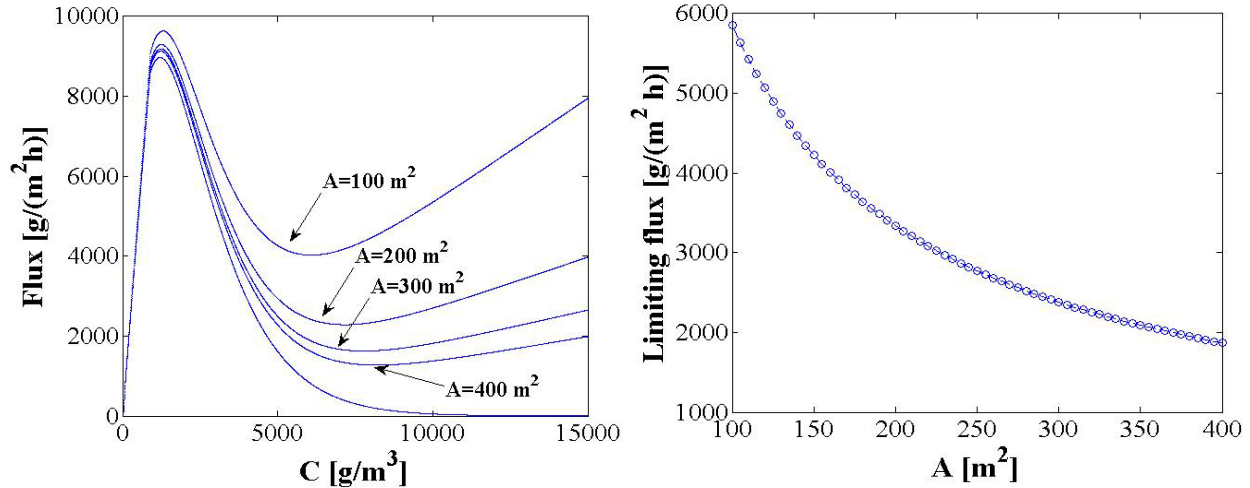
Fig.5.3 - Total settling flux profile (left) and the limiting flux profile (right) in different SST size conditions.

As shown in Fig.5.4 (left), the required volume decreases with increasing area. Adjustment of either bioreactor or SST's size can requires a compensating modification of the other, thereby restricting the whole ASP size.

5.5.2. Economic plausibility

For all relative cost conditions, the system capital cost decreases with the increase of SSTs' area initially, and then increases, therefore an economic optimal point exists, as shown in Fig.5.4 (right). What differs is the location of the least cost point. The relative cost is a significant weighting factor greatly impacting the relative size of bioreactor and SST, and a large relative cost shifts the economic optimal point toward the smaller SST surface area. If economic plausibility is the only consideration, the least cost point reduces capital investment (10~20% reduction). However, an important consideration is whether the least cost design can provide sufficient contaminant removal and simultaneously avoid solids overloading failures, which we will discuss in the next section.
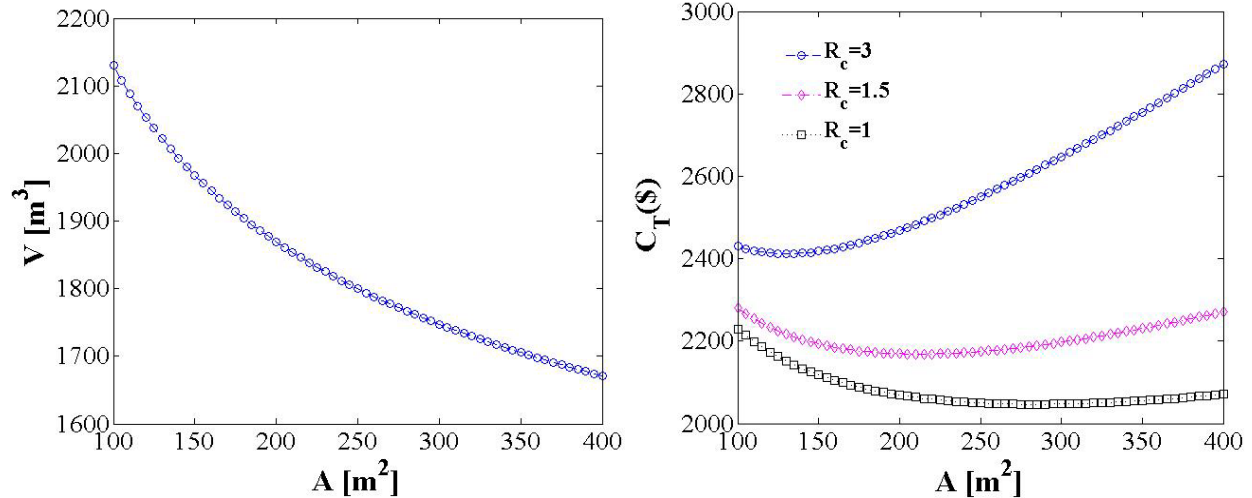
Fig.5.4 - Scale relationship between SSTs and bioreactors (left) and total cost of alternative ASP designs in three typical relative cost conditions (right).

5.5.3. Overall treatment efficiency

In an underloading condition, biomasses are shifted from bioreactor to SST, and finally reach a balance. And as shown in Fig.5.5 (left), the stored biomass amount in larger SSTs is 2 to 3 times more than it in smaller ones.

Nevertheless, the gradient of SST biomass storage actually has little effect on the total slurry distribution: the maximum SST biomass is no larger than 5% of the total. This indicates that all alternatives (A=100~400m^2) are able to retain most biomass (95~98%) in bioreactors. Additionally, since the total biomass amount is almost the same, there is no significant difference in the total bioreactor biomass storage regardless of the small variations in the SST biomass storage. This implies all alternative ASP designs can meet the high overall treatment efficiency requirement.
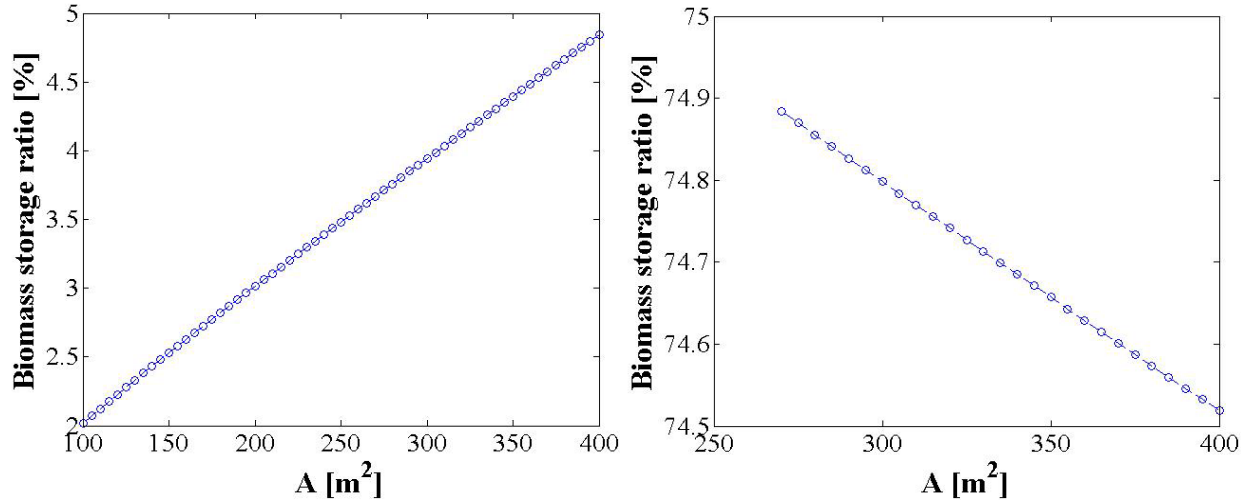
Fig.5.5 - SST biomass storage ratio in underloading steady state (left) and large size SST biomass storage ratio when the flux loading statues changes from overloading to critical loading (right).

5.5.4. System robustness evaluation

A lengthy time to reach biomass distribution equilibrium between bioreactor and SST implies a more stable process, since a longer time to reach equilibrium provides more time to respond in the event of an overload. This section illustrates this point by evaluating the time-to-failure of a 20-h hydraulic shock loading simulation (Fig.5.6 left) and deterioration of sludge settleability (Fig.5.6 right).

It is notable that the estimated time-to-failure provided by Takács model is much smaller than what the improved model predicts. This corresponds well to the conclusion presented earlier in the numerical accuracy section of this chapter that the Takács model overestimates the sludge blanket height due to numerical inaccuracies. This shortage can eventually cause a conservative design. For instance, the Takács model shows for a hypothetical hydraulic shock loading, the SST surface area should be at least 285 m^2 to provide sufficient capacity, while the improved model indicates 195 m^2 is sufficient.

139
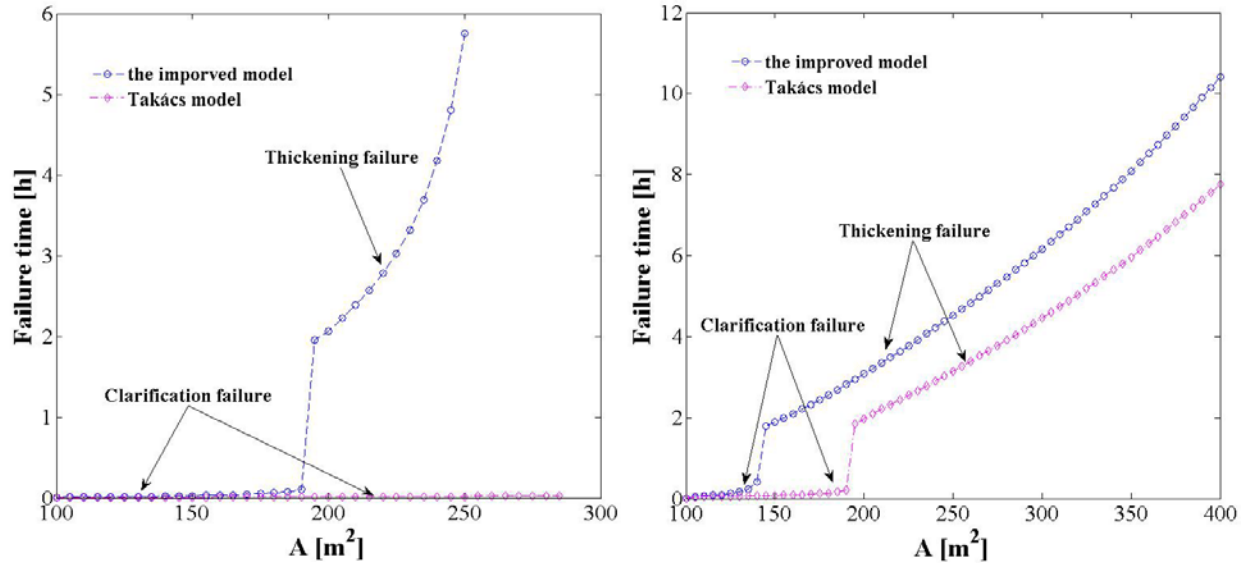
Fig.5.6 - SSTs' time-to-failure corresponding to hydraulic shock loading (left) and settleability deterioration (right).

The time-to-failure predicted by the improved model can be used for system robustness analysis. According to Fig.5.6 (left), the hydraulic shock loading failure time of smaller SST alternatives (A=100 to 185 m^2) is less than 0.1 h. It increases to 2-5.8 h, a great improvement in overloading endurance, when SSTs are enlarged to medium size (A=190 to 260 m^2). No failure will occur if the SST is larger than 260 m^2. Fig.5.7 presents the 20-h dynamic biomass accumulation processes in small, medium and large SSTs (A=120, 230, 350 m^2). For the case of a small SST, most biomasses are directly conveyed to the clarification zone by the overflow instead of settling to the thickening zone, causing a clarification failure in less than 0.1h. This helps explain why small SSTs have extremely short time-to-failure. A gradual sludge blanket rise is observed in medium SSTs, and causes a thickening failure when it reaches the inlet. An area of 195 m^2 is the demarcation point between clarification failure and thickening failure, and a state point analysis also shows this distinction (Keinath 1985). Compared with a clarification failure, the thickening failure is a relatively slow process as the sludge blanket must rise from the bottom to top, which usually occurs over several hours. If the SST can afford sufficient storage capacity of biomass in

the thickening zone, the solids loading condition can be reduced from overloading to critical loading. This explains why neither clarification failure nor thickening failure occurs when the SST area is greater than 260 m^2. Fig.5.5 (right) shows the biomass distribution for a large, overloaded SST and most (75%) of the biomass is stored in the thickening zone, which is much larger than for the under loaded case (2~5%).

Compared to hydraulic shock loading, where the failure is caused by a sudden increase of operating flux, failure due to poor biomass settleability (sludge bulking), is attributed to a decrease in the limiting flux. In this case, failure can be avoided only by increasing the limiting flux, such as changing the recycle rate or contacting pattern (Stenstrom and Andrews 1979b).

5.5.6. Comprehensive selection

An overall selection of SST size relative to the bioreactor size must include considerations other than capital investment. Simultaneously achieving an economically justifiable sizing, high contaminant removal and system stability can be difficult. It may be tempting to use the least cost alternative, such as an area of 130 m^2 when R_c=3 (Fig.5.4 right), but this selection produces a situation with no ability to tolerate overloading from either a hydraulic shock or deterioration in sludge settling properties. When the SST is less expensive relative to the bioreactor (R_c =1), a larger SST can be provided (A=285m^2) and much greater stability is obtained. Comprehensive selection of ASP design using a 1-D SST model is a tool for the designer to evaluate capital cost, overall treatment efficiency and process stability.
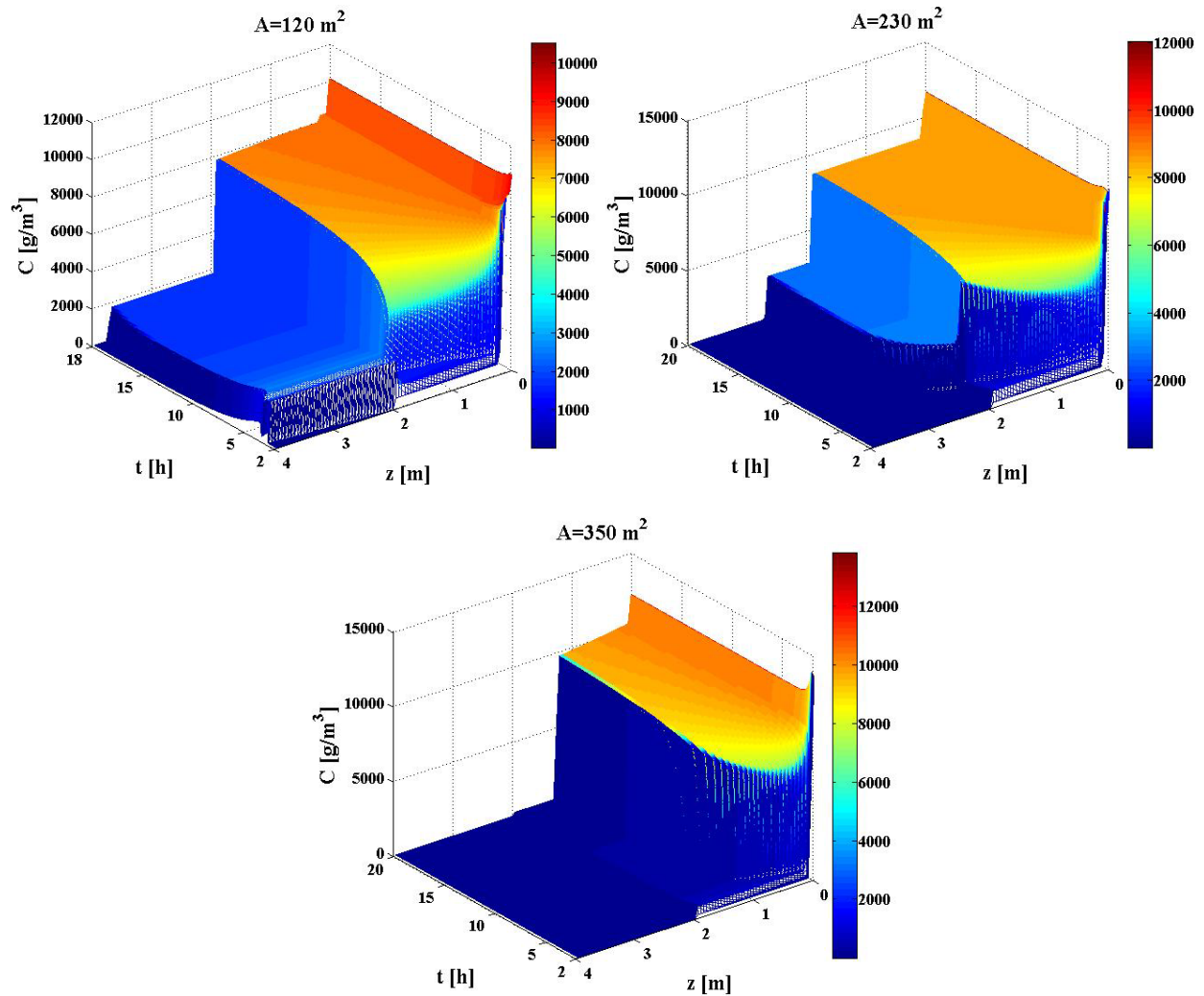
Fig.5.7 - Dynamic solids concentration profiles in hydraulic shock loading for different surface areas: 120 m^2, 230 m^2 and 350 m^2.

5.6. Conclusion

The conclusions of this chapter can be summarized as follows:

- The improved model with solution-sensitive PDE solver can determine the calculation behavior in terms of the solution gradient, therefore providing more numerically and physically acceptable solutions. The discretization level sensitivity test demonstrates that the improved model can provide uniform solids concentration and storage

predication, while Takács' model is sensitive to number of layers, and can even overestimate the sludge blanket level and underestimate the underflow concentration.

- For an activated sludge process design, the bioreactor and SST should be designed as a whole, and a safety constraint can be introduced in the design process to greatly improve the system's efficiency and reliability. The designed alternatives based on the safety constraint show that the requirement of bioreactor volume decreases with an increase of SST size, and this can help to prevent overdesigning the ASP size and land waste.

- A comprehensive selection of the designed alternatives should consider three aspects: economic plausibility, contaminant removal efficiency, and system robustness. Least-cost points can usually be attained, but their locations will vary depending on the weighting of the relative cost factor. In a solids underloading condition, all designed alternatives are able to provide sufficiently high contaminant removal with only 2%~5% total of the biosolids storage in the SST.

- Both hydraulic shock loading and settleability deterioration can cause solids overloading problems. ASPs with small size SSTs may suffer clarification failure in less than 0.1h, and the medial size ones can have a thickening failure problem in 2~5h due to the continuously rising sludge blanket level. If the SST is large enough to store 75% of the biomass in the thickening zone, no failure occurs, and ASP system will be robust. In most cases, it is difficult to prioritize these three criterions, which requires trade-offs for system optimization.

6. A sensitivity and model reduction analysis of 1-D SST models under wet-weather flow and sludge bulking conditions

6.1. Introduction

The activated sludge process is the most widely used technique to remove organic matter and reduce nutrients such as nitrogen and phosphorus in wastewater treatment plants (WWTPs). Generally, efficient solids-liquid separation techniques are needed to provide low turbidity effluent by removing the biomass from the liquid, and the secondary settling tanks (SSTs), where biomass is settled by gravity, are the most commonly used (Li and Stenstrom 2014d). Mathematical modeling approaches, where the activated sludge models, comprised of a set of ordinary differential equations (ODEs), are coupled with the SST models, comprised of a set of partial differential equations (PDEs), are being increasingly used in wastewater treatment process studies for three purposes 1): learning, which means the model simulation results are able to improve the understanding of wastewater treatment process; 2): design, the model can be used to evaluate various design alternatives via simulation, and 3): process optimization and control, simulating different sceneries to optimize the process efficiency and avoid possible failure problems (Hulsbeek et al. 2002, Petersen et al. 2002, Gernaey et al. 2004).

The family of Activated Sludge Models (Henze et al. 1987, Henze et al. 1995, Gujer et al. 1999) provide a comprehensive description of the significant biological processes of the activated sludge system, and are widely accepted in the research and industrial communities as a useful tool for scientific study and practical applications. However, compared with the well-developed scientific knowledge on characterizing the metabolic processes and contaminant removal in the bioreactor, various settling behavior occurring in the SST still remain poorly understood, thus

making the SST model a potential error source in process simulation (Plósz et al. 2011). The one-dimensional (1-D) 10-layer model, also known as the Takács model (Takács et al. 1991), is the most commonly used SST model and has been implemented in most commercial simulators as a reference model. Although the Takács model has achieved a degree of success in predicting the SST performance, its shortcomings are not negligible, such as the insufficient description of various settling behaviors and inaccuracy of numerical solutions, which have been demonstrated in previous studies (Jeppsson and Diehl 1996, Plósz et al. 2011, Bürger et al. 2012, Li and Stenstrom 2014a, Li and Stenstrom 2014b).

In last two decades, to compensate for the limitations of the Takács model, several advanced SST models have been developed as alternatives, which can be classified into three groups based on their advantages:

1. First-order hindered-only models with reliable numerical techniques: for these models, the model formula remains the same as the Takács model, considering only the hindered settling behavior, but using more reliable numerical techniques. Reliable techniques such as the Godunov numerical flux, the Yee-Roe-Davis (YRD) numerical flux, and finer discretization levels (more than 30-layers), are used to construct both numerically and physically acceptable solutions (Jeppsson and Diehl 1996, Li and Stenstrom 2014a, Li and Stenstrom 2015).

2. Second-order hindered-compression models additionally accounting for compression settling: the improved understanding of activated sludge rheology has facilitated the development of phenomenological theory of sedimentation-consolidation. The phenomenological theory is then expressed in the compression model, which allows a more

rigorous description of the compression settling behavior (Bürger 2000, Bürger et al. 2000a). Compared with the hindered-only model, the hindered-compression model is expected to provide more realistic predictions of the sludge blanket level and the underflow concentration.

3. Second-order hindered-dispersion models additionally accounting for hydraulic dispersion: for these models, an explicit hydraulic dispersion term is added to the model formula to account for the potential impact of hydraulics on the biomass settling behavior (Plósz et al. 2007, Ramin et al. 2014a). The hydraulic dispersion model possesses the advantage of simulating the hydraulics of SSTs over a wider range of dynamic flow conditions (Watts et al. 1996, Plósz et al. 2007). From the numerical point of view, adding the explicit flow-dependent dispersion term also decreases the difficulty in solving the hindered-dispersion model.

Recently, a new 1-D SST model, the Bürger-Diehl model (the hindered-compression-dispersion model), has been presented (Bürger et al. 2011), which accounts for phenomena that may impact the SST behavior, such as hindered settling, compression settling and hydraulic dispersion. The Bürger-Diehl model is also based on the reliable numerical solution of its governing model formula by appropriate methods (Torfs et al. 2015). Therefore, the Bürger-Diehl model is able to provide more realistic predictions of the SST performance.

Despite the advantages of the Bürger-Diehl model, its practical application is limited, which can be attributed to two main reasons:

1. The difficulty of calibration: great efforts have been made to facilitate model calibration, for example by evaluating the hindered-only and hindered-dispersion models, Ramin et al.

(Ramin et al. 2014a, Ramin et al. 2014c) identified the potential parameter subsets suitable for the calibration of WWTP models under various simulation conditions. However, calibrating the 1-D SST models accounting for the compression settling still remains a challenge due to the insufficient understanding of the influence of compression settling on the SST performance.

2. The increased implementation complexity and computation burden: technically, the currently used hindered-only, hindered-compression and hindered-dispersion models can be considered as the sub-models of the Bürger-Diehl model, and their successful applications in SST simulation implies that the Bürger-Diehl model in some cases can be reduced to these sub-models without sacrificing the quality of prediction. However, how to reliably reduce the Bürger-Diehl model, particularly under non-ideal flow and settling conditions, still remains unclear.

In this study, we provided a comprehensive sensitivity and model reduction analysis of the Bürger-Diehl model under non-ideal flow and settling conditions. The Benchmark Simulation Model No.1 (BSM1) (Alex et al. 2008) is used as the simulation platform, because of its well documented model inputs. The influence of the uncertainty of model parameters to the variance of model outputs, such as the sludge blanket level, is quantified by using global sensitivity analysis (GSA), and the reliability of the Bürger-Diehl model reduction is evaluated based on uncertainty analysis.

The main objectives of this chapter are (i) identify the suitable parameter subsets for the Bürger-Diehl model calibration under non-ideal flow and settling conditions; (ii) evaluate the influence of imposed flow and settling conditions on the sensitivity of the Bürger-Diehl model outputs to

the parameters; (iii) demonstrate how reliable reduction of the Bürger-Diehl model can be achieved based on GSA results ; (IV) assess the reliability of the Bürger-Diehl model reduction for different modeling purposes based on uncertainty analysis results.

6.2. Materials and method

6.2.1. Model structure and simulation description

As shown by Fig.6.1, BSM1 is used as the simulation platform, where ASM1 is combined with the SST model to describe the biological and settling processes of the activated sludge system. For further details about ASM1, the reader is referred to literature (Henze et al. 1987). With regards to the SST model, the Bürger-Diehl model is used to replace the Takács model.
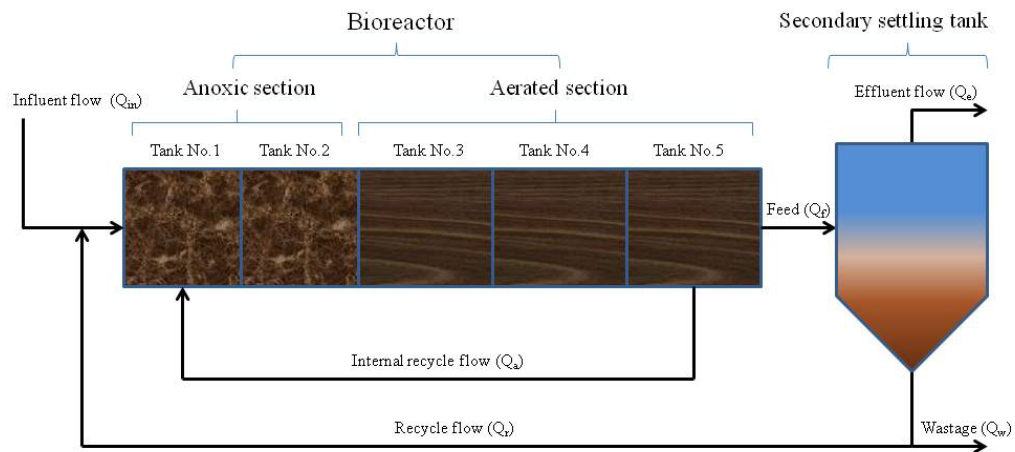
Fig.6.1 - Layout of the Benchmark Simulation Model NO.1 (BSM1).

The formula of the Bürger-Diehl model can be expressed as eq.(6.1) on the basis of the mass and momentum conservation:

$$\frac{\partial C}{\partial t} + \frac{\partial}{\partial x} F(C,x,t) = \frac{\partial}{\partial x}\left((d_{disp}(v_{ov}) + d_{comp}(C))\frac{\partial C}{\partial x} \right) + \frac{Q_f(t)C_f(t)}{A}\delta(t) \tag{6.1}$$

where C is the solids concentration, t is time, x is the depth from the feed layer, v_{ov} is the overflow velocity, Q_f is the feed flow rate, A is the SST surface area, C_f is the feed solids concentration, δ is the Dirac delta distribution and the transport flux F can be written as eq.(6.2) (Diehl 1996):

$$F(C,x,t) = \begin{cases} -\dfrac{Q_e}{A}C_e & \text{\textit{effluent region}} \\[2mm] v_{hs}(C)C - \dfrac{Q_e}{A}C & \text{\textit{clarification zone}} \\[2mm] v_{hs}(C)C + \dfrac{Q_u}{A}C & \text{\textit{thickening zone}} \\[2mm] \dfrac{Q_u}{A}C_u & \text{\textit{underflow region}} \end{cases} \tag{6.2}$$

where Q_e is the effluent flow rate, Q_u is the underflow rate, C_e is the effluent solids concentration and C_u is the underflow concentration. The hindered settling velocity, v_{hs}, is calculated by the double-exponential equation (Takács et al. 1991):

$$v_{hs} = v_0\left(e^{-r_h(C-f_{ns}C_f)} - e^{-r_p(C-f_{ns}C_f)} \right) \tag{6.3}$$

The compression function is approximated by eq.(6.4) recommended by previous publications (De Clercq et al. 2008, Bürger et al. 2011):

$$d_{comp}(C) = \begin{cases} 0 & 0 \le C < C_g \\[3mm] \dfrac{\rho_s \cdot \alpha \cdot v_{hs}(C)}{g(\rho_s - \rho_f)(\beta + C - C_g)} & C \ge C_g \end{cases} \tag{6.4}$$

where ρ_s is the solids density, ρ_f is the liquid density. The dispersion function developed by Plósz et al. (2007) is used to characterize the hydraulic dispersion, shown as eq.(6.5):

$$D_{disp}(v_{ov}) = \begin{cases} D_{c,0} & v_{ov} < v_{ov,c} \\ D_{c,0} + \gamma(v_{ov} - v_{ov,c})^2 & v_{ov} \geq v_{ov,c} \end{cases} \tag{6.5}$$

Quantifying prior uncertainty of all model parameters is one of the most important but difficult task for reliable sensitivity analysis. Table 6.1 shows the definition and prior uncertainty of parameters. The uncertainty of hindered settling parameters (v_0, r_h, r_p and f_n), compression settling parameters (C_g, α and β) and dispersion parameter, $v_{ov,c}$, are determined based on literature references and expert knowledge. Since the dispersion parameters, $D_{c,0}$ and γ, are not well documented in previous studies, we introduce a relative uncertainty (50%) based on the default values reported by Plósz et al. (Plósz et al. 2007) to reasonably quantify their uncertainties. The probability distributions of all model parameters are assumed uniform because of no prior knowledge (Ramin et al. 2014c).

To comprehensively evaluate the 1-D SST models, three scenarios of non-ideal flow and settling conditions are selected to run the BSM1 as following:

1. Wet-weather inflow but good biomass settleability: based on the values of ASM1 inputs and parameters follows the dry-weather data set provided by Alex et al. (2008), and a constant inflow rate (18446 m³/d), a 150-day simulation is conducted to obtain steady-state, and then a wet-weather condition (14.4-hour) is imposed by increasing the influent flow rate to four times of the average dry-weather inflow rate.

2. Dry-weather inflow but filamentous bulking: The same strategy as scenario 1 is used to reach steady state. Then, the filamentous bulking condition is simulated as long as 9.6 hours on the basis of the parameter uncertainty of bulking as shown in Table 6.1; (Since no significant association is found between compression parameters and filamentous abundance (Wágner et al. 2015), same uncertainty ranges of compression parameters are used under bulking condition as those used under good settling condition.)

3. Wet-weather inflow and filamentous bulking: the steady-state is obtained by 150-day simulation similar as scenarios 1 and 2. A 4.8-hour simulation of the wet-weather inflow and bulking condition is conducted by increasing the influent flow rate twice of the average dry-weather inflow rate, and using the settling parameter set of bulking;

Table 6.1 - Uncertainty of the Bürger-Diehl model parameters under good settling and bulking conditions.

		Good settling		Bulking	
	Unit	Min	Max	Min	Max
v_0	m/d	355.5	592.5	177.75	296.25
r_h	m³/kg	0.432	0.721	0.75	1.25
r_p	m³/kg	2.7	10	2.7	10
f_{ns}	-	0.00123	0.00259	0.00123	0.00259
C_g	kg/m³	6.06	10.12	6.06	10.12
α	Pa	0	20	0	20
β	kg/m³	1	10	1	10
$D_{c,0}$	m²/d	1.98	5.92	1.98	5.92
γ	d	1.1E-2	3.3E-2	1.1E-2	3.3E-2
$v_{ov,c}$	m/d	10	22	10	22

*Uncertainty is determined based on literature review and expert knowledge

6.2.2. Global sensitivity analysis

To improve the model understanding, global sensitivity analysis is usually introduced to investigate the dependence of model outputs on the uncertainties of model factors (defined as both model parameters and inputs). This is informative for various purposes, such as quantifying the individual contribution of the uncertain parameters to the model output uncertainty to identify influential parameters.

The global sensitivity technique used in this study is the Extended-Fourier Amplitude Testing (Extended-FAST), originally developed by Cukier et al. (1973) and Schaibly and Shuler (1973), and later extended by Satelli et al. (1999). Compared with frequently used regression-based and screening methods, the Extended-FAST possesses the advantages of providing accurate sensitivity measures in various model structures (linearity, monotonicity etc.) without the necessary of making any assumptions of model behaviors. As a variance-based approach, the Extended-FAST has its root in the general theorem that the total variance can be decomposed into conditional variances, as shown in eq.(6.6):

$$Var(sy) = Var(E(sy \mid \theta_i)) + E(Var(sy \mid \theta_i)) \qquad (6.6)$$

where *Var* and *E* is the variance and expectancy operator respectively, *sy* denotes a vector of scalar values for the model output and θ_i is the *i*th model factor. The Extended-FAST converts the multidimensional integral over all the uncertain parameters in a one-dimensional integral using a transformation function that scans the entire parameter space, and the contribution of the individual parameters to the variance of the model output is calculated by using a Fourier decomposition (Saltelli et al. 2004, Brockmann and Morgenroth 2007). The Extended-FAST

implementation strategy used in this study is based on Satelli et al. (1999), and the transformation function is given as eq.(6.7):

$$\theta_i = \frac{1}{2} + \frac{1}{\pi}\arcsin(\sin(\omega_i s + \varphi_i)) \qquad (6.7)$$

where s ranges from $-\pi/2$ to $\pi/2$, ω is a set of different frequencies and φ_i is a random phase-shift. The total number of model evaluation required can be determined by eq.(6.8):

$$N_s = m\left(2M\omega_{max} + 1\right) \qquad (6.8)$$

where m is the number of model parameters, M is the interference frequencies, and w_{max} is the maximum frequency. For further information about Extended-FAST implementation strategy, such as the selection of ω, the reader is referred to the literature (Saltelli et al. 1999).

Generally, Extended-FAST provides three kinds of sensitivity measures: the first-order effect index (S_i), which represents the contribution of the variance of individual parameters to the output variance without considering the interaction with other parameters, and can be used to identify the most significant factors (factors prioritization); the total effect index (S_{Ti}), which accounts for the total contribution of the parameter to the output variance, and is informative for determining factors that can be fixed without greatly reducing output variance (factor fixing); the interaction (S_{Si}), which can be used to evaluate the interactions among parameters.

6.2.3. Uncertainty analysis with Monte Carlo procedure

Uncertainty analysis can be understood as the propagation of the uncertainty of parameters to model outputs, which is beneficial for design and control decision-making. The model uncertainty analysis in this study involves the following steps as listed by Sin et al. (2009):

1. Specifying input uncertainty: for each scenario, only the SST model parameters are considered as uncertainty source;

2. Sampling input uncertainty: Latin hypercube sampling is applied;

3. Propagating input uncertainty to obtain prediction uncertainty: Monte Carlo simulation is used;

4. Representation and interpretation of results: the predicted uncertainty results are represented using mean, percentiles and cumulative distribution functions;

The possible correlations among parameters are not considered here, since there is no detailed information available about the correlation matrix.

6.2.4. Numerical setting and comparison of SST models

The discretization level of SST models is 30-layer. Given that the GSA and reduction analysis are made based on the numerical solutions of the Bürger-Diehl model, reliable numerical techniques are needed: the solids transport flux is approximated by Yee-Roe-Davis numerical flux, and the compression and dispersion terms are approximated following the strategy provided by Bürger et al. (2013). For Extended-FAST, M and ω_{max} is 4 and 8 respectively. Only factors with S_i larger than 0.01 or S_{Ti} larger than 0.1 are considered to be important according to Cosenza et al. (2013). To provide an effective coverage of model output uncertainty, the BSM1 model

with different SST models is simulated 500 times for each scenario following the benchmark simulation strategy.

Five significant model outputs: sludge blanket height (SBH), C_e, C_u, sludge inventory (SI) and operating flux ($flux_{op}$), are used to characterize the SST performance, since they are closely related to the SST robustness, the mostly interesting topic under non-ideal flow and settling conditions.

6.3. Results and discussion

6.3.1. Global sensitivity analysis of the Bürger-Diehl model under non-ideal flow and settling conditions

In this section, the GSA results of Bürger-Diehl model are provided in order to identify the potential parameter subsets suitable for model calibration. Table 6.2 shows the sensitivity measures (S_i and S_{Ti}) of the Bürger-Diehl model under the wet-weather condition (scenario 1). The high sensitivity indices ($S_i > 0.01$) of v_0 and r_h indicate their strong influence on the model outputs as well as implying the important role hindered settling plays in determining the SST performance. In contrast, the hindered settling parameter, r_p, is non-influential to SST behavior, with only one notable exception: C_e, where r_p contributes more than 50% percent of the total variance. It means that to accurately predict C_e, r_p needs to be carefully calibrated. Regarding the compression settling parameters, the gel concentration, C_g, is another significant parameter strongly impacting the SST performance, particularly, in the case of C_u, SI and $flux_{op}$, where C_g contributes more than 30% of the total variance. The other two compression settling parameters, α and β, are moderately influential to C_u, SI and $flux_{op}$ as well. The high sensitivity of C_u, SI and

flux$_{op}$ to the compression settling parameters can be interpreted by the fact that the sludge with high compressibility can be easily compacted in the thickening zone, thus leading to the increase of C_u and *flux$_{op}$*, but a decrease of *SI*. The hydraulic dispersion parameters, γ and $v_{ov,c}$, are important for SST behavior too, especially in the case of C_e, where γ ranks the second of most influential parameters. This is due to the explicit hydraulic term accounts for some of the variations in hydraulic feathers of SST under the wet-weather condition, as reported by Ramin et al. (Ramin et al. 2014c). f_n and $D_{c,0}$, are identified as non-influential parameters, since their sensitivity measures are much smaller than the corresponding thresholds.

Table 6.2 - Parameter sensitivity indices of the Bürger-Diehl model outputs in scenario 1.

		Wet-weather and good settling
		v_0	r_h	r_p	f_n	C_g	α	β	$D_{c,0}$	γ	$v_{ov,0}$
SBH	S_i	**0.071**	**0.461**	0.004	0.002	**0.046**	9.1E-4	6.7E-4	0.003	**0.085**	**0.067**
	S_{Ti}	0.086	**0.471**	0.014	0.016	0.063	0.004	0.005	0.007	0.097	0.086
C_e	S_i	**0.199**	**0.209**	**0.544**	3.5E-4	**0.011**	0.001	1.7E-4	0.001	**0.299**	**0.093**
	S_{Ti}	**0.438**	**0.453**	**0.593**	0.039	0.048	0.027	0.011	0.008	**0.578**	**0.186**
C_u	S_i	**0.046**	**0.261**	0.002	8.1E-4	**0.333**	**0.018**	0.008	1.6E-4	0.009	**0.031**
	S_{Ti}	0.067	**0.299**	0.012	0.013	**0.394**	0.027	0.016	0.002	0.013	0.049
SI	S_i	**0.019**	**0.282**	0.008	9.4E-4	**0.374**	**0.024**	**0.011**	2.9E-4	0.001	0.007
	S_{Ti}	0.052	**0.427**	0.021	0.012	**0.438**	0.036	0.024	0.004	0.005	0.029
Flux$_{op}$	S_i	**0.046**	**0.254**	0.001	7.8E-4	**0.351**	**0.017**	0.007	1.6E-4	0.008	**0.031**
	S_{Ti}	0.067	**0.295**	0.012	0.012	**0.411**	0.027	0.015	0.002	0.012	0.048

The sensitivity measures of model parameters under the bulking condition are shown in Table 6.3. It is interesting to find that the sensitivity measures of compression settling parameters, C_g, α and β, are smaller than the thresholds regardless of the model outputs, which means that the compression settling is not influential to SST performance under the bulking condition. The hindered settling parameters, v_0 and r_h, are the most influential parameters, which contributes

more than 95% of total variance to most model outputs, thus demonstrating the importance of reliably calibrating v_0 and r_h under the bulking condition. According to Table 6.3, C_e is most sensitive to the change of r_p, which contributes more than 80% of total variance of C_e. Therefore, reliable calibration of r_p is highly needed for accurate prediction of C_e when sludge bulking occurs. Similar as r_p, f_n is only influential to C_e with 6% contribution of total variance. The hydraulic dispersion parameter found to be important is $D_{c,0}$, even though its contribution of variance is relatively small compared those made by hindered settling parameters. Consequently, hindered settling process is most influential to the SST performance under the bulking condition, while the effect of compression settling is almost negligible.

Table 6.3 - Parameter sensitivity indices of the Bürger-Diehl model outputs in scenario 2.

		Dry-weather and filamentous bulking									
		v_0	r_h	r_p	f_n	C_g	α	β	$D_{c,0}$	γ	$v_{ov,0}$
SBH	S_i	**0.125**	**0.895**	0.001	5.6E-4	0.004	8.7E-4	0.001	**0.051**	0.001	0.001
	S_{Ti}	**0.143**	**0.911**	0.008	0.006	0.029	0.006	0.011	0.071	0.009	0.007
C_e	S_i	**0.191**	**0.138**	**0.823**	**0.063**	0.003	0.003	0.002	**0.062**	0.006	0.001
	S_{Ti}	**0.355**	**0.336**	**0.866**	**0.142**	0.022	0.054	0.021	**0.103**	0.043	0.029
C_u	S_i	**0.076**	**0.931**	8.2E-5	5.4E-6	4.9E-5	1.6E-5	5.7E-6	**0.016**	6.4E-6	4.1E-6
	S_{Ti}	0.078	**0.933**	0.003	0.001	0.004	0.001	0.003	0.021	0.003	0.001
SI	S_i	**0.079**	**0.933**	1.7E-5	1.2E-5	8.9E-5	1.4E-5	1.4E-5	**0.019**	1.1E-5	7.7E-6
	S_{Ti}	0.081	**0.935**	0.003	0.001	0.004	0.001	0.003	0.022	0.003	0.001
$Flux_{op}$	S_i	**0.083**	**0.924**	0.001	5.5E-6	6.7E-5	2.1E-5	6.7E-6	**0.016**	9.4E-6	7.2E-6
	S_{Ti}	0.085	**0.926**	0.003	0.001	0.004	0.001	0.003	0.021	0.003	0.001

According to Table 6.4, four parameters, v_0, r_h, r_p and $D_{c,0}$, are important for model calibration under the wet-weather and filamentous bulking condition, since their sensitivity measures are larger than the thresholds. For *SBH* and C_e, they are highly sensitive to the change of both hindered and hydraulic dispersion parameters, which means they are results of hindered settling

and hydraulic dispersion effects. However, in contrast to scenarios 1 and 2 where C_e is most sensitive to r_p, C_e in scenario 3 is mostly determined by r_h, which accounts for more than 50% of the total variance. The hindered settling process primarily impacts C_u, SI and $flux_{op}$, because the hindered settling parameters, v_0 and r_h, are the only influential parameters. Consequently, the reliable calibration of v_0 and r_h can greatly reduce the uncertainty of model outputs, hence producing an adequate description of the SST behavior under the wet-weather and bulking condition.

Table 6.4 - Parameter sensitivity indices of the Bürger-Diehl model outputs in scenario 3.

		Wet-weather and filamentous bulking									
		v_0	r_h	r_p	f_n	C_g	α	β	$D_{c,0}$	γ	$v_{ov,0}$
SBH	S_i	**0.132**	**0.929**	9.8E-4	2.1E-4	7.6E-4	4.7E-4	8.3E-4	**0.013**	0.001	0.006
	S_{Ti}	**0.152**	**0.947**	0.008	0.004	0.018	0.003	0.006	0.022	0.007	0.012
C_e	S_i	**0.222**	**0.509**	**0.025**	0.004	6.8E-4	0.001	0.004	**0.039**	0.008	0.003
	S_{Ti}	**0.591**	**0.801**	0.091	0.019	0.029	0.005	0.059	**0.181**	0.089	0.018
C_u	S_i	**0.088**	**0.952**	1.3E-4	2.6E-5	1.1E-4	3.4E-5	2.2E-5	0.006	4.9E-4	0.003
	S_{Ti}	0.091	**0.954**	0.003	0.002	0.005	0.001	0.003	0.01	0.004	0.006
SI	S_i	**0.056**	**0.937**	4.7E-4	7.2E-4	3.1E-4	1.1E-4	3.7E-4	0.007	4.1E-4	0.006
	S_{Ti}	**0.106**	**0.987**	0.004	0.004	0.006	0.003	0.002	0.011	0.003	0.009
$Flux_{op}$	S_i	**0.115**	**0.919**	0.001	2.4E-5	2.2E-4	4.2E-5	3.6E-5	0.005	3.1E-4	0.002
	S_{Ti}	**0.118**	**0.922**	0.004	0.002	0.005	0.001	0.003	0.009	0.003	0.005

6.3.2. Parameter interactions of the Bürger-Diehl model under non-ideal flow and settling conditions

Although the analysis of S_i greatly facilitates the SST model calibration by identifying influential parameters suitable for prioritization, it is important to emphasize that the analysis of S_{Ti} is still required; for parameters having small S_i, they cannot be simply fixed as non-influential

parameters because of the possible interactions reflected by their high S_{Ti} values. In this study, the interactions among parameters are characterized by the ratio of the sum of S_i to the sum of S_{Ti}, as shown in Fig.6.2 (left). As can be seen, the sum of S_i is always smaller than the sum of S_{Ti}, which indicates the existence of interactions. This result is more pronounced for C_e, where the ratio of the sum of S_i to the sum of S_{Ti} is smaller than 60% for all scenarios. However, for C_u, SI and $Flux_{op}$ in scenarios 2 and 3, the sum of S_i is close to the sum of S_{Ti}, which means the model is almost additive without parameter interactions affecting model outputs.
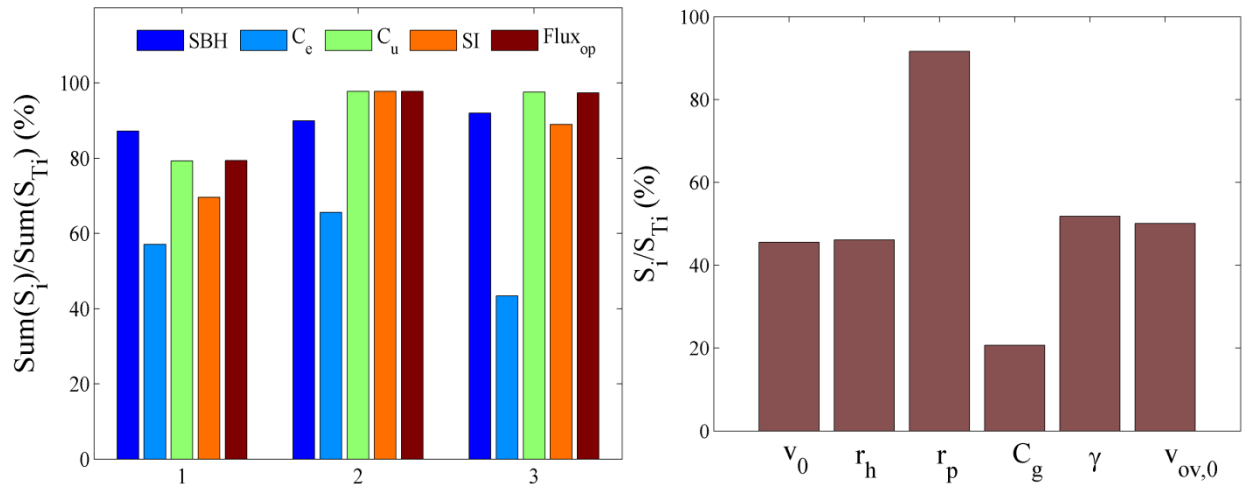
Fig.6.2 - Ratio of sum(S_i) to sum(S_{Ti}) of the Bürger-Diehl model outputs in scenarios 1 to 3(left), and ratio of S_i and S_{Ti} of the Bürger-Diehl model parameters in scenario 1.

To further investigate the parameter interactions, we take the parameter interaction analysis of C_e under the wet-weather condition as an example, where the ratio of the sum of S_i to the sum of S_{Ti} for important parameters are shown as Fig.6.2 (right). According to Fig.6.2 (right), strong parameter interactions are observed in most parameters, which implies that the effluent concentration under the wet-weather condition is strongly influenced by hindered settling, compression settling and hydraulic dispersion. What is surprising is that even though r_p is the most influential parameter on C_e, its interactions with other parameters are negligible, as

indicated by the high ratio of S_i to S_{Ti}. This may be attributed to the fact that r_p is a parameter used to describe settling behavior in low solids concentration range, while other parameters, especially the compression parameters, mostly affect the medium and high concentration domains. Based on the results of parameter interaction analysis, simple GSA techniques, such as the Standard Regression Coefficients method or Morris screening method, are sufficient for the sensitivity analysis of C_u, SI and $Flux_{op}$ in scenarios 2 and 3, while the advanced GSA methods, such as Extended-FAST, are needed for the sensitivity analysis of C_e.

6.3.3. Influence of imposed flow and settling conditions on the sensitivity of the Bürger-Diehl model outputs to parameters

In this study, the influence of imposed flow and settling conditions on the sensitivity of the Bürger-Diehl model outputs to the parameters are analyzed on the basis of the similarity of parameters identified to be important as well as the similarity of ranking of sensitivity indices. The Venn diagrams, Fig.6.3, are used for the comparison of important parameter identified in different scenarios. The significant hindered settling parameters found in scenarios 1 to 3, are almost identical regardless to the model outputs, with only one exception: f_n which is only important for the prediction of C_e in scenario 2. The important parameters found in scenarios 2 and 3 are similar, and moreover, all influential parameter in scenario 3 are important in scenario 2. The main difference between scenarios 2 and 3 is that the dispersion parameter, $D_{c,0}$, is influential for the predication of C_u and SI in scenario 2, which implies the SST performance under the bulking condition is sensitive to the hydraulic dispersion. Great differences can be observed between scenario 1 and the other two scenarios in terms of the significance of the compression parameters. The compression settling parameters, especially C_g, are strongly

influential on SST performance in scenario 1, while none of the compression parameters are important in scenarios 2 and 3. Another interesting observation is that significant hydraulic dispersion parameters found in scenarios 1 and 2 are different: γ and $v_{ov,c}$ are influential on SST behavior in scenario 1, while $D_{c,0}$ is the only hydraulic dispersion parameter important in scenario 2.

Table 6.5 - Spearman's rank index of the comparison of the similarity of sensitivity measure ranking.

Model outputs	N_s (rank of wet *vs.* rank of bulking)	N_s (rank of wet *vs.* rank of wet+bulking)	N_s (rank of bulking *vs.* rank of wet+bulking)
SBH	0.539	0.709	0.831
C_e	0.515	0.479	0.769
C_u	0.261	0.333	0.661
SI	0.442	0.224	0.467
$Flux_{op}$	0.358	0.333	0.842

The similarity of ranking of sensitivity indices in scenarios 1 to 3 is quantitatively investigated based on the Spearman's rank correlation index (N_S), and the high similarity of ranking leads to large N_S. According to Table 6.5, the rankings of sensitivity measures obtained in scenarios 2 and 3 are similar in terms of the model output variables *SBH*, C_e and $Flux_{op}$, where N_s values are larger than 0.7. However, for most model outputs, the ranking of sensitivity measures obtained in scenario 1 differs greatly from those obtained in scenarios 2 and 3, which is demonstrated by the small N_s. For instance, C_g is the most important parameter for the change of C_u, *SI* and $Flux_{op}$ in scenario 1, while in scenarios 2 and 3, most of the variance of C_u, *SI* and $Flux_{op}$ are contributed by r_h. Therefore, it should be noted that for the Bürger-Diehl model, sensitivity of model outputs to parameters strongly depends on the imposed flow and settling conditions, and suitable parameter subsets used for model calibration need to be determined based on flow and settling conditions to improve the calibration efficiency and reliability.

6.3.4. Reduction of the Bürger-Diehl model based on GSA results

Reduction of the Bürger-Diehl model, to some extent, is useful to facilitate its practical application, such as inclusion in the popular commercial simulators. Therefore, in this section, we focus on how to reliably reduce the Bürger-Diehl model for specific modeling purposes based on the GSA results.
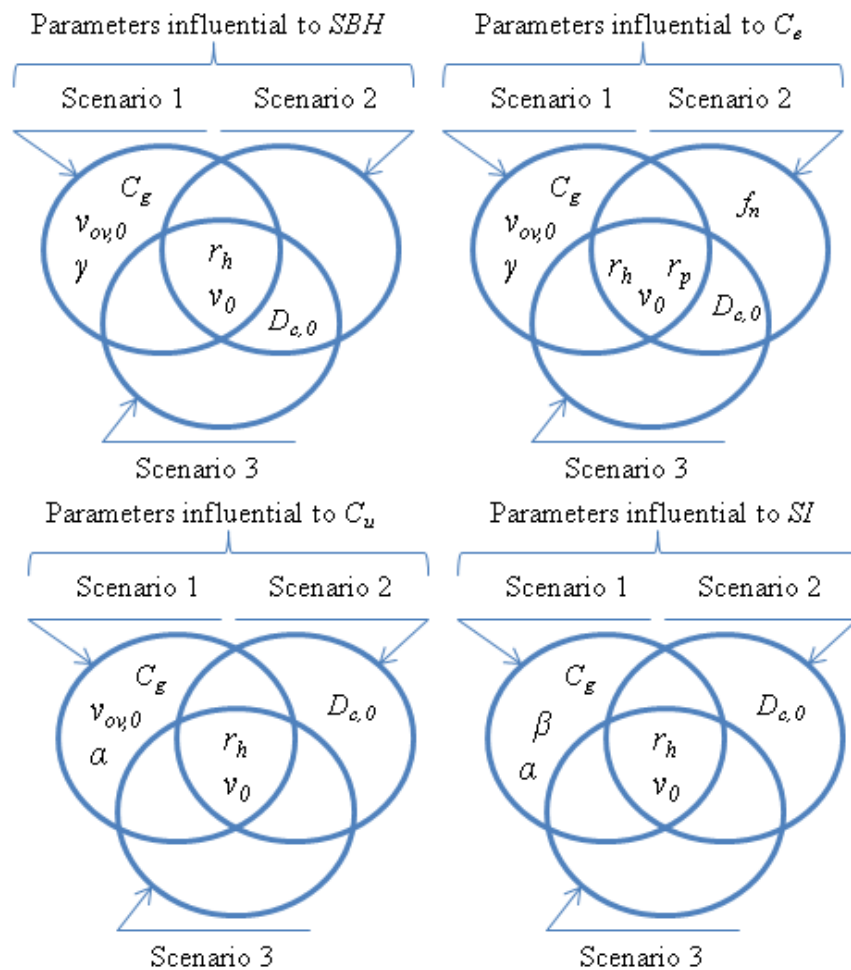
Fig.6.3 - Venn diagram related to the comparison of important parameters in scenarios 1 to 3.

According to Table 6.2, C_g is the only compression settling parameters influential on *SBH* and C_e in scenario 1 with sensitivity measures close to the threshold. It implies that if the primary modeling interests are *SBH* and C_e under the wet-weather condition, the Bürger-Diehl model (hindered-compression-dispersion) can be reduced to the hindered-dispersion model without greatly deteriorating prediction quality. However, in the case of *SI*, which is sensitive to all of the compression settling parameters, it is not reliable to reduce the Bürger-Diehl model to the hindered-dispersion model. To demonstrate this point, we compare the Bürger-Diehl model and the hindered-dispersion model based on the prediction of *SBH*, C_e and *SI*. The Monte Carlo simulations were run 300 times for each model. For each run, the hindered-dispersion and Bürger-Diehl models shared the same hindered and dispersion parameters. The similarity of model outputs obtained from the Bürger-Diehl and hindered-dispersion models is characterized by the scatter plot and the Pearson correlation index (N_p), as shown in Fig.6.4. As can be seen, in terms of the variable C_e, the predictions of the hindered-dispersion model are almost identical to those obtained from the Bürger-Diehl model, which is also confirmed by the high value of N_p, close to 1. The comparison of the *SBH* prediction shows that the *SBH* values predicated by the hindered-dispersion model agree well with those obtained from the Bürger-Diehl model. The discrepancy for these two models in the prediction of *SBH* is larger than it in the prediction of C_e. This can be expected, since C_g is more influential on *SBH* than it on C_e. When it comes to *SI*, the predictions obtained from the Bürger-Diehl model and the hindered-dispersion model differ greatly with a low N_p (0.647), which means the reduction of the Bürger-Diehl model to the hindered-dispersion model is not reliable in terms of the *SI* prediction.

Under the filamentous bulking condition, all compression settling parameters are non-influential regardless of model outputs, as shown in Table 6.3, thus making the reduction of the Bürger-

Diehl model to the hindered-dispersion model reliable for all model outputs. As Fig.6.4 shows, in terms of model outputs *SBH*, C_e and *SI*, the performance of the hindered-dispersion model is equivalent to the Bürger-Diehl model, which is confirmed by the high value of N_P. This means under the bulking condition, the Bürger-Diehl model can be reliably reduced to the hindered-dispersion model to reduce the implementation complexity and computation cost.

Further reduction of the Bürger-Diehl model to hindered-only model can, to some degree, deteriorate the quality of model prediction; for instance an obvious discrepancy can be observed between the Bürger-Diehl and hindered-only models in the prediction of C_e, where N_p is as low as 0.871. This is due to the strong sensitivity of C_e to the hydraulic dispersion parameter $D_{c,0}$ under the bulking condition, thus making the hydraulic effect not negligible in SST modeling if C_e is the primary interest.
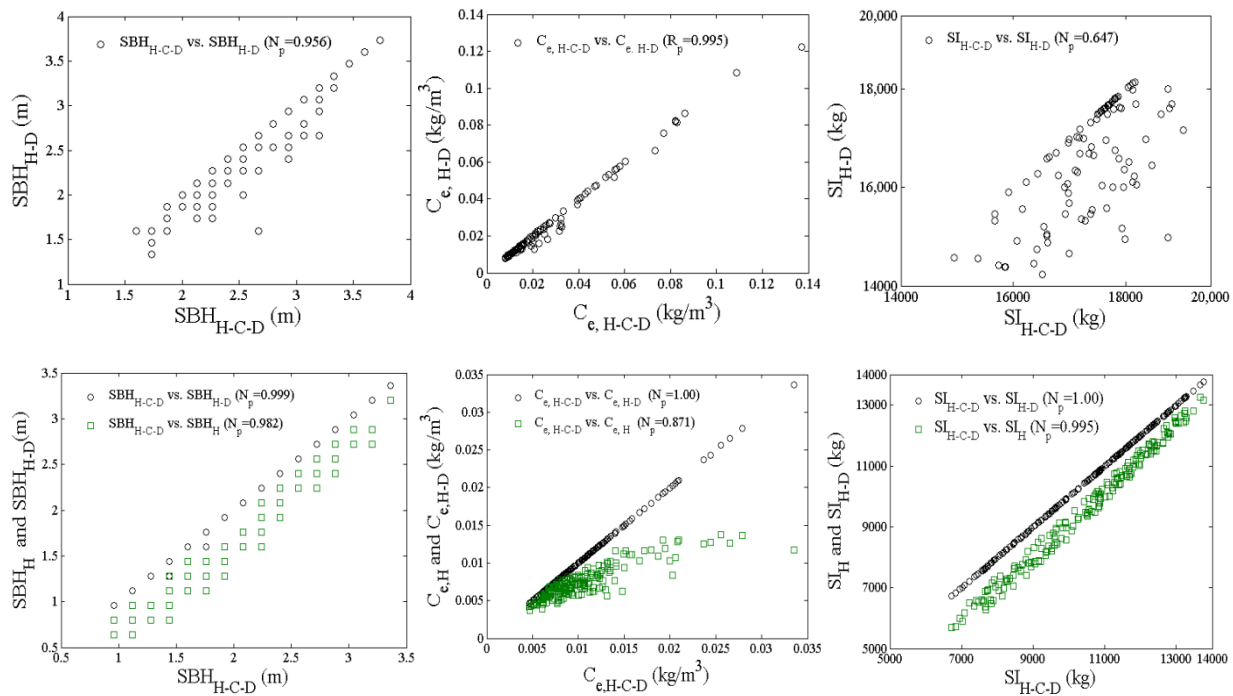
Fig.6.4 - Scatter plots and the Pearson correlation index comparing the similarity of model outputs of the Bürger-Diehl model and the reduced models (upper: scenario 1, bottom: scenario 2,

and subscripts H-C-D, H-D and H denote the Bürger-Diehl model, the hindered-compression model and the hindered-only model respectively).

6.3.5. Investigating the reliability of the Bürger-Diehl model reduction based on uncertainty analysis

In this section, the reliability of the Bürger-Diehl model reduction under non-ideal flow and settling conditions is further evaluated based on uncertainty analysis of the prediction of SBH, C_e, C_u and SI. Three typical reduced models, the hindered-only model, the hindered-dispersion model and the hindered-compression model, are considered, and the Bürger-Diehl model is used as the reference model to evaluate reliability of model reduction.
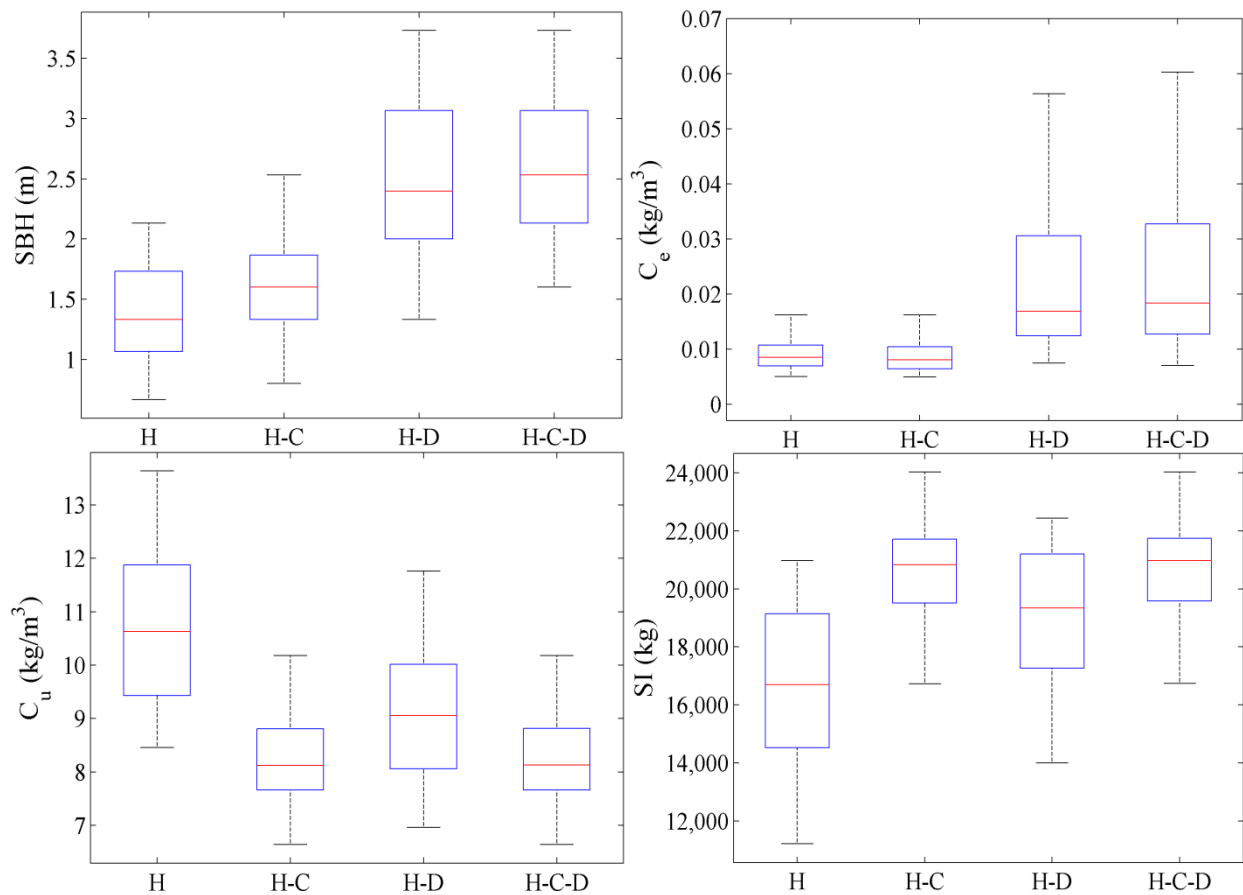
Fig.6.5 - Results of the Monte Carlo simulations of BSM1 for scenario 1. On each box, the central mark is the mean value, the edges of the box are the 25th and 75th percentiles, and the whiskers extend to the most extreme data points (subscripts H, H-C, H-D and H-C-D denote the hindered-only, hindered-compression, hindered-dispersion and Bürger-Diehl models respectively).

Fig. 6.5 is the boxplot of uncertainty of SST model outputs under the wet-weather condition. It is easy to observe that there is considerable uncertainty concerning all model outputs. With regard to *SBH* and C_e, reduction of the Bürger-Diehl model to the hindered-only and hindered-compression models cannot produce reliable predictions; for example the 75th percentiles of *SBH* and C_e predicted by the hindered-only and hindered-compression models are lower than the 25% percentile predicted by the Bürger-Diehl model. In contrast, the uncertainties of *SBH* and C_e obtained from the hindered-dispersion model are similar to those of the Bürger-Diehl model, which reveals that it is reliable to reduce the Bürger-Diehl model to the hindered-compression model in terms of model outputs *SBH* and C_e. In the case of C_u and *SI*, reducing the Bürger-Diehl model to hindered-compression model is acceptable, since the hindered-compression model can provide satisfactory uncertainty results similar as those of the Bürger-Diehl model.

The uncertainties of SST model outputs under the filamentous bulking condition are shown as Fig.6.6. As expected, the prediction uncertainties of the hindered-dispersion model are identical to those obtained from the Bürger-Diehl model, which agree with the conclusion that the SST performance under the bulking condition is not sensitive to the compression settling, and the Bürger-Diehl model can be reliably reduced to the hindered-dispersion model without significantly deteriorating the accuracy of model predictions. However, the prediction uncertainty of the hindered-only and hindered-compression models differ from those obtained from the hindered-dispersion and Bürger-Diehl models as Fig.6.6 shows; for example *SBH*, C_e and *SI* predicted by the hindered-only and hindered-compression models are much smaller than

those of hindered-dispersion and Bürger-Diehl models, while in the case of C_u, the hindered-only and hindered-compression models provide higher predictions than the hindered-dispersion and Bürger-Diehl models. Therefore, reducing the Bürger-Diehl model to the hindered-only and hindered-compression models is unreliable under the bulking condition, which may introduce considerable errors to the model uncertainty analysis.
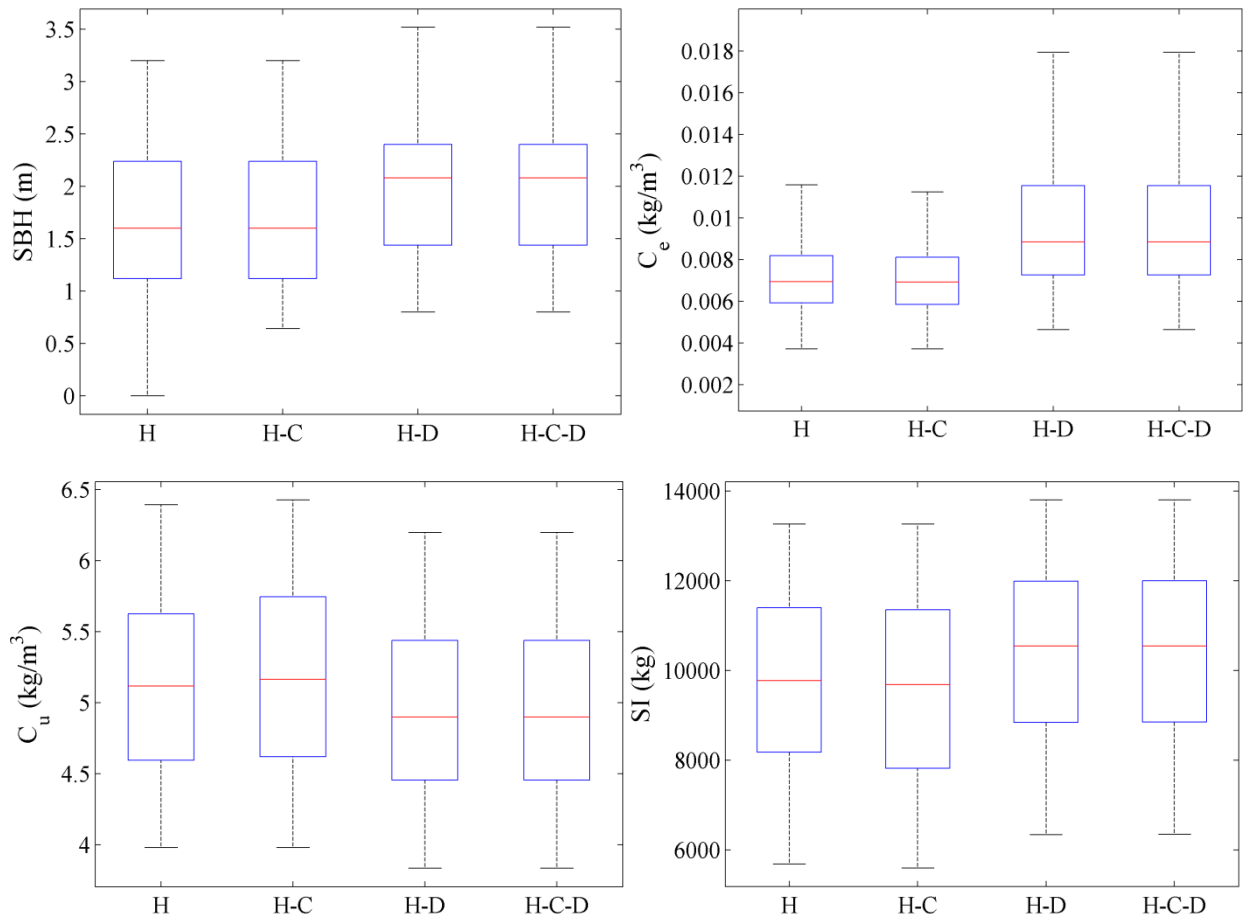
Fig.6.6 - Results of the Monte Carlo simulations of BSM1 for scenario 2. On each box, the central mark is the mean value, the edges of the box are the 25th and 75th percentiles, and the whiskers extend to the most extreme data points (subscripts H, H-C, H-D and H-C-D denote the hindered-only, hindered-compression, hindered-dispersion and Bürger-Diehl models respectively).

For scenario 3 (wet-weather and bulking), to show the influence of the Bürger-Diehl model reduction on the decision making in SST design and control, the cumulative function distribution

plots of *SBH* and C_e are given as Fig.6.7 to represent the uncertainty results. When wet-weather and sludge bulking occur, the sludge blanket can propagate from the SST bottom to effluent weir, which will cause system failure. If the effluent limit of TSS is set as 0.03 kg/m^3, Fig.6.7 shows that based on the uncertainty results, violation of effluent TSS limit always has the opportunity to occur under the wet-weather and bulking condition regardless of the SST model structure. However, it is notable that using different SST models leads to inconsistent probabilities of violation: the probabilities predicted by the hindered-only and hindered-compression models are 37%, which are smaller than 45% obtained from the hindered-dispersion and Bürger-Diehl models. If a more strict system robustness requirement is imposed, for example no thickening failure is allowed, the primary interest of uncertainty analysis is to investigate probability that the sludge blanket will rise above the feed inlet (*SBH* > 2.2 m). According to the Fig.6.7, the probabilities of thickening failure predicted by the hindered-only and hindered-compression models are 70% which are much smaller than 83% predicted by the hindered-dispersion and Bürger-Diehl models. Therefore, it is noteworthy that in terms of the violation of effluent TSS limit and thicken failure, the unreliable reduction of the Bürger-Diehl model to the hindered-only and hindered-compression models can lead to the underestimation the risk of system failure, thus negatively impact the decision making of the system design and control under the wet-weather and bulking condition.
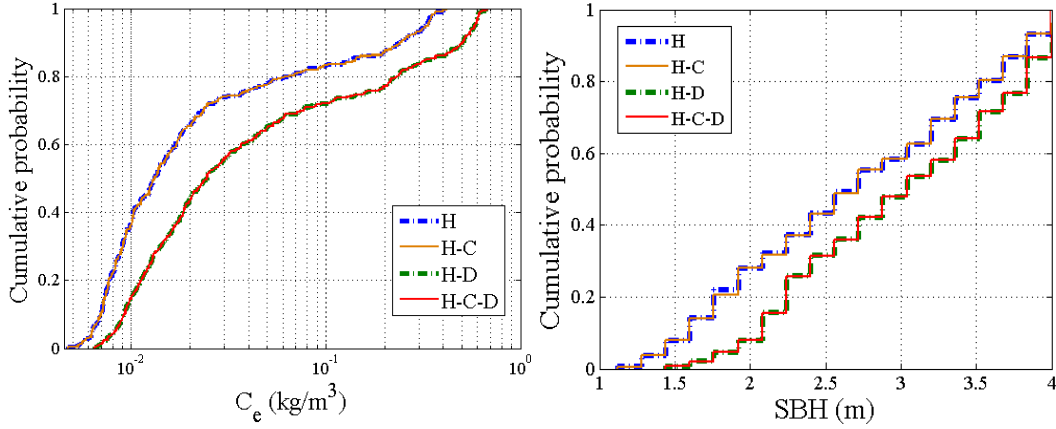
Fig.6.7 - Representation of the uncertainties of C_e and *SBH* for scenario 3 by the cumulative distribution function (subscripts H, H-C, H-D and H-C-D denote the hindered-only, hindered-compression, hindered-dispersion and Bürger-Diehl models respectively).

6.4. Conclusions

In the last decade, great efforts have been made to improve the SST simulation. In this study, by using the benchmark simulation model No.1 as the simulation platform, we provide the sensitivity and reduction analysis of the Bürger-Diehl model under non-ideal flow and settling conditions. The following specific conclusions can be made:

1. Based on the GSA results, the important parameters are identified for the Bürger-Diehl model calibration under non-ideal flow and settling conditions. All model parameters, except f_n and $D_{c,0}$, are influential to SST performance under the wet-weather condition. When filamentous bulking occurs, the outputs of the Bürger-Diehl model are most sensitive to the hindered settling parameters, v_0 and r_h, which need to be accurately calibrated.

2. The analysis of the total sensitivity measure (S_{Ti}) shows that the parameter interactions impact the model output differently. In the case of C_e where strong parameter interactions exist, advanced GSA techniques, such as Extended-FAST, are required for reliable GSA results. However, for C_u, *SI* and *Flux$_{op}$* under the bulking condition, the model is almost

additive with negligible parameter interactions. Therefore, simple GSA techniques, such as Standard Regression Coefficients method or Morris screening method, are sufficient to provide reliable GSA results.

3. The sensitivity of the Bürger-Diehl model outputs to parameters is highly impacted by the imposed simulation conditions, resulting in different parameter subsets for model calibration. For example, under the wet-weather condition, the compression settling parameters can be as important as the hindered settling parameters, particularly in the cases of C_u, SI and $Flux_{op}$. Imposing the sludge bulking in scenarios 2 and 3 greatly increases the influence of the hindered settling parameters (v_0 and r_h), while decreasing the influence of the compression settling parameters. Different simulation conditions can also lead to different influential dispersion parameters; for example γ and $v_{ov,c}$ are found to be influential in scenario 1, while $D_{c,0}$ is important in scenarios 2 and 3.

4. Reliable reduction of the Bürger-Diehl model can be achieved based on GSA results. For example, under the wet-weather condition, in terms of the prediction of C_e, the Bürger-Diehl model can be reduced to the hindered-dispersion model without deteriorating model performance, since the compression settling parameters are not as influential to C_e as the hindered settling and dispersion parameters. Under the bulking condition, the Bürger-Diehl model can be reduced to the hindered-dispersion model without impacting model outputs, which occurs because none of model outputs are sensitive to the compression settling parameters.

5. The reliability of the Bürger-Diehl model reduction can be evaluated based model uncertainty analysis. Unreliable reduction of the Bürger-Diehl model can introduce considerable errors to model predictions, thus negatively impact SST design and control.

7. Practical Identifiability and Uncertainty Analysis of the One-Dimensional Hindered-Compression Continuous Settling Model

7.1. Introduction

As the mostly used solids-liquid separation unit in wastewater treatment process, secondary settling tanks (SSTs) are able to remove finely dispersed solids to produce low turbidity effluent, and to concentrate the solids in an underflow for it to be recycled or disposed in the least volume. The two functions are known as clarification and thickening. The traditional SST design and operation strategies tend to be empirical and conservative, which may cause an unanticipated performance fluctuation of the SST itself and a low efficiency of energy and land use (Li and Stenstrom 2014a, Li and Stenstrom 2014d).

For design and operation optimization purposes, various SST mathematical models have been developed to provide a reasonable prediction of the effluent solids concentration, underflow solids concentration, sludge blanket level and sludge inventory which are specifically important during hydraulic shock loading and sludge settleability deterioration. In most commercial simulators, one-dimensional (1-D) SST models are most often used due to their simplicity and less computation burden, especially if long term simulations are needed (Bürger et al. 2011). Most early 1-D models, such as the well-known Takács model (Takács et al. 1991), are derived considering only local mass conservation and hindered settling. In last decade, the improved understanding of activated sludge rheology has facilitated the development of phenomenological theory of sedimentation-consolidation, which provides a more rigorous description of the compression settling behavior (Bürger 2000). The phenomenological theory is subsequently expressed in the 1-D model from the mass and linear momentum balance, allowing the

development of hindered-compression models, such as the Bürger-Diehl model (Bürger et al. 2012, Bürger et al. 2013). Compared with the hindered-only models, the hindered-compression models have the advantage of providing improved compression settling simulations, thus allowing more accurate predictions of the underflow concentration, sludge blanket level under unusual conditions, for example the wet-weather condition (Torfs et al. 2015).

Given the variety of simulation conditions, such as the sludge settleability and compressibility, 1-D settling models are not considered to be universal for all SST systems, and model parameter adjustment based on experiment data, usually referred as model calibration, is usually required for specific SST simulations. The calibration methodology of the hindered-only settling models are well developed, and can be classified into two categories: 1) the conventional approach using hindered settling velocities obtained from multiple batch settling tests; 2) the direct parameter estimation approach by fitting a single batch settling curve (Vanderhasselt and Vanrolleghem 2000). It is noticeable that the hindered-compression settling models cannot be calibrated straightforwardly following these two approaches because of the inclusion of the additional compression parameters. Several proposed calibration methods require the use of advanced techniques, such as radiotracing, to measure the dynamic concentration distribution during batch settling experiments (Kinnear 2002, De Clercq et al. 2005, De Clercq et al. 2008), which is beyond the accessibility of most practical application cases (Li and Stenstrom 2014d, Ramin et al. 2014d). Therefore, to promote the application of the hindered-compression settling model, great efforts are needed to facilitate its calibration. For example Ramin et al. (2014c, 2014d) reported that calibrating the hindered-compression model based on the additional measurement of the batch bottom concentration, beside the batch settling curves, has achieved some degree of success.

173

The limited observational data of practical batch experiments naturally gives rise to the problem of the poorly identifiable parameters, which means it is difficult to identify a unique set of all parameters used in the hindered-compression models due to possible parameter correlation (Brun et al. 2002, Brockmann et al. 2008). To avoid this problem, it is important to understand the practical identifiability of the model and select a suitable subset of parameters which can be reliably identified by the available experiment measurements (Weijers and Vanrolleghem 1997, Brun et al. 2001, Ruano et al. 2007).

In the wastewater treatment process modeling field, two alternative approaches have been most used to analysis the parameter identifiability problem. The first method is on the basis of scalar functions calculated from the Fisher Information Matrix (FIM), and the D and mod-E criteria can be used to select the best identifiable parameter subset (Weijers and Vanrolleghem 1997). The second method developed by Brun et al. (2001) uses a diagnostic regression and focuses on the analysis of parameter interdependency by calculating the collinearity index. Both methods are proven to be efficient in selecting the best identifiable parameter subset from limited experiment measurements (Weijers and Vanrolleghem 1997, Brun et al. 2001, Ruano et al. 2007, Brockmann et al. 2008). Recently, the Generalized Likelihood Uncertainty Estimation (GLUE) method has also been demonstrated as a reliable alternative for the identifiability analysis of the hindered-compression settling model by Torfs et al. (2013).

Nevertheless, despite the efficiency of the two most used approaches in addressing parameter identifiability problem, they still have drawbacks which may greatly impact the analysis results, at least in the hindered-compression settling model study. Both approaches are based on the calculation of local sensitivity functions for a set of reasonable parameters values within the

parameter space, and in most activated sludge model (ASM) identifiability studies, the initial parameter set is determined as default values reported in literature. For example the practical identifiability analysis of ASM2d by Brun et al. (2002) used the default values presented by Henze et al. (1999) as the starting point values. Given the fact that very limited parameter values have been reported in hindered-compression settling model studies, especially those related to the compression rheology, the initial parameter set values cannot be determined by the default value strategy, which implies that the choice of the initial parameter values may significantly impact the parameter identifiability. Beyond that, fixing some parameters, such as the non-influential parameters determined by the local sensitivity analysis, at prior values according to lecture and practical experience can introduce bias to the parameter estimates, which have been reported in pervious investigations (Weijers and Vanrolleghem 1997, Brun et al. 2001, Omlin et al. 2001, Brun et al. 2002).

From a practical point of view, the uncertainty analysis of wastewater treatment plant models is particularly important for design and operation decision making, and one of main uncertainty sources is the model input uncertainty, such as characterizing the model parameter values over a reliable range to reflect the limited knowledge of their exact values (Sin et al. 2009). To facilitate the practical application of the hindered-compression settling models by providing a guidance for experiment design, it is important to know which parameters can be obtained under what experimental conditions, and how large the model prediction uncertainties can be. This knowledge can be very beneficial in understanding the uncertainties of SST performance, such as the sludge blanket height (SBH), the recycle solids concentration under wet-weather and sludge settleability deterioration conditions.

The first objective of this chapter is to evaluate the parameter identifiability of the hindered-compression model based on different experimental layouts to show which parameter is identifiable in which experimental layout, as well as to study the influence of initial parameter selection on parameter identifiability analysis. The second goal of this chapter aims to investigate the influence of the choice of initial parameter values on parameter identifiability and the bias of the parameter estimates caused by fixing unidentifiable parameters. The third part focuses on the model prediction uncertainty analysis by showing how the estimates obtained from different layouts impact the model prediction uncertainty.

7.2. Materials and methods

7.2.1. Model structure

Although having a similar rheological basis, most established hindered-compression models can be distinguished by their modeling approach of the compression settling process (Li and Stenstrom 2014b). In this study, we selected the recently presented Bürger-Diehl model (no hydrodynamic dispersion considered) as an example for identifiability and uncertainty analysis because of its flexibility in application and available implementation details (Bürger et al. 2011, Bürger et al. 2013). The frame of the Bürger-Diehl model can be expressed as eq.(7.1):

$$\frac{\partial C}{\partial t} + \frac{\partial}{\partial x} F(C,x,t) = \frac{\partial}{\partial x}\left(d_{comp}(C)\frac{\partial C}{\partial x}\right) + \frac{Q_f(t)C_f(t)}{A}\delta(t) \tag{7.1}$$

where C is the solids concentration, t is time, x is deep from the SST bottom, d_{comp} is the compression function, A is SST surface area, Q_f is the feed flow rate, C_f is the feed solids

concentration, δ is the Dirac delta distribution, and the solids transport flux F can be written as eq.(7.2):

$$F(C,x,t) = \begin{cases} -\dfrac{Q_e}{A}C_e & \text{effluent region} \\[2mm] v_{hs}(C)C - \dfrac{Q_e}{A}C & \text{clarification zone} \\[2mm] v_{hs}(C)C + \dfrac{Q_u}{A}C & \text{thickening zone} \\[2mm] \dfrac{Q_u}{A}C_u & \text{underflow region} \end{cases} \tag{7.2}$$

where Q_e is the effluent flow rate, Q_u is the underflow rate, C_e is the effluent solids concentration, C_u is the underflow solids concentration, and v_{hs} is the hindered settling velocity calculated by the Vesilind equation (Vesilind 1968), shown as eq.(7.3):

$$v_{hs} = v_0 \exp(-r_h C) \tag{7.3}$$

The compression function, eq.(7.4), is derived by Bürger et al. (2012, 2013) which based on the logarithmic compression stress function developed by De Clercq et al. (2008):

$$d_{comp}(C) = \begin{cases} 0 & 0 \leq C < C_g \\[3mm] \dfrac{\rho_s \cdot \alpha \cdot v_{hs}(C)}{g(\rho_s - \rho_f)(\beta + C - C_g)} & C \geq C_g \end{cases} \tag{7.4}$$

where α and β are the compression parameters, and C_g denotes the gel concentration (the threshold compression concentration). Recently, Ramin et al. (2014c) found that the logarithmic compression stress function, as the state-of-the-art function, is not effective for model calibration,

even if the additional concentration profile measurements are provided, which implies the need of more accurate mathematical description of the compression behavior.
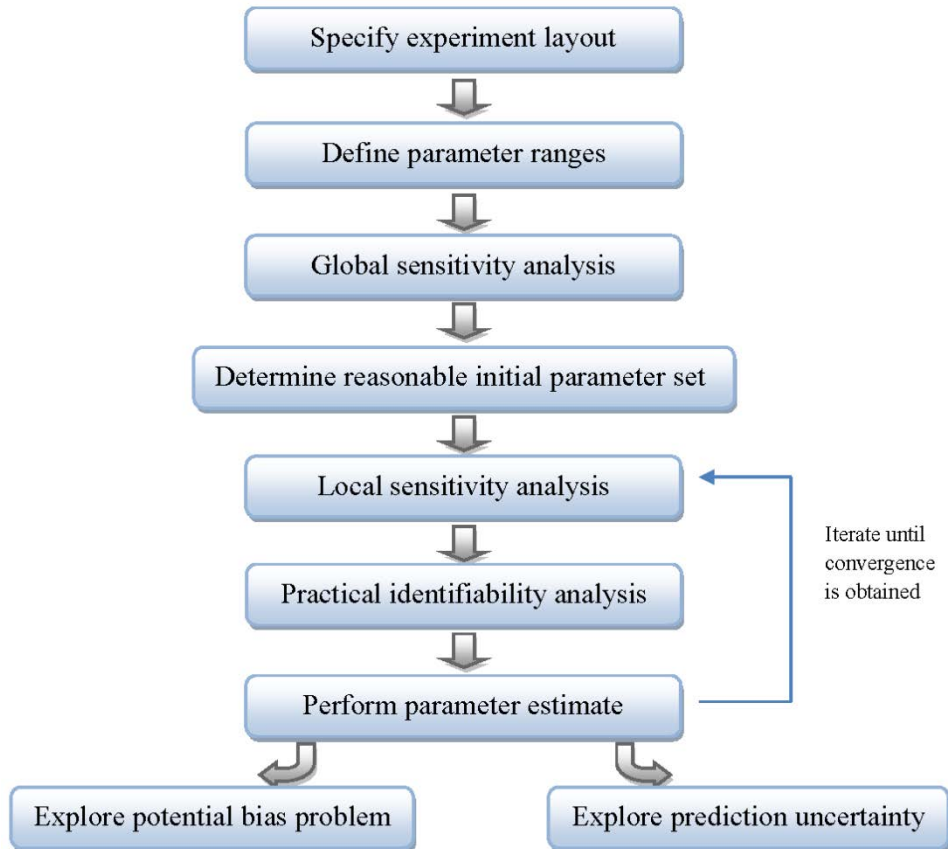
Fig.7.1 - Steps of a systematic procedure of identifiable parameter subset selection and estimation.

7.2.2. Experimental layouts

Currently in both academic research and practical application, the calibration of advanced settling models strongly relies on batch settling measurements, which remains labor intensive and information limited. The lack of high resolution data sets, especially those outside the hindered settling range, greatly challenges the model advancement test and application. Kinnear's data set (Kinnear 2002) is one of few published data sets that contain both the batch settling

curves and concentration profile measurements, which implies it can be used for a comprehensive model performance evaluation. In this study, we select the Salt Lake City Water Reclamation Plant (SLCWRP) subset of the Kinnear's data set, and design four modeling scenarios with increasing difficulty of data collection, as shown in Table 7.1, to evaluate the influence of experimental layouts on the analysis of parameter identifiability and prediction uncertainty. Since there is no information about the possible measurement error available, the measurement error is not considered in this study. For further information about methodology of data collection, the reader is referred to the literature (Kinnear 2002).

Table 7.1 - The design of batch settling experiments and comments.

Scenario	Experimental Design	Comments
1	Collecting sludge blanket curves with initial concentrations at 1.74, 3.42, 5.46, 8.25, 8.95 kg/m^3 (119 data points);	The sludge blanket curve data is most often collected in batch settling measurements. The linear part of the curve is informative for Vesilind parameter estimation;
2	Collecting sludge blanket curves with initial concentrations at 1.74, 3.42, 5.46, 8.25, 8.95 kg/m^3, and concentration at the static sediment top at 3.42 kg/m^3 (120 data points);	Theoretically, the solids concentration at the static sediment top equals to the gel concentration, the only physically measurable parameter within the hindered-compression settling model;
3	Collecting solids concentration profile of the static sediment with the initial concentration at 3.42 kg/m^3 (7 data points);	The solids concentration profile of the static sediment is difficultly measurable but highly recommended being collected in proposed hindered-compression calibration strategies;
4	Collecting sludge blanket curves with initial concentrations at 1.74, 3.42, 5.46, 8.25, 8.95 kg/m^3, as well as solids concentration profile of the static sediment with initial concentration at 3.42 kg/m^3 (126 data points);	The most informative data set, which is expected to provide information about both the hindered and compression settlings;

7.2.3. Identifiability analysis

Fig.7.1 shows the procedure for obtaining identifiable parameter subset in different experimental layouts. First, the experimental layout needs to be specified, as shown in Table 7.1. The proper

179

assessment of prior parameter uncertainties is significant for the subsequent analysis steps, but usually difficult and laborious. The hindered settling parameters (v_0, r_h) are well reported in previous studies (Plósz et al. 2011, Ramin et al. 2014a), while the compression parameters (C_g, α, β) remain poorly understood. Table 7.2 gives the parameter uncertainties used in this study, which are reasonably estimated based on literature reviews and modeling experience.

Table 7.2- Uncertainty of the hindered-compression model parameters.

Symbol	Definition	Uncertainty	Reference
V_0	hindered settling parameter [m/hr]	3.47 - 9.71	Plósz et al. 2011, Ramin et al. 2014a
r_h	hindered settling parameter [m^3/kg]	0.15 - 0.63	Plósz et al. 2011, Ramin et al. 2014a
C_g	Gel concentration [kg/m^3]	5.06 - 15.27	Kinnear 2002
α	compression settling parameter [Pa]	0 - 20	De Clercq et al. 2008, Bürger et al. 2013
β	compression settling parameter [kg/m^3]	1 - 10	De Clercq et al. 2008, Bürger et al. 2013

By evaluating model outputs which correspond to the experimental data set, the global sensitivity analysis (GSA) has been proved as a reliable approach to preliminarily select the parameter subset which can be reasonably estimated based on the available information content (Brockmann et al. 2008). Compared with the expert knowledge approach recommended by Brun et al. (2002), GSA is expected to be more objective by considering the whole range of uncertainty of each parameter, and allocating model output uncertainties to the parameter uncertainties (Saltelli et al. 2004). The GSA is carried out by the extended-Fourier Amplitude Testing (e-FAST), originally developed by Cukier et al. (1973) and Schaibly and Shuler (1973), and later extended by Satelli et al. (1999). As a variance based technique, the e-FAST has its root in the general theorem that the total variance can be decomposed into conditional variances, as shown in eq.(7.5):

$$Var(sy) = Var(E(sy | \theta_i)) + E(Var(sy | \theta_i)) \tag{7.5}$$

where *Var* and *E* is the variance and expectancy operator respectively, *sy* denotes a vector of scalar values for the model output and θ_i is the *i*th model factor. The Extended-FAST implementation strategy used in this study is based on Satelli et al. (1999), and the transformation function is given by eq.(7.6):

$$\theta_i = \frac{1}{2} + \frac{1}{\pi} \arcsin(\sin(\omega_i s + \varphi_i)) \tag{7.6}$$

where *s* ranges from -π/2 to π/2, w_i is a set of different frequencies and φ_i is a random phase-shift. The total number of model evaluation required can be determined by:

$$N_s = m\left(2M\omega_{max} + 1\right) \tag{7.7}$$

where *m* is the number of factors, *M* is the interference frequencies, and w_{max} is the maximum frequency. In this study, *M* and ω_{max} is 4 and 8 respectively. For further information about Extended-FAST implementation strategy, such as the selection of ω, the reader is referred to the literature (Saltelli et al. 1999).

Technically, the e-FAST is able to provide two kinds of sensitivity measures: S_i, which does not consider the interaction among factors, and S_{Ti}, which accounts for the total contribution of the factor to the output variance. According to Cosenza et al. (2014), S_{Ti} is more informative for determining non-influential factors. Therefore, the global mean sensitivity ($\delta_j^{G,msqr}$) of the model output to the change in θ_j is calculated by:

$$\delta_j^{G,msqr} = \sqrt{\frac{1}{n}\sum_{k=1}^{n}(S_{Ti})^2} \tag{7.8}$$

where n is number of observations. A large $\delta_j^{G,msqr}$ indicates the parameter θ_j is influential to the overall model outputs, and only parameters with $\delta_j^{G,msqr}$ larger than 0.1 are considered to be influential in this study. Given that the global sensitivity measures quantify the averaged influence of parameters on the model outputs, it may not be able to accurately reflect the parameter importance at specific local points, especially for those having global mean sensitivity measures close to the critical value. Therefore, the local mean sensitivity measures, which can calculated by eq.(7.9), are used as a supplement to further evaluate the significance of parameters.

As mentioned above, selecting the suitable value of initial parameter set remains a challenge due to the insufficient prior knowledge of biomass settleability and compressibility, as well as the limited number of reported parameter values. The parameters that cannot be reasonably estimated are fixed as the values reported by De Clercq et al. (2008) and Bürger et al. (2013). For the influential parameters, the initial hindered parameter values can be estimated by the conventional hindered settling velocity approach if batch settling curve observations are available, such as in experimental layouts 1, 2 and 4. The initial value of gel concentration (C_g) can be approximated by the concentration at the static sediment top, such as in experimental layouts 2, 3 and 4. Otherwise, the initial influential parameter values are determined by artificial manipulation until an acceptable fit to the experimental observations is obtained.

Parameter identifiability is investigated using the approach proposed by Brun et al. (2001), which is based on the collinearity calculation of the scaled local sensitivity functions ($s_{k,j}$), shown as eq.(7.9):

$$s_{k,j} = \frac{\Delta\theta_j}{sc_k}\frac{\partial sy_k}{\partial\theta_j} \quad and \quad \tilde{s}_{k,j} = \frac{s_{k,j}}{\|s_j\|} \tag{7.9}$$

where $\partial sy_k/\partial\theta_j$ denotes the absolute local sensitivity of model output sy_k to the parameter θ_j; $\Delta\theta_j$ and sc_k are two scale factors which denote the prior uncertainty range of the parameter θ_j and the typical magnitude of the corresponding observations respectively. $\|s_j\|$ is the Euclidean norm of the jth column of S ($S = \{s_{k,j}\}$). The perturbation factor used is 5%, which is found to be suitable for all the model parameters.

Poor parameter identifiability can be caused by a small sensitivity of the model output to the parameter, or by a high linear dependence of local sensitivity functions (Reichert and Vanrolleghem 2001). The significance of parameters is determined by the local mean sensitivity function $\delta_j^{L,msqr}$:

$$\delta_j^{L,msqr} = \sqrt{\frac{1}{n}\sum_{k=1}^{n}(s_{k,j})^2} \tag{7.10}$$

The collinearity index is defined as eq.(7.11) to evaluate the linear dependence:

$$\gamma_k = \frac{1}{\min_{\|\beta\|=1}\|\tilde{S}\eta\|} = \frac{1}{\sqrt{\min(EV[\tilde{S}^T\tilde{S}])}} \tag{7.11}$$

where $\tilde{S} = \{\tilde{s}_{k,j}\}$, η is the vector of coefficients, and *EV* denotes the eigenvalue of $[\tilde{S}^T \tilde{S}]$. A large γ_k indicates that the sensitivity functions are highly linearly dependent, which means the changes of model outputs caused by a small change of parameters, such as θ_j, can be mostly compensated by the change of other parameters (Brun et al. 2002). In this study, the parameter subset is considered to be poorly identifiable, if the corresponding γ_k exceeds 10, the threshold recommended by Brun et al. (2001).

To combine the information of the collinearity index and the local sensitivity function, the determinant measure ρ_k is defined as eq.(7.12), which can be useful in parameter identifiability comparison of different parameter subsets (Brun et al. 2002).

$$\rho_N = \det\left(S_N^T S_N\right)^{1/(2N)} \tag{7.12}$$

Where *det( )* is the determinant function, and *N* is the number of parameters in the corresponding subset. Since the value of ρ_N strongly depends on the choice of $\Delta\theta_j$, ρ_N is a relative measure suited for comparison of parameter identifiability of different subsets, and cannot be simply evaluated based on an absolute threshold value (Brun et al. 2002). The large $\delta_j^{L,msqr}$ and small γ_k result a large ρ_N, which indicates a good identifiability.

Based on the parameter identifiability analysis results, the parameter estimation is performed by minimizing the weighted residual sum of squares (WRSS):

$$WRSS = (Y - sy(\boldsymbol{\theta}))^T W (Y - sy(\boldsymbol{\theta})) \tag{7.13}$$

where Y is the experimental observation vector, $\boldsymbol{\theta}$ is the parameter vector, and $W = diag(1/sc_1^2, 1/sc_2^2, \cdots 1/sc_j^2, \cdots 1/sc_M^2)$ is a diagonal weighting matrix. The parameter identifiability analysis and estimation are repeated until convergence is achieved. Since the collinearity measures are calculated based on local sensitivity measures, steps (local sensitivity analysis, practical identifiability analysis, perform parameter estimate) have to be redone after adjusting the initial parameter values, until the convergence of estimates is achieved.

The selection of initial parameter values can profoundly impact the local sensitivity measures, thus potentially influencing parameter identifiability for nonlinear systems (Weijers and Vanrolleghem 1997). In this study, the influence of initial values selection on parameter identifiability is evaluated based on the approach developed by Brockmann et al. (2008) by using experimental layouts 3 and 4 as examples. Parameters are sampled 800 times over the entire uncertainty space using Latin hypercube sampling, and the corresponding WRSS values are calculated. Only the sampled parameter sets with WRSS smaller than 25 percentile of the total calculated WRSS are considered to provide acceptable predictions and used to investigate the influence of selecting initial parameter values on parameter identifiability.

7.2.4. Exploring the estimate bias and model prediction uncertainty

In most cases, estimating identifiable parameter subsets from insufficient experimental observations are conditional on the values of prior fixed parameter, which may lead to biased estimates (Brun et al. 2002). To evaluate the influence of the values of fixed parameters on estimates, we reestimate the parameter subset by varying β in the entire prior uncertainty space in layouts 3 and 4.

It is also interesting to investigate the maximum possible model prediction uncertainty reduction if the identifiable parameter subsets are reliably estimated. The prediction uncertainty analysis involves the following steps recommended by Sin et al. (2009):

1. Specifying input uncertainty: because of the reliable estimation of identifiable parameters, the only uncertainty source is the non-identifiable parameters, and their uncertainty has been shown in Table 7.2;

2. Sampling input uncertainty: Latin hypercube sampling strategy is applied;

3. Propagating input uncertainty to obtain prediction uncertainty: Monte Carlo simulation is applied;

4. Representation and interpretation of results: the prediction certainty results are represented using mean and percentiles.

7.3. Results and discussion

7.3.1. Parameter selection for identifiability analysis

The global sensitivity functions of the four experimental layouts are shown in Table 7.3. Compared with layout 1, the additional measurement of the top concentration of the static sediment in layout 2, provides a good initial approximation of the gel concentration, but does not impact the sensitivity functions calculation. Hence, the global sensitivity functions of the experimental layouts 1 and 2 are identical. When only the batch settling curve observations are available, such as in experimental layouts 1 and 2, the hindered settling parameters are much more influential than the compression parameters. The large difference of sensitivity functions

between hindered and compression parameters may be attributed to the fact that the duration of most batch settling experiments, usually 0.5~1 *hr*, is sufficient to collect hindered settling velocities, but not long enough to obtain compression settling behavior. This implies that calibration approaches based solely on batch settling curves need to be used with caution for hindered-compression model calibration. When concentration profile observations are available, compression parameter sensitivities greatly increase, especially in experimental layout 3, where sensitivity functions of several compression parameters can be even larger than those of hindered settling parameters. This finding shows that the solids concentration distribution in the high concentration range is profoundly influenced by the compression settling behavior, thus making the concentration profile measurements informative for compression parameter calibration, which agrees with the previous conclusion that collecting concentration profile data is recommended for hindered-compression model calibration (Kinnear 2002, De Clercq et al. 2008, Ramin et al. 2014c).

Initial parameter values as well as the corresponding local mean sensitivity measures, are also shown in Table 7.3. The important parameters found by the local measures are almost identical to those determined by the global measures, with only one exception: layout 4 where the global and local sensitivity measures cannot reach a consensus of the importance of β. This demonstrates that global sensitivity analysis is reliable for preliminary selection of important parameters, and local sensitivity analysis is also necessary to further evaluate the parameter selection. The influence of selecting initial parameter values to the local sensitivities is also obtained: the change of initial values of C_g and α from 6.00 and 0.31 in experimental layout 1 to 11.06 and 1.94 in experimental layout 2 impact local sensitivities. It demonstrates that a proper assessment of initial parameter values is particularly important.

Table 7.3 - Initial values, global and local mean sensitivity measures of the model parameters of layouts 1-4.

Parameter	Layout 1			Layout 2			Layout 3			Layout 4		
	θ^{ini}	$\delta^{G,msqr}$	$\delta^{L,msqr}$	θ^{ini}	$\delta^{G,msqr}$	$\delta^{L,msqr}$	θ^{ini}	$\delta^{G,msqr}$	$\delta^{L,msqr}$	θ^{ini}	$\delta^{G,msqr}$	$\delta^{L,msqr}$
V_0	7.61	0.235	0.421	7.61	0.235	0.487	9.18	0.159	0.107	7.61	0.208	0.506
r_h	0.34	0.815	0.681	0.34	0.815	0.699	0.38	0.245	0.675	0.34	0.701	0.997
C_g	6.00	0.214	0.129	11.06	0.214	0.213	11.06	0.735	0.332	11.06	0.322	0.398
α	0.31	0.168	0.145	1.94	0.168	0.136	0.617	0.271	0.136	0.38	0.146	0.214
β	4.00	0.029	0.056	4.00	0.029	0.011	4.72	0.158	0.103	2.10	0.079	0.119

7.3.2. Parameter identifiability analysis and parameter estimation

To be identifiable, a parameter subset is expected to satisfy two criteria: 1) parameters within the parameter subset must be sufficiently sensitive, which means their local mean sensitivity functions need to be larger than 0.1; 2) the local sensitivity functions of the parameter subset cannot be approximately linearly dependent, and this point is addressed by setting a maximum of the collinearity index as 10. Only if parameter subsets fulfill both criteria, those having high determinant measures are considered to be best identifiable.

The collinearity indices and determinant measures of parameter subsets are shown in Table 7.4. For layouts 1 and 2, all parameter subsets comprising influential parameters are identifiable with collinearity measures as low as 1.00, which means almost no interdependency exists. It is interesting to learn that although in previous studies, batch settling curves (experimental layout 1 and 2) were usually considered to be less informative for calibrating the compression parameters, weak interdependency exists between compression parameters C_g and α. In contrast, parameter subsets including the hindered parameters have a relatively stronger interdependency as their collinearity measures is more than 2. Combining hindered settling parameters (V_0, r_h) and compression settling parameters (C_g and α) does not deteriorate the parameter identifiability. Therefore, parameter subset {V_0, r_h, C_g, α} is used for parameter estimation due to its acceptable identifiability.

For experimental layout 3, even though all parameter subsets of size 2 are identifiable with collinearity measures less than 10, subset {α, β} shows a strong interdependency as its collinearity index is close to the critical value. As expected, parameter subsets comprising {α, β} are clearly unidentifiable with collinearity measures larger than 10. It is noticeable that although

the concentration profile observations are informative for both hindered and compression parameter calibration, simultaneously estimating all parameters is unlikely to be successful based upon the initial parameter selection as shown in Table 7.3, and the maximum size of identifiable parameter subsets is found to be 3. Consequently, parameter subset $\{r_h, C_g, \alpha\}$ is selected for estimation due to its low collinearity measure ($\gamma=2.86$) and high determinant measure ($\rho=0.738$).

Table 7.4 - Collinearity indices and determinant measures of parameter subsets of experimental layouts 1-4.

Set number	Parameters	Layout 1		Layout 2		Layout 3		Layout 4	
		γ_k	ρ_k	γ_k	ρ_k	γ_k	ρ_k	γ_k	ρ_k
1	V_0, r_h	2.23	0.775	2.67	0.714	3.67	0.615	2.21	0.779
2	V_0, C_g	1.22	0.972	1.01	1.00	1.18	0.979	1.25	0.967
3	V_0, α	1.00	1.00	1.00	1.00	1.63	0.884	2.24	0.968
4	V_0, β	-	-	-	-	1.45	0.923	1.24	0.968
5	r_h, C_g	1.21	0.975	1.05	0.998	1.36	0.943	1.81	0.850
6	r_h, α	1.19	0.978	1.11	0.991	1.63	0.884	1.81	0.848
7	r_h, β	-	-	-	-	1.52	0.908	1.80	0.849
8	C_g, α	1.00	1.00	1..00	1.00	2.59	0.724	4.78	0.541
9	C_g, β	-	-	-	-	3.43	0.635	5.31	0.514
10	α, β	-	-	-	-	9.21	0.391	**26.1**	0.233
11	V_0, r_h, C_g	2.23	0.827	2.71	0.797	4.23	0.675	3.08	0.732
12	V_0, r_h, α	2.59	0.806	2.91	0.778	3.67	0.663	3.14	0.728
13	V_0, r_h, β	-	-	-	-	3.71	0.678	3.14	0.729
14	V_0, C_g, α	1.22	0.981	1.01	0.999	3.88	0.689	4.78	0.649
15	V_0, C_g, β	-	-	-	-	4.52	0.658	5.32	0.627
16	V_0, α, β	-	-	-	-	**15.9**	0.418	**26.2**	0.370
17	r_h, C_g, α	1.32	0.967	1.13	0.992	2.86	0.738	4.78	0.593
18	r_h, C_g, β	-	-	-	-	3.63	0.689	5.31	0.574
19	r_h, α, β	-	-	-	-	**10.6**	0.476	**26.2**	0.339
20	C_g, α, β	-	-	-	-	**20.8**	0.319	**31.7**	0.232
21	V_0, r_h, C_g, α	2.59	0.838	2.94	0.826	**12.2**	0.481	4.79	0.578
22	V_0, r_h, C_g, β	-	-	-	-	**11.6**	0.476	5.33	0.564
23	V_0, r_h, α, β	-	-	-	-	**33.7**	0.339	**26.2**	0.380
24	V_0, C_g, α, β	-	-	-	-	**32.7**	0.340	**31.9**	0.328
25	r_h, C_g, α, β	-	-	-	-	**28.9**	0.367	**32.1**	0.306
26	$V_0, r_h, C_g, \alpha, \beta$	-	-	-	-	**36.5**	0.289	**32.1**	0.342

With respect to layout 4, the parameter subsets comprising $\{\alpha, \beta\}$ are poorly identifiable as well. Nevertheless, in contrast to layout 3 where no parameter subsets with size more than 3 are

identifiable, two subsets of size 4, $\{V_0,\ r_h,\ C_g,\ \alpha\}$ and $\{V_0,\ r_h,\ C_g,\ \beta\}$, are clearly identifiable in layout 4. The comparison of the determinant measures of $\{V_0,\ r_h,\ C_g,\ \alpha\}$ and $\{V_0,\ r_h,\ C_g,\ \beta\}$ shows that the former one is more promising for further evaluation.

Parameter estimation is performed based on the parameter identifiability analysis, and Table 7.5 summarizes the estimation results and the corresponding correlation matrix information. The low absolute off-diagonal elements of correlation matrixes of all experimental layouts confirm the conditional identifiability of the selected parameter subsets. Estimates of hindered parameters (V_0, r_h) and gel concentration (C_g) differ only slightly from their corresponding initial values, and in contrast, the difference between final estimates and initial values of α can be as large as 30~60%.

To compare the sludge settling properties characterized by the parameter estimates obtained from different experimental layouts, the batch settling flux and compressive solids stress which reflect the sludge settleability and compressibility respectively are calculated and shown in Fig.7.2. The estimated settling fluxes are similar or identical with only one notable exception: the batch flux of layout 3, which implies a better sludge settleability, especially in medium and high concentration range. This discrepancy possibly can be caused by the difference in obtaining initial hindered parameter values; the same initial values of hindered parameters are used in layout 1, 2 and 4 which are determined by the conventional hindered settling velocity approach. In layout 3 where no batch settling curve observations are available, the initial values of the hindered settling parameters are selected by experience or manual parameter adjustment. Fig.7.2 also shows that the estimated sludge compressibility characterized by compressive solids stress curves of different layouts are inconsistent, which is mostly reflected by the difference of estimated gel concentrations and magnitude of effective solids stress. The effective solids stress

curve estimated in experimental layout 1 possesses the smallest gel concentration and magnitude, which is consistent with the smallest initial values of *Cg* and *α* used in this case as compared with other layouts. Estimated effective solids stress curves of layout 2, 3 and 4 are similar in gel concentration, but greatly differ in stress magnitude, which can be attributed to the fact that in these layouts, similar gel concentration estimates but different *α* estimates are obtained.
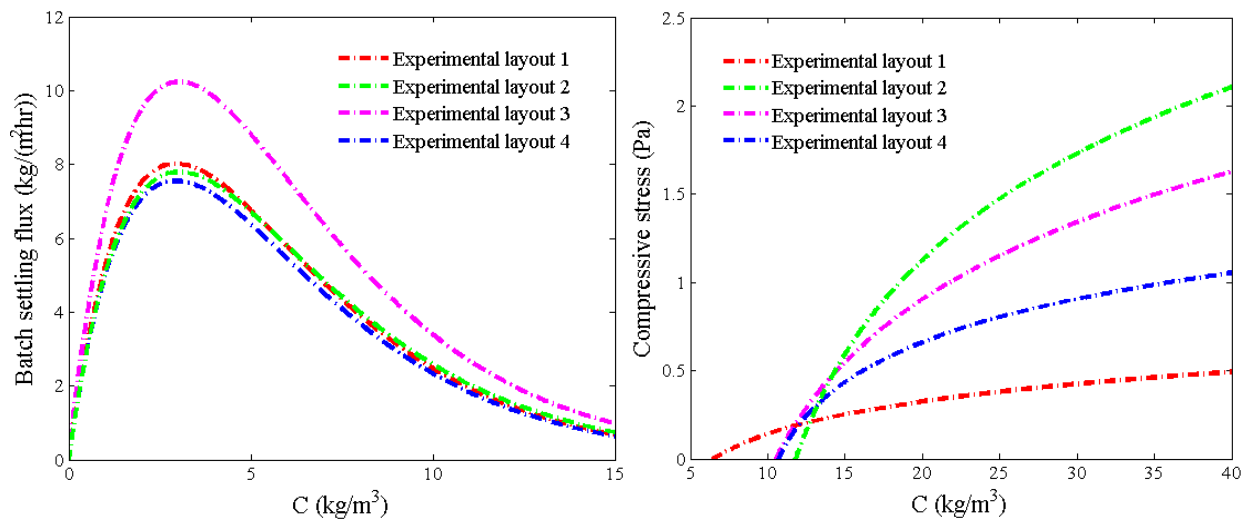
Fig.7.2 - The estimated batch settling flux functions (left) and compressive stress functions (right) calculated based on the Vesilind equation (Vesilind 1968) and the logarithmic compression stress equation (De Clercq et al. 2008).

To facilitate an understanding of the limitations of each layout in model calibration, we compare model simulations based on parameter estimates of layouts 1-4 to complete experiment observations (batch settling curves and concentration profiles), shown in Fig.7.3. As expected, model simulations based on estimates obtained in layout 4 fit well with both batch settling curves and concentration profiles. Simulations of layout 3 provide the best fit with concentration profile observations, while the predicted batch settling curves are much lower than experiment observations, which implies that the estimated batch settling flux of layout 3 cannot represent real sludge settleability. Accurate predictions of static concentration profiles in layout 3 may be

achieved by overestimating the sludge settleability while underestimating its compressibility. Therefore, estimating sludge settleability and compressibility by only using static concentration observations, such as experimental layout 3, may be questionable. Simulations of layout 1 and 2 provide fairly good fits to observed batch settling curves. Simulations of layout 1 slightly overestimate batch settling curves of 8.25, 8.95 kg/m^3, which may be caused by the underestimated gel concentration. Although simulations based upon layout 2 succeed in predicting the top concentration of static sediment, the predicted concentration within the sediment is lower than the experiment observations due to the relatively large estimated compressive solids stress as shown in Fig.7.2. Consequently, accurately estimating compressibility remains a challenge if using only batch settling curve observations.

Table 7.5 - Initial values, final estimates, standard errors and correlation matrixes of the parameter subsets selected in experimental layouts 1-4.

		Experiment layout 1									**Experiment layout 2**					
		Standard error		Correlation matrix						Standard error		Correlation matrix			
Parameter	θ^{est}	absolute	relative	V_0	r_h	C_g	α	Parameter	θ^{est}	absolute	relative	V_0	r_h	C_g	α
V_0	7.41	0.072	0.009	1				V_0	6.99	0.098	0.014	1			
r_h	0.34	0.004	0.011	0.446	1			r_h	0.33	0.004	0.013	0.538	1		
C_g	6.46	0.549	0.085	0.053	-0.081	1		C_g	11.8	0.196	0.017	0.356	-0.007	1	
α	0.22	0.028	0.127	-0.042	-0.297	0.084	1	α	1.01	0.086	0.085	0.100	-0.039	0.018	1

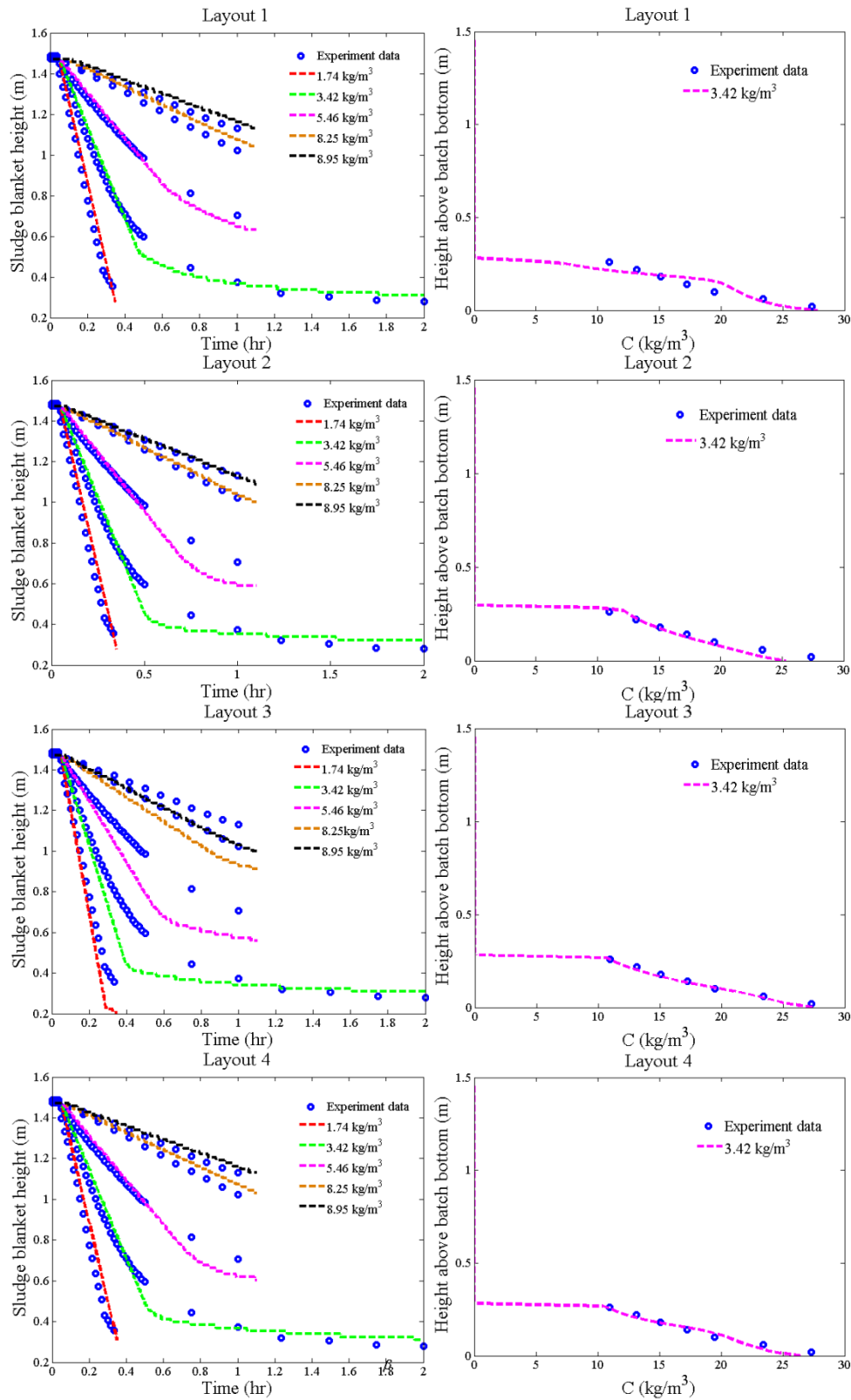|		**Experiment layout 3**								**Experiment layout 4**					
		Standard error		Correlation matrix					Standard error		Correlation matrix			
Parameter	θ^{est}	absolute	relative	r_h	C_g	α	Parameter	θ^{est}	absolute	relative	V_0	r_h	C_g	α
r_h	0.33	0.015	0.045	1			V_0	6.98	0.096	0.014	1			
C_g	10.51	0.866	0.082	-0.424	1		r_h	0.34	0.004	0.011	0.542	1		
α	0.82	0.109	0.133	0.406	0.838	1	C_g	10.7	0.177	0.017	0.376	0.405	1	
							α	0.39	0.433	0.111	-0.121	-0.408	-0.428	1

Fig.7.3 - Simulation results (batch settling curves and concentration profile) based on parameter subset estimations of experiment layouts 1-4.

7.3.3. Influence of selecting initial parameter values on parameter identifiability

The selection of parameter initial values impacts parameter identifiability in two ways: 1) impact local parameter sensitivity functions; 2) impact collinearity measures of parameter subsets. If initial values of C_g and hindered parameters are determined by measuring the top concentration of static sediment and hindered settling velocities respectively, the sensitivity analysis of parameter identifiability to initial parameter selection only needs to consider the remaining parameters (V_0, r_h, α, β in experimental layout 3, and α, β in experimental layout 4), which may have different initial values.

Fig.7.4 shows the change of local mean sensitivity functions with different initial parameter values. For experimental layout 3, changes of parameter initial values mostly influence the local mean sensitivity functions of V_0, r_h α and β. In spite of the variance of sensitivity functions, the gel concentration, C_g, remains influential as its 25% percentile is above the critical value defined as 0.1 in this study. Fig.7.4 also shows that compared with other parameters, C_g possesses the highest median of the local mean sensitivity functions, which agrees with the global sensitivity analysis conclusion that C_g is the most influential parameter in layout 3. In layout 4, the hindered settling parameters, V_0 and r_h, are the most influential parameters, and their sensitivity functions are almost insensitive to the initial value changes of α and β. Even though a moderate variance of the sensitivity measures of C_g is observed, it remains as a significant parameter with 5th percentile above the critical value. The only potentially non-influential parameters are α and β, whose 75th percentiles are close to the critical value.
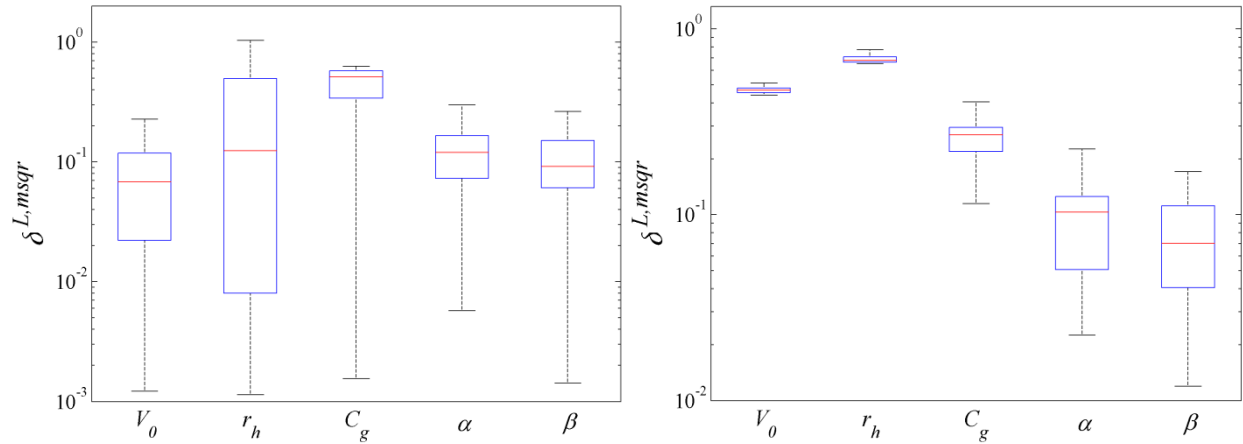
Fig.7.4 - Box-Whisker plot of the local mean sensitivity measures of model parameters in layouts 3 and 4. The upper and lower boundaries of the box mark the 75th and 25th percentile, and line within the box marks the median. Whiskers above and below indicate the 95th and 5th percentile. (left: experimental layout 3; right: experimental layout 4).

Box-Whisker plots for collinearity indices of parameter subsets calculated based on sampled parameters are shown in Fig.7.5. For experimental layout 3, the parameter subsets of size 2 are mostly identifiable, and their collinearity measures are not sensitive to the change of initial parameter values. Poor identifiability only can be obtained in subsets 1 $\{V_0, r_h\}$ and 10 $\{\alpha, \beta\}$ for their median and 75 percentile are above the critical value. This implies that parameter subsets comprising $\{V_0, r_h\}$ or $\{\alpha, \beta\}$ can be less identifiable than others. For subsets of size 3 and 4, the increase of parameter subset size leads to the variation of collinearity measures as well as the deterioration of identifiability, with only one notable exception: subset 14 $\{r_h, C_g, \alpha\}$, which is clearly identifiable independently of change of initial parameter values. This agrees well with the conclusion that parameter subsets that do not include $\{V_0, r_h\}$ or $\{\alpha, \beta\}$ show a better identifiability. Subset 26 $\{V_0, r_h, C_g, \alpha, \beta\}$ is poorly identifiable as the 5th percentile is above the critical value, thus making it unreliable for estimating all parameters simultaneously. Compared to layout 3, collinearity measures of parameter subsets of layout 4 are less sensitive to initial parameter value selection. Clearly, most parameter subsets are identifiable regardless of the

initial parameter values, and for several of them, for example the subsets of size 2, the collinearity measures are smaller than 1.5, indicating the absence of interdependence. Consequently, for layout 4, the size of parameter set that can be reliably estimated can be as large as 5, if parameters included are found to be influential to the experiment observations.
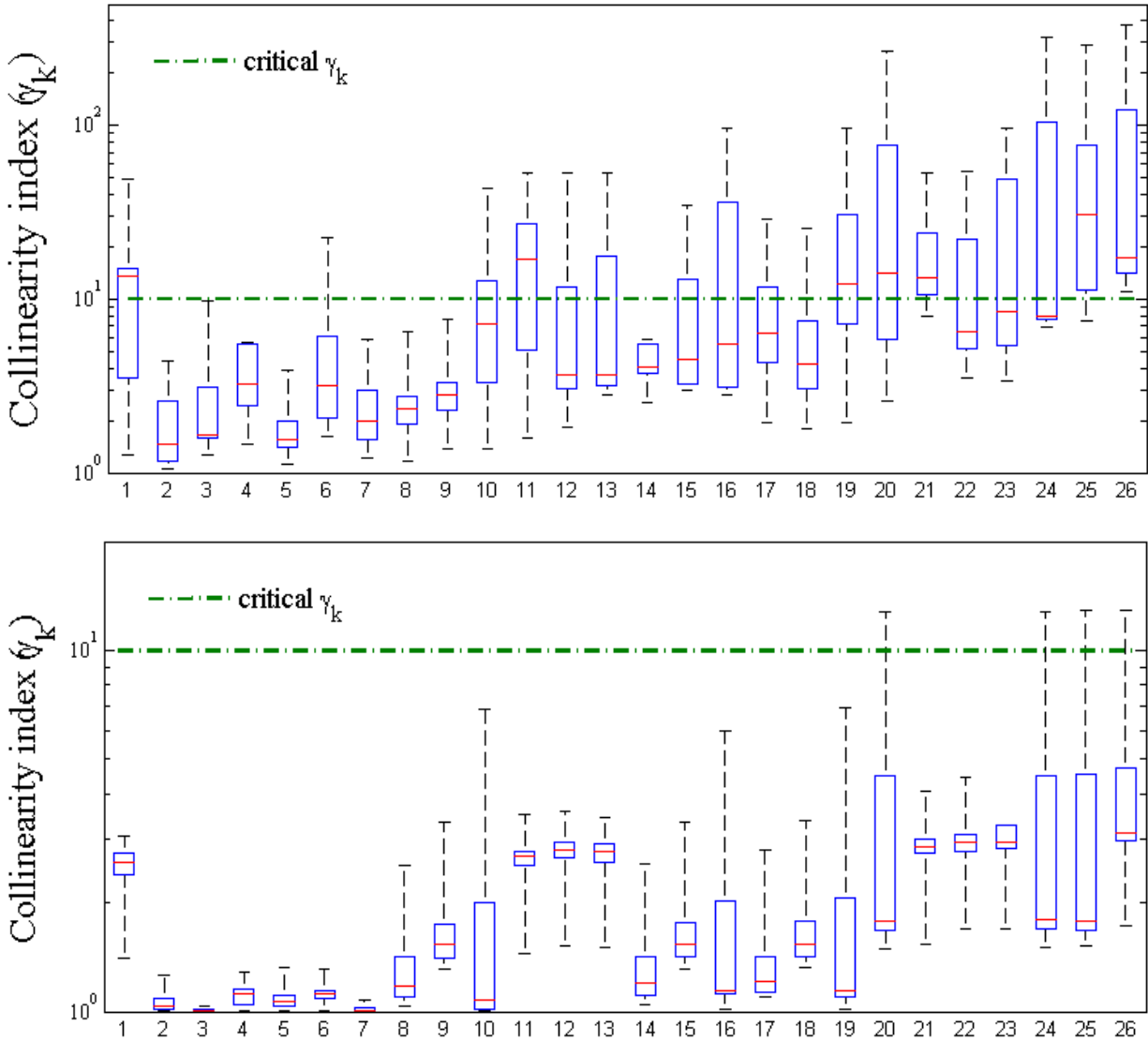
Fig.7.5 - Box-Whisker plot of the calculated collinearity indices for all parameter subsets of size 2-5. (the order of the parameter subsets is the same as the parameter set number as shown in Table 7.4). The upper and lower boundaries of the box mark the 75th and 25th percentile, and line within the box marks the median. Whiskers above and below indicate the 95th and 5th percentile. (top: experimental layout 3; bottom: experimental layout 4).

7.3.4. Exploring potential bias problem and prediction uncertainty

It is noteworthy that the estimates obtained by identifiable parameter subset estimation are clearly conditional on fixed values of unidentifiable parameters, hence potentially causing estimate bias problems (Brun et al. 2002). Fig.7.6 shows the reestimated results of layouts 3 and 4 using the parameter estimates shown in Table 7.5 as references, and Table 7.6 provides the average collinearity measures of all parameter subsets of size 2, composed of one identifiable parameter plus the fixed parameter, and the average estimate change of the corresponding identifiable parameter. As can be seen, the large average change is always associated with the large average collinearity measure, which indicates that the stronger the parameter is correlated to the fixed parameter, the more sensitive the estimate is to the change of the fixed parameter value. For layout 3, the small average collinearity measures of subsets $\{r_h, \beta\}$, $\{V_0, \beta\}$ indicate the week interdependency between r_h and β, C_g and β, and as a result, the estimates of the r_h and C_g are almost insensitive to β, which is demonstrated by the low average changes (<10%). However, concerning α, the increase of β leads to a significant increase of α, and the corresponding average change can be as high as 49.7%. The strong sensitivity of the estimate of α to the fixing β can be attributed to the significant interdependency of α and β with average collinearity measure as high as 19, which means that changes in β can be compensated by corresponding changes of α. When it comes to layout 4, almost no interdependency exists in subsets $\{V_0, \beta\}$, $\{r_h, \beta\}$ and $\{C_g, \beta\}$ as their corresponding average collinearity indices approach to 1. Conversely, the collinearity measures of $\{\alpha, \beta\}$ are relatively larger, which leads to poor identifiability problem. Obviously, the estimates of α in layouts 3 and 4 can only be seen as reasonable values which leads to a sufficient description of experiment observations rather than "true parameter value".

Table 7.6 - The average collinearity indices of parameter subsets of size 2 consisting of one identifiable parameter plus the fixed parameter, and the average changes of the estimates of identifiable parameters.

	Experimental layout 3			Experimental layout 4		
Parameter	Average γ	Average change (%)	Parameter	Average γ	Average change (%)
r_h	3.13	4.95	V_0	1.15	4.39
C_g	5.41	8.43	r_h	1.31	3.02
α	16.78	49.7	C_g	2.52	3.19
			α	3.10	98.4

To obtain prediction uncertainty of the hindered-compression model, we assume uncorrected parameters with the prior uncertainties as shown in Table 7.2, and zero uncertainty for the identifiable parameters of each layout. The model prediction uncertainty is calculated by using Latin hypercube sampling and Monte Carlo simulation. We consider the SST with the same configuration as proposed by Bürger et al. (2013), the volumetric flow Q_u=80 m^3/hr and Q_f is modeled by the harmonic function developed by Carstensen et al. (1998). The feed concentration is chosen as

$$C_f(t) = \begin{cases} 6 & 0 \leq t < 48\,hr \\ 7.5 & 48 \leq t < 72\,hr \\ 4 & 72 \leq t < 168\,hr \end{cases} \qquad (12)$$
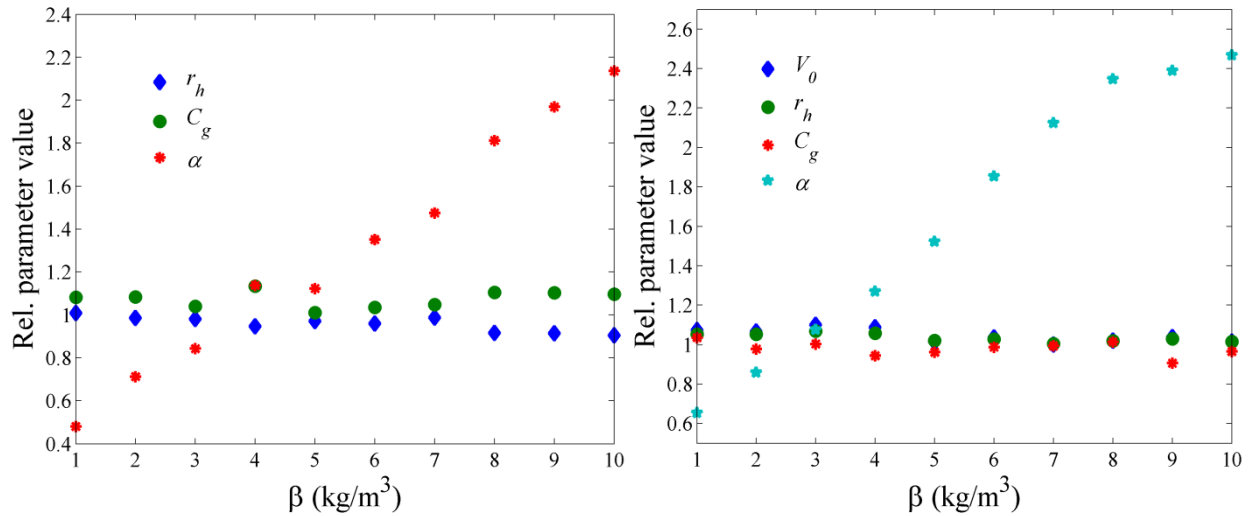
Fig.7.6 - Relative values of estimated parameter for different values of fixed parameters (left: experimental layout 3; right: experimental layout 4).

Fig. 7.7 shows the uncertainty ranges of SBH which is one of the most significant model outputs for system robustness and efficiency analysis. Given that model simulations based on estimation results of layouts 1, 2 and 4 possess the same uncertainty source - the non-identifiable β, it is interesting to compare their corresponding prediction uncertainties. Clearly, after estimating the identifiable parameter subsets of layouts 1, 2 and 4, the model prediction uncertainties become low, and the 5th percentile almost overlaps with the 95th percentile for SBH in layouts 1 and 4. Similar tendencies of SBH are obtained; however the difference in the prediction of peak SBH uncertainties can cause a discrepancy in developing control strategies. For layout 2 and 4, the 5th percentile of peak SBH is above 3m (the feed inlet), which indicates a high opportunity of thickening failure, and the 95th percentile is close to 4m (the effluent weir), which implies the potential risk of clarification failure. Hence, in order to avoid failure, a proper operating adjustment is needed from t= 48 to 72 hr, such as increasing the underflow rate. Conversely, for layout 1, since the 95th percentile of peak SBH uncertainty is below 3.5m, failure is not expected. For layout 3 where two uncertainty sources (V_0 and β) exist, the uncertainty of SBH remains

large, which implies that SBH is sensitive to these two parameters. If the unidentifiable parameters characterize the sludge with good settleability and compressibility, the growth of SBH can be moderate as the 5th percentile line shows. However, if the unidentifiable parameters lead to poor settleability and compressibility, a rapid change of SBH is expected as 95th percentile line shows, which can potentially cause thickening and clarification failures. Therefore, further operational adjustments are required to account for the shock increase of the solids flux for layout 3.
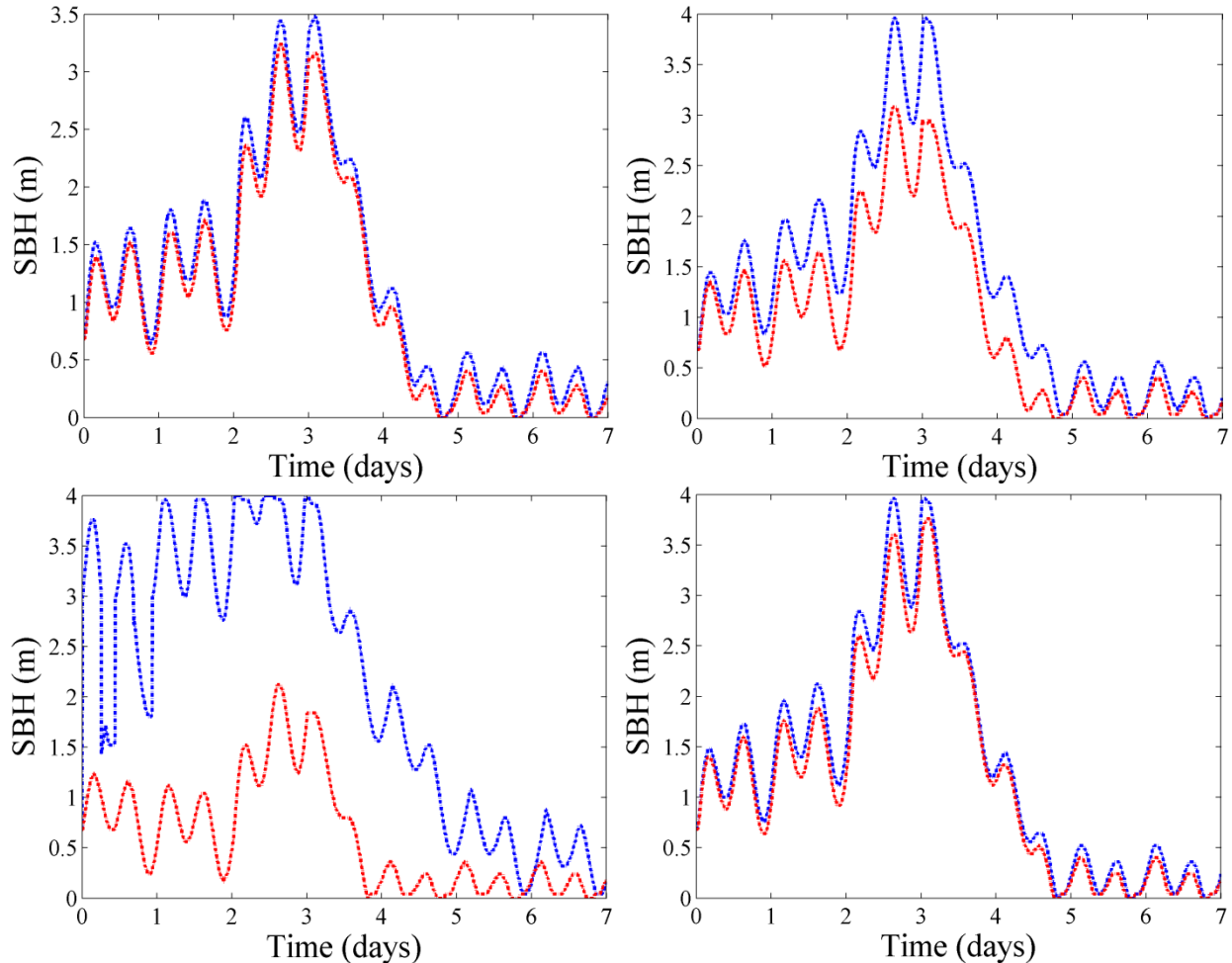

Fig.7.7 - Uncertainty of SBH based on parameter subset estimation of experimental layout 1-4. The blue and red dot lines indicate the 95th and the 5th percentile respectively. (top left: experimental layout 1; top right: experimental layout 2; bottom left: experimental layout 3; bottom right: experimental layout 4).

7.4. Conclusion

In this chapter, we provide a systematic analysis of model parameter identifiability in different experimental layouts, as well as the influence of selecting initial parameter values on parameter identifiability. Additionally, we further investigate the bias introduced by fixing parameters, and evaluate the model prediction uncertainties based on the estimation of identifiable parameter subsets. Specific conclusions can be made as follows:

1. As shown by the global sensitivity results, the hindered settling parameters are more influential in situations where only batch settling curve observations are available, while the sensitivity to compression parameters can be greatly increased if concentration profile observations are included. This supports the previous conclusion that concentration profile observations are informative for compression parameter calibration.

2. The identifiability analysis shows that at least three model parameters are conditionally identifiable, and β is most difficult to identify. Parameter estimates obtained from data sets only including the batch settling curves or the concentration profile fail to provide adequate description of the concentration profile observations and batch settling curve observations respectively, which implies the risk of calibrating model by using experimental measurements without sufficient information content.

3. Because of the application of local sensitivity functions, the parameter identifiability analysis can be sensitive to the initial parameter value selection. Determining the initial values of the hindered parameters and C_g by measuring the hindered settling velocities and the top concentration of the static sediment respectively is highly recommended to

minimize the sensitivity of parameter subset identifiability to the change of initial parameter values.

4. Estimates obtained by identifiable parameter subsets estimation are conditional on the values of fixed parameters. For these identifiable parameters, the more correlated they are to fixed parameters, the more sensitive their estimates are to the change of the fixed parameters. Reliably estimating identifiable parameters can reduce the model prediction uncertainty of SBH to some degree. However, in terms of the prediction uncertainty of peak SBH, the uncertainty analysis based on the estimates of different layouts cannot lead to consistent operation strategies, which implies that the hindered-compression continuous settling model cannot be used as quantitative prediction tool if calibrated without comprehensive data measurements.

It is worthy to note that in this chapter, we investigate the practical identifiability of SST model mostly based on the state-of-the-art settling model, since the prior uncertainty of all parameters in the model are well documented in previous investigations. Currently, several more advanced settling models have been developed to improve the model predictions, for example the hindered-transient-compression model developed by Ramin et al. (2014c) have been demonstrated to be more effective than the state-of-the-art settling model for batch settling predication. For these advanced SST models, the increase of model complexity can be expected, such as the size of model parameters can be close 10. The procedures and techniques used in this study, can also be a reliable framework for the parameter identifiability analysis of these advanced SST models.

8. Conclusion

This dissertation focuses on the one-dimensional (1-D) modeling of secondary settling tanks (SSTs), including the numerical analysis to introduce and select efficient (high accuracy and low computation cost) solution techniques, sensitivity and practical identifiability analysis to facilitate the reliable calibration of 1-D SST models, and evaluation the implications of secondary settling modeling on the design and control of waste water treatment plants. Specific conclusions of this dissertation can be made as follows:

1. Accurately solving the ideal continuous settling model is challenging because of solution discontinuities. As the only available method for analytical solution development of ideal continuous settling model, the method of characteristics has been successfully implemented to investigate the dynamics of SST for three typical solids loading transients: underloading-underloading, underloading-overloading and overloading-underloading.

2. The Yee-Roe-Davis method determines the calculation behavior in terms of the solution gradient, and provides both numerically and physically acceptable solutions that satisfy the Courant-Friedrichs-Lewy condition and entropy condition. Therefore, the Yee-Roe-Davis method is a reliable numerical technique for solving the nonlinear hyperbolic partial differential equation of the SST model, and can be an acceptable alternative to the Godunov and Enquist-Osher methods.

3. By using solutions of method of characteristics as reference, the convergence analysis of Methods Simplied-Godunov, Godunov and Yee-Roe-Davis shows that all are reliable, since they are able to provide arbitrarily close approximations to the reference solutions as

discretization is refined. For a given discretization level, the Yee-Roe-Davis method is most efficient in reducing error, and provides the most accurate approximations. However, this advantage of high accuracy of the Yee-Roe-Davis method is at the cost of larger computation time and coding complexity when compared with Methods Simplied-Godunov and Godunov. The simplified numerical flux calculation technique used in Method Simplied-Godunov increases error, but greatly reduces the coding complexity and computation cost. Method Godunov performs well in both accuracy and computation cost comparisons.

4. The choice of numerical methods can greatly impact the model outputs. Compared with the Yee-Roe-Davis method, using the Stenstrom-Vitasovic-Takács method can produce unrealistic solids accumulation during underloading condition, and underestimate the time-to-failure in thickening and clarification failures, thus potentially leading to conservative design and operation strategies.

5. Based on the global sensitivity analysis (GSA) results, the important parameters are identified for the hindered-compression-dispersion SST model (Bürger-Diehl model) calibration under non-ideal flow and settling conditions. Given that strong parameter interactions exist in the case of C_e prediction, advanced GSA techniques, such as Extended-Fourier Amplitude Testing, are required for reliable GSA results.

6. The sensitivity of the hindered-compression-dispersion SST model (Bürger-Diehl model) outputs to parameters is strongly impacted by the imposed simulation conditions, resulting in different parameter subsets for model calibration. Moreover, reliable reduction of the hindered-compression-dispersion SST model can be achieved based on GSA results; for example under the bulking condition, the hindered-compression-dispersion model can be

reduced to the hindered-dispersion model without impacting model outputs, which occurs because none of model outputs are sensitive to the compression settling parameters. The model uncertainty analysis is demonstrated as an efficient approach to evaluate the reliability of model reduction.

7. In terms of the calibration of hindered-compression-dispersion model, the global sensitivity analysis results show that the hindered settling parameters are more influential in situations where only batch settling data observations are available, while the sensitivity to compression parameters can be greatly increased if concentration profile observations are included. This supports the previous conclusion that concentration profile observations are informative for compression parameter calibration.

8. The practical identifiability analysis shows that parameter estimates obtained from data sets only including the batch settling curves or the concentration profile fail to provide adequate description of the concentration profile observations and batch settling curve observations respectively. This implies a risk of calibrating a model using experimental measurements without sufficient information content.

9. Because of the application of local sensitivity functions, the parameter identifiability analysis can be sensitive to the initial parameter value selection. Estimates obtained by identifiable parameter subsets estimation are conditional on the values of fixed parameters. For these identifiable parameters, the more correlated they are to fixed parameters, the more sensitive their estimates are to the change of the fixed parameters.

10. For an activated sludge process design, the bioreactor and SST should be designed as a

whole, and a safety constraint can be introduced in the design process to greatly improve the system's efficiency and reliability. The designed alternatives based on the safety constraint show that the requirement of bioreactor volume decreases with an increase of SST size, and this can help prevent overdesigning the activated sludge process size and land waste. A comprehensive selection of the designed alternatives should consider three aspects: economic plausibility, contaminant removal efficiency, and system robustness. Least-cost points can usually be attained, but their locations will vary depending on the weighting of the relative cost factor.

Reference

Alderton, J.L. (1963) Discussion of "Analysis of Thickener Operation." by V.C.Behn and J.C.Liebman. Jour. San. Eng. Div. ASCE 89(6), 57-59.

Alex, J., Benedetti, L., Copp, J., Gernaey, K.V., Jeppsson, U., Nopens, I., Pons, M., Rieger, L., Rosen, C., Steyer, J.P., Vanrolleghem, P.A. and Winkler, S. (2008) Benchmarking Simulation Model No.1 (BSM1). IWA Taskgroup on Benchmarking of Control Strategies for WWTP, IWA Publishing, London, UK.

Anderson, H.M. (1981) A dynamic simulation model for wastewater renovation systems. Ph.D Thesis, Wayne State University, Detroit.

Auzerais, F.M., Jackson, R. and Russel, W.B. (1988) The Resolution of Shocks and the Effects of Compressible Sediments in Transient Settling. Journal of Fluid Mechanics 195, 437-462.

Auzerais, F.M., Jackson, R., Russel, W.B. and Murphy, W.F. (1990) The Transient Settling of Stable and Flocculated Dispersions. Journal of Fluid Mechanics 221, 613-639.

Ballou, D.P. (1970) Solutions to Nonlinear Hyperbolic Cauchy Problems without Convexity Conditions. Transactions of the American Mathematical Society 152(2), 441-460.

Batchelo.Gk (1972) Sedimentation in a Dilute Dispersion of Spheres. Journal of Fluid Mechanics 52(Mar28), 245-&.

Batchelor, G.K. (1976) Brownian Diffusion of Particles with Hydrodynamic Interaction. Journal of Fluid Mechanics 74(Mar9), 1-29.

Behn, V.C. (1957) Settling behavior of waste suspensions. Jour. San. Eng. Div. ASCE 83(5), 1-20.

Bergstrom, L. (1992) Sedimentation of Flocculated Alumina Suspensions - Gamma-Ray Measurements and Comparison with Model Predictions. Journal of the Chemical Society-Faraday Transactions 88(21), 3201-3211.

Bergstrom, L., Schilling, C.H. and Aksay, I.A. (1992) Consolidation Behavior of Flocculated Alumina Suspensions. Journal of the American Ceramic Society 75(12), 3305-3314.

Berres, S., Bürger, R., Karlsen, K.H. and Tory, E.M. (2003) Strongly degenerate parabolic-hyperbolic systems modeling polydisperse sedimentation with compression. Siam Journal on Applied Mathematics 64(1), 41-80.

Brockmann, D. and Morgenroth, E. (2007) Comparing global sensitivity analysis for a biofilm model for two-step nitrification using the qualitative screening method of Morris or the quantitative variance-based Fourier Amplitude Sensitivity Test (FAST). Water Science and Technology 56(8), 85-93.

Brockmann, D., Rosenwinkel, K.H. and Morgenroth, E. (2008) Practical identifiability of biokinetic parameters of a model describing two-step nitrification in biofilms. Biotechnology and Bioengineering 101(3), 497-514.

Brun, R., Kuhni, M., Siegrist, H., Gujer, W. and Reichert, P. (2002) Practical identifiability of ASM2d parameters - systematic selection and tuning of parameter subsets. Water Research 36(16), 4113-4127.

Brun, R., Reichert, P. and Kunsch, H.R. (2001) Practical identifiability analysis of large environmental simulation models. Water Resources Research 37(4), 1015-1030.

Bryant, J. (1972a) Continuous Time Simulation of the Conventional Activated Sludge Wastewater Renovation System. Ph.D. Dissertation, Clemson University. Clemson, South Carolina.

Bryant, J.O. (1972b) Continuous tine simulation of the concentional activated sludge wastewater renovation system, Clemson University, Clemson, South Carolina, USA.

Bürger, R. (2000) Phenomenological foundation and mathematical theory of sedimentation-consolidation processes. Chemical Engineering Journal 80(1-3), 177-188.

Bürger, R., Bustos, M.C. and Concha, F. (1999) Settling velocities of particulate systems: 9. Phenomenological theory of sedimentation processes: numerical simulation of the transient behaviour of flocculated suspensions in an ideal batch or continuous thickener. International Journal of Mineral Processing 55(4), 267-282.

Bürger, R., Concha, F. and Karlsen, K.H. (2001) Phenomenological model of filtration processes: 1. Cake formation and expression. Chemical Engineering Science 56(15), 4537-4553.

Bürger, R., Concha, F. and Tiller, F.M. (2000a) Applications of the phenomenological theory to several published experimental cases of sedimentation processes. Chemical Engineering Journal 80(1-3), 105-117.

Bürger, R., Coronel, I. and Sepulveda, M. (2006) A semi-implicit monotone difference scheme for an initial-boundary value problem of a strongly degenerate parabolic equation modeling sedimentation-consolidation processes. Mathematics of Computation 75(253), 91-112.

Bürger, R., Diehl, S., Faras, S. and Nopens, I. (2012) On reliable and unreliable numerical methods for the simulation of secondary settling tanks in wastewater treatment. Computers & Chemical Engineering 41, 93-105.

Bürger, R., Diehl, S., Faras, S., Nopens, I. and Torfs, E. (2013) A consistent modelling methodology for secondary settling tanks: a reliable numerical method. Water Science and Technology 68(1), 192-208.

Bürger, R., Diehl, S. and Nopens, I. (2011) A consistent modelling methodology for secondary settling tanks in wastewater treatment. Water Research 45(6), 2247-2260.

Bürger, R., Evje, S., Karlsen, K.H. and Lie, K.A. (2000b) Numerical methods for the simulation of the settling of flocculated suspensions. Chemical Engineering Journal 80(1-3), 91-104.

Bürger, R. and Karlsen, K.H. (2008) Conservation laws with discontinuous flux: a short introduction. Journal of Engineering Mathematics 60(3-4), 241-247.

Bürger, R., Karlsen, K.H., Klingenberg, C. and Risebro, N.H. (2003) A front tracking approach to a model of continuous sedimentation in ideal clarifier-thickener units. Nonlinear Analysis-Real World Applications 4(3), 457-481.

Bürger, R., Karlsen, K.H., Risebro, N.H. and Towers, J.D. (2004) Numerical methods for the simulation of continuous sedimentation in ideal clarifier-thickener units. International Journal of Mineral Processing 73(2-4), 209-228.

Bürger, R., Karlsen, K.H., Torres, H. and Towers, J.D. (2010) Second-order schemes for conservation laws with discontinuous flux modelling clarifier-thickener units. Numerische Mathematik 116(4), 579-617.

Bürger, R., Karlsen, K.H. and Towers, J.D. (2005) A model of continuous sedimentation of flocculated suspensions in clarifier-thickener units. Siam Journal on Applied Mathematics 65(3), 882-940.

Bürger, R. and Narvaez, A. (2007) Steady-state, control, and capacity calculations for flocculated suspensions in clarifier-thickeners. International Journal of Mineral Processing 84(1-4), 274-298.

Buscall, R. (1990) The Sedimentation of Concentrated Colloidal Suspensions. Colloids and Surfaces 43(1), 33-53.

Buscall, R., Goodwin, J.W., Ottewill, R.H. and Tadros, T.F. (1982) The Settling of Particles through Newtonian and Non-Newtonian Media. Journal of Colloid and Interface Science 85(1), 78-86.

Buscall, R., Mcgowan, I.J., Mills, P.D.A., Stewart, R.F., Sutton, D., White, L.R. and Yates, G.E. (1987) The Rheology of Strongly-Flocculated Suspensions. Journal of Non-Newtonian Fluid Mechanics 24(2), 183-202.

Buscall, R. and White, L.R. (1987) The Consolidation of Concentrated Suspensions .1. The Theory of Sedimentation. Journal of the Chemical Society-Faraday Transactions I 83, 873-891.

Bustos, M.C. (1988) On the Construction of Global Weak Solutions in the Kynch Theory of Sedimentation. Mathematical Methods in the Applied Sciences 10(3), 245-264.

Bustos, M.C. and Concha, F. (1992) Boundary-Conditions for the Continuous Sedimentation of Ideal Suspensions. Aiche Journal 38(7), 1135-1138.

Bustos, M.C., Concha, F. and Wendland, W. (1990a) Global Weak Solutions to the Problem of Continuous Sedimentation of an Ideal Suspension. Mathematical Methods in the Applied Sciences 13(1), 1-22.

Bustos, M.C., Paiva, F. and Wendland, W. (1990b) Control of Continuous Sedimentation of Ideal Suspensions as an Initial and Boundary-Value Problem. Mathematical Methods in the Applied Sciences 12(6), 533-548.

Cacossa, K.F. and Vaccari, D.A. (1994) Calibration of a Compressive Gravity Thickening Model from a Single Batch Settling Curve. Water Science and Technology 30(8), 107-116.

Chancelier, J.P., DeLara, M.C., Joannis, C. and Pacard, F. (1997) New insights in dynamic modeling of a secondary settler .1. Flux theory and steady-states analysis. Water Research 31(8), 1847-1856.

Channell, G.M. and Zukoski, C.F. (1997) Shear and compressive rheology of aggregated alumina suspensions. Aiche Journal 43(7), 1700-1708.

Chen, G.W., Chang, I.L., Hung, W.T. and Lee, D.J. (1996) Regimes for zone settling of waste activated sludges. Water Research 30(8), 1844-1850.

Cho, S.H., Colin, F., Sardin, M. and Prost, C. (1993) Settling Velocity Model of Activated-Sludge. Water Research 27(7), 1237-1242.

Coe, H.B. and Clevenger, G.H. (1916) Methods for determining the capacities of slime-settling tanks. Transactions of the American Institute of Mining and Metallurgical Engineers 55, 356-384.

Concha, F. and Bürger, R. (2003) Thickening in the 20(th) century: a historical perspective. Minerals & Metallurgical Processing 20(2), 57-67.

Cosenza, A., Mannina, G., Vanrolleghem, P.A. and Neumann, M.B. (2013) Global sensitivity analysis in wastewater applications: A comprehensive comparison of different methods. Environmental Modelling & Software 49, 40-52.

Cukier, R.I., Fortuin, C.M., Shuler, K.E., Petschek, A.G. and Schaibly, J.H. (1973) Study of Sensitivity of Coupled Reaction Systems to Uncertainties in Rate Coefficients .1. Theory. Journal of Chemical Physics 59(8), 3873-3878.

David, D. (1968) Cost of waste water treatment processes. U.S. Department of the Interior Federal Water Pollution Control Administration Cincinnati, Ohio.

David, R., Saucez, P., Vasel, J.L. and Wouwer, A.V. (2009a) Modeling and numerical simulation of secondary settlers: A Method of Lines strategy. Water Research 43(2), 319-330.

David, R., Vasel, J.L. and Wouwer, A.V. (2009b) Settler dynamic modeling and MATLAB simulation of the activated sludge process. Chemical Engineering Journal 146(2), 174-183.

Davies, L., Dollimore, D. and Sharp, J.H. (1976) Sedimentation of Suspensions - Implications of Theories of Hindered Settling. Powder Technology 13(1), 123-132.

De Clercq, J. (2006) Batch and continuous settling of activated sludge: in-depth monitoring and 1D compression modelling. Ph.D Thesis, Ghent University.

De Clercq, J., Devisscher, M., Boonen, I., Vanrolleghem, P.A. and Defrancq, J. (2003) A new one-dimensional clarifier model - verification using full-scale experimental data. Water Science and Technology 47(12), 105-112.

De Clercq, J., Jacobs, F., Kinnear, D.J., Nopens, I., Dierckx, R.A., Defrancq, J. and Vanrolleghem, P.A. (2005) Detailed spatio-temporal solids concentration profiling during batch settling of activated sludge using a radiotracer. Water Research 39(10), 2125-2135.

De Clercq, J., Nopens, I., Defrancq, J. and Vanrolleghem, P.A. (2008) Extending and calibrating a mechanistic hindered and compression settling model for activated sludge using in-depth batch experiments. Water Research 42(3), 781-791.

de Kretser, R.G., Scales, P.J. and Bagley, D.M. (2003) Compressive rheology: An overview. Binding, D.M. and Walters, K. (eds), pp. 125-166, British Society of Rheology, Aberystwyth.

de Kretser, R.G., Usher, S.P., Scales, P.J., Boger, D.V. and Landman, K.A. (2001) Rapid filtration measurement of dewatering design and optimization parameters. Aiche Journal 47(8), 1758-1769.

Dick, R.I. (1965) Applicability of Prevailing Thickening Theories to Activaded Sludge, University of Illinois, Illinois.

Dick, R.I. (1970) Role of Activated Sludge Final Settling Tanks. Jour. San. Eng. Div. ASCE 96, 423-436.

Dick, R.I. and Ewing, B.B. (1967) Rheology of Activated Sludge. Journal Water Pollution Control Federation 39(4), 543-&.

Dick, R.I. and Ewing., B.B. (1967) Evaluation of Activated Sludge Thickening Theories. Jour. San. Eng. Div. ASCE 93(4), 9-29.

Diehl, S. (1995) On Scalar Conservation-Laws with Point-Source and Discontinuous Flux Function. Siam Journal on Mathematical Analysis 26(6), 1425-1451.

Diehl, S. (1996) A conservation law with point source and discontinuous flux function modelling continuous sedimentation. Siam Journal on Applied Mathematics 56(2), 388-419.

Diehl, S. (1997) Dynamic and steady-state behavior of continuous sedimentation. Siam Journal on Applied Mathematics 57(4), 991-1018.

Diehl, S. (2000) On boundary conditions and solutions for ideal clarifier-thickener units. Chemical Engineering Journal 80(1-3), 119-133.

Diehl, S. (2005) Operating charts for continuous sedimentation II: Step responses. Journal of Engineering Mathematics 53(2), 139-185.

Diehl, S. (2006) Operating charts for continuous sedimentation III: control of step inputs. Journal of Engineering Mathematics 54(3), 225-259.

Diehl, S. (2007) Estimation of the batch-settling flux function for an ideal suspension from only two experiments. Chemical Engineering Science 62(17), 4589-4601.

Diehl, S. (2008) The solids-flux theory - Confirmation and extension by using partial differential equations. Water Research 42(20), 4976-4988.

Diehl, S. and Faras, S. (2012) Fundamental nonlinearities of the reactor-settler interaction in the activated sludge process. Water Science and Technology 66(1), 28-35.

Diehl, S. and Jeppsson, U. (1998) A model of the settler coupled to the biological reactor. Water Research 32(2), 331-342.

Diplas, P. and Papanicolaou, A.N. (1997) Batch analysis of slurries in zone settling regime. Journal of Environmental Engineering-Asce 123(7), 659-667.

Dixon, D.C. (1977a) Momentum-Balance Aspects of Free-Settling Theory .1. Batch Thickening. Separation Science 12(2), 171-191.

Dixon, D.C. (1977b) Momentum-Balance Aspects of Free-Settling Theory .2. Continuous, Steady-State Thickening. Separation Science 12(2), 193-203.

Dixon, D.C. (1978) Momentum-Balance Aspects of Free-Settling Theory .3. Transient Compression Resistance. Separation Science and Technology 13(9), 753-766.

Dixon, D.C. (1981) Thickener Dynamic Analysis, Accounting for Compression Effects. Chemical Engineering Science 36(3), 499-507.

Dixon, D.C., Souter, P. and Buchanan, J.E. (1976) A study of inertial effects in sedimentation. Chemical Engineering Science 31, 737-740.

Dupont, R. and Dahl, C. (1995) A One-Dimensional Model for a Secondary Settling-Tank Including Density-Current and Short-Circuiting. Water Science and Technology 31(2), 215-224.

Eckenfelder, W.W. and Melbinger, N. (1957) Settling and Compaction Characteristics of Biological Sludges .1. General Considerations. Sewage and Industrial Wastes 29(10), 1114-1122.

Ekama, G.A., Barnard, J.L., Gunthert, F.W., Krebs, P., McConcordale, J.A., Parker, D.S. and Wahlberg, E.J. (1997a) Secondary settling tank: theory, modelling, design and operation. Scientific and Technical Report No.6, 105-116, IAWQ, London.

Ekama, G.A., Barnard, J.L., Gunthert, F.W., Krebs, P., McConcordale, J.A., Parker, D.S. and Wahlberg, E.J. (1997b) Secondary settling tank: theory, modelling, design and operation. Scientific and Technical Report No. 6., pp. 105-116, IAWQ, London.

Ekama, G.A. and Marais, P. (2002a) Hydrodynamic Modelling of Secondary Settling Tanks, WRC Report No. 835/1/02 Part 1, Water Resources Group, Department of Civil Engineering, University of Cape Town, South Africa.

Ekama, G.A. and Marais, P. (2002b) Hydrodynamic Modelling of Secondary Settling Tanks. WRC Report No. 835/1/02 Part 1, Water Resources Group, Department of Civil Engineering, University of Cape Town, South Africa.

Engquist, B. and Osher, S. (1981) One-Sided Difference Approximations for Non-Linear Conservation-Laws. Mathematics of Computation 36(154), 321-351.

Fitch, B. (1962) Sedimentation Process Fundamentals. Transactions of the Society of Mining Engineers of Aime 223(2), 129-137.

Fitch, B. (1979) Sedimentation of Flocculent Suspensions - State of the Art. Aiche Journal 25(6), 913-930.

Fitch, B. (1983) Kynch Theory and Compression Zones. Aiche Journal 29(6), 940-947.

Fitch, B. (1993) Thickening Theories - an Analysis. Aiche Journal 39(1), 27-36.

Font, R. (1988) Compression Zone Effect in Batch Sedimentation. Aiche Journal 34(2), 229-238.

Font, R. (1991) Analysis of the Batch Sedimentation Test. Chemical Engineering Science 46(10), 2473-2482.

Garrido, P., Bürger, R. and Concha, F. (2000) Settling velocities of particulate systems: 11. Comparison of the phenomenological sedimentation-consolidation model with published experimental results. International Journal of Mineral Processing 60(3-4), 213-227.

George, D.B. and Keinath, T.M. (1978) Dynamics of Continuous Thickening. Journal Water Pollution Control Federation 50(11), 2560-2572.

Gernaey, K.V., van Loosdrecht, M.C.M., Henze, M., Lind, M. and Jorgensen, S.B. (2004) Activated sludge wastewater treatment plant modelling and simulation: state of the art. Environmental Modelling & Software 19(9), 763-783.

Gladman, B., Usher, S.P. and Scales, P.J. (2006) Compressive rheology of aggregated particulate suspensions. Korea-Australia Rheology Journal 18(4), 191-197.

Gladman, B.R., Rudman, M. and Scales, P.J. (2010a) The effect of shear on gravity thickening: Pilot scale modelling. Chemical Engineering Science 65(14), 4293-4301.

Gladman, B.R., Rudman, M. and Scales, P.J. (2010b) Experimental validation of a 1-D continuous thickening model using a pilot column. Chemical Engineering Science 65(13), 3937-3946.

Godunov, S.K. (1959) A finite difference method for the numerical computations of discontinuous solutions of the equations of fluid dynamics. Mat. Sb 47, 271-306 (in Russian).

Gong, M., Xanthos, S., Ramalingam, K., Fillos, J., Beckmann, K., Deur, A. and McCorquodale, J.A. (2011) Development of a flocculation sub-model for a 3-D CFD model based on rectangular settling tanks. Water Science and Technology 63(2), 213-219.

Grace, H.P. (1953) Resistance and Compressibility of Filter Cakes. Chemical Engineering Progress 49(6), 303-318.

Grassia, P., Usher, S.P. and Scales, P.J. (2011) Closed-form solutions for batch settling height from model settling flux functions. Chemical Engineering Science 66(5), 964-972.

Green, M.D. (1997) Characterisation of suspensions in settling and compression. Ph.D Thesis, University of Melbourne, Melbourne.

Grieves, C.G. and Stenstrom, M.K. (1976a) Evaluation of Performance of the Texas City Refinery Wastewater Treatment Facilities.

Grieves, C.G. and Stenstrom, M.K. (1976b) Evaluation of Performance of the Texas City Refinery Wastewater Treatment Facilities. Project 4076-IF 551,641-2.

Grijspeerdt, K., Vanrolleghem, P. and Verstraete, W. (1995) Selection of One-Dimensional Sedimentation - Models for Online Use. Water Science and Technology 31(2), 193-204.

Gujer, W., Henze, M., Mino, T. and van Loosdrecht, M. (1999) Activated Sludge Model No. 3. Water Science and Technology 39(1), 183-193.

Gustavsson, K. and Oppelstrup, J. (2000) Consolidation of concentrated suspensions-numerical simulations using a two-phase fluid model. Computing and Visualization in Science 3, 39-45.

Hamilton, J., Jain, R., Antoniou, P., Svoronos, S.A., Koopman, B. and Lyberatos, G. (1992) Modeling and Pilot-Scale Experimental-Verification for Predenitrification Process. Journal of Environmental Engineering-Asce 118(1), 38-55.

Hassett, N.J. (1958) Design and Operation of Continuous Thickeners. Industrial Chemist 34, 116-120.

Henze, M., Grady, C.P.L.J., Gujer, W., Marais, G.v.R. and Matsuo, T. (1987) Activated Sludge Model No.1. IAWPRC Scientific and Technical Report NO.1, IAWPRC, London.

Henze, M., Gujer, W., Mino, T., Matsuo, T., Wentzel, M.C. and Marais, G.v.R. (1995) Activated Sludge Model No.2. IAWQ Scientific and Technical Report No.3, IAWQ, London.

Henze, M., Gujer, W., Mino, T., Matsuo, T., Wentzel, M.C., Marais, G.V.R. and Van Loosdrecht, M.C.M. (1999) Activated Sludge Model No.2d, ASM2d. Water Science and Technology 39(1), 165-182.

Holdich, R.G. and Butt, G. (1997) Experimental and numerical analysis of a sedimentation forming compressible compacts. Separation Science and Technology 32(13), 2149-2171.

Hulsbeek, J.J.W., Kruit, J., Roeleveld, P.J. and van Loosdrecht, M.C.M. (2002) A practical protocol for dynamic modelling of activated sludge systems. Water Science and Technology 45(6), 127-136.

Islam, M.A. and Karamisheva, R.D. (1998) Initial settling rate/concentration relationship in zone settling. Journal of Environmental Engineering-Asce 124(1), 39-42.

Javaheri, A.B. (1971) Continuous thickening of non-ideal suspensions, University of Illinois Urbana, Illinois.

Javaheri, A.B. and Dick, R.I. (1969) Aggregate size variations during thickening of activated sludge. Journal Water Pollution Control Federation 41, R197-R214.

Jeppsson, U. and Diehl, S. (1996) An evaluation of a dynamic model of the secondary clarifier. Water Science and Technology 34(5-6), 19-26.

Kammermeyer, K. (1941) Settling and thickening of aqueous suspensions. Industrial and Engineering Chemistry 33, 1484-1491.

Karl, J.R. and Wells, S.A. (1999) Numerical model of sedimentation/thickening with inertial effects. Journal of Environmental Engineering-Asce 125(9), 792-806.

Keinath, T.M. (1985) Operational Dynamics and Control of Secondary Clarifiers. Journal Water Pollution Control Federation 57(7), 770-776.

Keinath, T.M., Ryckman, M.D., Dana, C.H. and Hofer, D.A. (1977) Activated Sludge-Unified System-Design and Operation. Journal of the Environmental Engineering Division-Asce 103(5), 829-849.

Kinnear, D.J. (2002) Biological solids sedimentation: a model incorporating fundamental settling parameters. Ph.D. Thesis, University of Utah.

Kos, P. (1977) Fundamentals of Gravity Thickening. Chemical Engineering Progress 73(11), 99-105.

Kynch, G.J. (1952) A Theory of Sedimentation. Transactions of the Faraday Society 48(2), 166-176.

Landman, K.A. and White, L.R. (1992) Determination of the Hindered Settling Factor for Flocculated Suspensions. Aiche Journal 38(2), 184-192.

Landman, K.A., White, L.R. and Buscall, R. (1988) The Continuous-Flow Gravity Thickener - Steady-State Behavior. Aiche Journal 34(2), 239-252.

Lee, D.J., Chen, G.W., Liao, Y.C. and Hsieh, C.C. (1996) On the free-settling test for estimating activated sludge floc density. Water Research 30(3), 541-550.

Lee, D.J., Ju, S.P., Kwon, J.H. and Tiller, F.M. (2000) Filtration of highly compactible filter cake: Variable internal flow rate. Aiche Journal 46(1), 110-118.

Lee, T.T., Wang, F.Y. and Newell, R.B. (1999) Distributed parameter approach to the dynamics of complex biological processes. Aiche Journal 45(10), 2245-2268.

Li, B. and Stenstrom, M.K. (2014a) Dynamic one-dimensional modeling of secondary settling tanks and design impacts of sizing decisions. Water Research 50, 160-170.

Li, B. and Stenstrom, M.K. (2014b) Dynamic one-dimensional modeling of secondary settling tanks and system robustness evaluation. Water Science and Technology 69(11), 2339-2349.

Li, B. and Stenstrom, M.K. (2014c) Dynamic one-dimensional modeling of secondary settling tanks and system robustness evaluation. Water Science and Technology.

Li, B. and Stenstrom, M.K. (2014d) Research advances and challenges in one-dimensional modeling of secondary settling Tanks - A critical review. Water Research 65, 40-63.

Li, B. and Stenstrom, M.K. (2015) Construction of analytical solutions and numerical methods comparison of the ideal continuous settling model. Computers & Chemical Engineering 80, 211-222.

Li, D.H. and Ganczarczyk, J.J. (1987) Stroboscopic Determination of Settling Velocity, Size and Porosity of Activated-Sludge Flocs. Water Research 21(3), 257-262.

Loureiro, J.M. and Rodrigues, A.E. (1991) 2 Solution Methods for Hyperbolic Systems of Partial-Differential Equations in Chemical-Engineering. Chemical Engineering Science 46(12), 3259-3267.

Mazzolani, G., Pirozzi, F. and d'Antonoi, G. (1998) A generalized settling approach in the numerical modeling of sedimentation tanks. Water Science and Technology 38(3), 95-102.

Metcalf&Eddy (2002) Wastewater Engineering: Treatment and Reuse, McGraw-Hill Science/Engineering/Math, New York.

Michaels, A.S. and Bolger, J.C. (1962a) The plastic flow behavior of flocculated kaolin suspensions. Industrial & Engineering Chemistry Fundamentals 1, 153-165.

Michaels, A.S. and Bolger, J.C. (1962b) Settling Rates and Sediment Volumes of Flocculated Kaolin Suspensions. Industrial & Engineering Chemistry Fundamentals 1(1), 24-&.

Moncrieff, A.G. (1964) Theory of thickener design based on batch sedimentation tests. Transactions of the American Institute of Mining and Metallurgical Engineers 73, 729-761.

More, J.J. (1978a) The Levenberg-Marquardt algorithm: implementation and theory. Proceedings of the Biennial Conference on numerical analysis, 105-116.

More, J.J. (1978b) The Levenberg-Marquardt algorithm: implementation and theory. Proceedings of the Biennial Conference on numerical analysis 105-116.

Northcott, K.A., Snape, I., Scales, P.J. and Stevens, G.W. (2005) Dewatering behaviour of water treatment sludges associated with contaminated site remediation in Antarctica. Chemical Engineering Science 60(24), 6835-6843.

Oleinik, A.O. (1964) Uniqueness and stability of the generalized solution of the Cauchy problem for a quasi-linear equation. Am. Math. Soc. Trans. Ser 2(33), 285-290.

Omlin, M., Brun, R. and Reichert, P. (2001) Biogeochemical model of Lake Zurich: sensitivity, identifiability and uncertainty analysis. Ecological Modelling 141(1-3), 105-123.

Petersen, B., Gernaey, K., Henze, M. and Vanrolleghem, P.A. (2002) Evaluation of an ASM1 model calibration procedure on a municipal-industrial wastewater treatment plant. J. Hydroinformatics 4, 15-38.

Petty, C.A. (1975) Continuous Sedimentation of a Suspension with a Nonconvex Flux Law. Chemical Engineering Science 30(12), 1451-1458.

Pflanz, P. (1969) Performance of (activated sludge) secondary sedimentation basins. In Advances in Water Pollution Research (Edited by Jenkins, S.H.), 569-581.

Pitman, A.R. (1980) Settling Properties of Extended Aeration Sludge. Journal Water Pollution Control Federation 52(3), 524-536.

Plósz, B.G., De Clercq, J., Nopens, I., Benedetti, L. and Vanrolleghem, P.A. (2011) Shall we upgrade one-dimensional secondary settler models used in WWTP simulators? - An assessment of model structure uncertainty and its propagation. Water Science and Technology 63(8), 1726-1738.

Plósz, B.G., Weiss, M., Printemps, C., Essemiani, K. and Meinhold, J. (2007) One-dimensional modelling of the secondary clarifier-factors affecting simulation in the clarification zone and the assessment of the thickening flow dependence. Water Research 41(15), 3359-3371.

Ramalingam, K., Xanthos, S., Gong, M., Fillos, J., Beckmann, K., Deur, A. and McCorquodale, J.A. (2012) Critical modeling parameters identified for 3D CFD modeling of rectangular final settling tanks for New York City wastewater treatment plants. Water Science and Technology 65(6), 1087-1094.

Ramin, E., Flores-Alsina, X., Sin, G., Gernaey, K.V., Jeppsson, U., Mikkelsen, P.S. and Plósz, B.G. (2014a) Influence of selecting secondary settling tank sub-models on the calibration of WWTP models - A global sensitivity analysis using BSM2. Chemical Engineering Journal 241, 28-34.

Ramin, E., Flores-Alsina, X., Sin, G., Gernaey, K.V., Jeppsson, U., Mikkelsen, P.S. and Plósz, B.G. (2014b) Influence of selecting secondary settling tank sub-models on the calibration of WWTP models – A global sensitivity analysis using BSM2. Chemical Engineering Journal 241, 28-34.

Ramin, E., Sin, G., Mikkelsen, P.S. and Plósz, B.G. (2014c) Significance of settling model structures and parameter subsets in modelling WWTPs under wet-weather flow and filamentous bulking conditions. Water Research 63, 209-221.

Ramin, E., Wagner, D.S., Yde, L., Binning, P.J., Rasmussen, M.R., Mikkelsen, P.S. and Plosz, B.G. (2014d) A new settling velocity model to describe secondary sedimentation. Water Research 66, 447-458.

Richardson, J.F. and Zaki, W.N. (1954) The Sedimentation of a Suspension of Uniform Spheres under Conditions of Viscous Flow. Chemical Engineering Science 3(2), 65-73.

Riddell, M.D.R., Lee, J.S. and Wilson, T.E. (1983) Method for Estimating the Capacity of an Activated-Sludge Plant. Journal Water Pollution Control Federation 55(4), 360-368.

Roberts, E.J. (1949) Thickening - Art or Science. Transactions of the American Institute of Mining and Metallurgical Engineers 184(3), 61-64.

Ruano, M.V., Ribes, J., De Pauw, D.J.W. and Sin, G. (2007) Parameter subset selection for the dynamic calibration of activated sludge models (ASMs): experience versus systems analysis. Water Science and Technology 56(8), 107-115.

Ruth, B.F. (1946) Correlating Filtration Theory with Industrial Practice. Industrial and Engineering Chemistry 38(6), 564-571.

Saltelli, A., Tarantola, S., Campolongo, F. and Ratto, M. (2004) Sensitivity Analysis in Practice. A Guide to Assessing Scientific Models. In: Probability and Statistics Series, John Wiley & Sons.

Saltelli, A., Tarantola, S. and Chan, K.P.S. (1999) A quantitative model-independent method for global sensitivity analysis of model output. Technometrics 41(1), 39-56.

Schaibly, J.H. and Shuler, K.E. (1973) Study of Sensitivity of Coupled Reaction Systems to Uncertainties in Rate Coefficients .2. Applications. Journal of Chemical Physics 59(8), 3879-3888.

Scott, K.J. (1966) Mathematical Models of Mechanism of Thickening. Industrial & Engineering Chemistry Fundamentals 5(1), 109-&.

Scott, K.J. (1968a) Experimental Study of Continuous Thickening of a Flocculated Silica Slurry. Industrial & Engineering Chemistry Fundamentals 7(4), 582-&.

Scott, K.J. (1968b) Thickening of Calcium Carbonate Slurries - Comparison of Data with Results for Rigid Spheres. Industrial & Engineering Chemistry Fundamentals 7(3), 484-&.

Scott, K.J. and Alderton, J.L. (1966) Maximum solids handling capacity of continuous thickeners. Trans. Inst. Mining Met 75(C201-210).

Shannon, P.T., Stroupe, E. and Tory, E.M. (1963) Batch and Continuous Thickening - Basic Theory - Solids Flux for Rigid Spheres. Industrial & Engineering Chemistry Fundamentals 2(3), 203-&.

Shirato, M., Kato, H., Kobayashi, K. and Sakazaki, H. (1970) Analysis of settling of thick slurries due to consolidation. J. Chem. Eng. Jpn 3, 98-104.

Sin, G., Gernaey, K.V., Neumann, M.B., van Loosdrecht, M.C.M. and Gujer, W. (2009) Uncertainty analysis in WWTP model applications: A critical discussion using an example from design. Water Research 43(11), 2894-2906.

Smollen, M. and Ekama, G.A. (1984) Comparison of Empirical Settling-Velocity Equations in Flux Theory for Secondary Settling Tanks. Water Sa 10(4), 175-184.

Steinour, H.H. (1944) Rate of sedimentation - Nonflocculated suspensions of uniform spheres. Industrial and Engineering Chemistry 36, 618-624.

Stenstrom, M.K. (1976a) A dynamic model and computer compatible control strategies for wastewater treatment plants. Ph.D Thesis, Clemson University, Clemson, South Carolina, USA.

Stenstrom, M.K. (1976b) A dynamic model and computer compatible control strategies for wastewater treatment plants. Ph.D. Dissertation, Clemson University. Clemson, South Carolina.

Stenstrom, M.K. and Andrews, J.A. (1979a) Real-Time Control of Activated Sludge Process J. of Envr. Engr. Div, ASCE 105(2), 245-260.

Stenstrom, M.K. and Andrews, J.F. (1979b) Real-Time Control of Activated-Sludge Process. Journal of the Environmental Engineering Division-Asce 105(2), 245-260.

Takács, I. (2008) Experiments in activated sludge modelling, Ghent University Belgium.

Takács, I., Patry, G.G. and Nolasco, D. (1991) A Dynamic-Model of the Clarification Thickening Process. Water Research 25(10), 1263-1271.

Talmage, W.P. and Fitch, E.B. (1955) Determining Thickener Unit Areas. Industrial and Engineering Chemistry 47(1), 38-41.

Terzaghi, K. (1925) Modern concepts concerning foundation engineering. Trans. Boston Soc. Civ. Engng 12, 1-43.

Terzaghi, K. and Peck, P.B. (1948) Soli Mechanics in Engineering Practice, John Wiley, New York.

Tien, C. (2002) Cake filtration research - a personal view. Powder Technology 127(1), 1-8.

Tiller, F.M. and Khatib, Z. (1984) The Theory of Sediment Volumes of Compressible, Particulate Structures. Journal of Colloid and Interface Science 100(1), 55-67.

Tiller, F.M. and Shirato, M. (1964) The Role of Porosity in Filtration .6. New Definition of Filtration Resistance. Aiche Journal 10(1), 61-67.

Tiller, F.M. and Yeh, C.S. (1987) The Role of Porosity in Filtration .11. Filtration Followed by Expression. Aiche Journal 33(8), 1241-1256.

Torfs, E., Maere, T., Burger, R., Diehl, S. and Nopens, I. (2015) Impact on sludge inventory and control strategies using the benchmark simulation model no. 1 with the Burger-Diehl settler model. Water Science and Technology 71(10), 1524-1535.

Torfs, E., Vlasschaert, P., Amerlinck, Y., Bürger, R., Diehl, S., Faras, S. and Nopens, I. (2013) Towards improved 1-D settler modelling: calibration of the Bürger model and case study. Proceedings of the Water Environment Federation WEFTEC 2013: Session 47 through Session 53, 3953-3969

Tory, E.M. and Shannon, P.T. (1965) Reappraisal of Concept of Settling in Compression - Settling Behavior and Concentration Profiles for Initially Concentrated Calcium Carbonate Slurries. Industrial & Engineering Chemistry Fundamentals 4(2), 194-&.

Tracy, K.D. (1973) Mathematical Modeling of Unsteady-State Thickening of Compressible Slurries. Ph.D Thesis, Clemson University, Clemson South Carolina.

Traub, J.F. (1964) Iterative methods for solution of equations, Prentice-Hall, Englewood Cliffs, NJ.

Usher, S.P., De Kretser, R.G. and Scales, P.J. (2001) Validation of a new filtration technique for dewaterability characterization. Aiche Journal 47(7), 1561-1570.

Usher, S.P. and Scales, P.J. (2005) Steady state thickener modelling from the compressive yield stress and hindered settling function. Chemical Engineering Journal 111(2-3), 253-261.

Usher, S.P., Scales, P.J. and White, L.R. (2006) Prediction of transient bed height in batch sedimentation at large times. Aiche Journal 52(3), 986-993.

Vaerenbergh, E.V. (1980) Numerical computation of secondary settler area using batch settling data. Trib. Ceb 33, 369-374, 441-442.

Vand, V. (1948) Design of prototype thickeners from batch settling tests. Water & Sewage Works, 302-307.

Vanderhasselt, A. and Vanrolleghem, P.A. (2000) Estimation of sludge sedimentation parameters from single batch settling curves. Water Research 34(2), 395-406.

Vanduijn, C.J., Molenaar, J. and Deneef, M.J. (1995) The Effect of Capillary Forces on Immiscible 2-Phase Flow in Heterogeneous Porous-Media. Transport in Porous Media 21(1), 71-93.

Vanrolleghem, P., VanderSchueren, D., Krikilion, G., Grijspeerdt, K., Willems, P. and Verstraete, W. (1996) On-line quantification of settling properties with in-sensor-experiments in an automated settlometer. Water Science and Technology 33(1), 37-51.

Vesilind, P.A. (1968a) Discussion of "Evaluation of Activated Sludge Thickening Theories" By R. I. Dick and B. B. Ewing. Jour. San. Eng. Div. ASCE 94, 185-191.

Vesilind, P.A. (1968b) Discussion of "Evaluation of Activated Sludge Thickening Theories" By R.I.Dick and B.B. Ewing. Jour. San. Eng. Div. ASCE 94, 185-191.

Vitasovic, Z.Z. (1986a) An Integrated Control Strategy for The Activated Sludge Process. Ph.D Thesis, Rice University, Houston, Texas, USA.

Vitasovic, Z.Z. (1986b) An Integrated Control Strategy for The Activated Sludge Process. Ph.D. Dissertation, Rice University, Houston, Tex. .

Wágner, D.S., Ramin, E., Szabo, P., Dechesne, A. and Plósz, B.G. (2015) Microthrix parvicella abundance associates with activated sludge settling velocity and rheology - Quantifying and modelling filamentous bulking. Water Research 78, 121-132.

Watts, R.W., Svoronos, S.A. and Koopman, B. (1996) One-dimensional modeling of secondary clarifiers using a concentration and feed velocity-dependent dispersion coefficient. Water Research 30(9), 2112-2124.

Weijers, S.R. and Vanrolleghem, P.A. (1997) A procedure for selecting best identifiable parameters in calibrating activated sludge model no.1 to full-scale plant data. Water Science and Technology 36(5), 69-79.

Work, L.T. and Kohler, A.S. (1940) Sedimentation of suspensions. Industrial and Engineering Chemistry 32, 1329-1334.

Xanthos, S., Gong, M.W., Ramalingam, K., Fillos, J., Deur, A., Beckmann, K. and McCorquodale, J.A. (2011) Performance Assessment of Secondary Settling Tanks Using CFD Modeling. Water Resources Management 25(4), 1169-1182.

Yee, H.C., Klopfer, G.H. and Montagne, J.L. (1990) High-Resolution Shock-Capturing Schemes for Inviscid and Viscous Hypersonic Flows. Journal of Computational Physics 88(1), 31-61.

Yoshioka, N., Y.H., Tanaka, S., Naito, S. and Tsugami., S. (1957a) Continuous Thickening of Homogeneous Flocculated Suspensions. Kagaku Kogaku 21, 66-74.

Yoshioka, N., Hotta, Y., Tanaka, S., Naito, S. and Tsugami, S. (1957b) Continuous thickening of homogeneous flocculated slurries. Kagaku Kogaku 21, 66-74.

Zhang, D.J., Li, Z.L., Lu, P.L., Zhang, T. and Xua, D.Y. (2006) A method for characterizing the complete settling process of activated sludge. Water Research 40(14), 2637-2644.

Zheng, Y.S. and Bagley, D.M. (1998) Dynamic model for zone settling and compression in gravity thickeners. Journal of Environmental Engineering-Asce 124(10), 953-958.

Zheng, Y.S. and Bagley, D.M. (1999) Numerical simulation of batch settling process. Journal of Environmental Engineering-Asce 125(11), 1007-1013.

Zhou, S.P. and Mccorquodale, J.A. (1992a) Mathematical-Modeling of a Circular Clarifier. Canadian Journal of Civil Engineering 19(3), 365-374.

Zhou, S.P. and Mccorquodale, J.A. (1992b) Modeling of Rectangular Settling Tanks. Journal of Hydraulic Engineering-Asce 118(10), 1391-1405.

Zuber, N. (1964) On the Dispersed 2-Phase Flow in the Laminar Flow Regime. Chemical Engineering Science 19(11), 897-917.